Freie Universität Berlin

FACHBEREICH GEOWISSENSCHAFTEN

Reaktion des Auftriebsökosystems vor Namibia auf Klimaschwankungen im späten Holozän im Vergleich mit der Rezentsituation

Dissertation in kumulativer Form
zur Erlangung des Doktorgrades

vorgelegt von

Sandra Meisel

im Mai 2011

FACHBEREICH GEOWISSENSCHAFTEN

Inhaltsverzeichnis

Abkürzungsverzeichnis

ABF	Angola-Benguela Front
AIR	reference standard for nitrogen isotope analysis
AR	accumulation rates
AR_{bulk}	accumulation rates of bulk sediment
AR_{TOC}	accumulation rates of total organic carbon
BCC	Benguela Coastal Current
BOC	Benguela Oceanic Current
BP	before present; i.e. before AD1950
cal age	calendar age
C_{org}	organic carbon
C_{inorg}	inorganic carbon
$\delta^{13}C$	carbon isotope composition
$\delta^{13}C_{org}$	carbon isotope composition of organic carbon
$\delta^{15}N$	nitrogen isotope composition
$\delta^{15}N_{nitrate}$	nitrogen isotope composition of nitrate
$\delta^{15}N_{SPM}$	nitrogen isotope composition of suspended particulate matter
$\delta^{15}N_{sediment}$	nitrogen isotope composition in the sediment
$\delta^{18}O$	oxygen isotope composition
$\delta^{18}O_{calcite}$	oxygen isotope composition in foraminiferal calcite
DIC	dissolved inorganic carbon
ESACW	East South Atlantic Central Water
ITCZ	Innertropical Convergence Zone
LIA	Little Ice Age (±650 bis 100 BP)
MWE	Medieval Warm Epoch (±1050 bis 650 BP)
MS	measurement series
MUC	multicorer core
NADW	North Atlantic Deep Water
OM	organic matter
PN	particulate nitrogen
POC	particulate organic carbon
RCC	rapid climate change
SECC	South Equatorial Counter Current
SACW	South Atlantic Central Water
SPM	suspended particulate matter
SR	sedimentation rates
SST	sea surface temperature
$T_{\delta18O}$	water temperature reconstructed by means of $\delta^{18}O$-signals in foraminiferal calcite

TC	total carbon
TIC	total inorganic carbon
TOC	total organic carbon
ΔT	SST - $T_{\delta 18O}$
VPDB	Vienna Belemnite of the PeeDee Formation
VSMOW	Vienna Standard Mean Ocean Water
UK'37	alkenone unsaturation index

8

Summary

Our investigation deals with the central Namibian upwelling within the *Benguela Current Large Marine Eco-system* with particular emphasis on the shelf region. First, we are concentrating on the modern situation, deepening our understanding of today's dynamics above the central Namibian shelf. The investigation is based on an extensive compilation of surface sediments and suspended particulate matter collected along with hydrographic data. Against this background the variability in upwelling and nutrient dynamics since the middle Holocene is examined by means of three sediment cores from the diatomaceous muds coating the inner shelf up to 150 m depth.

Our main insight into the nutrient dynamics and oceanographic features comes from nitrogen isotope ratios (δ^{15}N) in organic matter. It was, therefore, in our very interest to investigate the deceptive influence of sample preparation on the original δ^{15}N-signal. We compared the effects of common processing methods in order to establish which can be most trusted with respect to the central Namibian shelf sediments. Each sample was subjected to three common types of pre-analysis processing methods. For comparative purposes, the first measurement series (MS-1) was carried out on untreated sediment. In MS-2, the sediment was rinsed with distilled water. In MS-3, analyses were carried out on decalcified and rinsed material, in MS-4 the samples were decalcified without being subsequently washed. Rinsing, irrespective of whether acidification was included (MS-3) or not (MS-2), induced substantial modifications in δ^{15}N compared to untreated sample splits (MS-1). Molar C_{org}/N ratios, on the other hand, were only affected by a combination of acidification and rinsing (MS-3). Our findings provide strong evidence of ammonium (NH_4^+) being responsible for the discrepancies observed. Firstly, nitrogen isotopes fractionate during NH_4^+-volatilisation in the heating oven, where the sediment is put to desiccate. Thereby, ^{14}N accumulates in gaseous NH_3, thus leaving ^{15}N-enriched NH_4^+ behind. Secondly, outgassing and concomitant fractionation only concerns NH_4^+-ions dissolved in the interstitial waters of the sediment; NH_4^+-ions adsorbed to negatively-charged SiO_2-surfaces (in the form of diatom frustrules) escape both the outgassing and fractionation and remain unaffected. Finally, the surface charge and, with it, adsorption capacity of SiO_2 increases with increasing pH of the pore water, hence with increasing carbonate content.
Taken together, our findings raise serious doubts about whether untreated sediment (MS-1) can provide reliable C_{org}/N and δ^{15}N-records in case that NH_4^+ is involved. This is because variations in $[C_{org}/N]_{untreated}$ and $\delta^{15}N_{untreated}$ may result from a misleading influence of NH_4^+, not necessarily having any nutrient-related background. We conclude that excessive confidence in MS-1 is inappropriate with respect to organic-rich and anoxic deposits, such as the northern Benguela shelf sediments, where NH_4^+ is abundantly produced and easily preserved. It is recommended that NH_4^+ (both adsorbed and dissolved) be removed prior to measuring C_{org}/N and δ^{15}N. This seems to be done best by a combination of acidification and subsequent rinsing (MS-3).

In order to investigate today's functioning of the coastal upwelling we compare δ^{15}N-records in surface sediments ($\delta^{15}N_{sediment}$) from the central Namibian shelf with suspended particulate matter ($\delta^{15}N_{SPM}$) from the surface ocean. Water column profiles provide an insight into changes of $\delta^{15}N_{SPM}$ with depth and elucidate potential offsets between $\delta^{15}N_{SPM}$ and $\delta^{15}N_{sediment}$. Investigating spatial and vertical changes in δ^{15}N along with temperature and productivity records (e.g. organic carbon and nitrogen contents), and combining data from sediments and suspended matter holds valuable clues to the principle controls on the δ^{15}N-signal.
Highest δ^{15}N-signatures are found right off the coast where water temperatures are lowest. This, together with pronounced nitrate deficits in coastal proximity and oxygen depletion in the bottom waters suggests the upwelling of denitrified source waters. With increasing distance offshore, δ^{15}N declines unexpectedly, reaching a minimum above the shelf break. Beyond that, the trend reverses to "normal" with δ^{15}N-signals continuously increasing towards the mesopelagic ocean.
The decrease in $\delta^{15}N_{sediment}$ and surface ocean $\delta^{15}N_{SPM}$ with increasing distance to the coast disagrees with the concept of Rayleigh fractionation kinetics, viz. the progressive ^{15}N-enrichment of the nitrate pool as it is gradually used up by phytoplankton growth. Interestingly, the oceanward decline in δ^{15}N represents an exact copy of the trend bottom water $\delta^{15}N_{nitrate}$ is expected to perform. Apparently, bottom nitrate somehow supports primary production in the photic zone over large areas of the continental shelf. An obvious explanation is that the penetration of wind- and wave-induced mixing is so deep as to tap the varyingly denitrified, subsurface waters. Nutrient replenishment via a second upwelling front at the shelf break represents an alternative scenario that might account for the unanticipated δ^{15}N-gradient. Both mechanisms are considered capable of working against the expected nutrient drawdown (i.e. ^{15}N-enrichment) as surface waters travel offshore. The results help to evaluate the applicability of $\delta^{15}N_{sediment}$ as a proxy of past nitrogen cycling, proving particularly useful when it comes to interpreting $\delta^{15}N_{sediment}$-fluctuations in the sediment cores.

The cores document climate variability in the northern Benguela Upwelling back to 5500 BP with resolutions ranging from multi-decadal (NAM1) over centennial (core 178) to millennial scale (core 226620). One of the key objectives was to examine the impact of past climate fluctuations on the system in order to assess its vulnerability to climate forcing and to gain a better understanding of what the system may await in the future. The study rests on nutrient (δ^{15}N, δ^{13}C) and productivity proxies (accumulation rates of total organic carbon; AR_{TOC}). Reconstructed sea surface temperatures (alkenone-derived SST) and temperatures at subsurface depths ($T_{\delta 18O}$; based on foraminiferal calcite) reflect the physical boundary conditions.

δ^{15}N-records indicate that denitrification seems to have prevailed since the modern shelf circulation system has established. Although the median values of the proxy indicators lie within today's range, the northern Benguela experienced pronounced and rapid perturbations during the middle and late Holocene, and apparently, not all are purely local in character. Properties and functioning of the northern Benguela system seem to be intimately linked to changes in both atmospheric circulation features and the thermohaline overturn. In this regard, the combined analysis of SST and $T_{\delta 18O}$ proved a useful tool in order to differentiate between climate signals transferred by the ocean or the atmosphere. SSTs are primarily controlled by the intensity of atmospheric circulation features, reflecting changes of upwelling-favourable winds. $T_{\delta 18O}$ records the temperature of the source water and often correlates with global ocean conveyor speed due to varying inputs of warm Agulhas Water. Besides that, it seems as though conveyor slowdown or acceleration not only affected the temperature of the source water but also its nutrient content.

Predictions concerning region-specific consequences of abrupt changes in NADW-production are still highly speculative. As regards the Benguela system, a severe slowdown of the ocean conveyor may have adverse effects on primary production and the ecosystem as a whole due to deteriorating amounts of nutrients in the source waters.

Zusammenfassung

Die Arbeit befasst sich mit dem Auftrieb vor der zentralnamibischen Küste als Teil des *Benguela Current Large Marine Ecosystem*. Das besondere Augenmerk gilt dabei der Schelfregion. An erster Stelle steht die Auseinandersetzung mit der Rezentsituation: Ziel ist ein umfassender Einblick in die Dynamik, Auftriebsmuster und das Nährstoffregime küstennaher Gewässer in ihrem heutigen Zustand. Die Probenpalette besteht aus Oberflächensedimenten, Schwebstoffen aus der Wassersäule und hydrographischen Messungen. Vor diesem Hintergrund widmen wir uns im Anschluss der Klima- und Auftriebsvariabilität der letzten 5500 Jahre. Die hierzu verwendeten Sedimentkerne (Kern 226620, Kern 178; Kern NAM1) entstammen dem organikreichen Diatommenschlammgürtel vom inneren, zentralnamibischen Schelf.

Einen großen Teil unseres Wissens über das Nährstoffregime inklusive ozeanographischer Randbedingungen beziehen wir aus der Stickstoffisotopensignatur (δ^{15}N) in organischem Material. Dementsprechend war es uns ein Anliegen, potentiellen Veränderungen des δ^{15}N-Signals als Folge der Probenaufbereitung auf den Grund zu gehen und herauszufinden, welche Aufbereitungsart die geeignetste Grundlage für unsere Untersuchungen darstellt.

Hierzu wurde jede Probe drei verschiedenen Aufbereitungsarten unterzogen. Zu Vergleichszwecken liegt der ersten Messserie (MS-1) unbehandeltes Sediment zugrunde. Für MS-2 wurde das Sediment vor der Messung mit destilliertem Wasser gespült. MS-3 basiert auf gesäuertem und gespültem Material, während für MS-4 zwar gesäuert, allerdings auf das anschließende Spülen verzichtet wurde. Wie unsere Daten zeigen, hat der Waschvorgang substanzielle Veränderungen im δ^{15}N-Signal zur Folge, unabhängig davon, ob zusätzlich gesäuert wurde (MS-3) oder nicht (MS-2). Die C_{org}/N-Verhältnisse reagieren stattdessen nur auf eine Kombination aus Säuern und anschließendem Waschen (MS-3).

Die teils dramatischen Unterschiede in den Kurvenverläufen von δ^{15}N als auch C_{org}/N werden auf den Einfluss von Ammonium (NH_4^+) zurückgeführt. Folgende Prozesse sind hierbei von Relevanz: Während des Trocknens kommt es zum Verlust von NH_4^+-N in Form von gasförmigem NH_3, wobei ^{14}N gegenüber ^{15}N den Übergang in die Gasphase bevorzugt. Allerdings sind nur die im Porenwasser gelösten NH_4^+-Ionen vom Ausgasen und der Fraktionierung betroffen. Adsorbiertes NH_4^+ scheint dem Ausgasen gegenüber immun. Die Adsorption erfolgt an negativ geladenen SiO_2-Partikeln (präsent in Form von Diatomeenschalen). Dabei führt ein Anstieg des pH-Werts im Porenwasser zu einer Erhöhung der negativen Oberflächenspannung und somit Adsorptionskapazität von SiO_2. Grund für einen pH-Anstieg ist ein höherer Karbonatanteil im Sediment.

Unsere Beobachtungen stellen die Verlässlichkeit von C_{org}/N and δ^{15}N-Daten aus unbehandeltem Sediment sehr in Frage. MS-1 täuscht Fluktuationen von C_{org}/N und δ^{15}N vor, die – statt von veränderten Umweltbedingungen zu zeugen – auf unkontrolliertes und variables Ausgasen von NH_3 zurückzuführen sind. Das Beisein von Ammonium erweist sich augenscheinlich als hoch problematisch. Da organikreiche und anoxische Sedimente Vorkommen und Erhalt von NH_4^+ begünstigen, empfiehlt es sich von der Verwendung unbehandelten Diatomeenschlamms (MS-1) abzusehen und stattdessen das Sediment vorab zu säuern und zu spülen (MS-3). Hierdurch scheint der irreführende Einfluss von NH_4^+-Ausgasen und -Fraktionierung auf C_{org}/N and δ^{15}N beseitigt.

Im Mittelpunkt der Rezentuntersuchung steht der Vergleich von δ^{15}N in suspendiertem partikulärem Material ($\delta^{15}N_{SPM}$) mit dem darunterliegenden Sediment ($\delta^{15}N_{Sediment}$). Wassersäulenprofile sollen zudem Aufschluss über Veränderungen des $\delta^{15}N_{SPM}$-Signals mit zunehmender Tiefe geben und Offsets zwischen $\delta^{15}N_{SPM}$ und $\delta^{15}N_{Sediment}$ erklären. Das Studium von δ^{15}N-Signalen in Sedimenten und Schwebstoffen in Kombination mit Temperatur- und Produktivitätsproxies liefert wertvolle Hinweise auf das Zustandekommen und die Anwendbarkeit von δ^{15}N zu Zeiten, da der direkte Einblick in die Wassersäule fehlt.

Die höchsten δ^{15}N-Signale befinden sich in Küstennähe, wo die Oberflächentemperaturen am niedrigsten sind. Gleichzeitig geringe Sauerstoff- und Nitratkonzentrationen im Bodenwasser lassen auf den Auftrieb denitrifizierten Nitrats schließen. Mit zunehmender Entfernung zur Küste sinken die δ^{15}N-Signale und erreichen ein Minimum über der Schelfkante. Hier kommt es zur Trendwende und entsprechend dem „normalen" Verlauf steigen die δ^{15}N-Werte nun gen Westen.

Die westwärtige Abnahme von δ^{15}N widerspricht dem Konzept der Rayleigh-Fraktionierung, d.h. der kontinuierlichen Anreicherung von ^{15}N-NO_3^- entlang des Strömungspfades infolge sukzessiver Nitratzehrung. Interessanterweise entsprechen die Beobachtungen exakt dem Trend, den man für $\delta^{15}N_{Nitrat}$ im Bodenwasser erwarten würde. Dies gibt Anlass zu der Vermutung, dass über weiten Teilen des Schelfs eine direkte Versorgung der photischen Zone mit Bodenwassernitrat stattfindet. Als Ursache wird intensive vertikale Durchmischung der relativ seichten Schelfgewässer diskutiert. Die Durchmischung scheint stark genug, um tiefere,

nährstoffreiche Wassermassen anzuzapfen und auf diese Weise der Nährstoffzehrung entgegenzuwirken. Eine zweite Auftriebsfront an der Schelfkante stellt ein Alternativszenario dar, wobei die Kombination beider Prozesse hinter dem unerwarteten δ^{15}N-Verlauf als wahrscheinlich anzunehmen ist. Das komplizierte Zusammenspiel nährstoffrelevanter und ozeanographischer Prozesse muss bei der folgenden Interpretation von δ^{15}N-Schwankungen entlang der Kernprofile berücksichtigt werden.

Hintergrund der Untersuchung an den Sedimentkernen ist die Frage des Einflusses holozäner Klimaschwankungen auf das Auftriebsgeschehen und Nährstoffregime. Von der Klimasensitivität des Systems in der Vergangenheit erhoffen wir uns eine klarere Vorstellung dessen, womit infolge des gegenwärtigen Klimawandels zu rechnen ist. Die Auflösung der Kerne reicht von multi-dekadisch (NAM1) über hundert- (Kern 178) bis tausendjährig (Kern 226620). Dabei setzen die ältesten Daten in etwa 5500 Jahre vor heute ein. Die Untersuchung fußt auf Nährstoff- (δ^{15}N, δ^{13}C) und Produktivitätsproxies (Akkumulationsraten von organischem Kohlenstoff; AR_{TOC}). Rekonstruktionen der Temperaturen im Oberflächenwasser (Alkenon-basierte SST; sea surface temperature) und unterhalb der durchmischten Schicht ($T_{\delta 18O}$; anhand planktischer Foraminiferen) spiegeln die physikalischen Randbedingungen wider.

Den δ^{15}N-Schwankungen zufolge, sind die Auftriebswässer seit Ausbildung der modernen Schelfzirkulation mehr oder weniger denitrifiziert. Im Mittel zeigen alle Proxyindikatoren Werte, die der Rezentsituation sehr nahe kommen. Dennoch gab es eine Reihe mehr oder wenig heftiger Fluktuationen im Laufe des mittleren und späten Holozän und wie der sorgfältige Vergleich mit Datenserien verschiedentlicher Herkunft zeigt (vom südafrikanischen Subkontinent, Südost- und Nordatlantik), ist deren Ursache oft nicht rein lokaler Natur.

Charakter und Eigenschaft des namibischen Auftriebs scheinen sowohl auf Veränderungen der Windsysteme als auch der thermohalinen Zirkulation zu reagieren. Die Kombination von SST- und $T_{\delta 18O}$-Daten erwies sich als äußerst nützlich, um zwischen dem Einfluss der Atmosphäre und des Ozeans hinsichtlich Transport und Ursache der Klimaschwankungen zu unterscheiden. SST-Signale sind primär von der Intensität der Passatwinde abhängig. $T_{\delta 18O}$ zeichnet hingegen Temperaturschwankungen im Auftriebswasser auf und korreliert dabei häufig mit der Geschwindigkeit der ozeanischen Förderbands aufgrund variablen Eintrags von warmem Agulhaswasser aus dem Indik. Ganz offensichtlich schlagen sich Veränderungen der thermohalinen Zirkulation neben der Temperatur auch im Nährstoffgehalt des Auftriebswassers nieder.

Abrupte Schwankungen der thermohalinen Zirkulation haben global unterschiedliche Konsequenzen und oft sind die zu erwartenden Auswirkungen auf eine bestimmte Region noch reine Spekulation. Eine als Folge des anthropogenen Klimawandels diskutierte Verlangsamung der Tiefenwasserproduktion könnte sinkende Nährstoffgehalte im Auftriebswasser verursachen und sich dementsprechend nachteilig auf die Primärproduktion und das Benguela-Ökosystem als Ganzes auswirken.

Reaktion des Auftriebssystems vor Namibia auf spätholozäne Klimaschwankungen im Vergleich mit der Rezentsituation - eine Übersicht

1. Einleitung

Der Einfluss küstennaher Auftriebssysteme auf das globale Klimageschehen ist sehr viel größer als ihre räumlich überschaubaren Ausmaße zunächst vermuten lassen. Nirgends ist die Primärproduktion und somit Bindung atmosphärischen CO_2 (CO_2-Sequestrierung) so hoch wie in den Schelfgewässern vor Peru bzw. Chile, Kalifornien, NW-Afrika und Namibia. Grund hierfür ist der windinduzierte Auftrieb von nährstoffreichem Tiefenwasser (Berger et al., 1989). Dennoch agieren Auftriebssysteme nicht gezwungenermaßen als CO_2-Senke. Unabhängig von der CO_2-Sequestrierung kommt es nämlich zum Ausgasen großer Mengen an CO_2, sobald das CO_2-reiche Auftriebswasser die Meeresoberfläche erreicht. Letztendlich hängt die CO_2-Bilanz davon ab, welcher der beiden Prozesse überwiegt. Im nördlichen Benguela scheint das Ausgasen der dominantere Prozess; dies wird aber durch höhere Sequestrierungsraten im südlichen Benguela ausgeglichen, so dass das System als Ganzes vermutlich als kleine CO_2-Senke fungiert (Shannon und O'Toole, 1999).

Ebenso bedeutend wie ihre Rolle im Kohlenstoffkreislauf ist der Einfluss von Auftriebssystemen auf den globalen und regionalen Wärmehaushalt. Beispielsweise spiegelt das Zusammentreffen der Angola-Benguela-Front (nördliche Begrenzung des Benguela-Auftriebssystems; s. unten) entlang 15° südlicher Breite mit den nördlichen Ausläufern der Namibwüste die enorme Bedeutung des kalten Auftriebswassers auf die Küstenregion Westafrikas wider (Brook et al., 1999; Shi et al., 2000; Berger und Wefer, 2002). Der Benguelastrom selbst ist Teil des weltumspannenden ozeanischen Förderbands und übernimmt zudem einen wichtigen Part hinsichtlich des Wärmetransfers in den Nordatlantik (Gordon, 1986; Berger und Wefer, 2002).

Auftriebssedimente stellen dank der hohen Akkumulationsraten (jährlich mehrere hundert Gramm organischer Kohlenstoff pro Quadratmeter; Berger und Wefer, 2002) beinahe so sensible Klimaarchive wie Eisbohrkerne dar. Änderungen im Auftriebsgeschehen und Nährstoffregime sind detailgenau aufgezeichnet und ermöglichen eine hochauflösende Rekonstruktion vergangener Umweltbedingungen.

2. Einführung in das Untersuchungsgebiet

Das Benguela-Auftriebssystem vor SW-Afrika entwickelte sich im späten Oligozän (Oberhänsli, 1991). Verglichen mit den Küstenauftriebsgebieten vor Südamerika (Peru, Chile), Nordamerika (Kalifornien) und Nordafrika (Marokko, Mauretanien, Senegal) weisen die namibischen Gewässer die höchste Primärproduktion auf (Lavik et al., 2009). Das *Benguela Current Large Marine Ecosystem* erstreckt sich von der Agulhas-Retroflektion im Süden bis zur Angola-Benguela-Front im Norden (Abb. 1). Das eigentliche Auftriebsgeschehen konzentriert sich dabei auf eine Handvoll Zellen. Die ganzjährig aktive Lüderitzzelle teilt das Gebiet in zwei beinahe unabhängige Subsysteme, den südlichen und nördlichen Benguela (Shannon und Nelson, 1996; Shannon und O'Toole, 2003; Mohrholz et al., 2008).

Die vorliegende Arbeit befasst sich mit dem Küstenabschnitt vor Walvis Bay (22 - 24°S) im nördlichen Benguela; ein besonderes Augenmerk gilt dabei der Schelfregion (Abb. 1). Nach eingehender Betrachtung der Rezentsituation (Meisel et al., 2011 a; S. 51ff) widmen wir uns im nächsten Schritt der Klima- und Auftriebsvariabilität der letzten 5500 Jahre (Meisel et al., 2011 b; S. 71ff). Bisherige Forschungsbemühungen beschränken sich größtenteils auf den Kontinentalhang und eiszeitliche Variabilitäten (z.B. Diester-Haass et al., 1988; Oberhänsli, 1991; Summerhayes et al., 1995; Kirst et al., 1999; Berger und Wefer, 2002; Kim et al., 2002). Nur wenige Studien haben sich bislang der holozänen Schelfsedimente bedient und vergleichsweise dürftig ist unser Wissen von der Dynamik küstennaher Gewässer sowie der jüngeren Auftriebsgeschichte.

Der Benguelastrom ist der östliche Grenzstrom des subtropischen Südatlantik-Wirbels (South Atlantic Gyre), welcher durch das Zusammenspiel der Südostpassatwinde im Norden und Westwinde im Süden angetrieben wird. In 28° südlicher Breite teilt sich der Benguelastrom in einen Küstenarm (BCC; Benguela Coastal Current)
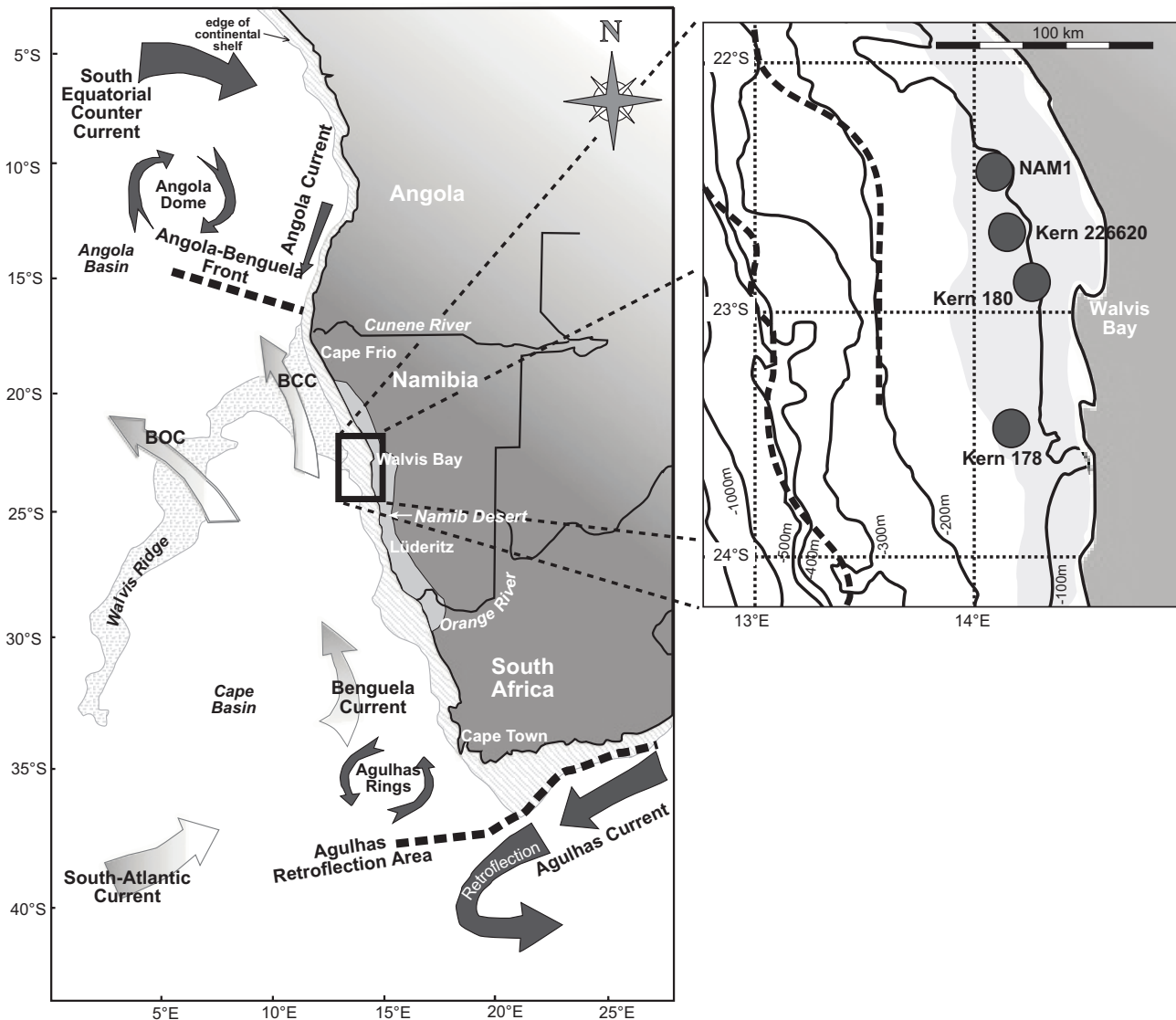
Abb. 1. Der Kartenausschnitt zeigt die Ozeanografie im Südost-Atlantik mit der Beschränkung auf oberflächennahe Strömungen (modifiziert nach Holmes et al. (1999)). Dunkle bzw. helle Pfeile geben die Bewegungsrichtung warmer bzw. kalter Wassermassen an. Über dem namibischen Schelf ist die Bewegung des Oberflächenwassers großteils windabhängig und dementsprechend nordwärts gerichtet (Shannon und O'Toole, 1999). Nur wenn der polwärtige Unterstrom (s. Text) saisonal bedingt an Kraft gewinnt, dreht der Netto-transport um 180°, d.h. gen Süden. Besonders ausgeprägt ist die Strömungsumkehr während El Niño-Ereignissen (Shannon und O'Toole, 1999; Tomczak, 2005; Mohrholz et al., 2008).

Die vergrößerte Darstellung zur Rechten zoomt auf das Untersuchungsgebiet. Rezent unterliegt es dem Einfluss der Zentralnamibischen Auftriebszelle. Nach Shannon und Nelson (1996), erstreckt sich diese von ungefähr 22.7 bis 24.5°S, wobei der Einfluss kalten Auftriebs-wassers bis zum obersten Kontinentalhang (ca. 200 km Entfernung zur Küste) reicht. Die ozeanwärtige Ausdehnung der Filament-zone beträgt ungefähr 600 km. Das Auftreten einer doppelten Schelfkante charakterisiert einen Großteil des zentralnamibischen Schelf, besonderes ausgeprägt ist sie allerdings vor Walvis Bay (Strichlinien).

An Kern 180 (22.88°S / 14.41°E; Wassertiefe 48 m) wird der Einfluss verschiedener Arten der Probenaufbreitung auf die δ^{15}N-Signale und C_{org}/N Verhältnisse untersucht (Meisel und Struck, 2011; S. 37ff). Die übrigen Kerne werden zur Rekonstruktion der Auftriebs- und Klimavariabilität der vergangenen 5500 Jahre herangezogen (Meisel et al., 2011 b; S. 71ff). NAM1 reicht von 62 bis 3036 BP (22.67°S / 14.02°E; Wassertiefe 125 m), Kern 178 von 1757 bis 3585 BP (23.76°S / 14.27°E; Wassertiefe 114 m), Kern 226620 (22.75°S / 14.31°E; Wassertiefe 81 m) deckt die längste Zeitspanne ab (879 bis 5610 BP), ist dabei aber auch am geringsten aufgelöst (s. Tabelle 4). Die Kerne entstammen allesamt dem organikreichen Diatomeenschlammgürtel (grau schattiert).

und einen nordwestwärts driftenden, ozeanischen Teilstrom (BOC; Benguela Oceanic Current) (Stramma und Peterson, 1989). Anders als andere küstennahe Auftriebsgebiete grenzt das Auftriebsgebiet beiderseits an Warmwasserregionen: den Angolastrom im Norden und den Agulhasstrom im Süden (Shannon und Nelson, 1996; Shannon und O'Toole, 1999). Der Angolastrom wird vom Südäquatorialen Gegenstrom (SECC; South Equatorial Countercurrent) gespeist. Er umfasst die oberen 200 m der Wassersäule und fliesst küsten-parallel bis auf die Höhe der Angola-Benguela-Front, wo er nach Westen abgelenkt wird (Moroshkin et al., 1970; Shannon und O'Toole, 1999). Den BCC ereilt von Süden her kommend das gleiche Schicksal (Stramma und Peterson, 1989) (Abb. 1).

Die Angola-Benguela-Front wandert saisonal zwischen 14° und 17° südlicher Breite. Ihre nördlichste Position erreicht sie gewöhnlich im Südwinter bzw. -frühjahr, wenn der Auftrieb im nördlichen Benguela am stärksten ist (September bis November) (Summerhayes et al., 1995; Shannon und Nelson, 1996). Im südlichen Benguela fällt die größte Intensität hingegen in das Südfrühjahr bzw. -sommer (Tomczak und Godfrey, 2003).

Ursache für den Auftrieb sind der Südostpassat und der entsprechend ablandige Ekman-Transport von Oberflächenwasser. Ein küstenwärts gerichteter Kompensationsstrom transportiert Zwischenwasser aus ungefähr 200 m Tiefe den namibischen Schelf hinauf (Calvert und Price, 1971; Mohrholz et al., 2008). Das Festland als Barriere, gelangt das nährstoffreiche Tiefenwasser in Küstennähe an die Überfläche, wo es die Grundlage für die hohe Primärproduktion bildet.

Das Auftriebswasser ist eine Mélange zweier zentraler Wassermassen, deren jeweiliger Anteil saisonal stark variiert (Mohrholz et al., 2008). Das Südatlantische Zentralwasser (SACW; South Atlantic Central Water) erhält seinen charakteristischen Fingerabdruck im Angola Dome (Abb. 1). Die lange Verweilzeit innerhalb dieses Wirbels führt infolge intensiven organischen Abbaus zu einer ebenso starken Anreicherung an Nährstoffen wie Verarmung an Sauerstoff. Der Angolastrom transportiert das SACW gen Süden. In den nördlichen Benguela gelangt es schließlich via eines Unterstroms, der die Angola-Benguela-Front über dem Schelf in mittleren bzw. bodennahen Tiefen durchbricht (Mohrholz et al., 2008).

Die zweite Wassermasse, Ost-Südatlantisches Zentralwasser (ESACW; East South Atlantic Central Water), stammt aus der Agulhas Retroflektion im Süden, wo dem Zentralwasser aus dem subtropischen Wirbel variable Mengen an warmem Agulhaswasser aus dem Indik beigemengt werden. Der Benguelastrom verfrachtet das ESACW entlang der Schelfkante gen Norden bis es sich vor der namibischen Küste mit dem hypoxischen SACW mischt (Gordon, 1986; Shannon und O'Toole, 2003; Mohrholz et al., 2008).

Der starke Einfluss von SACW auf den Sauerstoffhaushalt des nördlichen Benguela-Schelfs zeigt sich in der inversen Korrelation zwischen dem O_2-Gehalt und SACW-Anteil im Auftriebswasser (Mohrholz et al., 2008). Im Sommer ist der Anteil an SACW gegenüber dem an ESACW besonders groß und dementsprechend ausgeprägt ist die Sauerstoffarmut zu dieser Jahreszeit. Allerdings ist die Tendenz zum Sauerstoffmangel nicht allein dem O_2-armen SACW zuzuschreiben. Organischer Abbau (in der Wassersäule und am Ozeanboden) spielt eine zusätzliche Rolle. Remineralisation geht mit Sauerstoffzehrung einher und so ist das Ausmaß des Sauerstoffdefizits in tieferen Wasserschichten nicht bloß SACW, sondern auch der Primärproduktion direkt proportional (Chapman und Shannon, 1985; Codispoti und Christensen, 1985; Shannon und O'Toole, 1999; Tyrrell und Lucas, 2002; Gaye-Haake et al., 2005).

Sobald der Sauerstoffgehalt ein kritisches Level erreicht, setzt anaerober Abbau unter Bildung von Schwefelwasserstoff (H_2S) (Sulphatreduktion) ein (Shannon und O'Toole, 1999). Sulphatreduktion ist gegenüber Denitrifizierung (Nitratreduktion) zwar die energetisch ungünstigere, aufgrund des hohen Sulphatvorkommens dennoch die häufigere Form anaeroben Abbaus über dem zentralnamibischen Schelf (Tyrrell und Lucas, 2002). Zeitweise kommt es zu eruptivem Ausgasen großer Mengen an Methan (CH_4) und Schwefelwasserstoff (H_2S) aus den gasgesättigten Schelfsedimenten. H_2S führt zur Lähmung der intrazellulären Atmung und so haben die sogenannten *sulphur eruptions* Massensterben und die Abwanderung von wirtschaftlich bedeutenden Fischspezies zur Folge (Shannon und O'Toole, 1999; 2003; Bakun und Weeks, 2004; Brüchert et al., 2004; Emeis et al., 2004; Weeks et al., 2004). Nach Lavik et al. (2009) sind diese Ausgasereignisse die Ursache für den scheinbaren Widerspruch zwischen der hohen Primärproduktion und den unterdurch-schnittlichen Fangquoten.

Besonders ausgeprägt sind die Sauerstoffarmut und das Abwandern der Fischschwärme im Zuge sogenannter Benguela-Niños, während derer sich überdurchschnittlich große Mengen an warmem und O_2-armem Angolawasser über den nördlichen Benguela-Schelf ergießen. Benguela-Niños sind ein in dekadischen Abständen wiederkehrendes Phänomen, dem sich die Fischereiindustrie als zweitwichtigster Sektor der nami-bischen Wirtschaft (hinter Bergbau) gezwungenermaßen immer wieder aufs Neue stellt (van Zyl, 2010).

Weitere Merkmale von Benguela-Niños sind die Verlagerung der Angola-Benguela-Front nach Süden, eine dramatische Abschwächung des Auftriebs, ein Absinken der Thermokline sowie ungewöhnlich hohe Oberflächentemperaturen. Letztere bedingen zunehmende Verdunstungsraten und bescheren der Namibwüste ungewöhnlich hohe Niederschlagsmengen (Shannon et al., 1986; Shannon und O'Toole, 2003). Benguela-Niños sind schwächer und zudem seltener als ihr pazifisches Gegenstück, der El Niño vor Peru. Sie sind nicht notwendigerweise an ENSO (El Niño-Southern Oscillation) -Ereignisse gebunden und treten unabhängig von Schwankungen im Windsystem auf. Vielmehr scheinen sie mit Verlagerungen der Innertropischen Konvergenzzone im Zusammenhang zu stehen (Shannon et al., 1986).

Der namibische Schelf zählt zu den tiefsten und zugleich breitesten der Welt (Shannon, 1985). Im Untersuchungsgebiet liegt der Übergang zum Kontinentalhang in ca. 400 m Tiefe ungefähr 160 km von der Küste entfernt (Abb. 1). Eine zweite, wenngleich weniger markante Stufe in 100 km Entfernung zur Küste markiert die Grenze des inneren Schelf. Nach Smith (1995) fördern breite Schelfe die Ausbildung eines doppel-zelligen Auftriebsmusters. In der Tat bestätigen unsere Ergebnisse (Meisel et al., 2011 a; S. 51ff) frühere Studien, welche die Existenz einer zweiten, an die Schelfkante gebundenen Auftriebsfront nahelegen (Bang, 1971; Barange und Pillar, 1992; Summerhayes et al., 1995; Pichevin et al., 2005; Emeis et al., 2009).

Angesichts der hohen Primärproduktionsraten sind die Schelfsedimente vorwiegend biogener Natur. Der fluviatile und äolische Eintrag terrigener Partikel ist gegenüber der Masse an in-situ produziertem, organischem Material vernachlässigbar. Das Phytoplankton wird von Diatomeen dominiert und bis ungefähr 150 m Tiefe ist der Schelf von einem küstenparallel verlaufenden Diatomeenschlammgürtel bedeckt (Bremner und Willis, 1993). Gen Küste nimmt die Mächtigkeit der Ablagerungen auf über 10 m zu (Brüchert et al., 2004; Emeis et al., 2004). Lokale Variabilitäten sind auf die Morphologie des Basements zurückzuführen, das im Zuge der Holozänen Transgression überflutet wurde (Vogt, 2002). Im Mittel betragen die Sedimentations-raten 1mm/a (Bremner und Willis, 1993; Struck et al., 2002).

Nach Bremner und Willis (1993) zeichnen sich der äußere Schelf und obere Kontinentalhang durch eine kalkhaltigere Fazies aus (> 50wt% $CaCO_3$). Der abnehmende Opalanteil in Richtung Westen spiegelt die Abnahme der Diatomeenkonzentration von mehr als >10^6 Zellen/Liter in Küstennähe auf 10^2 Zellen/Liter über dem Kontinentalhang wider (Emeis et al., 2009).

3. Methoden und Proxies

Ein Proxy ist ein Indikator oder Ersatzmaß für ein nicht direkt erfassbares Phänomen oder eine nicht direkt erfassbare Größe. Unsere Untersuchungen basieren auf Temperatur- (UK'37-Index; $\delta^{18}O$), Nährstoff-($\delta^{15}N$, $\delta^{13}C$) und Produktivitätproxies (u.a. AR_{TOC}). Da die Arbeit mit stabilen Isotopen eine sehr zentrale Rolle einnimmt, vorweg ein kurzer Einblick in die theoretischen Grundlagen und Methodik.

3.1. Grundlagen zu der Arbeit mit stabilen Isotopen

Ein chemisches Element weist die gleiche Anzahl an Protonen wie Elektronen auf. Isotope sind Atome ein und desselben Elements, die sich hinsichtlich ihrer Anzahl an Neutronen und somit Massenzahl unterscheiden. Ihre chemischen Eigenschaften sind zwar identisch, aufgrund unterschiedlicher Massen weichen aber ihre physikalischen Eigenschaften voneinander ab. Der Massenunterschied hat sogenannte Isotopieeffekte zur Folge, die auf unterschiedlichen Bindungsenergien und Reaktionsgeschwindigkeiten beruhen. So steigen die Stärke kovalenter Bindungen und die Dissoziationsenergie mit der Atommasse, d.h. schwere Isotope bilden stärkere kovalente Bindungen. Molekülverbindungen, die das jeweils schwerere Isotop beinhalten, sind reaktionsträger und somit stabiler (Faure, 1992).

Natürlicherweise treten die stabilen Isotope eines Elements als Isotopengemisch auf. Isotopieeffekte können zu isotopischen Austauschreaktionen in chemischen und physikalischen Prozessen und einer messbaren Veränderung der Mischungsverhältnisse führen. Im Zuge einer solchen Fraktionierung kommt es zu einer relativen An- bzw. Abreicherung der jeweiligen Isotope, wobei das schwere Isotop die Verbindung mit der stärkeren chemischen Bindung generell bevorzugt (Bigeleisen, 1965). Oft ist das Ausmaß der Fraktionierung invers proportional der Temperatur (Faure, 1992).

Im Gegensatz zur Gleichgewichtsfraktionierung, die Hin- und Rückreaktion beinhaltet, sind kinetische Fraktionierungsprozesse entweder irreversibel (wie beispielsweise biologisch gesteuerte Prozesse) oder

Tabelle 1

Stabile Isotope von Stickstoff, Kohlenstoff und Sauerstoff, ihre Häufigkeiten und Darstellung als δ-Werte. [a)] nach Faure (1992).

Element	Stabile Isotope	mittlere Häufigkeit (%) [a)]	Isotopenverhältnis R	δ-Wert (‰)	Standard
Stickstoff	^{14}N	99.63	$^{15}N/^{14}N$	$\delta^{15}N$	AIR
	^{15}N	0.37			
Kohlenstoff	^{12}C	98.90	$^{13}C/^{12}C$	$\delta^{13}C$	VPDB
	^{13}C	1.10			
Sauerstoff	^{16}O	99.762	$^{18}O/^{16}O$	$\delta^{18}O$	VPDB; VSMOW
	^{17}O	0.038			
	^{18}O	0.200			

laufen unvollständig ab. In offenen Systemen wird die Rückreaktion häufig dadurch unterbunden, dass das Reaktionsprodukt entfernt wird (z.B. Evaporation von Wasser) (Faure, 1992).

Die Existenz von Isotopieeffekten innerhalb leichter Elemente wurde erstmals 1925 von H. Briscoe und P. Robinson vermutet. H. Urey hat die Forschung Mitte der 40er Jahre weiter vorangetrieben. Er erkannte ihr Potential hinsichtlich geochemischer Fragestellungen und lenkte die Arbeit mit stabilen Isotopen in seine heutigen Bahnen (Sharp, 2006).

Das Isotopenverhältnis einer Probe (R_P) wird mittels Massenspektrometrie bestimmt, mit dem eines Standards (R_{Std}) verglichen und als Abweichung in Promille (‰) dargestellt.

$$\delta\text{-Wert} = \frac{R_P - R_{Std}}{R_{Std}} \times 10^3 \qquad\qquad R = \frac{\text{schweres Isotop}}{\text{leichtes Isotop}}$$

Ein positiver δ-Wert zeugt von einer Anreicherung, ein negativer δ-Wert von einer Abreicherung des schweren Isotops relativ zum Standard. Der Standard dient als Referenz und vereinfacht den Vergleich der Isotopenverhältnisse verschiedener Substanzen untereinander. VPDB (Vienna Belemnite of the PeeDee Formation) ist ein internationaler Standard für Kohlenstoffisotope, VPDB und VSMOW (Vienna Standard Mean Ocean Water) für Sauerstoffisotope, für Stickstoff wird molekularer Luftstickstoff (N_2), AIR, als Referenz herangezogen (Tabelle 1).

3.2. Die Anwendung von $\delta^{15}N$- und $\delta^{13}C_{org}$-Signalen im Sediment und in partikulärem Material

Während der Assimilierung anorganischen Stickstoffs durch die Primärproduzenten wird ^{14}N gegenüber ^{15}N favorisiert. Infolge dessen wird der Stickstoffpool nicht nur sukzessive aufgebraucht, gleichzeitig wird das residuale Nitrat auch zunehmend „schwerer". Letzteres gilt ebenso für die Primärproduktion und entstehende Biomasse (Wada und Hattori, 1978; Wada, 1980, Montoya, 1994; Waser et al., 1998). Der Modellvorstellung zufolge findet in Auftriebsgebieten, wo der Nährstoffpool mitsamt des Oberflächenwassers lateral abtranspor-tiert wird, die als „Rayleigh-Fraktionierung" bezeichnete Anreicherung von ^{15}N entlang des Strömungspfades in Richtung Nordwesten statt (Montoya, 1994). Hinzugefügt werden muss, dass die Fraktionierung nur stattfindet, solange anorganischer Stickstoff ausreichend zur Verfügung steht (Ostrom und Macko, 1991; Francois et al., 1992; Altabet und Francois, 1994; Ostrom et al., 1997).

Dank der inversen Korrelation zwischen $\delta^{15}N$ und der Nitratkonzentration eignet sich sedimentäres $\delta^{15}N$-Signal zur Rekonstruktion zwar nicht des absoluten, wohl aber des relativen Stickstoffverbrauchs (Altabet et al., 1991; Montoya und McCarthy, 1995; Holmes et al., 1996); so können $\delta^{15}N$-Schwankungen sowohl auf Veränderungen der Nährstoffmengen als auch der Photosyntheseraten hindeuten.

Sedimentären $\delta^{13}C$-Signalen kommt in der Rekonstruktion der Paläoproduktivität und vergangener Nährstoffregimes eine ähnliche Rolle zu wie $\delta^{15}N$. Während der Assimilierung anorganischer Kohlenstoff-dioxidkomponenten (CO_2, HCO_3^-) durch das Phytoplankton werden analog zum Stickstoff die „leichten" Isotope den „schweren" vorgezogen. Dies hat eine ^{13}C-Anreicherung der DIC-Komponenten (dissolved inorganic carbon) im Oberflächenwasser zur Folge (Mulitza et al., 1999; Ganssen und Kroon, 2000).

In der Wassersäule und am Ozeanboden wird die in der photischen Zone produzierte, isotopisch „leichte" Biomasse abgebaut. Die Nährstoffe werden wieder freigesetzt und gelangen mit dem Auftriebswasser zurück an die Oberfläche, wo sie erneut assimiliert werden. Nährstoffreichtum hat hohe Photosyntheseraten zur Folge und äußert sich typischerweise in niedrigeren $\delta^{15}N$-Werten (geringer relativer Nitratverbrauch) bei

gleichzeitig hohen Akkumulationsraten von organischen Material (AR_{TOC}) (Holmes et al., 1999). Anders verhält sich dabei häufig das $\delta^{13}C$-Signal. Oft gehen hohe AR_{TOC} mit niedrigen $\delta^{15}N$-, aber hohen $\delta^{13}C$-Werten einher (Ostrom et al., 1997); dies obwohl $\delta^{13}C$ genauso wie $\delta^{15}N$ invers mit der Nährstoffkonzentration korreliert (Mulitza et al., 1999; Ganssen und Kroon, 2000). Solch entgegengesetzte Entwicklung von $\delta^{13}C$ und $\delta^{15}N$ zeigt sich auch in unseren Daten (z.B. Meisel et al., 2011 b; S. 79, Fig. 3, 3600 und 3400 BP, core 178). Sie ist darauf zurückzuführen, dass das Ausmaß der Fraktionierung mit der Verfügbarkeit der Nährstoffe sinkt und Nitrat, im Gegensatz zu DIC, häufig nur in geringen Mengen vorhanden ist (Montoya, 1994; Ostrom et al., 1997). Dies hat zur Folge, dass der Nitratpool anders als der DIC-Pool bereits maximal an „schweren" Isotopen angereichert ist. Verstärkter Auftrieb von frischem, NO_3^--reichem Bodenwasser und ein resultierender Anstieg der Primärproduktion äußert sich folglich in zunehmenden $\delta^{13}C$-Werten (Zunahme des relativen DIC-Verbrauchs) bei gleichzeitig sinkenden $\delta^{15}N$-Signalen im Primärprodukt (Abnahme des relativen Nitrat-verbrauchs; NB: Allerdings nimmt der relative Nitratverbrauch nur ab, solange der Anstieg der Primär-produktion die Zufuhr von Nitrat nicht übersteigt).

Wie die sprunghafte Zunahme an Publikationen zeigt, hat die Anwendung stabiler Stickstoffisotope zu Beginn der 90er Jahre enorm an Popularität gewonnen (s. ISI-Science Citation Index; Suchbegriff „nitrogen isotopes"). Zu dieser Zeit wurden erstmals $\delta^{15}N$-Signale in Tiefseesedimenten mit der Nährstoffdynamik in Zusammenhang gebracht (Calvert et al., 1992; Francois et al., 1992; Altabet et al., 1994, 1995; Montoya, 1994). Jüngere Studien aus der Ostsee (Struck et al., 2000, 2004), dem Mittelmeer (Struck et al., 2001) und küstennahen Auftriebsgebieten (Libes und Deuser, 1988; Holmes et al., 1999, 2002; Struck et al., 2002) bestätigen den hohen Nutzen der Stickstoffisotopie in paläoozeanographischen Fragestellungen.

Aufgrund der Vielzahl biochemischer Reaktionspfade ist der Stickstoffkreislauf allerdings um einiges komplexer als der Kohlenstoffkreislauf (Montoya, 1994). Neben Assimilation durch Primärproduzenten gibt es eine Reihe weiterer N-relevanter Prozesse wie Nitrifizierung, Remineralisation, Annamox (anaerobe Ammonium-Oxidation; Kuypers et al., 2005), Sulfid-Oxidation mit Nitrat als Oxidationsmittel (Lavik et al., 2009), N_2-Fixierung und Denitrifizierung; ihre jeweilige Auswirkung auf die $\delta^{15}N$-Signatur von Ammonium und Nitrat ist nicht immer hinreichend geklärt. Obwohl dies Unsicherheiten mit sich bringt, lassen sich andererseits oft nützliche Informationen hinsichtlich der Nährstoffsituation ableiten.

Von Denitrifizierung (Nitratreduktion) weiß man, dass sie die Isotopensignatur von Nitrat erheblich zu beeinträchtigen vermag. Denitrifizierung ist ein anaerober Abbaupfad, im Zuge dessen NO_3^- die Rolle als Elektronenakzeptor (Oxidationsmittel) übernimmt sobald der Sauerstoffgehalt 0.2 ml/l unterschreitet. Aufgrund der Vorliebe denitrifizierender Mikroorganismen für ^{14}N-NO_3^- erhöht sich das Isotopensignal im residualen Nitratpool sukzessive um mehrere Promille (Cline und Kaplan, 1975).

In Auftriebsgebieten ist Denitrifizierung ein häufiges Phänomen. Dies ist auf die hohe Primärproduktion und entsprechend vermehrten Sauerstoffbedarf durch organischen Abbau zurückzuführen (Libes und Deuser, 1988; Tyrrel und Lucas, 2002). Die Anwendbarkeit von $\delta^{15}N$ als Indikator für relativen Nährstoffverbrauch wird durch Denitrifizierung enorm in Mitleidenschaft gezogen. Eine korrekte Interpretation von $\delta^{15}N_{Sediment}$-Schwankungen verlangt deshalb neben Photosyntheseraten und Nährstoffzufuhr die Berücksichtigung veränderter Durch-lüftung des Bodenwassers.

Qualität und Nutzen der Isotopensignale in Kernsedimenten hängen sehr vom verlässlichen Transfer des Ursprungsignals zum Ablagerungsort ab (Thornton und McManus, 1994). In der Vergangenheit wurde der Einfluss mikrobiellen Abbaus auf die Isotopensignatur organischen Materials bereits rege und nicht selten widersprüchlich diskutiert. Am weitesten verbreitet scheint die Auffassung, dass Remineralisation von einer Diskriminierung gegenüber ^{15}N begleitet wird und demzufolge einen Anstieg der $\delta^{15}N$-Werte im Residual mit sich bringt (Saino und Hattori, 1980; Altabet, 1988; Altabet et al., 1991; Fry et al., 1991; Schäfer und Ittek-kot, 1993; Altabet und Francois, 1994; Ostrom et al., 1997; Sachs und Repeta, 1999; Freudenthal et al., 2001). Allerdings kommen andere Studien zu entgegengesetzten Ergebnissen (Wada, 1980; Holmes et al., 1999; Lehmann et al., 2002). Dies mag an der Art des untersuchten Materials liegen und daran, dass unterschiedliche Fraktionen organischen Materials mit jeweils individueller Isotopensignatur verschieden anfällig auf Abbau-prozesse reagieren (e.g. Harvey et al., 1995). Ob der Abbau unter oxischen oder anoxischen Bedingungen stattfindet, scheint ein weiteres Kriterium für die Fraktionierungsrichtung zu sein (Lehmann et al., 2002; Gaye-Haake et al., 2005), wobei der Abbau unter Sauerstoffarmut die Erhaltung des Ursprungsignals generell begünstigt (Altabet et al., 1999; Sachs und Repeta, 1999; Lehmann et al., 2002).

Wie unsere Untersuchungen zeigen, findet der $\delta^{15}N$-Anstieg im organikreichen Diatomeenschlamm nur scheinbar während des Abbaus selbst statt, ist in Wirklichkeit aber auf das Ausgasen isotopisch leichten NH_3 (Ammoniak) zurückzuführen (Kapitel 4.1.; Meisel und Struck, 2011; S. 37ff). NH_4^+ (Ammonium) ist ein

Produkt organischen Abbaus. Beim Übergang in gasförmiges NH_3 während des Trocknens verbleibt ^{15}N-NH_4^+ bevorzugt in Lösung, was den beobachteten Anstieg der $\delta^{15}N$-Werte zur Folge hat. In gespültem Sediment (unabhängig davon, ob vorher gesäuert wurde oder nicht) ist die ausgasungsbedingte Erhöhung des $\delta^{15}N$-Signals beseitigt und man kommt der Realität vermutlich sehr nahe, $\delta^{15}N$-Schwankungen lediglich vor dem Hintergrund veränderten Nährstoffverbrauchs und Denitrifizierung zu interpretieren (Meisel und Struck, 2011; S. 37ff).

3.3. Temperaturrekonstruktion mittels der Karbonat- und Alkenon-Paläothermometrie

Zur Rekonstruktion der Paläotemperaturen in mittleren Wassertiefen machen wir uns die $\delta^{18}O$-Signale im Schalenkalzit ($\delta^{18}O_{calcite}$) der planktischen Foraminifere *O. universa* zunutze. Foraminiferen sind Einzeller und werden der Gruppe der Rhizaria zugeordnet. Zum Aufbau ihrer Karbonatgehäuse verwenden sie im Meerwasser gelöstes CO_2 (Wefer und Berger, 1991; Niebler et al., 1999).
Die Nutzung der temperaturabhängigen Fraktionierung der Sauerstoffisotope zwischen Wasser und CO_2 geht auf Harold Urey zurück (Urey, 1947, 1948; Urey et al., 1951). Bei der Lösung von CO_2 im Meerwasser reichert sich CO_2 gegenüber H_2O in ^{18}O an. Aufgrund dessen ist Karbonat isotopisch „schwerer" als jenes Wasser, aus dem es ausfällt. Das Ausmaß der Fraktionierung ist umgekehrt proportional der Temperatur (s. Kapitel 3.1.), d.h. je geringer die Umgebungstemperatur, desto „schwerer" der Schalenkalzit (Niebler et al., 1999). Das $\delta^{18}O$-Signal des Meerwassers kann für den untersuchten Zeitraum als konstant betrachtet werden (Meisel et al., 2011 b); somit deuten $\delta^{18}O$-Schwankungen alleinig auf veränderte Umgebungstemperaturen ($T_{\delta18O}$) hin.
O. universa bewohnt, wie andere planktonische Foraminiferen auch, kein bevorzugtes Tiefenhabitat, sondern passt sich den für die jeweilige Wassermasse typischen Bedingungen an (Ravelo und Fairbanks, 1992; Hemleben und Bijma,1994; Tedesco et al., 2007). Grob reicht die Kalzifizierungstiefe von der Thermokline hinab in die durchmischte Schicht. An die Verfügbarkeit von Nährstoffen oder den Mondzyklus gebundene Schwankungen führen zu einer relativ starken Streuung des $T_{\delta18O}$-Signals. Von diesem Hintergrundrauschen abgesehen, werden $T_{\delta18O}$-Schwankungen entweder auf variable Intensität wind- und welleninduzierter Durchmischung der oberen Wassersäule oder Temperaturschwankungen im Auftriebswassers zurückgeführt.

Der Alkenon-Untersättigung-Index (UK'37-Index) stellt ein weiteres Paläothermometer dar. Anders als *O. universa*-$\delta^{18}O_{calcite}$ dienen Alkenone aber der Rekonstruktion der Oberflächentemperatur (SST; sea surface temperature). Alkenone sind langkettige, unverzweigte und ungesättigte C37-C39 Methyl- und Ethylketone. Sie werden bei der Photosynthese von in obersten Wasserschichten lebenden Coccolithophoriden, darunter v.a. Emiliania huxleyi, gebildet (Emeis et al., 2009).
SST-Variationen zeugen von schwankender Auftriebsintensität und erlauben Rückschlüsse auf die Stärke der Passatwinde. Einschränkend sei bemerkt, dass sich Temperaturschwankungen des Auftriebswassers auch im SST-Datensatz niederschlagen und es deshalb nicht immer einfach ist, zwischen Auftriebswasser- und windbedingten SST-Variationen zu unterscheiden.
Die Differenz zwischen SST und $T_{\delta18O}$ (ΔT) spiegelt die Stratifizierung der oberen Wassersäule wider. Eine Abnahme von ΔT wird entweder durch verstärkten Auftrieb oder tieferes Eindringen wind- und welleninduzierter Durchmischung verursacht.

3.4. Primärproduktionsraten

Die Höhe der Primärproduktion liefert indirekt Hinweise auf die Nährstoffsituation, dies wiederum auf die Auftriebsintensität und die Windbedingungen. In Oberflächensedimenten ist die räumliche Variabilität der Produktivität im Anteil organischen Kohlenstoffs (TOC, total organic carbon) überliefert. Der Vergleich mit Konzentrationen partikulären, organischen Materials (PN- und POC-Konzentrationen; particulate nitrogen, particulate organic carbon) an der Meeresoberfläche soll klären, ob ursprüngliche Produktivitätsgradienten mikrobiellen Abbaus zum Trotz erhalten bleiben (Meisel et al., 2011 a; Seite 51ff). Zu beachten ist, dass variable Anteile anderer Komponenten (z.B. Diatomeen- oder Karbonatschalen) eine scheinbare An- bzw. Abreicherung an TOC zur Folge haben können. Sedimentäre TOC-Konzentrationen stellen somit keine absolute Messgröße dar, weswegen der relativ große Schwankungsbereich nicht überinterpretiert werden sollte. In Kernsedimenten wird dieser Verdünnungseffekt durch die Angabe von Akkumulationsraten (AR_{TOC}) umgangen (Meisel et al., 2011 b; Seite 71ff).

4. Kurzfassung der Publikationen

4.1. Der störende Einfluss von NH_4^+ auf sedimentäre $\delta^{15}N$-Signale und C_{org}/N-Verhältnisse und die Rolle der Probenaufbereitung (Meisel und Struck, 2011; Seite 37ff)

4.1.1. Fragestellung und Zielsetzung

Aufgrund der zentralen Rolle von $\delta^{15}N$ in unseren Untersuchungen war es uns ein Anliegen, den Einfluss unterschiedlicher Probenaufbereitung auf die Stickstoffisotopensignatur im Diatomeenschlamm zu prüfen. Das Wissen um die Anfälligkeit des ursprünglichen $\delta^{15}N_{Sediment}$-Signals auf verschiedene Aufbereitungsarten bildet die Grundlage einer korrekten Interpretation. Welches der $\delta^{15}N_{Sediment}$-Signale verdient aber die Bezeichnung „ursprünglich"?

Hinsichtlich dieser Frage stellt Kern 180 ein dankbares Versuchsobjekt dar. Kern 180 zeichnet sich durch eine ausgeprägte Homogenität aus. Das Fehlen jeglicher Laminierung wird auf eruptive Ausgas-Ereignisse (*sulphur eruptions*; Kapitel 2) zurückgeführt, im Zuge derer die ursprüngliche Schichtung zerstört wurde. Aufgrund der natürlichen Durchmischung gingen wir von einem möglichst geradlinigen $\delta^{15}N$-Verlauf entlang des Kernprofils und – wenn überhaupt – nur geringfügigen Schwankungen aus. Wie sich zeigte, wurden nicht alle Messreihen dieser Erwartung gerecht.

Die Anfälligkeit von $\delta^{15}N$ auf die Probenaufbereitung wurde anhand verschiedenster Probenmaterialien (Algen, Cyanobakterien, Seegras, Sediment, Gewebe von Fischen und Mollusken) bereits vielfältig diskutiert. Dabei führte die Frage, welche Form der Aufbereitung das verlässlichste Signal liefert, zu teils widersprüchlichen Ergebnissen (Bunn et al., 1995; Holmes et al., 1999; Kennedy et al., 2005; Carabel et al., 2006; Ng et al., 2007).

Beispielsweise wird das Waschen der Proben mit destilliertem Wasser häufig angewandt, um Säurereste zu entfernen (Stoner und Zimmerman, 1988; Kang et al., 2003). Aufgrund des möglichen Verlusts organischen Materials raten einige Autoren allerdings vehement davon ab (Nieuwenhuize et al., 1994; Bunn et al., 1995; Jacob et al., 2005; Carabel et al., 2006). Andere Studien zeigen, dass das Entfernen von Karbonat durch Säuern nicht nur $\delta^{13}C$ verändert, sondern auch Spuren im $\delta^{15}N$-Signal hinterlässt (Bunn et al., 1995; Jacob et al., 2005; Carabel et al., 2006; Ng et al., 2007). Aus diesem Grund verzichten viele auf das Säuern und geben unbehandeltem Sediment für $\delta^{15}N$-Messungen den Vorrang (Goering et al., 1990; Thornton und McManus, 1994; Bunn et al., 1995; Bouillon et al., 2002; Carabel et al., 2006). Wie unsere Ergebnisse allerdings eindeutig belegen, ist weder a priori von Spülen abzuraten, noch das Verwenden unbehandelten Materials uneingeschränkt zu empfehlen.

Bereits an dieser sei Stelle vermerkt, dass sich im Laufe der Untersuchungen die Gegenwart von Ammonium (NH_4^+) als die Kernursache für irreführende Shifts im $\delta^{15}N$-Signal herauskristallisierte. Dies hat zur Folge, dass die C_{org}/N-Verhältnisse gleichermaßen betroffen und Inhalt der Untersuchungen sind.

4.1.2. Material

Kern 180 besteht aus organikreichem Diatommenschlamm und entstammt dem inneren, zentral-namibischen Schelf (Abb. 1). Seine Länge beträgt 5 m, der durchschnittliche Anteil an organischem Kohlenstoff (C_{org}) 5.5 %. Dem Kern wurden insgesamt 100 Spritzenproben entnommen. Diese wurden bei 40°C getrocknet und gemörsert. Mit dem Ziel, an jeder der Proben vier verschiedene Messserien (MS) auszuführen, wurde – wie aus Abb. 2 ersichtlich – jede Probe geviertelt. Der ersten Messreihe (MS-1) liegt unbehandeltes Sediment zugrunde, die übrigen drei Teilproben wurden vor der Messung einer jeweils individuellen Aufbereitung unterzogen:

Für MS-2 wurde das Material mit destilliertem Wasser gewaschen und erneut getrocknet. Für MS-3 wurde das Sediment nach Hinzufügen von 2N HCL mit destilliertem Wasser gewaschen und ebenfalls erneut getrocknet. MS-4 basiert auf in-situ Azidifizierung unter Verzicht auf den Spülvorgang. Das Hinzufügen von Säure in MS-3 und MS-4 dient dem Entfernen vorhandenen Karbonats und der Bestimmung von C_{org}. Anschließendes Trocknen bei 40°C gewährleistet die Eliminierung von Säureresten durch Verdampfen.

Nach entsprechender Aufbereitung wurden die Proben zur Messung der Stickstoffisotopenverhältnisse ($\delta^{15}N$) sowie der Elementkonzentrationen von Kohlenstoff und Stickstoff in ein Massenspektrometer überführt.

Unabhängig davon wurde das Waschwasser von MS-2 und MS-3 auf NH_4^+-Gehalte untersucht (mittels des 'LCK 303 Ammonium Cuvette Test' von Hach-Lange; http://www.hach-lange.co.uk). Eine Zusammenfassung der untersuchten Parameter findet sich in Tabelle 2.

Tabelle 2

Untersuchte Parameter und Anzahl an Daten. NB: MS-1 und MS-2 geben aufgrund fehlenden Säuerns bloß Aufschluß über den Gesamtkohlenstoffanteil (TC; total carbon), nicht aber C_{org}. Deswegen müssen $[C_{org}/N]_{untreated}$ (MS-1) und $[C_{org}/N]_{H2O}$ (MS-2) indirekt bestimmt werden (Näheres hierzu in Meisel und Struck, 2011; S. 37ff). Es sei außerdem darauf hingewiesen, dass MS-2 nur ein Teil der Proben unterzogen wurde (n = 22).

	TC (%)	C_{org} (%)	N (%)	C_{org}/N	$\delta^{15}N$ (‰)	NH_4^+ im Spülwasser
MS-1	100		98	97	100	
MS-2	22		22	21	22	22
MS-3		100	100	100	100	22
MS-4		98	100	98	100	
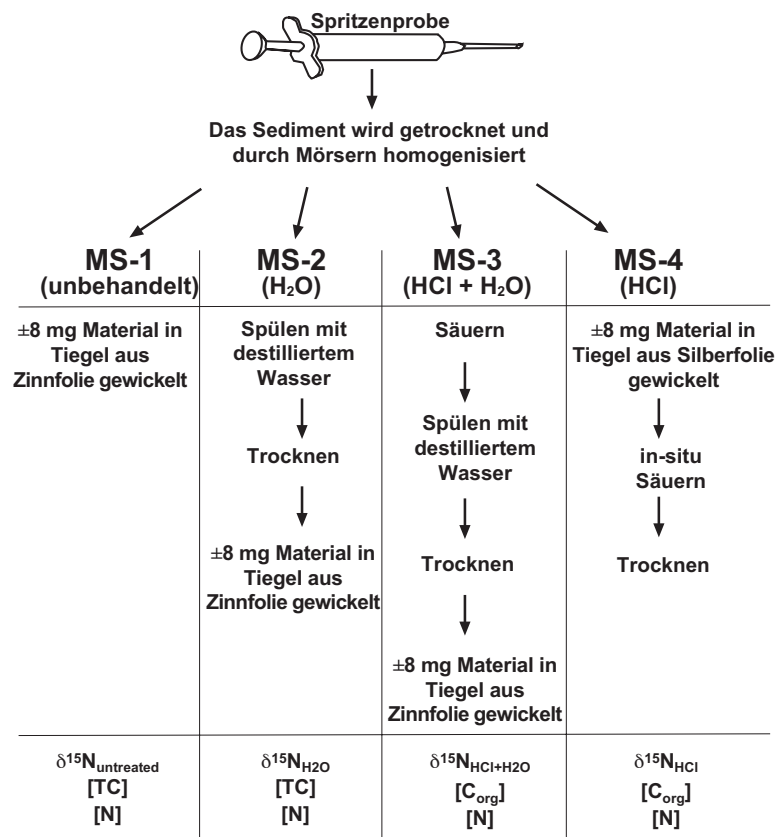
Abb. 2. Die einzelnen Messserien (MS) im Überblick. MS-1 und MS-2 liefern den Gesamtkohlenstoffanteil (TC, total carbon). MS-3 und MS-4 geben infolge des Säuerns Aufschluss über den Anteil an organischem Kohlenstoff (C_{org}).

4.1.3. Ergebnisse und Interpretation

Untersucht wurde die Anfälligkeit von C_{org}/N und $\delta^{15}N$ in organikreichen, anoxischen Sedimenten auf gängige Arten der Probenaufbereitung. Motivation der Arbeit war die Frage, welche der Messreihen dem Originalsignal am nächsten kommt und demzufolge die geeignetste Grundlage für paläoklimatische Studien im nördlichen Benguela darstellt.

Wie unsere Daten zeigen, bringt der Waschvorgang sowohl große Verluste an NH_4^+ (nicht gezeigt) als auch substanzielle Veränderungen der $\delta^{15}N$-Signatur mit sich (Abb. 3). Beide Beobachtungen gelten gleichermaßen für MS-2 wie MS-3, also unabhängig davon, ob zusätzlich gesäuert wurde oder nicht. Die C_{org}/N-Verhältnisse reagieren stattdessen nur infolge einer Kombination aus Säuern und anschließendem Waschen (MS-3) (Abb. 4).

Unserer Theorie zufolge sind die teils dramatischen Unterschiede in den Kurvenverläufen von C_{org}/N und $\delta^{15}N$ auf Ammonium zurückzuführen (NB: NH_4^+ entsteht im Zuge organischen Abbaus):

(i) Während des Trocknens kommt es zum Verlust von NH_4^+-N in Form von gasförmigem NH_3. Dabei scheint ^{14}N gegenüber ^{15}N den Übergang in die Gasphase zu bevorzugen. Dies hat sowohl höhere C_{org}/N als auch $\delta^{15}N$-Signale in unbehandeltem Sediment (MS-1) zur Folge .

(ii) Adsorbierte NH_4^+-Ionen (s.u.) scheinen dem Ausgasen und somit der Fraktionierung gegenüber immun. Je größer der Anteil unadsorbierter, also gelöster NH_4^+-Ionen, umso ausgeprägter demzufolge der Shift zu höheren C_{org}/N und $\delta^{15}N$-Werten.
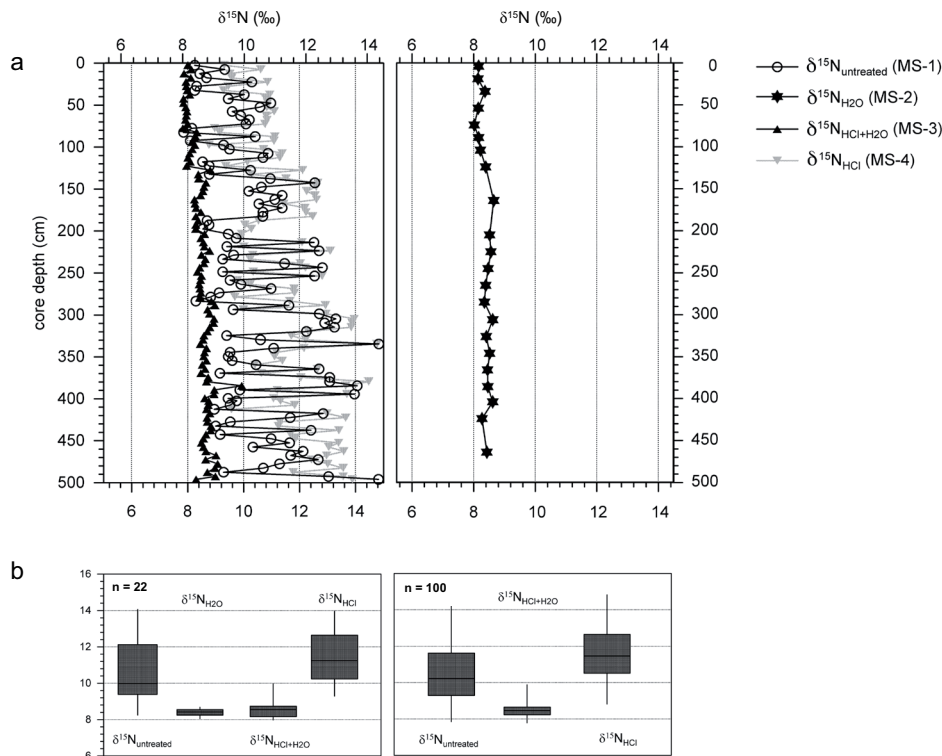
Abb. 3. (a) Der Verlauf von $\delta^{15}N$ im Kernprofil. Aus Gründen der Übersichtlichkeit wird $\delta^{15}N_{H2O}$ (MS-2) separat gezeigt. (b) $\delta^{15}N$-Boxplots. Zur besseren Vergleichbarkeit von MS-2 mit den übrigen Messreihen basieren alle Boxplots zur Linken auf derselben Auswahl an Proben, die MS-2 unterzogen wurden.
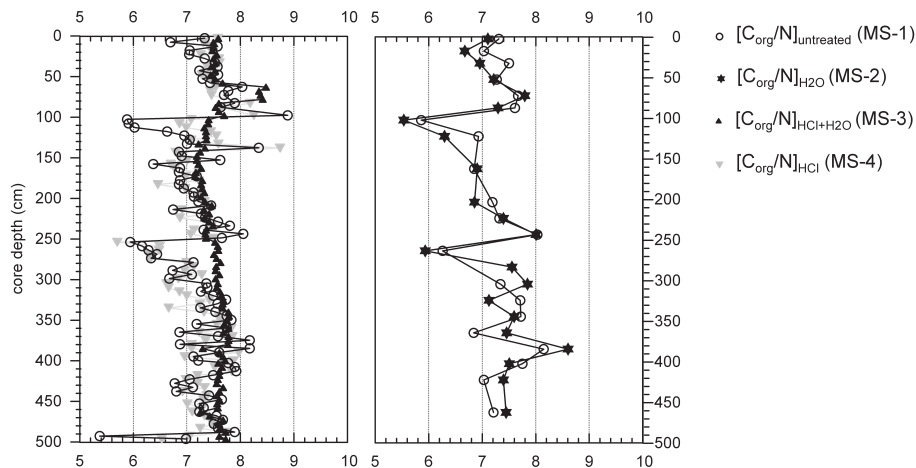
Abb. 4. Der Verlauf von C_{org}/N im Kernprofil. Das Diagramm zur Rechten zeigt $[C_{org}/N]_{H2O}$ (MS-2) nebst entsprechenden $[C_{org}/N]_{untreated}$-Daten und legt die enorme Ähnlichkeit beider Datensätze offen.
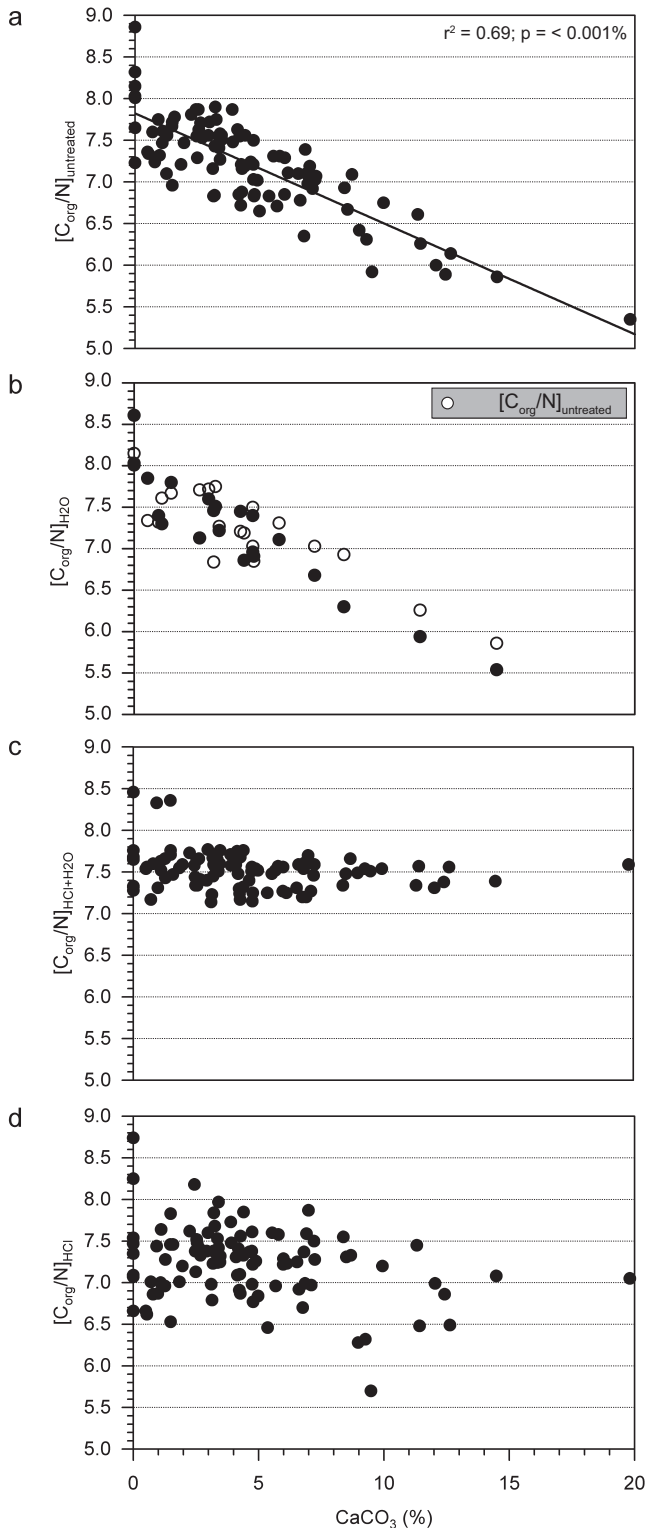
Abb. 5. C_{org}/N vs. $[CaCO_3]$: Mit der Zunahme des Karbonatanteils (und infolgedessen pH-Werts des Interstitialwassers) steigt die negative Oberflächenladung von SiO_2 und somit die Zahl adsorbierter NH_4^+-Ionen. Dies erklärt die inverse Korrelation zwischen C_{org}/N und $[CaCO_3]$ in MS-1 (a). Säuern wirkt der NH_4^+-Adsorbtion entgegen. Anders als in MS-3 (c) werden die im Interstitialwasser gelösten NH_4^+-Ionen im Zuge der Aufbereitung für MS-4 aber nicht fortgespült (d). Stattdessen wird davon ausgegangen, dass einige der ehemals adsorbierten NH_4^+-Ionen während des Trocknens über die Gasphase (NH_3) entweichen. Das Ausgasen wird als der Grund für die Störung der ursprünglich inversen Korrelation angesehen.

Wie im folgenden ausgeführt scheint die Menge adsorbierter NH_4^+-Ionen vom pH-Wert des Porenwassers abhängig, der pH-Wert selbst wiederum vom Karbonatanteil im Sediment. Aufgrund der alkalischen Wirkung des Karbonat-Ions (CO_3^{2-}) steigt der pH-Wert des Interstitialwassers, sobald Karbonat in Lösung geht (Faure, 1992).

$$CaCO_3 + H_2O \longleftrightarrow Ca^{2+} + CO_3^{2-} + H_2O$$

$$CO_3^{2-} + H_2O \longleftrightarrow HCO_3^- + OH^-$$

Ein Anstieg des pH erhöht die negative Oberflächenspannung und somit Adsorptionskapazität von SiO_2 (präsent in Form von Diatomeenschalen) (Brunelle, 1978). Unserer Theorie zufolge führt die pH-abhängige Polarisierung von SiO_2 und Adsorption von NH_4^+-Kationen zu der negativen Korrelation zwischen C_{org}/N und $[CaCO_3]$ in MS-1 (Abb. 5a).

Wie bereits aus Abb. 4 ersichtlich, ist der Einfluss von Säuern und Waschen (MS-3) auf C_{org}/N beachtlich. Gleiches zeigt Abb. 5, wo die ursprünglich so klare Korrelation zwischen C_{org}/N und $[CaCO_3]$ infolge Säuerns und Waschens komplett ausradiert ist (Abb. 5c).

Was aber geschieht im Zuge der Probenaufbereitung für MS-3? Das Säuern bewirkt eine pH-Erniedrigung im Interstitialwasser. Die negative Oberflächenspannung von SiO_2 nimmt ab, und ehemals adsorbierte NH_4^+-Ionen werden mitsamt des Karbonats im Waschwasser fortgespült. Ein Anstieg von C_{org}/N ist die Folge.

Das Beisein von Ammonium erweist sich augenscheinlich als hoch problematisch. Da organikreiche und anoxische Sedimente das Vorkommen von NH_4^+ begünstigen, empfiehlt es sich entgegen weitläufiger Empfehlung (Kapitel 4.1.1.), von der Verwendung unbehandelten Diatomeenschlamms (MS-1) abzusehen. MS-1 täuscht Fluktuationen von $\delta^{15}N$ und C_{org}/N vor, die – statt von veränderten Umweltbedingungen zu zeugen – auf unkontrolliertes und variables Ausgasen von NH_3 zurückzuführen sind. In MS-3 scheint der irreführende Einfluss von NH_4^+ auf $\delta^{15}N$ und C_{org}/N beseitigt. Das Säuern und anschließende Spülen mobilisiert neben adsorbiertem NH_4^+ ebenso das an ^{15}N angereicherte, gelöste NH_4^+. Außerdem passt der geradlinige Verlauf von $[C_{org}/N]_{HCl+H2O}$ und $\delta^{15}N_{HCl+H2O}$ zum erwähnten Homogenisierungsszenario, was die Glaubwürdigkeit von MS-3 und Richtigkeit unserer Gedankenstränge zusätzlich bestätigt.

4.2. Nährstoffregime und ozeanographische Charakteristika im zentralnamibischen Auftrieb, abgebildet in $\delta^{15}N$-Signalen von suspendiertem Material und Oberflächensedimenten (Meisel et al., 2011 a; Seite 51ff)

4.2.1. Fragestellung und Zielsetzung

Dieser Teil der Arbeit befasst sich mit der Rezentsituation im zentralnamibischen Auftrieb und basiert in erster Linie auf dem Vergleich von $\delta^{15}N$-Signalen in partikulärem Material des Oberflächenwassers ($\delta^{15}N_{SPM}$) mit dem darunterliegenden Sediment ($\delta^{15}N_{Sediment}$). Wassersäulenprofile sollen zudem Aufschluss über Veränderungen des $\delta^{15}N_{SPM}$-Signals mit zunehmender Tiefe geben und mögliche Offsets zwischen $\delta^{15}N_{SPM}$ und $\delta^{15}N_{Sediment}$ erklären. Im Mittelpunkt stehen folgende Fragen: Welche nährstoffrelevanten bzw. ozeanographischen Prozesse verursachen die Trends von $\delta^{15}N_{SPM}$ im Oberflächenwasser und entlang der Wassersäule? Zweitens, inwieweit repräsentiert $\delta^{15}N_{Sediment}$ ein verlässliches Abbild pelagialer Prozesse zu Zeiten, da der direkte Einblick in die Wassersäule fehlt?

4.2.2. Material

Die Probenpalette setzt sich aus (i) hydrographischen Messungen, (ii) suspendiertem partikulärem Material (SPM) sowie (iii) Oberflächensedimenten (0 - 1 cm) zusammen. Eine übersichtliche Auflistung der Parameter inklusive Anzahl der Messungen (=n) findet sich in Tabelle 3. Von der Mehrzahl der TOC-Daten abgesehen, wurden die Sedimentdaten bereits anderorts publiziert (s. Tabelle 3). Ein erneutes Veröffentlichen ist dennoch gerechtfertigt, denn vom Vergleich mit SPM erwarten wir wertvolle Einblicke in die Anwendbarkeit sedimentärer $\delta^{15}N$-Signale in Paläountersuchungen. Eine derartige Gegenüberstellung ist für den nördlichen Benguela-Schelf bislang einzigartig.

Die $\delta^{15}N_{SPM}$-Werte basieren auf gesäuertem Probenmaterial. Spülen ist hier ausgeschlossen, da die Messung von SPM an Filterpapier vorgenommen wurde. Delta$^{15}N_{Sediment}$ wurde an unbehandeltem Material gemessen (Pichevin, 2005; Emeis et al., 2009 zzgl. dortiger Ref.). Wegen fehlenden Spülens muss sowohl für $\delta^{15}N_{Sediment}$ als auch $\delta^{15}N_{SPM}$ davon ausgegangen werden, dass NH_4^+ bzw. das Ausgasen in Form von NH_3 indirekt abbaubedingte Spuren im $\delta^{15}N$-Signal hinterlässt (Meisel und Struck, 2011; s. Kapitel 3.2. und 4.1.). Für weitere Informationen hinsichtlich der Probennahme und -aufbereitung sei auf die eigentliche Publikation verwiesen.

4.2.3. Ergebnisse und Interpretation

Der Theorie zufolge sind in Auftriebsgebieten der Nitratgehalt und $\delta^{15}N$ entlang des Strömungspfades invers korreliert (s. Kapitel 3.2.). Wie eine Reihe von Studien belegt, scheint dieses Modell die Prozesse westlich des kontinentalen Schelfs auch recht genau zu beschreiben (Conkright et al., 1998; Holmes et al., 1998, 1999, 2003). Auf küstennähere Gewässer lässt es sich hingegen nicht übertragen. Wie Oberflächenwasser-SPM und Sediment gleichermaßen zeigen, verhält sich $\delta^{15}N$ dort genau entgegengesetzt der Theorie. Auf dem ca. 160 km langen Weg über den zentralnamibischen Schelf sinkt $\delta^{15}N_{SPM}$ von ±10‰ in Küstennähe auf ±4‰ über der Schelfkante ($\delta^{15}N_{Sediment}$ verläuft etwas flacher; Abb. 6). Hier kommt es zur Trendwende und entsprechend dem „normalen" Verlauf steigen die $\delta^{15}N$-Werte nun gen Westen.

Das küstennahe $\delta^{15}N$-Maximum wird auf den Auftrieb denitrifizierten Nitrats zurückgeführt. Hohe Akkumulations- bzw. Produktivitätsraten (ersichtlich aus PN, POC und sedimentärem TOC) und geringe O_2-Konzentrationen im Bodenwasser stützen diese Annahme. Dennoch, die westwärtige Abnahme der $\delta^{15}N$-

Tabelle 3

Probenmaterial und jeweilige Proxies. Referenzen für die Sedimentdaten sind wie folgt: [a] Emeis et al. (2009) und Pichevin et al. (2005); [b] Emeis et al. (2009); [c] Mollenhauer et al. (2002). Bislang unpublizierte sedimentäre TOC-Daten stammen von der METEOR M48-2 Fahrt (August 2000) und der POS 250 Expedition (April 1999).

Hydrographische Messungen		SPM		Oberflächensedimente	
Oberflächenwasser (n = 63)	Wassersäulenprofil (n = 28)	Oberflächenwasser (n = 62)	Wassersäulenprofil (n = 31)		
Temperatur	Temperatur (°C)	$\delta^{15}N_{SPM}$ (‰)	$\delta^{15}N_{SPM}$ (‰)	$\delta^{15}N_{Sediment}$ (‰) [a]	(n = 98)
	Sauerstoff (ml/l)	PN (mg/l)	PN (mg/l)	SST (UK-37) (°C) [b]	(n = 123)
	Chlorophyll *a* (mg/l)	POC (mg/l)	C_{org}/N (molar)	TOC (%) [c]	(n = 68; 43 bisher unpubl.)
		C_{org}/N (molar)			
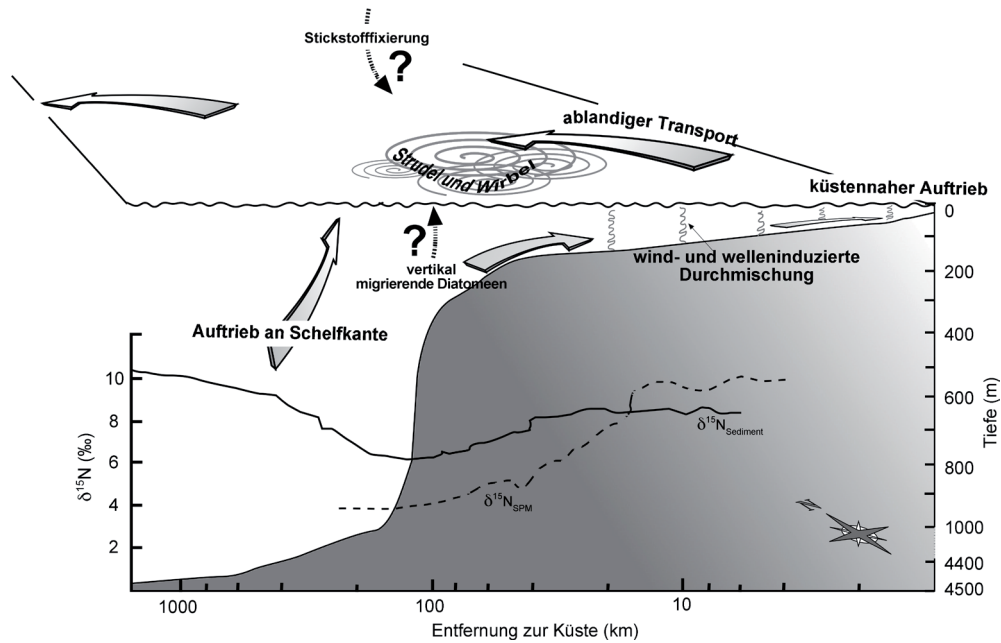
Abb. 6. Während sich die meisten $\delta^{15}N_{SPM}$-Werte auf den Schelf beschränken, reichen einige $\delta^{15}N_{Sediment}$-Daten weit über den Kontinentalhang. Die Abnahme von Oberflächenwasser-$\delta^{15}N_{SPM}$ und $\delta^{15}N_{Sediment}$ in Richtung Westen zeugt von einer kontinuierlichen Reduzierung des relativen Nährstoffverbrauchs. Dem Modell zufolge profitiert die Primärproduktion über weiten Teilen des Schelf von starker vertikaler Durchmischung und dem Anzapfen tiefer, nährstoffreicher Wassermassen. Zudem transportieren auftriebsgebundene Turbulenzen die an der Schelfkante zugeführten Nährstoffe bis über den mittleren Schelf und wirken so der sukzessiven Nährstoffzehrung gen Westen entgegen. Zusätzliche Details sind der eigentlichen Publikation zu entnehmen (S. 45ff).

Signale widerspricht dem Konzept der Rayleigh-Fraktionierung, d.h. der kontinuierlichen Anreicherung von ^{15}N-NO_3^- entlang des Strömungspfades infolge sukzessiver Nitratzehrung (Montoya, 1994) (Kapitel 3.2.). Ursache für den unerwarteten Trend scheint eine Reduzierung des relativen Nährstoffverbrauchs gen Westen. Dies resultiert aus geringerer Primärproduktion zum einen und erhöhter Nährstoffzufuhr zum anderen. Einen Beitrag zur Nährstoffzufuhr liefert die vertikale Durchmischung der relativ seichten Schelfgewässer. Die Durchmischung scheint stark genug, um tiefere, nährstoffreichere Wassermassen anzuzapfen und auf diese Weise der erwarteten Nährstoffzehrung entgegenzuwirken. Eine zusätzliche Versorgung mit Nährstoffen findet via einer zweiten Auftriebsfront an der Schelfkante statt (Abb. 6). Unserer Theorie nach führt der Auftrieb über der Schelfkante zur Bildung von Strudeln und Wirbeln, deren Einflussbereich bis weit über den mittleren Schelf reicht. In einer breiten Mischungszone treffen nun die westwärts driftenden, denitrifizierten Wässer des küstennahen Auftriebs und der Nährstoffpool von der Schelfkante aufeinander. Infolge der Durchmischung beider Wassermassen kommt es zu der beobachteten Abnahme der $\delta^{15}N$-Signatur in Richtung Westen.

Wie die parallele Entwicklung von $\delta^{15}N_{Sediment}$ und $\delta^{15}N_{SPM}$ über den Schelf hinweg zeigt, sind die Spuren sekundärer Prozesse wie mikrobiellen Abbaus offensichtlich nicht signifikant genug, um räumliche Trends im Ursprungssignal zu zerstören und $\delta^{15}N_{SPM}$ auf seinem Weg zum Ozeanboden in großem Stil zu beeinflussen. Letzteres gilt insbesondere für den inneren Schelf; die hohen Akkumulationsraten in Küstennähe gewährleisten einen raschen, ungestörten Transfer des partikulären Materials zum Sediment, was den Erhalt des Ursprungssignals enorm begünstigt.

Trotz der überschaubaren Einflüsse durch frühe Abbauprozesse empfiehlt es sich dennoch, Kernsedimente vor der Messung zu spülen (mit oder ohne vorherigem Säuern), um so eine mögliche Erhöhung des $\delta^{15}N$-Signals durch NH_3-Ausgasung auszuschließen (Kapitel 4.1.). Der authentische Transfer von $\delta^{15}N_{SPM}$ allein macht $\delta^{15}N_{Sediment}$ – auch nach entsprechender Probenaufbereitung – allerdings noch nicht zum verlässlichen Werkzeug. Dazu muss erst die Gesamtheit aller möglichen Prozesse, die zur Entstehung des Ursprungssignals beigetragen haben könnten berücksichtigt werden. Darunter fallen der Einfluss denitrifizierter Auftriebswässer in Küstennähe, der Eintrag zusätzlicher Nährstoffe an der Schelfkante sowie das Anzapfen bodennaher, nährstoffreicher Wassermassen dank ausgeprägter vertikaler Durchmischung über weiten Teilen des Schelf.

4.3. Nährstoffregime und Auftrieb im nördlichen Benguela seit dem mittleren Holozän in globalem Kontext – eine Multiproxy-Studie (Meisel et al., 2011 b; Seite 71ff)

4.3.1. Fragestellung und Zielsetzung

Der dritte Teil der Arbeit befasst sich mit dem Einfluss holozäner Klimaschwankungen auf das Auftriebsgeschehen und Nährstoffregime im nördlichen Benguela. Von der Klimasensitivität des Systems in der Vergangenheit erhoffen wir uns eine klarere Vorstellung dessen, womit infolge des gegenwärtigen Klimawandels zu rechnen ist.

Wie einleitend (Kapitel 2) dargelegt, ist das Untersuchungsgebiet aus räumlicher wie zeitlicher Sicht extrem heterogen. Werden globale Klimaschwankungen überhaupt überliefert oder aber von der lokalen Dynamik komplett überlagert? Eine der größten Herausforderungen ist dabei die Unterscheidung globaler und regionaler Ereignisse von lokalen Schwankungen. Auf welchem Weg globale Klimasignale den nördlichen Benguela erreichen, gilt es außerdem zu klären.

4.3.2. Material

Unsere Untersuchungen basieren auf drei Sedimentkernen vom inneren, zentralnamibischen Schelf (Abb.1). Die ältesten Daten reichen bis etwa 5500 Jahre zurück. Das ist ungefähr 1000 Jahre, bevor der Meeresspiegel auf sein heutiges (d.h. vorindustrielles) Niveau angestiegen ist und sich die moderne Schelfzirkulation ausgebildet hat (Emeis et al., 2009). Den Kernen wurden Spritzen- und Schlitzproben entnommen (Tabelle 4). Die Auflösung ersterer reicht von multi-dekadisch (NAM1) über hundert- (Kern 178) bis tausendjährig (Kern 226620).

Die Karbonatgehäuse der planktonischen Foraminifere *O. universa* aus den Schlitzproben dienen der ^{14}C-Altersdatierung und δ^{18}O-Analysen zur Temperaturrekonstruktion ($T_{\delta180}$). Delta^{13}C$_{org}$, δ^{15}N, TOC und SST entstammen den Spritzenproben. Die Isotopenanalysen der Kerne 226620 und 178 wurden an gesäuertem und gewaschenem Sediment durchgeführt. In NAM1 basieren die Messungen hingegen auf in-situ gesäuertem Material (bereits veröffentlicht in Struck et al., 2002), weswegen die Möglichkeit einer ausgasungsbedingten Erhöhung des δ^{15}N$_{Sediment}$-Signals nicht außer Acht gelassen werden sollte (Meisel und Struck, 2011; s. Kapitel 3.2. und 4.1.). Davon abgesehen resultieren δ^{15}N$_{Sediment}$-Schwankungen primär aus Veränderungen der Denitrifizierungsrate und des relativen Nährstoffverbrauchs.

4.3.3. Ergebnisse und Interpretation

Die N-S-Anordnung der Kerne dokumentiert küstenparallele Bewegungen der Auftriebszelle durch die Zeit (Abb. 1). Aus heutiger Sicht liegt Kern 178 im Zentrum der Zentralnamibischen Zelle, NAM1 und Kern 226620 unter ihrem nördlichen Rand, wo die modernen Oberflächentemperaturen durchschnittlich leicht höher sind. Gemäß der SST-Daten scheint das Auftriebsgeschehen über den untersuchten Zeitraum hinweg kaum räumlicher Veränderung unterworfen gewesen zu sein. Trotz teils beachtlicher Schwankungen spiegeln die Durchschnittstemperaturen das N-S-Temperaturgefälle wider und stimmen auch hinsichtlich ihrer mittleren Absolutwerte mit der rezenten Situation überein (NAM1: 16.0°C; Kern 226620: 15.1°C; Kern 178: 15.0°C).

Tabelle 4

Proxies der Spritzen- und Schlitzproben unter Angabe des Probenmaterials und der Aufbereitung. Quellenstudien bereits veröffentlichten Materials sind wie folgt: [a] Struck et al. (2002); [b] Emeis et a. (2009). [*] Delta^{15}N-Daten von unbehandeltem Sediment wurden bereits in Emeis et al. (2009) veröffentlicht.

Probenaufbereitung und Proxies	NAM1	178	226620
Spritzenproben	in 1 cm-Intervallen (∅ 5.5 a)	in 5 cm-Intervallen (∅ 16.5 a)	in 5 cm-Intervallen (∅ 62.5 a)
TOC (wt%)	in-situ gesäuert [a]	in-situ gesäuert	in-situ gesäuert
δ^{13}C$_{org}$ (‰)	in-situ gesäuert [a]	gesäuert und gewaschen	gesäuert und gewaschen
δ^{15}N (‰)	in-situ gesäuert [a]	gesäuert und gewaschen	gesäuert und gewaschen [*]
SST (°C)	UK'37	UK'37	UK'37 [b]
Schlitzproben	die obersten 50 cm (~330 BP) in 5 cm dicke Scheiben geschnitten; dann 1 cm dicke Scheiben	5 cm dicke Scheiben	alle 4 cm wurden 2 cm dicke Scheiben entnommen
$T_{\delta180}$ (°C)	Foraminiferenkalzit	Foraminiferenkalzit	Foraminiferenkalzit
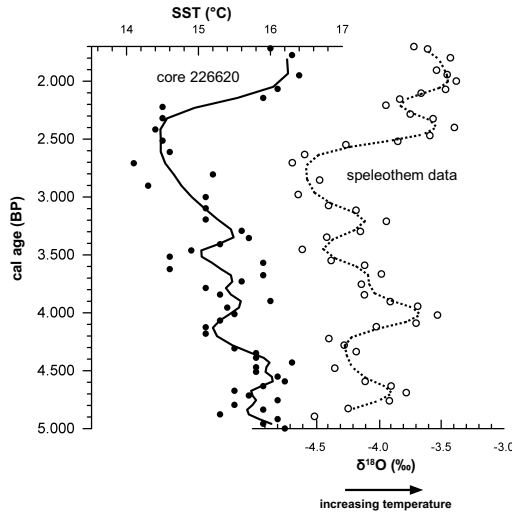
Abb. 7. Der Vergleich von SST aus Kern 226620 mit dem $T_{\delta18O}$-Datensatz vom Cold Air Cave im Nordosten Südafrikas (Holmgren et al., 2003) macht die ausgesprochen ähnliche Temperaturentwicklung im namibischen Auftrieb und Kontinentinneren sichtbar.
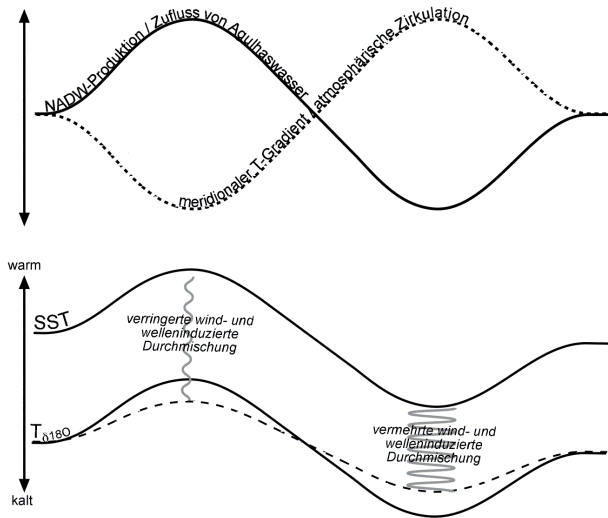
Abb. 8. Eine Beschleunigung der thermohalinen Zirkulation und NADW-Produktion hat eine Erwärmung der hohen nördlichen Breiten zur Folge (Bianchi und McCave, 1999). Der globale Temperaturgradient sinkt, wiederum lässt die Geschwindigkeit der Passatwinde und somit die Auftriebsintensität nach. Die oberflächennahen Wasserschichten wärmen sich auf und SST steigt (Rühlemann et al., 1999; Berger und Wefer, 2002; Kim et al., 2002). Der gleichzeitige Anstieg von $T_{\delta18O}$ ist auf den vermehrten Zufluss von warmem Agulhaswasser zurückzuführen, sobald das ozeanische Förderband beschleunigt. Entgegengesetzt ist die Entwicklung bei verringerter NADW-Produktion. Dem Modell nach vermag wind- und welleninduzierte Durchmischung den Verlauf von $T_{\delta18O}$ etwas zu glätten (gestrichelte Linie).

Die $\delta^{15}N$-Werte fallen selten unter 5.5‰ (dem $\delta^{15}N$-Signal des Tiefenwassers; Wada et al., 1975; Montoya, 1994; Sigman et al., 1997; Brandes und Devol, 2002), ein Anzeichen dafür, dass Denitrifizierung das $\delta^{15}N$-Signal seit jeher signifikant beeinflusst.

Im Mittel zeigen alle Proxyindikatoren Werte, die der Rezentsituation sehr nahe kommen. Dennoch gab es offensichtlich eine Reihe mehr oder wenig heftiger Fluktuationen im Laufe des mittleren und späten Holozän und wie der sorgfältige Vergleich mit Datenserien verschiedentlicher Herkunft zeigt (vom südafrikanischen Subkontinent, Nordatlantik, Südostatlantik), ist deren Ursache oft nicht rein lokaler Natur.

Wie beispielsweise aus Abb. 7 ersichtlich, folgen die Temperaturen im nördlichen Benguela und im Nordosten Südafrikas einem ausgesprochen ähnlichen tausendjährigen Trend. Der ausgeprägte Temperaturanstieg um 2200 BP fällt zudem mit dem Romanischen Klimaoptimum zusammen und ist auch in anderen, gleichermaßen marinen wie terrestrischen Datensätzen aus südafrikanischem Raum überliefert (Cohen et al., 1992; Talma und Vogel, 1992). Angesichts der Distanz zwischen den einzelnen Beprobungsorten ist die Veränderung atmosphärischer Zirkulationsmuster offensichtlich von überregionaler Größenordnung.

Auch „populäre" Schwankungen wie die Kleine Eiszeit oder das Klimaoptimum im mittleren Holozän schlagen sich in den Datensätzen nieder. Beispielsweise scheint während der frühen Stadien der Kleinen Eiszeit (±650 bis 100 BP) der Auftrieb zuzunehmen. Entsprechendes wurde auch von anderen Orten berichtet und passt außerdem – dem Modell von Cohen und Tyson (1995) entsprechend (Meisel et al., 2011 b; s. S. 88) – zu den gleichzeitig erhöhten Niederschlagsraten im Kontinentinneren.

Offensichtlich ging die globale Klimageschichte des Holozän nicht spurlos am nördlichen Benguela vorüber. In der Tat sind die Übereinstimmungen und Parallelitäten nicht nur häufiger, sondern auch um einiges klarer, als angesichts der systemimmanenten Heterogenität erwartet. Wie aber kommen diese Korrelationen zustande? Die Rolle der Atmosphäre und des Ozeans im globalen Transfer von Klimasignalen ist bereits ausgiebig und nicht selten widersprüchlich diskutiert worden (z.B. Vidal et al., 1999). Unsere Daten legen nahe, dass Charakter und Schwankungen des namibischen Auftriebs von beiderlei Komponenten beeinflusst werden. Entsprechende Zusammenhänge und Auswirkungen auf SST und $T_{\delta18O}$ sind in Abb. 8 schematisch dargestellt. Der dort abgebildete Einfluss des thermohalinen Förderbands auf die Atmosphäre und somit auf den interhemisphärischen
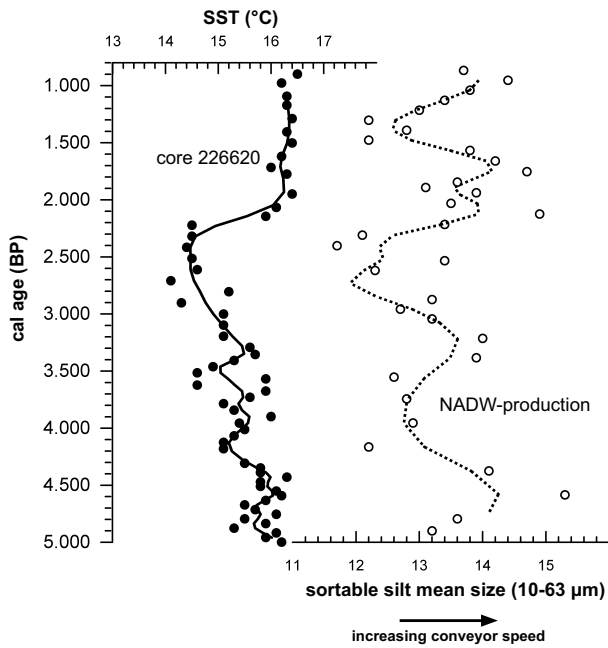
Abb. 9. SST-Verlauf von Kern 226620 neben NADW-Produktion (Rekonstruktion Letzterer aus Bianchi und McCave, 1999). Der Temperaturabfall bis ca. 2200 BP rührt der Theorie gemäß (Abb. 8) vom steileren meridionalen Temperaturgefälle und stärkeren Passatwinden. Die Trendwende um 2200 BP fällt mit dem Romanischen Optimum zusammen und wird auf ein flacheres meridionales Temperaturgefälle und Abflauen des Südostpassats zurückgeführt.

Transfer von Klimasignalen über die Windsysteme zeigt sich in dem parallelen Verlauf der Oberflächentemperaturen (SST) in Kern 226620 und NADW-Produktion in Abb. 9.

Eine zusätzliche Beobachtungen ist, dass die thermohaline Zirkulation Temperatur und Nährstoffgehalt des Auftriebswassers beeinflusst. Verlangsamte NADW-Produktion wird häufig von sinkenden $T_{\delta 180}$ und verringerten Primärproduktionsraten begleitet, wobei Letzteres als Zeichen von Nährstoffmangel interpretiert wird. Unter beschleunigten NADW-Bildungsraten kehren sich die Verhältnisse um.

Die meisten Arbeiten machen lediglich von einem Paläothermomter, d.h. Temperaturproxy, Gebrauch. Um allerdings zwischen ozeanisch und atmosphärisch verursachten Temperaturschwankungen zu unterscheiden, erwies sich die Kombination von SST und $T_{\delta 180}$ als äußerst nützlich. Insgesamt bildet die Auswahl an Proxies eine solide Basis für Paläoklimarekonstruktionen. Kern 178 liefert dabei oft die schlüssigsten Einblicke in die vorherrschenden Prozesse.

5. Schlussfolgerung und Ausblick

Vom Einfluss küstennaher Auftriebssysteme auf den globalen CO_2- und Wärmehaushalt war zu Beginn die Rede. Dass Auftriebssysteme dank ihres Fischreichtums die Ernährung und den Lebensunterhalt von Millionen Menschen sichern, blieb bislang unerwähnt. Nach Zahlen der FAO (Stand 2007) deckt der Verzehr von Fisch bei mehr als 1,5 Milliarden Menschen 20 % des Bedarfs an tierischem Eiweiß (FAO, 2009). Das Ziel einer verantwortungsvollen Fischereipolitik ist daher von globalem Interesse. Für die ansässigen Küstenbewohner, deren Lebensunterhalt unmittelbar von der Intaktheit des Ökosystem abhängt, ist ein nachhaltiges Ressourcenmanagement besonders von Brisanz.

Allerdings setzen Maßnahmen zum nachhaltigen Schutz ein tiefes Verständnis der Prozesse voraus. Die vorliegende Arbeit leistet dafür einen nicht unwesentlichen Beitrag, indem sie anhand geochemischer Hilfsmittel die Nährstoffsituation, Primärproduktion sowie das Auftriebsgeschehen unter die Lupe nimmt und dabei sowohl die Rezentsituation (Meisel et al., 2011 a) als auch Schwankungen durch die Zeit (Meisel et al., 2011 b) betrachtet.

Wie in Kapitel 2 ausgeführt, unterliegt das Untersuchungsgebiet der Interaktion küstenparalleler, den Schelf querender und vertikaler Strömungen. Die beteiligten Wassermassen unterscheiden sich hinsichtlich ihrer Herkunft, Charakteristika sowie ihrer jahreszeitlich variierender Bedeutung. Dementsprechend dynamisch gestaltet sich erwartungsgemäß auch das Nährstoffregime. Der Komplexität zum Trotz erwiesen sich unsere Rezentuntersuchungen vor dem Hintergrund früherer Erkenntnisse als solide Grundlage für Paläoklimarekonstruktionen. Allerdings fehlt es bislang noch an einem umfassenden $[NO_3^-]$- und $\delta^{15}N_{Nitrat}$-Datensatz, um unsere Theorien zu untermauern. Aktuell wird viel Arbeit in eine entsprechende Datenerhebung investiert und so ist mit der Beseitigung noch vorhandener Unsicherheiten hinsichtlich der Interpretation von $\delta^{15}N_{Sediment}$ und der Identifizierung der Nährstoffquellen in naher Zukunft zu rechnen.

Der anhand dreier Sedimentkerne unternommene Blick in die Vergangenheit liefert wertvolle Informationen über die Anfälligkeit des Systems auf externes Forcing (Antrieb). Seit der Ausbildung der Schelfzirkulation im mittleren Holozän schwankten die Primärproduktionsraten teilweise gewaltig; von entsprechenden Auswirkungen auf die Nahrungskette und Fischgründe ist sicherlich auszugehen. Unsere Ergebnisse zeigen,

dass Änderungen im Auftriebsgeschehen und Nährstoffhaushalt häufig auf Fluktuationen in der atmosphärischen und / oder thermohalinen Zirkulation zurückzuführen sind. Diese Beobachtungen können hinsichtlich einer Vorhersage möglicher Auswirkungen des gegenwärtigen Klimawandels auf den namibischen Auftrieb von großem Nutzen sein und tragen gegebenenfalls zu einer Verbesserung bestehender Klimamodelle bei. Wir brauchen verlässliche Zukunftsszenarien, um adäquat und vor allem rechtzeitig auf klimabedingte Veränderungen reagieren zu können.

Wie fehleranfällig allerdings bereits die Phase der Datenerhebung sein kann, zeigen Meisel und Struck (2011). Die je nach Art der Probenaufbereitung eklatant unterschiedlichen δ^{15}N-Werte und C_{org}/N-Verhältnisse machen deutlich, dass der Entscheidung für eine Aufbereitungsart eine kritische und vor allem materialspezifische Untersuchung vorangehen sollte. Im Falle des organikreichen Diatomenschlamms scheint der störende Einfluss von Ammonium auf δ^{15}N und C_{org}/N in unbehandeltem Sediment eindeutig belegt.

Referenzen

Altabet, M.A., (1988) Variations in nitrogen isotopic composition between sinking and suspended particles: implications for nitrogen cycling and particle transformation in the open ocean. *Deep-Sea Research*, 35, 535-554.

Altabet, M., Deuser, W.G., Honjo, S., Stienen, C., (1991) Seasonal and depth-related changes in the source of sinking particles in the North Atlantic. *Nature*, 354, 136-139.

Altabet, M.A., Francois, R., (1994) Sedimentary nitrogen isotopic ratio as a recorder for surface ocean nitrate utilization. *Global Biogeochemical Cycles*, 8, 103-116.

Altabet, M.A., Francois, R., Murray, D.W., Prell, W.L., (1995) Climate-related variations in denitrification in the Arabian Sea from ^{15}N/^{14}N-ratios. *Nature*, 373, 506-509.

Altabet, M.A., Pilskaln, C., Thunnel, R., Pride, C., Sigman, D., Chavez, F., Francois, R., (1999) The nitrogen isotope biogeochemistry of sinking particles from the margin of the Eastern North Pacific. *Deep Sea Research I*, 46, 655-679.

Bakun, A., Weeks, S.J., (2004) Greenhouse gas buildup, sardines, submarine eruptions and the possibility of abrupt degradation of intense marine upwelling ecosystems. *Ecology Letters*, 7, 1015-1023.

Bang, N.D., (1971) The southern Benguela current region in February, 1966: Part II. Bathythermography and air-sea interactions. *Deep-Sea Research*, 18, 209-224.

Barange, M., Pillar, S.C., (1992) Cross-shelf circulation, zonation and maintenance mechanisms of *Nyctiphanes capensis* and *Euphausia hanseni* (Euphausiacea) in the northern Benguela upwelling system. *Continental Shelf Research*, 12(9), 1027-1042.

Berger, W.H., Smetacek, V.S., Wefer, G., (1989) Productivity of the ocean: present and past, pp. 471. John Wiley and Sons, Chichester.

Berger, W.H., Wefer, G., (2002) On the reconstruction of upwelling history: Namibia upwelling in context. *Marine Geology*, 180, 3-28.

Bianchi, G.G., McCave, N., (1999) Holocene periodicity in North Atlantic climate and deep-ocean flow south of Iceland. *Nature*, 397, 515-517.

Bigeleisen, J., (1965) Chemistry of isotopes. *Science*, 147, 463-471.

Bouillon, S., Raman, A.V., Dauby, P., Dechairs, F., (2002) Carbon and nitrogen isotope ratios of subtidal benthic invertebrates in an estuarine mangrove ecosystem (Andhra Pradesh, India). *Estuarine, Coastal and Shelf Science*, 54(901-913).

Brandes, J.A., Devol, A.H., (2002) A global marine-fixed nitrogen isotopic budget: Implications for Holocene nitrogen cycling. *Global Biogeochemical Cycles*, 16(4), 1120.

Bremner, J.M., Willis, J.P., (1993) Mineralogy and geochemistry of the clay fraction of sediments from the Namibian continental margin and the adjacent hinterland. *Marine Geology*, 115, 85-116.

Brook, A.B., Marais, E., Cowart, J.B., (1999) Evidence of wetter and drier conditions in Namibia from tufas and submerged speleothems. *Cimbebasia*, 15, 29-39.

Brüchert, V., Altenbach, A.V., Bening, G., Bockelmann, F., Currie, B., Donath, J., Dübecke, J., Endler, R., Erdmann, S., Ertan, T., Fuchs, B., Klockgether, G., Krüger, S., Kuypers, M.M.M., Lass, H.U., Lavik, G., Lilienthal, S., Leipe, T., Nickel, G., Noli-Peard, K., Ohde, T., Schulz, B., Schulz, H., Siegel, H., Struck, U., Wulf, J., Zitzmann, S., Zonneveld, K., (2004) The Benguela Upwelling System 2003, Part 3, Cruise No. 57, Leg 3, March 15 – April 13, 2003, Walvis Bay, Namibia - Dakar. In: *Meteor Berichte*, 4, pp. 53.

Bunn, S.E., Loneragan, N.R., Kempster, M.A., (1995) Effects of acid washing on stable isotopes ratios of C and N in penaeid shrimp and seagrass: implications for food-web studies using multiple stable isotopes. *Limnology and Oceanography*, 40(3), 622-625.

Brunelle, J.P., (1978) Preparation of catalysts by metallic complex adsorption on mineral oxides. *Pure and Appied Chemistry*, 50, 1211-1229.

Calvert, S.E., Price, N.B., (1971) Upwelling and nutrient regeneration in the Benguela Current, October, 1968. *Deep-Sea Research*, 18, 505-523.

Calvert, S.E., Nielsen, B., Fontugne, M.R., (1992) Evidence from nitrogen isotope ratios for enhanced productivity during formation of eastern Mediterranean sapropels. *Nature*, 359, 223-225.

Carabel, S., Godínez-Domínguez, E., Verísimo, P., Fernández, L., Freire, J., (2006) An assessment of sample processing methods for stable isotope analyses of marine food webs. *Journal of Experimental Marine Biology and Ecology*, 336, 254-261.

Chapman, P., Shannon, L., (1985) The Benguela ecosystem Part II. Chemistry and related processes. *Oceanography and Marine Biology Annual Review* 23, 183-251.

Cline, J.D., Kaplan, I.R., (1975) Isotopic fractionation of dissolved nitrate during denitrification in the eastern tropical North Pacific Ocean. *Marine Chemistry*, 3, 271-299.

Codispoti, L.A., Christensen, J.P., (1985) Nitrification, denitrification and nitrous oxide cycling in the eastern tropical South Pacific Ocean. *Marine Chemistry*, 16, 277-300.

Cohen, A.L., Parkington, J.E., Brundrit, G.B., van der Merwe, N.J., (1992) A Holocene Marine Climate Record in Mollusc Shells from the Southwest African Coast. *Quaternary Research*, 38, 379-385.

Cohen, A.L., Tyson, P.D., (1995) Sea-surface temperature fluctuations during the Holocene off the south coast of Africa: implications for terrestrial climate and rainfall *Holocene*, 5(3), 304-312.

Diester-Haass, L., Heine, K., Rothe, P., Schrader, H., (1988) Late Quaternary history of continental climate and the Benguela Current off South West Africa. *Palaeogeography, Palaeoclimatology, Palaeoecology*, 65, 81-91.

Emeis, K.-C., Brüchert, V., Currie, B., Endler, R., Ferdelman, T., Kiessling, A., Leipe, T., Noli-Peard, K., Struck, U., Vogt, T., (2004) Shallow gas in shelf sediments of the Namibian coastal upwelling ecosystem. *Continental Shelf Research*, 24(6), 627-642.

Emeis, K.-C., Struck, U., Leipe, T., Ferdelman, T.G., (2009) Variability in upwelling intensity and nutrient regime in the coastal upwelling system offshore Namibia: results from sediment archives. *International Journal of Earth Sciences* 98, 309-326.

FAO Fisheries and Aquaculture Information and Statistics Service, (2009) *FAO yearbook. Fishery and Aquaculture Statistics. 2007*. Rome, FAO. 2009.

Faure, G., (1992) *Principles and applications of inorganic geochemistry - A comprehensive textbook for geology students*. Maxwell Macmillan International Editions, New York, Toronto, Oxford.

Francois, R., Altabet, M.A., Burckle, L.H., (1992) Glacial to interglacial changes in surface nitrate utilization in the Indian sector of the southern ocean as recorded by sediment δ^{15}N. *Paleoceanography*, 7, 589-606.

Freudenthal, T., Wagner, T., Wenzhöfer, F., Zabel, M., Wefer, G., (2001) Early diagenesis of organic matter from sediments of the eastern subtropical Atlantic: Evidence from stable nitrogen and carbon isotopes. *Geochimica et Cosmochima Acta*, 65(11), 1795-1808.

Fry, B., (1988) Food web structure on Georges Bank from stable C, N, and S isotopic compositions. *Limnology and Oceanography*, 33, 1182-1190.

Fry, B., Jannasch, H., Molyneaux, S.J., Wirsen, C.O., Muramoto, J.A., King, S., (1991) Stable isotope studies of the carbon, nitrogen and sulfur cycles in the Black Sea and the Cariaco Trench. *Deep-Sea Research*, 38(S2), 1003-1019.

Ganssen, G.M., Kroon, D., (2000) The isotopic signature of planktonic foraminifera from NE Atlantic surface sediments: implications for the reconstruction of past oceanic conditions. *Journal of Geological Society*, 157, 693-699.

Gaye-Haake, B., Lahajnar, N., Emeis, K.-C., Unger, D., Rixen, T., Suthhof, A., Ramaswamy, V., Schulz, H., Paropkari, A.L., Guptha, M.V.S., Ittekkot, V., (2005) Stable nitrogen isotopic ratios of sinking particles and sediments from the northern Indian Ocean. *Marine Chemistry*, 96, 243-255.

Goering, J., Alexander, V., Haubenstock, N., (1990) Seasonal variability of stable carbon and nitrogen isotope ratios of organism in a North Pacific Bay. *Estuarine, Coastal and Shelf Science*, 30(239-260).

Gordon, A.L., (1986) Interocean Exchange of Thermocline Water. *Journal of Geophysical Research*, 91(C4), 5037-5046.

Harvey, H.R., Tuttle, J.H., Bell, J.T., (1995) Kinetics of phytoplankton decay during simulated sedimentation: Changes in biochemical composition and microbial activity under oxic and anoxic conditions. *Geochimica et Cosmochimica Acta*, 59(16), 3367-3377.

Hemleben, C., Bijma, J., (1994) Foraminiferal population dynamics and stable carbon isotopes In: *Carbon Cycling in the Glacial Ocean: Constraints on the Ocean´s Role in Global Change*, *17* (Ed. by R. Zahn, T.F. Pedersen, M.A. Kaminski, L. Labeyrie), pp. 145-166. Springer-Verlag.

Holmes, M.E., Müller, P.J., Schneider, R.R., Segl, M., Pätzold, J., Wefer, G., (1996) Stable nitrogen isotopes in Angola Basin surface sediments. *Marine Geology*, 134, 1-12.

Holmes, B., Eichner, C., Struck, U., Wefer, G., (1999) Reconstructions of surface ocean nitrate utilization using stable nitrogen isotopes in sinking particles and sediments. In: *Use of Proxies in Paleoceanography: Examples from the South Atlantic* (Ed. by G. Fischer, G. Wefer), pp. 447-468. Springer, Berlin.

Holmes, E., Lavik, G., Fischer, G., Segl, M., Ruhland, G., Wefer, G., (2002) Seasonal variability of δ^{15}N in sinking particles in the Benguela upwelling region. *Deep-Sea Research I*, 49, 377-394.

Jacob, U., Mintenbeck, K., Brey, T., Knust, R., Beyer, K., (2005) Stable isotope food web studies: a case for standardized sample treatment. *Marine Ecology Progress Series*, 287, 251-253.

Kang, C.-K., Kim, B.J., Lee, K.-S., Kim, J.B., Lee, P.-Y., Hong, J.-S., (2003) Thropic importance of benthic microalgae to macrozoobenthos in coastal bay systems in Korea: dual stable C and N isotope analyses. *Marine Ecology Progess Series*, 259, 79-92.

Kennedy, P., Kennedy, H., Papadimitriou, S., (2005) The effect of acidification on the determination of organic carbon, total nitrogen and their stable isotopic composition in algae and marine sediment. *Rapid Communications in Mass Spectrometry*, 19, 1063-1068.

Kim, J.-H., Schneider, R.R., Müller, P.J., Wefer, G., (2002) Interhemispheric comparison of deglacial sea-surface temperature patterns in Atlantic eastern boundary currents. *Earth and Planetary Science Letters*, 1994, 383-393.

Kirst, G.J., Schneider, R.R., Müller, P.J., von Storch, I., Wefer, G., (1999) Late Quaternary Temperature Variability in the Benguela Current System Derived from Alkenones. *Quaternary Research*, 52, 92-103.

Kuypers, M.M.M., Lavik, G., Woebken, D., Schmid, M., Fuchs, B.M., Amann, R., Jørgensen, B.B., Jetten, M.S.M., (2005) Massive nitrogen loss from the Benguela upwelling system through anaerobic ammonium oxidation. *PNAS*, 102(18), 6478-6483.

Lavik, G., Stührmann, T., Brüchert, V., van der Plas, A., Mohrholz, V., Lam, P., Mußmann, M., Fuchs, B.M., Amann, R., Lass, U., Kuypers, M.M.M., (2009) Detoxification of sulphidic African shelf waters by blooming chemolithotrophs. *Nature*, 459, 581-585.

Lehmann, M.F., Bernasconi, S.M., Barbieri, A., McKenzie, J.A., (2002) Preservation of organic matter and alteration of its carbon and nitrogen isotope composition during simulated and in situ early sedimentary diagenesis. *Geochimica et Cosmochimica Acta*, 66, 3573-3584.

Libes, S.M., Deuser, W.G., (1988) The isotope geochemistry of particulate nitrogen in the Peru Upwelling Area and the Gulf of Maine. *Deep-Sea Research*, 35(4), 517-533.

Meisel, S., Struck, U., (2011) The potential distortion of sedimentary δ^{15}N and C_{org}/N ratios by NH_4^+ and the effects of pre-analysis sample treatment. *Fossil Record,* 14(2), 141-152.

Meisel, S., Struck, U., Emeis, K.-C., (2011, a) Nutrient dynamics and oceanographic features in the central Namibian upwelling region as reflected in δ^{15}N-signals of suspended matter and surface sediments. *Fossil Record,* 14(2), 153-169.

Meisel, S., Emeis, K.-C., Struck, U., Kristen, I., (2011, b) Nutrient regime and upwelling in the northern Benguela since the middle Holocene in a global context – a multi-proxy approach. *Fossil Record,* 14(2), 171-193.

Mohrholz, V., Bartholomae, C.H., van der Plas, A.K., Lass, H.U., (2008) The seasonal variability of the northern Benguela undercurrent and its relation to the oxygen budget on the shelf. *Continental Shelf Research*, 28(3), 424-441.

Mollenhauer, G., Schneider, R.R., Müller, P.J., Spieß, V., Wefer, G., (2002) Glacial/interglacial variability in the Benguela upwelling system: Spatial distribution and budgets of organic carbon accumulation. *Global Biogeochemical Cycles*, 16(4), 1134.

Montoya, J.P., (1994) Nitrogen isotope fractionation in the modern ocean: Implications for the sedimentary record. In: *Carbon Cycling in the Glacial Ocean: Constraints on the Ocean´s Role in Global Change.*, 17, *NATO ASI Series* (Ed. by R. Zahn, T.F. Pedersen, M.A. Kaminski, L. Labeyrie), pp. 259-279. Springer-Verlag, Berlin.

Montoya, J.P., McCarthy, J.J., (1995) Isotopic fractionation during nitrate uptake by phytoplankton growth in continuous culture. *Journal of Plankton Research*, 17, 439-464.

Moroshkin, K.V., Bubnov, V.A., Bulatov, R.P., (1970) Water circulation in the eastern South Atlantic Ocean. *Oceanology*, 10(1), 27-34.

Mulitza, S., Arz, H., Kemle-von Mücke, S., Moos, C., Niebler, H.-S., Pätzold, J., Segl, M., (1999) The South Atlantic Carbon Isotope Record of Planktic Foraminifera In: *Use of Proxies in Paleoceanography: Examples from the South Atlantic* (Ed. by G. Fischer, G. Wefer), pp. 427-445. Springer-Verlag, Berlin Heidelberg.

Ng, J.S.S., Wai, T.-C., Williams, G.A., (2007) The effects of acidification on the stable isotope signatures of marine algae and molluscs. *Marine Chemistry*, 103, 97-102.

Niebler, H.-S., Huberten, H.-W., Gersonde, R., (1999) Oxygen Isotope Values of Planktic Foraminifera: A Tool for the Reconstruction of Surface Water Stratification In: *Use of Proxies in Paleoceanography: Examples from the South Atlantic* (Ed. by G. Fischer, G. Wefer), pp. 165-189. Springer-Verlag, Berlin Heidelberg.

Nieuwenhuize, J., Maas, Y.E.M., Middelburg, J.J., (1994) Rapid analysis of organic carbon and nitrogen in particulate materials. *Marine Chemistry*, 45, 217-224.

Oberhänsli, H., (1991) Upwelling signals at the northeastern Walvis Ridge during the past 500,000 years. *Paleoceanography*, 6(1), 53-71.

Ostrom, N.E., Macko, S.A., (1991) Late Wisconsinan to present sedimentation of organic matter off northern Newfoundland in response to climatological events. *Continental Shelf Research*, 11, 1285-1296.

Ostrom, N.E., Macko, S.A., Deibel, D., Thompson, R.J., (1997) Seasonal variation in the stable carbon and nitrogen isotope biogeochemistry of a coastal cold ocean environment. *Geochimica et Cosmochimica Acta*, 61(14), 2929-2942.

Pichevin, L., Martinez, P., Bertrand, P., Schneider, R., Giraudeau, J., Emeis, K., (2005) Nitrogen cycling on the Namibian shelf and slope over the last two climatic cycles: Local and global forcings. *Paleoceanography*, 20.

Ravelo, A.C., Fairbanks, R.G., (1992) Oxygen Isotopic Composition of Multiple Species of Planktonic Foraminifera: Recorders of the Modern Photic Zone Temperature Gradient *Paleoceanography*, 7(6), 815-831.

Rühlemann, C., Mulitza, S., Müller, P.J., Wefer, G., Zahn, R., (1999) Warming of the tropical Atlantic Ocean and slowdown of thermohaline circulation during the last deglaciation. *Nature*, 402, 511-514.

Sachs, J.P., Repeta, D.J., (1999) Oligotrophy and nitrogen fixation during eastern Mediterranean sapropel events. *Science*, 286, 2485-2488.

Saino, T., Hattori, A., (1980) ^{15}N natural abundance in oceanic suspended particulate matter. *Nature*, 283, 752-754.

Schäfer, P., Ittekkot, V., (1993) Seasonal variability of δ^{15}N in settling particles in the Arabian Sea and its paleogeochemical significance. *Naturwissenschaften*, 80, 511-513.

Shannon, L.V., (1985) The Benguela ecosystem. Part I. Evolution of the Benguela, physical features and processes. *Oceanography and Marine Biology Annual Review*, 23, 105-182.

Shannon, L.V., Boyd, A.J., Brundrit, G.B., Taunton-Clark, J., (1986) On the existence of an El Niño-type phenomenon in the Benguela system. *Journal of Marine Research*, 44(3), 495-520.

Shannon, L.V., Nelson, G., (1996) The Benguela: Large Scale Features and Processes and System Variability. In: *The South Atlantic: Present and Past Circulation* (Ed. by G. Wefer, W.H. Berger, G. Siedler, D. Webb), pp. 163-210. Springer, Berlin, Heidelberg.

Shannon, L.V., O'Toole, M.J., (1999) Integrated Overview of the Oceanography and Environmental Variability of the Benguela Current Region - Thematic Report NO.2. In: *Synthesis and Assessment of Information on the Benguela Current Large Marine Ecosystem (BCLME)*, Windhoek, Namibia.

Shannon, L.V., O'Toole, M.J., (2003) Sustainability of the Benguela: ex Africa semper aliquid novi. In: *Large marine ecosystems of the world: trends in exploitation, protection and research* (Ed. by G. Hempel, K. Sherman), pp. 227-253. Elsevier B.V., Amsterdam.

Sharp, Z., (2006) *Principles of Stable Isotope Geochemistry* Prentice Hall.

Shi, N., Dupont, L.M., Beug, H.-J., Schneider, R., (2000) Correlation between Vegetation in Southwestern Africa and Oceanic Upwelling in the Past 21,000 Years. *Quaternary Research*, 54, 72-80.

Sigman, D.M., Altabet, M.A., Michener, R., McCorkle, D.C., Fry, B., Holmes, R.M., (1997) Natural abundance-level measurement of the nitrogen isotopic composition of oceanic nitrate: an adaption of the ammonia diffusion method. *Marine Chemistry*, 57(3-4), 227-242.

Smith, R.L., (1995) The physical processes of coastal ocean upwelling systems. In: *Upwelling in the Ocean: Modern Processes and Ancient Records* (Ed. by C.P. Summerhayes, K.-C. Emeis, M.V. Angel, R.L. Smith, B. Zeitzschel), pp. 39-64. John Wiley & Sons

Stoner, A.W., Zimmerman, R.J., (1988) Food pathways associated with penaeid shrimps in a mangrove-fringed estuary. *Fisheries Bulletin*, 86, 543-552.

Stramma, L., Peterson, R.G., (1989) Geostrophic Transport in the Benguela Current region. *Journal of Physical Oceanography*, 19, 1440-1448.

Struck, U., Emeis, K.C., Voss, M., Christiansen, C.C., Kunzendorf, H., (2000) Records of southern and central Baltic Sea eutrophication in δ^{13}C and δ^{15}N of sedimentary organic matter. *Marine Geology*, 164(3-4), 157-171.

Struck, U., Emeis, K.-C., Voss, M., Krom, M.D., Rau, G.H., (2001) Biological productivity during sapropel S5 formation in the Eastern Mediterranean Sea: Evidence from stable isotopes of nitrogen and carbon. *Geochimica et Cosmochimica Acta*, 65(19), 3241-3258.

Struck, U., Emeis, K.-C., Alheit, J., Schneider, R., Eichner, C., Altenbach, A.-V., (2002) Changes of the upwelling rates of nitrate preserved in the ^{15}N-signature of sediments and fish scales from the diatomaceous mud belt off Namibia. *GeoBios*, 35(EPA-special issue), 3-11.

Struck, U., Pollehne, F., Bauerfeind, E., v. Bodungen, B., (2004) Sources of nitrogen for the vertical particle flux in the Gotland Sea (Baltic Proper) - results from sediment trap studies. *Journal of Marine Systems*, 45, 91-101.

Summerhayes, C.P., Kroon, D., Rosell-Mele, A., Jordan, R.W., Schrader, H.-J., Hearn, R., Villanueva, J., Grimalt, J.O., Eglington, G., (1995) Variability in the Benguela Current upwelling system over the past 70,000 years. *Progress in Oceanography*, 35, 207-251.

Talma, S.A., Vogel, J.C., (1992) Late Quaternary Paleotemperatures Derived from a Speleothem from Cango Caves, Cape Province, South Africa. *Quaternary Research*, 37, 203-213.

Tedesco, K., Thunell, R., Astor, Y., Muller-Karger, F., (2007) The oxygen isotope composition of planktonic foraminifera from the Cariaco Basin, Venezuela: Seasonal and interannual variations. *Marine Micropaleontology*, 62, 180-193.

Thornton, S.F., McManus, J., (1994) Application of organic carbon and nitrogen stable isotope and C/N ratios as source indicators of organic matter provenance in estuarine systems: evidence from the Tay Estuary, Scotland. *Estuarine, Coastal and Shelf Science*, 38(219-233).

Tomczak, M., Godfrey, J.S., (2003) *Regional Oceanography: An Introduction*. Daya Publishing House.

Tyrrell, T., Lucas, M.I., (2002) Geochemical evidence of denitrification in the Benguela upwelling system. *Continental Shelf Research*, 22, 2497-2511.

Urey, H.C., (1947) The thermodynamic properties of isotopic substances. *Journal of the Chemical Society*, 562-581.

Urey, H.C., Epstein, S., McKinney, C., McCrea, J., (1948) Method for measurement of paleotemperatures. *Bulletin of the Geological Society of America (abstract)*, 59, 1359-1360.

Urey, H.C., Epstein, S., McKinney, C.R., (1951) Measurements of palaeotemperatures and temperatures of the Upper Cretaceous of England. *Bulletin of the Geological Society of America*, 62, 339-416.

van Zyl, B.J., (2010) A Decade of Namibian Fisheries and Biodiversity Management. *www.unep.org/bpsp/Fisheries/ Fisheries%20Case%20Studies/VANZYL.pdf*, Access date April 2010.

Vidal, L., Schneider, R.R., Marchal, O., Bickert, T., Stocker, T.F., Wefer, G., (1999) Link between the North and South Atlantic during the Heinrich events of the last glacial period. *Climate Dynamics*, 15, 909-119.

Vogt, T., (2002) Akustische Fazies auf dem Schelf und oberen Kontinentalrand vor Namibia - Auswertung von PARASOUND-Ergebnissen der Reise METEOR 48-2, *M.Sc. Thesis*, pp. 80. University of Greifswald, Greifswald.

Wada, E., (1980) Nitrogen isotope fractionation and its significance in biogeochemical processes occurring in marine environments. In: *Isotope Marine Chemistry* (Ed. by E.D. Goldberg, Y. Horibe, K. Saruhashi), pp. 375-398. Uchida Rokakuho, Japan.

Wada, E., Kadonaga, T., Matsuo, S., (1975) ^{15}N abundance in nitrogen of naturally occurring substances and global assessment of denitrification from isotopic viewpoint. *Geochem. J.*, 9, 139-148.

Wada, E., Hattori, A., (1978) Nitrogen isotope effects in the assimilation of inorganic nitrogenous compounds by marine diatoms. *Geomicrobiology Journal*, 1, 85-101.

Waser, N.A.D., Turpin, D.H., Harrison, P.J., Nielsen, B., Calvert, S.E., (1998) Nitrogen isotope fractionation during uptake and assimilation of nitrate, nitrite, ammonium and urea by a marine diatom. *Limnology and Oceanography*, 43, 215-224.

Weeks, S.J., Currie, B., Bakun, A., Peard, K.R., (2004) Hydrogen sulphide eruptions in the Atlantic Ocean off southern Africa: implications of a new view based on SeaWiFS satellite imagery. *Deep-Sea Research I*, 51, 153-172.

Wefer, G., Berger, W., (1991) Isotope paleontology: growth and composition of extant calcareous species. *Marine Geology*, 100, 207-248.

Erklärung

Die vorliegende Arbeit wurde in kumulativer Form verfasst und gliedert sich in drei Manuskripte. Diesen geht eine Einführung in deutscher Sprache voran, die den Einstieg in die Fragestellung und Thematik erleichtern soll. Hier werden neben einem umfassenden Einblick in die angewandten Methoden ebenso die wichtigsten Ergebnisse gezeigt.

Koordination und Ausführung der Probenaufbereitung, Laborarbeiten und Datenerhebung erfolgte mit Unterstützung von PD Dr. Ulrich Struck in seiner Rolle als Leiter des Isotopenlabors. Wie nebenan tabellarisch aufgeführt, wurden eigens erhobene Daten bereits veröffentlichten Daten gegenübergestellt und um diese erweitert. Interpretation, Evaluierung der Messergebnisse und Diskussion sind das Ergebnis sorgfältiger Literaturrecherche sowie des intensiven Dialogs und Austauschs mit meinem Betreuer (PD Dr. Ulrich Struck) und den Co-Autoren.
Niederschrift und Erstellung der Grafiken erfolgten eigenständig und ich versichere, die vorliegende Arbeit ausschließlich unter Verwendung der angegebenen Quellen und Mittel verfasst zu haben. Ebenso wurden alle Passagen, die inhaltlich und argumentativ auf anderen Werken beruhen, anhand entsprechender Referenz kenntlich gemacht.

Die Manuskripte befinden sich im Druck und werden in noch in diesem Jahr in *Fossil Record,* Ausgabe 14 (2), erscheinen. Die Arbeit hat in gleicher oder ähnlicher Form noch keiner Prüfungsbehörde vorgelegen.

Stavanger, 20. Mai 2011

Zusammenstellung der dieser Arbeit zugrundeliegenden Daten unter Angabe der Anzahl an Proben. Daten in roter Schrift wurden bereits anderweitig veröffentlicht (Referenzen finden sich im Text). Daten in blauer Schrift sind bis dato unveröffentlicht; sie wurden allerdings nicht von der Autorin selbst erhoben sondern von den Co-Autoren zur Verfügung gestellt.

(A) Daten der Publikation "*The potential distortion of sedimentary $\delta^{15}N$ and C_{org}/N ratios by NH_4^+ and the effects of pre-analysis sample treatment*" (Seite 37ff). [1] an unbehandeltem Sediment; [2] an gespültem Sediment; [3] an gesäuertem und gespültem Sediment; [4] an in-situ gesäuertem Sediment.

	TC (%)	C_{org} (%)	N (%)	C_{org}/N	$\delta^{15}N$ (‰)	NH_4^+ im Spülwasser
Messreihe 1 [1]	100	-	98	97	100	-
Messreihe 2 [2]	22	-	22	21	22	22
Messreihe 3 [3]	-	100	100	100	100	22
Messreihe 4 [4]	-	98	100	98	100	-

(B) Daten der Publikation "*Nutrient dynamics and oceanographic features in the central Namibian upwelling region as reflected in $\delta^{15}N$-signals of suspended matter and surface sediments*" (Seite 51ff).

hydrographische Messungen		suspendiertes partikuläres Material (SPM)		Oberflächensedimente	
Oberflächenwasser (n = 63)	Wassersäulenprofil (n = 28)	Oberflächenwasser (n = 62)	Wassersäulenprofil (n = 31)		
Temperatur	Temperatur (°C)	$\delta^{15}N_{SPM}$ (‰)	$\delta^{15}N_{SPM}$ (‰)	$\delta^{15}N_{Sediment}$ (‰)	(n = 98)
	Sauerstoff (ml/l)	PN (mg/l)	PN (mg/l)	SST (°C)	(n = 123)
	Chlorophyll *a* (mg/l)	POC (mg/l)	C_{org}/N (molar)	TOC (%)	(n = 68; 43 bisher unpubl.)
		C_{org}/N (molar)			

(C) Daten der Publikation "*Nutrient regime and upwelling in the northern Benguela since the middle Holocene in a global context – a multi-proxy approach*" (Seite 71ff).

	Kern NAM1	Kern 178	Kern 226620
TOC (wt%)	540	103	74
$\delta^{13}C_{org}$ (‰)	528	129	74
$\delta^{15}N$ (‰)	541	129	74
SST (°C)	355	128	74
$T_{\delta 18O}$ (°C)	428	108	33

The potential distortion of sedimentary δ^{15}N and C_{org}/N ratios by NH_4^+ and the effects of pre-analysis sample treatment

Sandra Meisel [a], Ulrich Struck [a,*]

[a] *Museum für Naturkunde, Leibniz-Institut für Evolutions- und Biodiversitätsforschung an der Humboldt-Universität zu Berlin, Invalidenstraße 43, 10115 Berlin, Germany*

KEYWORDS

ammonium,
C/N ratios,
isotope fractionation,
nitrogen isotopes,
sample treatment

ABSTRACT

We examined the susceptibility of δ^{15}N-signals and C_{org}/N ratios in organic-rich sediments to pre-analysis sample treatment. Each sample was subjected to three different kinds of processing. For comparative purposes, the first measurement series (MS-1) was carried out on untreated sediment. In MS-2, the sediment was rinsed with distilled water. In MS-3, analyses were carried out on decalcified and rinsed material, in MS-4 the samples were decalcified without being subsequently washed.

The sediment yielded conspicuously different results depending on the type of processing it was subjected to. Rinsing, irrespective of whether acidification was included or not, induced substantial modifications in δ^{15}N accompanied by a pronounced loss of NH_4^+ (up to 14wt% of the initial N-content). Molar C_{org}/N ratios, on the other hand, were only affected by a combination of acidification and rinsing.

The discrepancies are ascribed to the influence of decomposition-derived ammonium (NH_4^+). In untreated sediment (MS-1), NH_4^+ seems to produce misleading shifts in both δ^{15}N-signals and C_{org}/N ratios. Presumed mechanisms involved are as follows: Firstly, nitrogen isotopes fractionate during NH_4^+-volatilisation in the heating oven, where the sediment is put to desiccate. Secondly, NH_4^+-ions are able to escape that fractionation when adsorbed to negatively-charged SiO_2-surfaces. The adsorption capacity of SiO_2 increases with increasing pH of the pore water and hence with increasing carbonate content.

Our findings raise serious doubts about whether untreated sediment (MS-1) can provide reliable C_{org}/N and δ^{15}N-records. Pre-analysis acidification plus rinsing (MS-3) seems to eliminate the deceptive influence of NH_4^+-adsorption and -outgassing.

1. Introduction

Nitrogen isotope abundance ratios (δ^{15}N) and C/N ratios are both important instruments in the study of marine food webs. Their value - as with every proxy indicator - depends on the reliable recording of the original phenomenon in the absence of the direct measure. In this regard, the deceptive influence of sample preparation on the original C/N ratios and δ^{15}N-signals is of great interest and has already been addressed by several authors (Nieuwenhuize et al., 1994; Bunn et al., 1995; Holmes et al., 1999; Jacob et al., 2005; Kennedy et al., 2005; Carabel et al., 2006; Ng et al., 2007).

Various studies have shown, for instance, that the removal of carbonate via acidification not only alters δ^{13}C but may likewise bias δ^{15}N (Bunn et al., 1995; Jacob et al., 2005; Carabel et al., 2006; Ng et al., 2007). As a consequence, many authors now refrain from pre-analysis decalcification when measuring δ^{15}N and prefer to conduct independent measurements using untreated subsamples (Goering et al., 1990; Thornton and McManus, 1994; Bunn et al., 1995; Bouillon et al., 2002; Carabel et al., 2006).

Our findings clearly indicate that this approach is not applicable to all kinds of material. The goal of this study is to investigate the effects of common processing methods on the organic-rich sediments from the central Namibian shelf and to establish which can be most trusted with respect to the δ^{15}N- and C/N record.

* Corresponding author. Tel.: +49 (0)30 2093-8552;
  Fax: +49 (0)30 2093-8565.

  E-mail address: Ulrich.Struck@mfn-berlin.de (U. Struck).

2. Material and methods

2.1. Core 180

Core 180 was retrieved from the northern Benguela Upwelling area during METEOR cruise M57-3 (15/03/2003 to 08/04/2003) (Fig. 1). The 5 m long core consists of organic-rich diatomaceous ooze (average opal 54.3%, average organic matter 9.8%, average carbonate 5.9%; Bremner and Willis, 1993), which coats the inner shelf as a belt running parallel to the coast at a depth of up to 150 m (Shannon and O'Toole, 1999; Struck et al., 2002; Brüchert et al., 2004). Its presence testifies to the high productivity of the region. The deposit has an average thickness of 5.1 m, an estimated age of 5000 years with a mean sedimentation rate amounting to 1 mm/a (Bremner and Willis, 1993).

The total organic carbon content of core 180 averages 5.5wt%. The sediment is primarily made up of phytoplankton remains, mainly diatom frustules (Vavilova, 1990; Graml, 2001). This explains the high percentage of biogenic silica (opal) and why unaltered $\delta^{15}N$ should more or less correspond to the isotopic signature of the first trophic level. A dilution by higher trophic levels as well as terrestrial detritus (i.e. clay minerals) is considered negligible (Holmes et al., 1998; Pichevin et al., 2005).
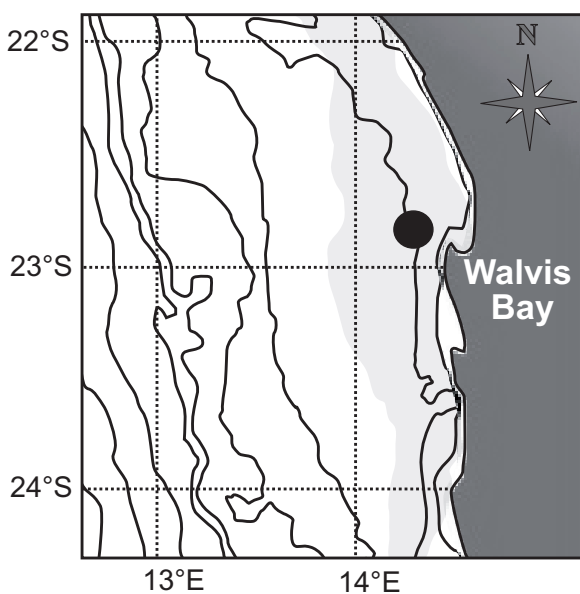
Fig. 1. The provenance of core 180 (22.88°S / 14.41°E; water depth 48 m). The organic-rich diatomaceous ooze coating the inner shelf is shaded grey.

2.2. Sample processing and isotopic measurements

A total of 100 syringe samples were taken at 5 cm-intervals. The sediments were desiccated in a heating oven (40°C) and homogenised using an agate mortar. Each sample was subsequently split into four parts with each subsample being subjected to an individual pre-analysis sample treatment (Fig. 2):

(1) The first measurement series (MS-1) was carried out on ±8 mg of untreated sediment wrapped in tin-foil cups. [N] and [TC] (total carbon) measured relate to the bulk sediment volume.

(2) In MS-2, the material was rinsed, shaken, and centrifuged a total of 3 times at 3000 rpm before being desiccated a second time (40°C). The measurement was carried out on ±8 mg of sediment wrapped in tin-foil cups. Note that only about a quarter of the samples was subjected to this type of treatment (n = 22). As some compounds may be lost during rinsing, [N] and [TC] measured in MS-2 relate to a smaller sediment volume than [N] and [TC] in MS-1. This makes [N] and [TC] appear proportionally larger compared to MS-1.

(3) In order to determine the amount of organic carbon (C_{org}), carbonate needs to be eliminated via acid treatment prior to measurement. Acidification was conducted in two different ways: In the first case (MS-3), the sediment was put into a centrifuge tube and treated with 2N hydrochloric acid. It was then thoroughly rinsed with distilled water and centrifuged a total of 3 times at 3000 rpm. Measurements were made on ±8 mg of dried (40°C) sample material wrapped in tin-foil cups. As some compounds (including carbonate) are lost during rinsing, [N] and [C_{org}] in MS-3 again relate to a smaller sediment volume than [N] and [TC] in MS-1.

(4) In MS-4 the samples were directly acidified in tarred silver cups by adding 2N hydrochloric acid until no more CO_2 was released. Prior to analysis, the acid was allowed to evaporate in the heating oven (40°C). Different from MS-3, [N] and [C_{org}] relate to the bulk sediment volume since no subsequent washing was applied (NB: Note that the sample's weight was taken before adding the acid.).

The isotopic composition of nitrogen ($\delta^{15}N$) and total weight percent (wt%) of carbon and nitrogen were determined with a Thermo Flash EA 1112 Elemental Analyser connected to an isotope-ratio mass-spectrometer (Finnigan, Delta V). The reference gas was pure N_2 nitrogen from a cylinder calibrated against IAEA-standards N-1 and N-2. The external reproducibility of the isotope measurements was

tested with an internal standard (peptone) after every 5th measurement. As regards the concentrations of C and N, reproducibility is ±3% of the original amount present. For $\delta^{15}N$, the analytical precision of the lab standard was ±0.2‰ (1σ standard deviation). The isotope abundance ratios are reported in the conventional δ-notation in per mil (‰) with respect to atmospheric N_2 (AIR).

2.3. Ammonia concentration in the rinsing water

Ammonium (NH_4^+) is a by-product of organic matter decomposition. In organic-rich and anoxic sediments NH_4^+ is abundantly produced and easily preserved.
As outlined below, our findings gave strong reason to believe that NH_4^+ exerts a deceptive influence on the original $\delta^{15}N$- and C_{org}/N record. In order to substantiate that assumption, we decided to test the rinsing water in MS-2 and MS-3 for NH_4^+. The measurements were made on the same selection of samples subjected to MS-2 (n = 22). The concentration of NH_4^+ was measured by means of the photometrical

test 'LCK 303 Ammonium Cuvette Test' of Hach-Lange (http://www.hach-lange.co.uk). For MS-3, the pH was adjusted to 7 by the addition of 1 molar NaOH-solution. The amount of NH_4^+ always lay within the accepted methodological range (2 - 47 mg/l).

3. Results

3.1. Delta^{15}N vs. depth

The down-core distributions of $\delta^{15}N_{HCl}$ and $\delta^{15}N_{untreated}$ are similar in both quality (pattern) and quantity (isotope composition) (Fig. 3a). Both records show large but comparable variations spanning roughly 8 to 15‰ ($\delta^{15}N_{untreated}$) and 9 to 15‰ ($\delta^{15}N_{HCl}$). Median $\delta^{15}N_{HCl}$ (11.4‰) is slightly higher than median $\delta^{15}N_{untreated}$ (10.2‰) (Fig. 3b; Table 1).

Washing with distilled water, irrespective of whether prior acid treatment is included (MS-3) or not (MS-2), entails strong modifications in the down-core development of $\delta^{15}N$ (Fig. 3a; Table 1). In both measurement series, the range of $\delta^{15}N$-variation is
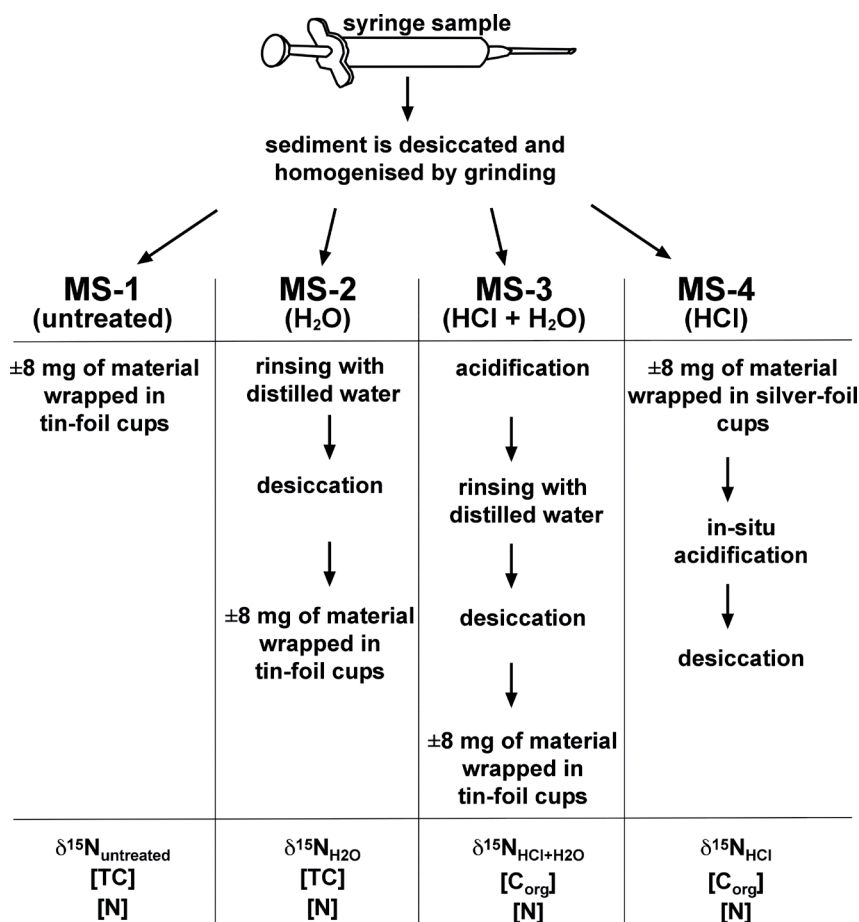
Fig. 2. The single measurement series (MS) in brief. MS-1 and MS-2 yield the total carbon content (TC), whereas, due to the acidification process, MS-3 and MS-4 yield the amount of organic carbon (C_{org}).

Table 1
Standard deviation, median, minimum and maximum values of C_{org}/N and $\delta^{15}N$. MS-2 is limited to a selection of samples (n = 22). Values in brackets are based on this same selection of samples. This is in order to ensure a better comparability of MS-2 with the other measurement series.

	MS-1 untreated	MS-2 H_2O	MS-3 $HCl+H_2O$	MS-4 HCl		MS-1 untreated	MS-2 H_2O	MS-3 $HCl+H_2O$	MS-4 HCl
C_{org}/N					$\delta^{15}N$ (‰)				
standard deviation	0.6 (0.5)	0.7	0.2 (0.2)	0.4 (0.4)	standard deviation	1.7 (1.8)	0.2	0.4 (0.5)	1.4 (1.5)
median	7.2 (7.3)	7.4	7.5 (7.5)	7.3 (7.3)	median	10.2 (10.0)	8.4	8.5 (8.5)	11.4 (11.2)
minimum	5.4 (5.9)	5.5	7.1 (7.2)	5.7 (6.9)	minimum	7.9 (8.3)	8.0	7.8 (7.9)	8.8 (9.3)
maximum	8.9 (8.2)	8.6	8.5 (8.4)	8.7 (7.7)	maximum	14.8 (14.1)	8.7	9.9 (9.9)	14.8 (14.0)

reduced to within the standard error inherent in the method. Both data sets appear much smoother than $\delta^{15}N_{untreated}$.

The lowering from mean 10.2‰ (or 10.0‰; see Table 1) in MS-1, to 8.5‰ in MS-3 and 8.4‰ in MS-2 suggests a mobile phase with comparably high $\delta^{15}N$-values (Fig. 3b). The offsets distinctly exceed the measurement precision and are almost equivalent to the isotopic difference between two trophic levels (Fry, 1988). Given the magnitude of this discrepancy, the records would lead to completely different conclusions regarding nutrient supply and consumption.

3.2. C_{org}/N ratios vs. depth

With MS-3 and MS-4 it is possible to directly calculate C_{org}/N. In contrast, MS-1 and MS-2, not having been acidified, provide no information about $[C_{org}]$. This means that we must derive this information from elsewhere. As regards MS-1, we can easily use $[C_{org}]$ of MS-4, as both [N] from MS-1 and $[C_{org}]$ from MS-4 refer to the bulk sediment volume [a]. This is not possible with MS-2 because [N] refers to an amount smaller than the bulk sediment volume. For the sake of legibility, the calculation of $[C_{org}]$ in MS-2 is shown elsewhere (see caption next to Fig. 4).
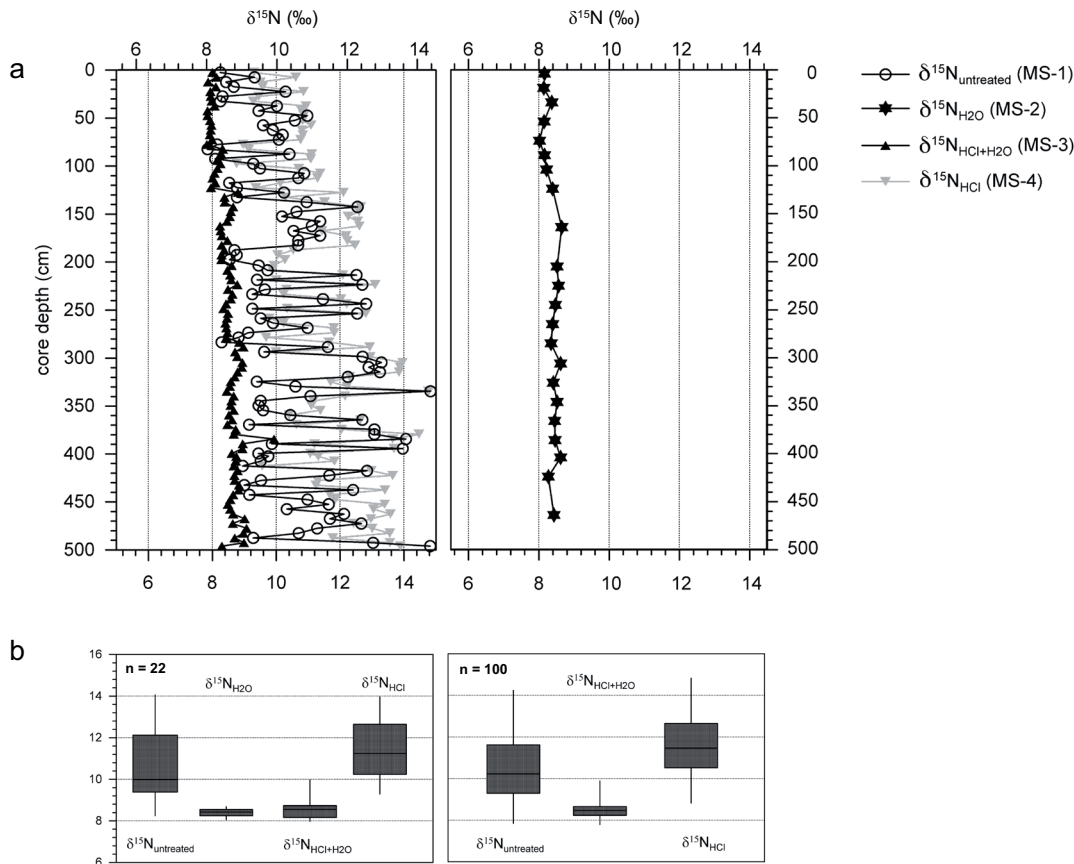
Fig. 3. (a) Downcore development of $\delta^{15}N$. For reasons of clarity, $\delta^{15}N_{H2O}$ (MS-2) is shown separately. (b) Delta^{15}N-data pooled in boxplots. For better comparison of MS-2 with the other measurement series, the boxplots to the left are based on the same selection of samples processed in MS-2.

C_{org}/N ratios are neither affected by washing nor by in-situ acidification. $[C_{org}/N]_{H2O}$ and $[C_{org}/N]_{untreated}$ show a markedly similar development (Fig. 4, right chart) and $[C_{org}/N]_{HCl}$ deviates only sporadically from $[C_{org}/N]_{untreated}$. C_{org}/N strongly reacts, however, to acidification plus rinsing (MS-3). The combination of acidification and rinsing leads to pronounced downcore data-smoothing, accompanied by a slight increase of median C_{org}/N (from 7.2 in untreated material to 7.5 in acidified plus rinsed material; Table 1).

3.3. Ammonium in rinsing water

The rinsing water from MS-2 and MS-3 contains - as expected - significant amounts of ammonium nitrogen. In MS-2, the loss averages 3.5wt%, ranging from 0.4 to 10.8wt% (Fig. 5). In MS-3, the loss averages 6.3wt%, spanning 1.1 to 14wt%. The offset between the losses in MS-2 and MS-3 averages 2.1wt%. Obviously, prior acidification (MS-3) somehow mobilises an even greater quantity of NH_4^+.

4. Discussion

A study of the available literature shows that the effects of sample preparation on δ¹⁵N and C/N are far from unanimous. Bunn et al. (1995), for instance, found that acidification and subsequent rinsing increased the mean δ¹⁵N-signatures of shrimp tissue and decreased those of seagrass to a degree that may confuse the interpretation of food webs. Rinsing is a common practice applied in order to remove acid remains (Stoner and Zimmerman, 1988; Kang et al., 2003) but the fact of the matter is that several authors strongly advise against it in order to minimise the loss of dissolved organic matter (Nieuwenhuize et al., 1994; Bunn et al., 1995; Jacob et al., 2005; Carabel et al., 2006). Still, acidification alone does not guarantee the stability of organic compounds, either: Ng et al. (2007) and Jacob et al. (2005) reported elevated C/N ratios in decalcified sample volumes, suggesting a proportionally greater loss of N relative to C. Moreover, the δ¹⁵N-signature of sedimentary matter (Kennedy et al., 2005; Carabel et al., 2006), marine algae
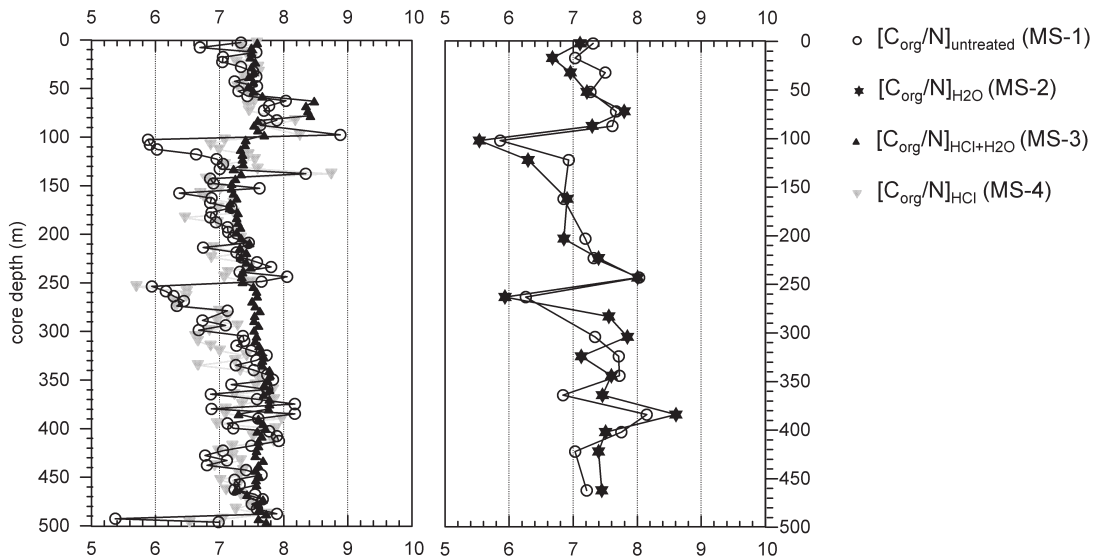
Fig. 4. Downcore development of C_{org}/N. The right chart shows $[C_{org}/N]_{H2O}$ (MS-2) along with the corresponding $[C_{org}/N]_{untreated}$ data (MS-1), revealing their striking similarity. Since rinsing eliminates no carbonate, the amount of organic carbon in MS-2, i.e. $[C_{org}]_{MS-2}$, had to be calculated in an indirect manner.

$[C_{inorg}] = [TC]_{MS-1} - [C_{org}]_{MS-4}$ $[TC]_{MS-1}$ and $[C_{org}]_{MS-4}$ both refer to the bulk sediment volume and are thus comparable (section 2.2.).

$[C_{org}]_{MS-2} = [TC]_{MS-2} - [C_{inorg}]$

Note that $[TC]_{MS-2}$ refers to a smaller sediment volume (due to the loss of various compounds in the course of rinsing) than $[C_{inorg}]$ (which refers to the bulk sediment volume). For this reason, $[C_{inorg}]$ turns out to be slightly underestimated when applied in the equation. The underestimation of $[C_{inorg}]$ results in an overestimation of $[C_{org}]_{MS-2}$ and consequently $[C_{org}/N]_{H2O}$. Overall, however, the error is expected to be small. Besides that, our conclusions are based on down-core patterns rather than absolute values.

---

[a] The δ¹³C-values in MS-4 oscillate minimally around -19.5‰ (not shown), which indicates that the removal of carbonate was complete.
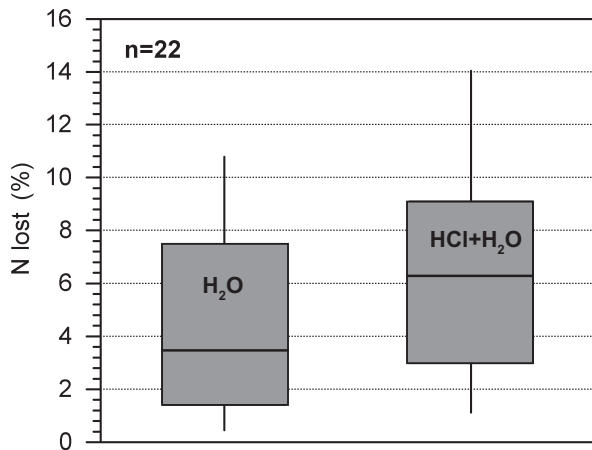
Fig. 5. The amount of NH_4^+-N washed away by the rinsing water in MS-2 (H_2O) and MS-3 ($HCl+H_2O$). The losses relate to the amount of nitrogen present in untreated sediment (MS-1). The measurements were made on the same selection of samples subjected to MS-2 (n = 22). On average, acidification plus rinsing mobilises 2.1% more NH_4^+-N than rinsing alone.

and cyanobacteria (Ng et al., 2007), invertebrates and fish (Jacob et al., 2005) decreased significantly in response to in-situ acidification. In contrast, mollusc tissue (Ng et al., 2007) and algal material examined by Kennedy et al. (2005) proved rather resistant.

In tests conducted by Holmes et al. (1999) neither the application of weak hydrochloric acid nor subsequent rinsing significantly affected sedimentary $\delta^{15}N$.

It clearly shows that the influence of sample preparation is as variable and manifold as the types of material investigated. According to our own results, washing may leave pronounced marks on the $\delta^{15}N$-record while C_{org}/N is only affected when samples are subjected to both acidification and rinsing. The questions are: first, which record can be trusted to provide the prime isotopic signal required for palaeoceanographic reconstructions? Second, can the loss of NH_4^+ be held responsible for the changes of C_{org}/N and $\delta^{15}N$ occurring in the course of sample processing? We pre-empt the answer - yes, there is a variety of evidence that substantiates the influence of ammonium on both C_{org}/N and $\delta^{15}N$.

4.1. The potential impact of NH_4^+ on C_{org}/N and the role of carbonate

C_{org}/N ratios are a widely used instrument in distinguishing between marine and terrestrial organic matter (Schubert and Calvert, 2001). The observation that NH_4^+ is capable of biasing the original C/N ratio and causing misinterpretation is not new. Several studies have already reported fixation and adsorption of NH_4^+ in and onto clay minerals and accordingly low C/N ratios (e.g. Müller, 1977 and ref. therein; Rosenfeld, 1979; von Breymann and Suess, 1988; Schubert and Calvert, 2001; Morse and Morin, 2005). In core 180, clay minerals are negligible and so is their significance in this context. There must be another reason for the observed deviations of C_{org}/N. On the evidence of the excellent correlation between [$CaCO_3$] and C_{org}/N in MS-1 (Fig. 6a), carbonate appears to be the key to the answer.

Due to the alkaline nature of the carbonate ion (CO_3^{2-}), the pH of the interstitial water is slightly raised while carbonate dissolves (Faure, 1992). An increasing pH promotes the adsorption of dissolved ammonium ions to silicate surfaces (Brunelle, 1978). Biogenic silica is abundant in the form of diatom frustules (section 2.1.). The isoelectronic point of silica is around pH 1 [b]. However, the negative polarisation of silicate surfaces only becomes significant at a pH above 7. This is the threshold above which the amount of NH_4^+ adsorbed to silica surfaces increases rapidly (Brunelle, 1978). The pH in marine sediments oscillates around 8, held more or less stable due to the buffering qualities of ammonium and carbonate (Ben-Yaakov, 1973). At these pH-ranges (pH > 7) even slight changes in the H^+/OH^--ratio have pronounced effects on NH_4^+-adsorption (Brunelle, 1978).

The negative correlation between C_{org}/N and [$CaCO_3$] in MS-1 (Fig. 6a) is ascribed to the combination of NH_4^+-adsorption and -outgassing: The amount of adsorbed ammonium rises along with the carbonate content as the adsorption capacity of SiO_2 is enhanced at higher pH-values. At the same time, it is predominantly adsorbed (as opposed to dissolved) ammonium that is kept from outgassing in the form of NH_3 in the heating oven (more on the ammonium loss due to outgassing in the following chapter).

Note that our reasoning requires the pore water to be undersaturated with respect to carbonate (if the solution was already supersaturated, rising [$CaCO_3$]

---

[b] The isoelectric point (IEP) is the pH at which a particular molecule carries no net electrical charge. The surfaces of mineral oxides that are surrounded by a solution with a pH higher than its IEP result negatively charged which is compensated for by adsorbed cations. The reverse ist true if the particle is dipped in a medium with a pH lower than its IEP (Brunelle, 1978).

would not lead to enhanced dissociation of $CaCO_3$), a prerequisite that is met by the high partial pressures of CO_2 (produced by OM matter decay) and the comparably low temperatures (Faure, 1992).

Also note that NH_4^+ has NH_3 as a conjugate base. This implies that the amount of NH_4^+ decreases in favour of NH_3 as the pH rises. However, this effect is seemingly outweighed by the concomitantly increasing adsorption capacity of SiO_2 as the pH increases. The fact that the solubility of SiO_2 increases as the pore waters get more basic (Brunelle, 1978; Faure, 1992) does not disturb the pattern either.

Acidification plus rinsing has a considerable impact on the C_{org}/N ratios. In MS-3, the originally inverse correlation between $[CaCO_3]$ and C_{org}/N is completely erased (Fig. 6c). Lower C_{org}/N ratios of carbonate-rich sample splits are adapted to the C_{org}/N ratios in carbonate-poor sample splits and mean C_{org}/N is slightly raised (see also Table 1).

What happens in the course of acidification plus rinsing? As the pH is lowered, the SiO_2-adsorption capacity diminishes and the SiO_2-surfaces result over-saturated with respect to ammonium. Ammonium is released into the water and carried away in the course of rinsing. C_{org}/N consequently rises.

In-situ acidification (MS-4) brings about the same release of formerly adsorbed NH_4^+. However, in contrast to MS-3, the liberated NH_4^+-molecules are not washed away. In the heating oven some of them outgas to form gaseous NH_3 (see below). This outgassing is considered the reason for the disturbance of the originally inverse correlation between $[CaCO_3]$ and C_{org}/N (Fig. 6d).

Note that the amount of ammonium lost in MS-2 still averages more than half of the amount lost in MS-3 (Fig. 5). Assuming that rinsing alone releases hardly any adsorbed NH_4^+, the bulk of the ammonium lost in MS-2 represents dissolved NH_4^+. If this hypothesis is right, how is it that the leaching of dissolved NH_4^+

does not result in rising C_{org}/N ratios? $[C_{org}/N]_{untreated}$ and $[C_{org}/N]_{H2O}$ are virtually identical (Figs. 4 and 6b). The most likely explanation is the simultaneous loss of dissolvable organic matter with high C_{org}/N ratios: Organic matter that has already been subjected to some microbial activity usually exhibits higher C_{org}/N ratios than fresh organic matter. This is because nitrogen is more susceptible to decay than carbon and, therefore, preferentially lost (Rosenfeld, 1981; Lehmann, et al. 2002).
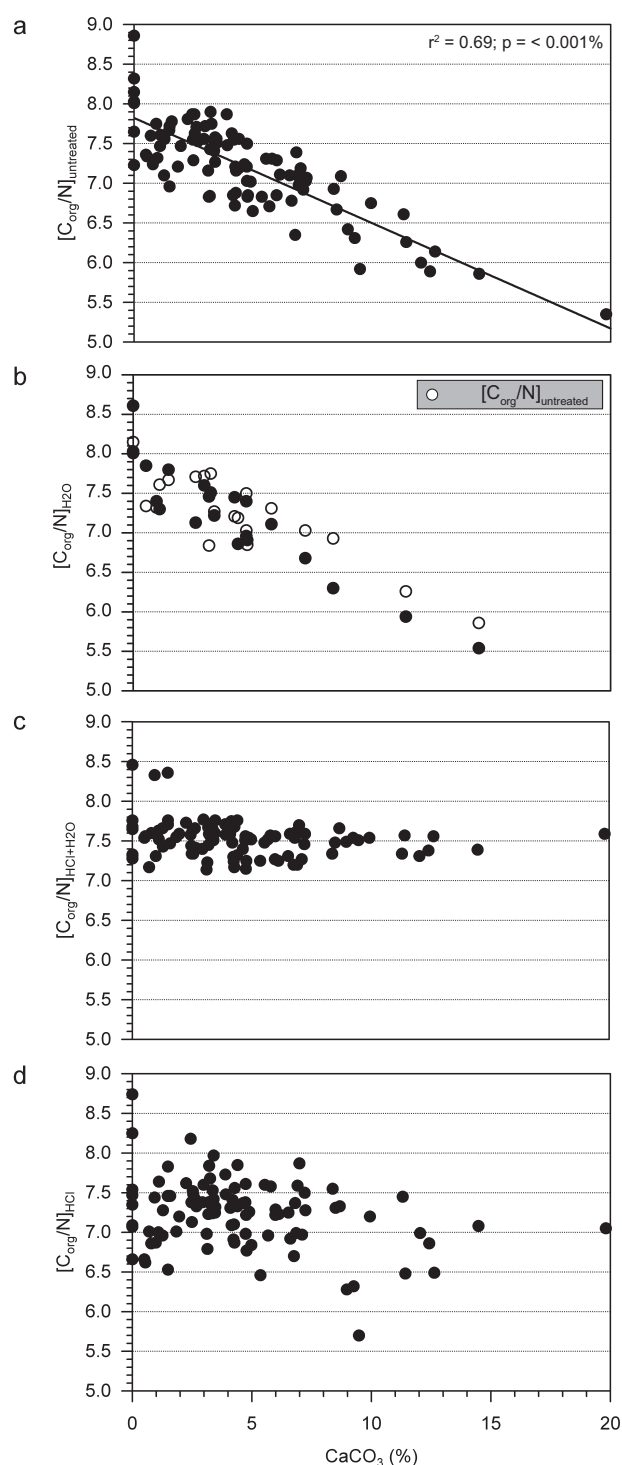
Fig. 6. C_{org}/N vs. $[CaCO_3]$: $[CaCO_3]$ was calculated by subtracting $[C_{org}]$ (MS-4) from the total amount of carbon (MS-1). The resulting amount of inorganic carbon was multiplied by 8.33, according to the molar relationships in $CaCO_3$.

$$CaCO_3 = ([TC]_{MS-1} - [C_{org}]_{MS-4}) \times 8.33$$

The negative correlation in (a) testifies to the increasing number of NH_4^+-ions adsorbed to negatively charged SiO_2-surfaces, the higher the amount of carbonate. The dissolution of carbonate lifts the pH in the interstitial water, which increases the surface polarisation and adsorption capacity of SiO_2. The higher the percentage of adsorbed NH_4^+-ions the lower the N-loss due to outgassing. Acidification lowers the adsorption capacity of SiO_2, causing the release of adsorbed NH_4^+-ions. During subsequent rinsing they are washed away with the rinsing water. This is why the negative correlation is completely erased in MS-3 (c).

Apparently these compounds are sufficiently unstable to be leached away together with dissolved NH_4^+, thus inhibiting the increase in C_{org}/N. In contrast, acidification plus rinsing is capable of additionally mobilising originally adsorbed NH_4^+; this additional loss leads to the observed increase of C_{org}/N ratios in MS-3.

The weakness of the correlations notwithstanding, Fig. 7 substantiates our hitherto held ideas and confirms the control of carbonate, or rather pH, on the mobility of NH_4^+ in MS-2 and MS-3. The less $CaCO_3$, the less adsorbed NH_4^+ and the greater the loss during rinsing (Fig. 7a). The positive correlation in Fig. 7b further corroborates the assumption that acidification plus rinsing (MS-3) mobilises both adsorbed and dissolved NH_4^+, while rinsing alone (MS-2) mobilises only the latter.

4.2. The potential impact of NH_4^+ on $\delta^{15}N$

Rinsing caused average $\delta^{15}N$ to drop by 1.6‰ (Fig. 3b; Table 1). According to our above line of reasoning, rinsing does predominantly (if not exclusively) mobilise dissolved NH_4^+. This implies a $\delta^{15}N$-enrichment in dissolved NH_4^+ compared to the resid-

ual sediment. The ^{15}N-enrichment in dissolved NH_4^+ may be due to nitrogen isotope fractionation during the drying process. When NH_4^+ transforms to gaseous NH_3, the light isotope (^{14}N) may accumulate in the gaseous phase, thus leaving ^{15}N-enriched NH_4^+ behind (Fig. 8b). The process is comparable to kinetic isotope fractionation of oxygen isotopes during the vaporisation of water and can reach pronounced proportions. In a study conducted on simulated urine patches on grassland soils, the isotopic composition of the NH_3 volatilised was depleted by up to almost 30‰ compared to the original urea-N added (Frank et al., 2004).

The inverse relation between $\delta^{15}N$ and [N] in untreated material (Fig. 9a) substantiates that ammonia volatilisation - accompanied by the discrimination against ^{15}N - is taking place. The outgassing of ^{15}N-depleted NH_3 results both in the reduction of [N] and an increase of the $\delta^{15}N$-signatures. After rinsing, the negative correlation is completely erased (Fig. 9b); this agrees with the leaching of ^{15}N-enriched ammonium ions as illustrated in Fig. 8c.

Acidification plus rinsing (MS-3) and rinsing alone (MS-2) yield extremely similar $\delta^{15}N$-patterns (Figs. 3, 9b and 9c). Apparently, the mobilisation of originally
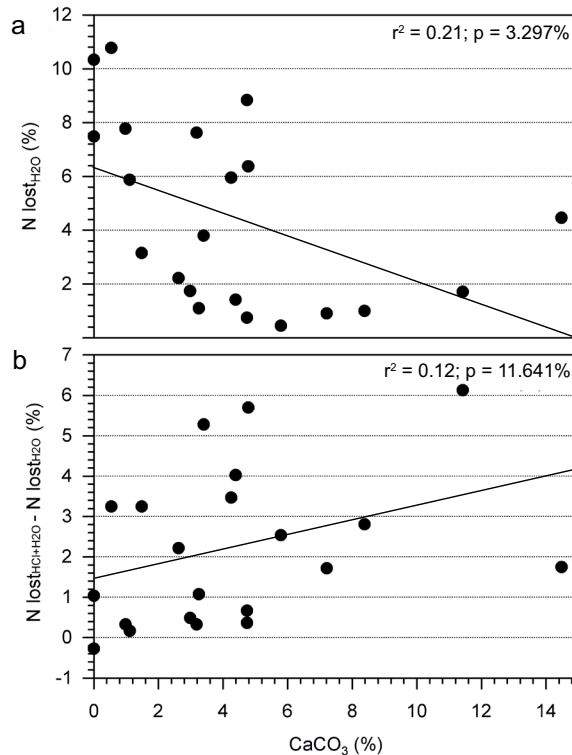
Fig. 7. The control of $CaCO_3$ on the fate of NH_4^+ during sample treatment. Both charts substantiate the ability of $CaCO_3$ to promote NH_4^+-adsorption. (a) Samples containing lower carbonate tend to loose more NH_4^+ during rinsing (MS-2). This is attributed to the slightly lower pH of the pore waters, the consequently less negative surface charge of the SiO_2-particles and the higher percentage of NH_4^+ dissolved in interstitial waters. Chart (b) testifies to the rising proportion of adsorbed NH_4^+ as carbonate and the pH increases. Acidification plus rinsing mobilises both adsorbed and dissolved NH_4^+ while rinsing alone mobilises only dissolved NH_4^+. At low $CaCO_3$, where only few NH_4^+ is adsorbed, the offset between N lost$_{HCl+H2O}$ and N lost$_{H2O}$ tends to be low. The increasing offset with higher [$CaCO_3$] is due to the rising proportion of adsorbed NH_4^+ and its loss in the course of acidification plus rinsing.

adsorbed NH_4^+ in MS-3 has no additional effect on the isotopic signature of the sediment. This suggests that adsorbed NH_4^+ is resistant to both the outgassing and fractionation during the drying process (Figs. 8b and 8d).

On the basis of the available evidence, $\delta^{15}N$ is strongly controlled by dissolved NH_4^+. As outlined in the above section, the amount of dissolved NH_4^+ depends on the adsorption capacity of SiO_2, which co-varies with the amount of carbonate, or rather, the pH of the interstitial waters. The lower the carbonate content, the lower the pH and the higher the amount of dissolved NH_4^+, which is the fraction liable to fractionation in the heating oven. Fig. 10 reflects the anticipated relationship between carbonate and $\delta^{15}N$ reasonably well. The lower the carbonate content, the more pronounced the shift towards higher $\delta^{15}N_{untreated}$-values (Fig. 10a). Due to the leaching of isotopically "heavy" NH_4^+-molecules in both MS-2 and MS-3, the negative correlation is lost and average $\delta^{15}N$ is again lowered (Figs. 10b and 10c).

In-situ acidification (MS-4) increases the amount of dissolved NH_4^+-molecules (Fig. 8e) compared to the amount already present in the original sediment (Fig. 8b). This enhances the loss of ^{15}N-depleted NH_3 during desiccation and might explain why average $\delta^{15}N_{HCl}$ is slightly higher than average $\delta^{15}N_{untreated}$ (Fig. 3b). Fig. 10d furthermore reveals that the increase of $\delta^{15}N$ is more pronounced where $CaCO_3$ is abundant, i.e. where we expect a higher proportion of NH_4^+ to be released.

The presence of NH_4^+ seems equally problematic with $\delta^{15}N$ as with C_{org}/N. NH_4^+ is generated during OM decayal. As our data indicates, the decayal itself does not seem to produce the observed ^{15}N-enrichment in the residual sediment. This is worth noting because it disagrees with the widely held belief in nitrogen isotope fractionation during protein hydrolysis (e.g. Melander, 1960; Gaebler et al., 1966; Saino and
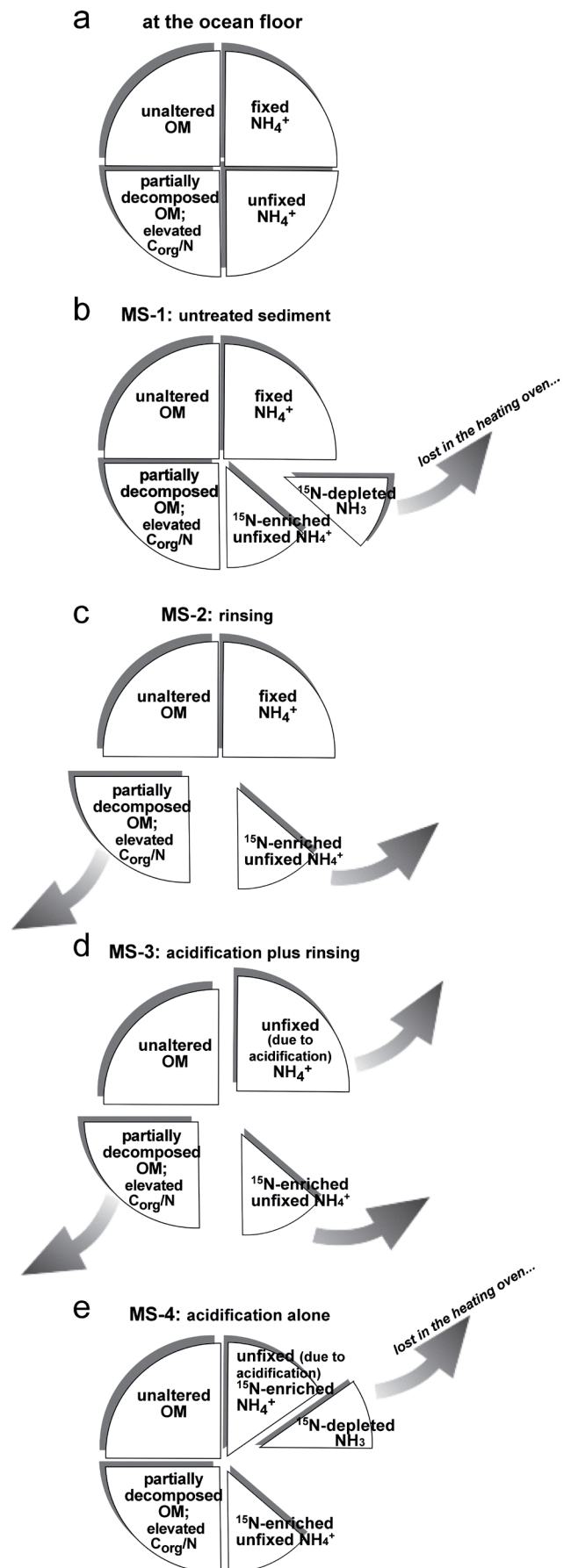
Fig. 8. Schematic summary of the processes occurring during various methods of sample preparation. Arrows mark the fractions lost during processing. Chart (a) identifies the fractions that are relevant as regards the modification of C_{org}/N and $\delta^{15}N$ during sample treatment. NH_4^+ is excreted in the course of organic matter (OM) decayal, leaving partially decomposed OM with elevated C_{org}/N behind. If not stated otherwise, C_{org}/N and $\delta^{15}N$-values reflect unaltered OM.

In the heating oven, some of the dissolved NH_4^+ is lost in the form of ^{15}N-depleted NH_3, thus leaving a ^{15}N-enriched residual behind (b). (c) Rinsing mobilises intermediate and by-products resulting from deanimation reactions, exept for adsorbed NH_4^+. Adsorbed NH_4^+-ions are released during acidification. (d) The subsequent rinsing in MS-3 induces their loss. (e) In MS-4, unfixed NH_4^+ are not washed away but fractionate during desiccation, thereby increasing the ^{15}N-enrichment in the residual.
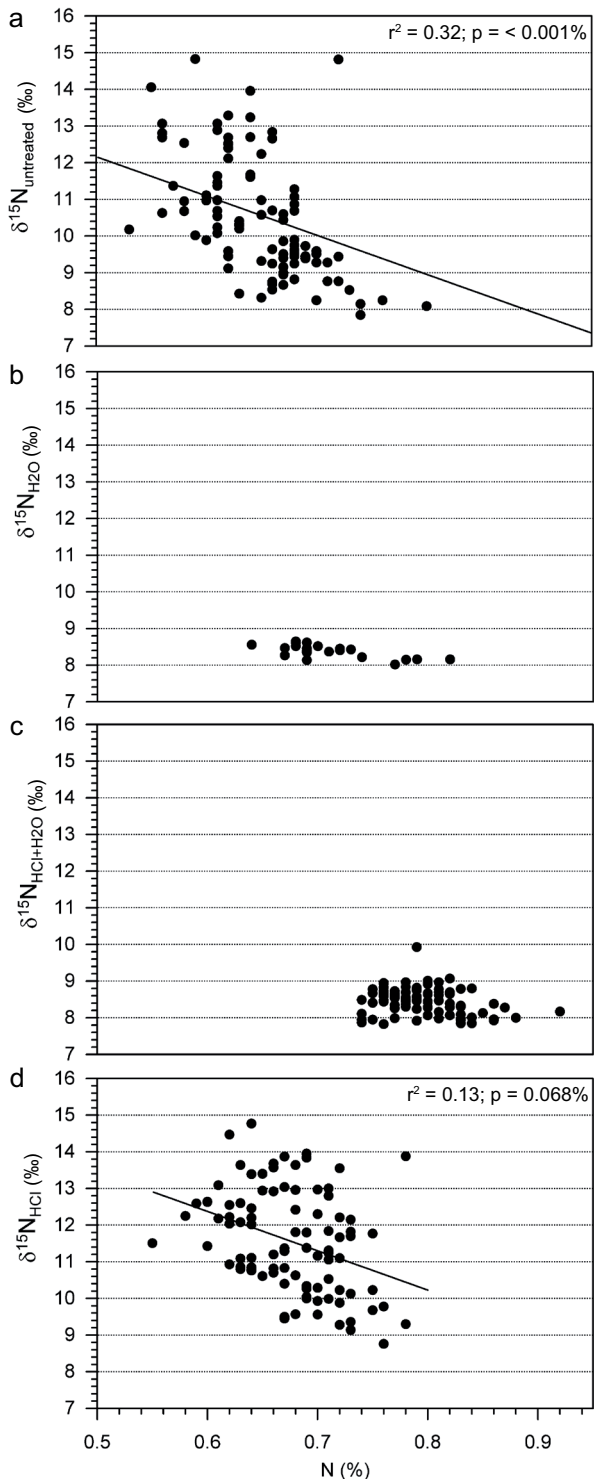
Fig. 9. $\delta^{15}N$ vs. [N]. Dissolved NH_4^+ is lost in the form of gaseous, ^{15}N-depleted NH_3. (a) Its outgassing results in the simultaneous reduction of [N] and accumulation of ^{15}N-enriched NH_4^+ in the residual, hence the inverse relation. (b, c) The negative correlation is erased in both MS-2 and MS-3, implying that rinsing alone provokes the leaching of ^{15}N-enriched NH_4^+. The acid-induced loss of adsorbed NH_4^+ in MS-3 has no additional influence on $\delta^{15}N$, because adsorbed NH_4^+ has not undergone any fractionation. (d) As ^{15}N-enriched NH_4^+ is not washed away in MS-4, the negative correlation remains.

NB: In MS-1 and MS-4, [N] refers to the bulk sediment volume. In MS-2 and MS-3, the sample splits have already undergone processing and consequently lost a certain amount of components when being weighed. This is why the percentage of [N] appears somewhat higher in MS-2 and MS-3 (b, c).

Hattori, 1980; Altabet and McCarthy, 1985; Schäfer and Ittekkot, 1993; Altabet and Francois, 1994; Montoya, 1994; Ostrom et al., 1997; Sachs and Repeta, 1999).

What makes us so certain that deanimation occurred without fractionation is that MS-2 and MS-3 yield so markedly similar $\delta^{15}N$-signatures (Fig. 3b). The acid-induced mobilisation of adsorbed NH_4^+ in MS-3 does not additionally influence the isotopic signature of the sediment. Apparently, adsorbed NH_4^+ is unfractionated per se. Its $\delta^{15}N$-signature seemingly corresponds to that of fresh organic matter, otherwise its loss during acidification plus rinsing should have induced additional isotopic shifts. Our data clearly demonstrates that the observed shift towards higher $\delta^{15}N$-signals in MS-1 truly results from kinetic isotope fractionation during the drying process, i.e. during the transformation of NH_4^+ to gaseous NH_3.

4.3. Which record to trust

It appears that the use of untreated material for $\delta^{15}N$-analyses is not, contrary to popular belief (section 1.), advisable a priori. Our findings have shown that the down-core scattering of $[C_{org}/N]_{untreated}$ and $\delta^{15}N_{untreated}$ is primarily to be ascribed to the misleading influence of NH_4^+, rather than being indicative of environmental fluctuations.

If interested in the original signal, it is recommended that NH_4^+ be removed prior to measuring $\delta^{15}N$ and C_{org}/N. This appears to be done best by a combination of acidification and subsequent rinsing (MS-3). Acidification plus rinsing eliminates the effects of NH_4^+-adsorption and -outgassing and restores the original signal of both C_{org}/N and $\delta^{15}N$. If $\delta^{15}N$ is the sole parameter of interest, it is enough to remove dissolved NH_4^+ as it is only dissolved NH_4^+ that undergoes fractionation during desiccation; then rinsing alone suffices (MS-2) in order to eliminate the decomposition-, or more precisely, outgassing-derived shift towards higher $\delta^{15}N$-signals.

5. Conclusions and recommendations

[1] Our data provide strong evidence of nitrogen isotope fractionation during desiccation when NH_4^+ transforms into gaseous NH_3. Thereby, ^{14}N accumulates in the gaseous phase, thus leaving ^{15}N-enriched NH_4^+ behind.

[2] The outgassing and fractionation only concerns NH_4^+-ions dissolved in the pore waters. In contrast, NH_4^+-molecules adsorbed to negatively-charged SiO_2-surfaces remain unaffected. The adsorption capacity

of SiO_2 increases with increasing pH, i.e. rising carbonate content.

[3] We conclude that excessive confidence in untreated material is inappropriate when NH_4^+-molecules are involved: Ammonia volatilisation is capable of producing misleading fluctuations in $\delta^{15}N_{untreated}$ without any environmentally-triggered background. Our results clearly indicate that the higher the amount of dissolved NH_4^+, the more we must suspect unwanted shifts towards higher $\delta^{15}N$ in untreated sediment. At the same time, it remains unclear how many of the dissolved NH_4^+-ions turn into gaseous NH_3. Due to this uncontrollable and variable outgassing, $[C_{org}/N]_{untreated}$ is likewise considered unreliable.

[4] Acidification plus rinsing seems capable of wiping out the effects of NH_4^+-adsorption and -outgassing and associated distortions of $\delta^{15}N$ and C_{org}/N: Acidification reduces the negative surface polarisation of SiO_2 and liberates adsorbed ammonium ions. Subsequent rinsing ideally mobilises all decomposition-derived intermediate products, including both dissolved and formerly bound ammonium. Certainly we cannot exclude the possibility of parts of "fresh" organic matter being concomitantly washed away.

[5] In organic-rich and anoxic sediments, where the conditions are favourable for the presence of NH_4^+, we assume acidified and rinsed material to deliver the trustworthiest record with decayal-derived influences being eliminated.

Several authors have called for a standardisation of pre-analysis sample treatment, fearing that the different methodology may hamper the comparability of data (e.g. Jacob et al., 2005; Ng et al., 2007). We do only support this view as long as it is the same type of material analysed.

Due to compositional differences, however, sediments may require completely different approaches in order to overcome possible misinterpretations of C_{org}/N ratios and $\delta^{15}N$-values (e.g. Schubert and Calvert, 2001). The chemistry of the interstitial waters, the porosity and the solid/water ratio are further aspects to consider.

Our results certainly do not warrant any generalisation. Instead, they highlight the importance of carefully investigating the varying effects of different processing methods, rather than following a simple recipe. It is recommended that random measurements be conducted on acidified plus rinsed sample splits in addition to untreated material, in order to better evaluate the potential influence of ammonium on $\delta^{15}N$ and C_{org}/N.
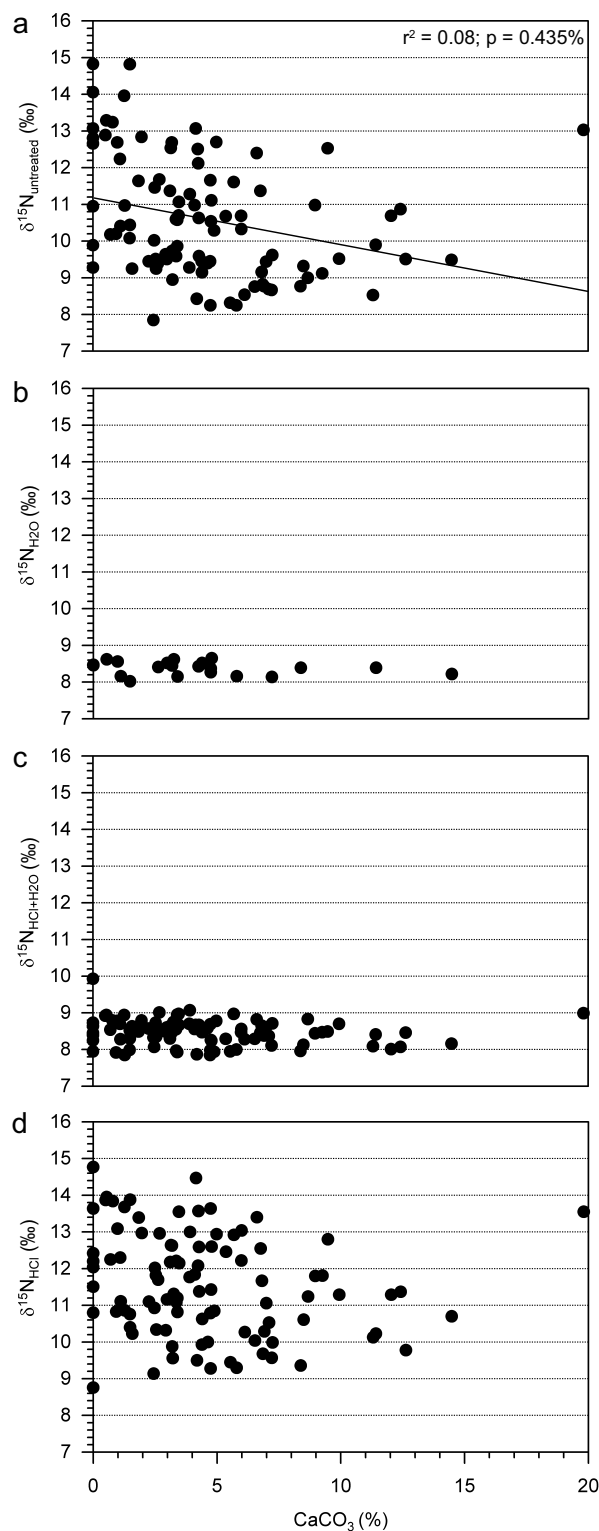
Fig. 10. $\delta^{15}N$ vs. $[CaCO_3]$. The negative correlation in MS-1 (a) reflects the enhanced outgassing of ^{15}N-depleted NH_3 the lower the amount of carbonate, i.e. the lower the negative surface polarisation of SiO_2. Only dissolved NH_4^+ is able to outgas and fractionate. For further details see text.

References

Altabet, M.A., McCarthy, J.J., (1985) Temporal and spatial variations in the natural abundance of ^{15}N in PON from a warm-core ring. *Deep-Sea Research*, 32, 755-772.

Altabet, M.A., Francois, R., (1994) Sedimentary nitrogen isotopic ratio as a recorder for surface ocean nitrate utilization. *Global Biogeochemical Cycles*, 8, 103-116.

Bakun, A., Weeks, S.J., (2004) Greenhouse gas buildup, sardines, submarine eruptions and the possibility of abrupt degradation of intense marine upwelling ecosystems. *Ecology Letters*, 7, 1015-1023.

Ben-Yaakov, S., (1973) pH Buffering of Pore Water of Recent Anoxic Sediments. *Limnology and Oceanography,* 18(1), 86-94.

Bouillon, S., Raman, A.V., Dauby, P., Dechairs, F., (2002) Carbon and nitrogen isotope ratios of subtidal benthic invertebrates in an estuarine mangrove ecosystem (Andhra Pradesh, India). *Estuarine, Coastal and Shelf Science*, 54, 901-913.

Bremner, J.M., Willis, J.P., (1993) Mineralogy and geochemistry of the clay fraction of sediments from the Namibian continental margin and the adjacent hinterland. *Marine Geology*, 115, 85-116.

Brüchert, V., Altenbach, A.V., Bening, G., Bockelmann, F., Currie, B., Donath, J., Dübecke, J., Endler, R., Erdmann, S., Ertan, T., Fuchs, B., Klockgether, G., Krüger, S., Kuypers, M.M.M., Lass, H.U., Lavik, G., Lilienthal, S., Leipe, T., Nickel, G., Noli-Peard, K., Ohde, T., Schulz, B., Schulz, H., Siegel, H., Struck, U., Wulf, J., Zitzmann, S., Zonneveld, K., (2004) The Benguela Upwelling System 2003, Part 3, Cruise No. 57, Leg 3, March 15 – April 13, 2003, Walvis Bay, Namibia - Dakar. In: *Meteor Berichte*, *4*, pp. 53.

Bunn, S.E., Loneragan, N.R., Kempster, M.A., (1995) Effects of acid washing on stable isotopes ratios of C and N in penaeid shrimp and seagrass: implications for food-web studies using multiple stable isotopes. *Limnology and Oceanography*, 40(3), 622-625.

Carabel, S., Godínez-Domínguez, E., Verísimo, P., Fernández, L., Freire, J., (2006) An assessment of sample processing methods for stable isotope analyses of marine food webs. *Journal of Experimental Marine Biology and Ecology*, 336, 254-261.

Emeis, K.-C., Brüchert, V., Currie, B., Endler, R., Ferdelman, T., Kiessling, A., Leipe, T., Noli-Peard, K., Struck, U., Vogt, T., (2004) Shallow gas in shelf sediments of the Namibian coastal upwelling ecosystem. *Continental Shelf Research*, 24(6), 627-642.

Faure, G., (1992) *Principles and applications of inorganic geo-chemistry - A comprehensive textbook for geology students*. Maxwell Macmillan International Editions, New York, Toronto, Oxford.

Frank, D.A., Evans, R.D., Tracy, B.F., (2004) The role of ammonia volatilization in controlling the natural ^{15}N abundance of a grazed grassland. *Biogeochemistry*, 68, 169-178.

Fry, B., (1988) Food web structure on Georges Bank from stable C, N, and S isotopic compositions. *Limnology and Oceanography*, 33, 1182-1190.

Gaebler, O.H., Vitti, T.G., Vukmirovich, R., (1966) Isotope effects in metabolism of ^{14}N and ^{15}N from unlabeled dietary proteins.

Canadian Journal of Biochemistry, 44, 1249-1257.

Goering, J., Alexander, V., Haubenstock, N., (1990) Seasonal variability of stable carbon and nitrogen isotope ratios of organism in a North Pacific Bay. *Estuarine, Coastal and Shelf Science*, 30(239-260).

Graml, M., (2001) Sedimentfazielle- und isotopenanalytische Untersuchungen an rezenten Schelfsedimenten im Auftriebsgebiet des Süd-Ost-Atlantiks vor Namibia. In: *Institut für Paläontologie und Historische Geologie*, pp. 63. Ludwig-Maximilians-Universität, Munich.

Holmes, M.E., Müller, P.J., Schneider, R.R., Segl, M., Wefer, G., (1998) Spatial variations in euphotic zone nitrate utilization based on $\delta^{15}N$ in surface sediments. *Geo-Marine Letters*, 18(1), 58-65.

Holmes, B., Eichner, C., Struck, U., Wefer, G., (1999) Reconstructions of surface ocean nitrate utilization using stable nitrogen isotopes in sinking particles and sediments. In: *Use of Proxies in Paleoceanography: Examples from the South Atlantic* (Ed. by G. Fischer, G. Wefer), pp. 447-468. Springer, Berlin.

Jacob, U., Mintenbeck, K., Brey, T., Knust, R., Beyer, K., (2005) Stable isotope food web studies: a case for standardized sample treatment. *Marine Ecology Progress Series*, 287, 251-253.

Kang, C.-K., Kim, B.J., Lee, K.-S., Kim, J.B., Lee, P.-Y., Hong, J.-S., (2003) Trophic importance of benthic microalgae to macrozoobenthos in coastal bay systems in Korea: dual stable C and N isotope analyses. *Marine Ecology Progess Series*, 259, 79-92.

Kennedy, P., Kennedy, H., Papadimitriou, S., (2005) The effect of acidification on the determination of organic carbon, total nitrogen and their stable isotopic composition in algae and marine sediment. *Rapid Communications in Mass Spectrometry*, 19, 1063-1068.

Lehmann, M.F., Bernasconi, S.M., Barbieri, A., McKenzie, J.A., (2002) Preservation of organic matter and alteration of its carbon and nitrogen isotope composition during simulated and in situ early sedimentary diagenesis. *Geochimica et Cosmochimica Acta*, 66, 3573-3584.

Melander, L., (1960) *Isotope effects on reaction rates*. Ronald Press, New York.

Montoya, J.P., (1994) Nitrogen isotope fractionation in the modern ocean: Implications for the sedimentary record. In: *Carbon Cycling in the Glacial Ocean: Constraints on the Ocean´s Role in Global Change.*, *17*, *NATO ASI Series* (Ed. by R. Zahn, T.F. Pedersen, M.A. Kaminski, L. Labeyrie), pp. 259-279. Springer-Verlag, Berlin.

Müller , P.J., (1977) C/N ratios in Pacific deep-sea sediments: Effect of inorganic ammonium and organic nitrogen compounds sorbed by clays. *Geochimica et Cosmochimica Acta*, 41(6), 765-776.

Ng, J.S.S., Wai, T.-C., Williams, G.A., (2007) The effects of acidification on the stable isotope signatures of marine algae and molluscs. *Marine Chemistry*, 103, 97-102.

Nieuwenhuize, J., Maas, Y.E.M., Middelburg, J.J., (1994) Rapid analysis of organic carbon and nitrogen in particulate materials. *Marine Chemistry*, 45, 217-224.

Ostrom, N.E., Macko, S.A., Deibel, D., Thompson, R.J., (1997) Seasonal variation in the stable carbon and nitrogen isotope biogeochemistry of a coastal cold ocean environment. *Geochimica et Cosmochimica Acta*, 61(14), 2929-2942.

Pichevin, L., Martinez, P., Bertrand, P., Schneider, R., Giraudeau, J., Emeis, K., (2005) Nitrogen cycling on the Namibian shelf and slope over the last two climatic cycles: Local and global forcings. *Paleoceanography*, 20.

Rosenfeld, J.K., (1981) Nitrogen diagenesis in Long Island Sound sediments. *American Journal of Sciences*, 281, 436-462.

Sachs, J.P., Repeta, D.J., (1999) Oligotrophy and nitrogen fixation during eastern Mediterranean sapropel events. *Science*, 286, 2485-2488.

Saino, T., Hattori, A., (1980) ^{15}N natural abundance in oceanic suspended particulate matter. *Nature*, 283, 752-754.

Schäfer, P., Ittekkot, V., (1993) Seasonal variability of $\delta^{15}N$ in settling particles in the Arabian Sea and its paleogeochemical significance. *Naturwissenschaften*, 80, 511-513.

Schubert, C.J., Calvert, S.E., (2001) Nitrogen and carbon isotopic composition of marine and terrestrial organic matter in Arctic Ocean sediments: implications for nutrient utilization and organic matter composition. *Deep-Sea Research I*, 48, 789-810.

Shannon, L.V., O'Toole, M.J., (1999) Integrated Overview of the Oceanography and Environmental Variability of the Benguela Current Region - Thematic Report NO.2. In: *Synthesis and Assessment of Information on the Benguela Current Large Marine Ecosystem (BCLME)*, Windhoek, Namibia.

Stoner, A.W., Zimmerman, R.J., (1988) Food pathways associated with penaeid shrimps in a mangrove-fringed estuary. *Fisheries Bulletin*, 86, 543-552.

Struck, U., Emeis, K.-C., Alheit, J., Schneider, R., Eichner, C., Altenbach, A.-V., (2002) Changes of the upwelling rates of nitrate preserved in the $\delta^{15}N$-signature of sediments and fish scales from the diatomaceous mud belt off Namibia. *GeoBios*, 35(EPA-special issue), 3-11.

Thornton, S.F., McManus, J., (1994) Application of organic carbon and nitrogen stable isotope and C/N ratios as source indicators of organic matter provenance in estuarine systems: evidence from the Tay Estuary, Scotland. *Estuarine, Coastal and Shelf Science*, 38, 219-233.

Vavilova, V.V., (1990) Marine biology: phytoplankton of the Benguela upwelling system off Namibia in the austral summer of 1985. *Oceanology*, 30, 472-477.

Weeks, S.J., Currie, B., Bakun, A., Peard, K.R., (2004) Hydrogen sulphide eruptions in the Atlantic Ocean off southern Africa: implications of a new view based on SeaWiFS satellite imagery. *Deep-Sea Research I*, 51, 153-172.

Nutrient dynamics and oceanographic features in the central Namibian upwelling region as reflected in δ^{15}N-signals of suspended matter and surface sediments

Sandra Meisel [a], Ulrich Struck [a,*], Kay-Christian Emeis [b]

[a] Museum für Naturkunde, Leibniz-Institut für Evolutions- und Biodiversitätsforschung
    an der Humboldt-Universität zu Berlin, Invalidenstraße 43, 10115 Berlin, Germany

[b] Institut für Biogeochemie und Meereschemie, Universität Hamburg, Bundesstr. 55, 20146 Hamburg, Germany

KEYWORDS

Benguela Current,
denitrification,
nitrogen isotopes,
nutrient utilisation,
suspended matter,
two-celled upwelling

ABSTRACT

The study deals with the modern situation of the northern Benguela Upwelling, directing particular attention to the shelf region off central Namibia (21 to 24°S). At the centre of the investigation is the comparison of δ^{15}N-records in surface sediments (δ^{15}N$_{sediment}$) with suspended particulate matter (δ^{15}N$_{SPM}$) from the surface ocean. In addition to that, water column profiles (including hydrographic data) provide an insight into changes of δ^{15}N$_{SPM}$ with depth and elucidate potential offsets between δ^{15}N$_{SPM}$ and δ^{15}N$_{sediment}$.

The parallel spatial trend of δ^{15}N$_{sediment}$ and surface ocean δ^{15}N$_{SPM}$ shows that secondary processes are not so pronounced as to obliterate the signal generated in the surface waters. Highest δ^{15}N-signatures are found right off the coast where water temperatures are lowest. Concomitantly high productivity rates and low bottom oxygen suggest the upwelling of denitrified source waters. With increasing distance offshore, δ^{15}N declines unexpectedly, reaching a minimum above the shelf break. Beyond that, the trend reverses to "normal" with δ^{15}N-signals continuously increasing towards the mesopelagic ocean.

The decrease in δ^{15}N$_{sediment}$ and surface ocean δ^{15}N$_{SPM}$ with increasing distance to the coast disagrees with the concept of Rayleigh fractionation kinetics, viz. the progressive ^{15}N-enrichment of the nitrate pool as it is gradually used up by phytoplankton growth. On the basis of the available evidence, the downward trend of δ^{15}N results from decreased relative nitrate consumption, resting on a combination of reduced primary production and the existence of an ulterior source of nutrients. Nutrient replenishment seems to occur via an additional upwelling front at the edge of the shelf as well as tapping of subsurface nitrate through sufficiently deep penetration of wind- and wave-induced mixing over large areas of the shelf. Both mechanisms are considered capable of working against the expected nutrient drawdown (i.e. ^{15}N-enrichment) as surface waters travel offshore. It is important to keep these caveats in mind when interpreting δ^{15}N-variations in sediment cores retrieved from this area.

1. Introduction

The role of eastern boundary upwelling areas in the global climate system far outweighs their modest regional extent. The upwelling of cold and nutrient-rich subthermocline waters supports a powerful biological pump and the sequestration of organic carbon on a large scale (e.g. Berger et al., 1989; Berger and Wefer, 2002). Much effort has already been put into a deeper understanding of the Benguela upwelling system as a whole (e.g. Chapman and Shannon, 1985;

Shannon and Nelson, 1996; Shannon and O'Toole, 1999). Our investigation focuses on the central Namibian coastal section with particular emphasis on the shelf region, which has been largely neglected in literature so far.

Information about productivity patterns is derived from C_{org}/N ratios and N-contents in suspended matter as well as from the amount of total organic carbon (TOC) in the surface sediments. Temperature records (recorded in the sediments as well as through direct measurements) reflect the intensity and spatial extent of upwelling.

The main insight into nutrient dynamics and oceanographic features comes from the nitrogen isotope ratios of surface sediments (δ^{15}N$_{sediment}$) and suspended particulate matter (SPM) from the overlying

* Corresponding author. Tel.: +49 (0)30 2093-8552;
  Fax: +49 (0)30 2093-8565.

  E-mail address: Ulrich.Struck@mfn-berlin.de (U. Struck).

water column ($\delta^{15}N_{SPM}$). As for the Namibian shelf, this is actually the first time that such a compilation of surface sediment and water column data is presented. The influence of early alteration processes is investigated by tracking downward variations of $\delta^{15}N_{SPM}$ from the sea surface to the seafloor.

Over the last years, $\delta^{15}N$-records have gained growing importance in the study of marine nutrient regimes and food webs. However, the value of $\delta^{15}N_{sediment}$ as a potent biomarker in palaeo-studies depends on the sound knowledge about fractionation-relevant processes involved. Investigating spatial and vertical changes in $\delta^{15}N$, combining data from sediments and suspended matter, may hold some valuable clues to the principle controls on $\delta^{15}N$ above the central Namibian shelf. This helps to evaluate the usefulness of $\delta^{15}N_{sediment}$ in ancient sediments and gets particularly useful when it comes to interpreting biological and physical processes operating in the ocean at times that we lack direct insight in the water column (e.g. Meisel et al., 2011).

1.1. Nitrogen dynamics and nitrogen isotopes as a proxy parameter

Nitrate (NO_3^-) dominates the oceanic pool of combined nitrogen and supports most of the primary production (Montoya, 1994). As long as nutrients are in abundant supply, nitrogen isotopes are fractionated when assimilated by phytoplankton (Ostrom et al., 1997). Phytoplankton typically results depleted in ^{15}N (by ±5‰) relative to the inorganic source nitrogen used for growth. According to Rayleigh fractionation kinetics the remaining NO_3^--pool becomes progressively enriched in ^{15}N and with it the primary producers taking up nutrients from that pool (e.g. Wada and Hattori, 1978; Wada, 1980; Montoya, 1994; Waser et al., 1998). The greater the distance to the nutrient source, by inference, the higher $\delta^{15}N$ in both nitrate and the primary product. Without other processes interfering (such as nitrogen fixation, denitrification, etc.), high $\delta^{15}N$-values are thus associated with low nitrate concentrations and vice versa. Owing to this relationship, $\delta^{15}N$-records were extensively used as a proxy of relative nitrate utilisation in the photic zone, sometimes holding valuable clues about ocean circulation and trade wind pattern (e.g. Francois et al., 1992; Altabet and Francois, 1994; Montoya, 1994; Montoya and McCarthy, 1995; Voss et al., 1996; Holmes et al. 1998, 1999, 2002; Pichevin et al., 2005).

2. Study area

2.1. Coastal upwelling

The Benguela Current is the eastern boundary current of the South Atlantic anticyclonic gyre. Its eastern periphery is characterised by an upwelling area with a pronounced negative surface temperature anomaly found between 15 and 34°S (Shannon, 1985; Shannon and Nelson, 1996). Fig. 1 provides an insight in the modern large-scale flow pattern.

Upwelling concentrates on a number of cells along the southwest African coast. The principal centre is in the vicinity of Lüderitz (27°S) where strong upwelling occurs throughout the year. The zone represents an environmental boundary between the northern and southern Benguela, which represent two quasi-independent subsystems (Shannon and Nelson, 1996; Shannon and O'Toole, 2003; Mohrholz et al., 2008). The area under investigation lies within the Central Namibian Upwelling Cell in the northern Benguela (Shannon and Nelson, 1996).

The northern Benguela exhibits a late winter-spring maximum (September to November) and summer minimum (January to March) in upwelling activity (Hart and Currie, 1960; Stander, 1964; Nelson and Hutchings, 1983; Shannon, 1985). Upwelling is induced by the trade winds (e.g. Lutjeharms and Meeuwis, 1987). Surface waters are dragged offshore, giving rise to a pressure deficit that is compensated for by the advection of deeper water masses travelling up the shelf. Seasonal variability nonetheless, this cross-shelf circulation is maintained all year round. The offshore-directed surface layer is thickest in austral winter when upwelling is strongest (up to 35 m; in austral summer reaching 20 m only). At the same time the onshore compensation flow covers the entire water column below the surface mixed layer. In summer the onshore flow slackens and vanishes completely near the bottom (Mohrholz et al., 2008). Upwelling taps water from up to 200 m depths (Calvert and Price, 1971; Mohrholz et al., 2008). The upwelled water represents a mélange of two upper central water masses, namely nutrient-rich and oxygen-poor South Atlantic Central Water (SACW) and well-oxygenated and nutrient-poor Eastern South Atlantic Central Water (ESACW) (Table 1) (Mohrholz et al., 2008). SACW originates from the Brazil-Malvinas Confluence region of the Subtropical Convergence in the Southwest Atlantic. It is transported within the subtropical gyre and the equatorial current system into the Angola Dome region where continuous remineralisation of organic matter (OM) reduces its O_2-content while enriching its nutrient loads. From there, it is eventually advected along

the shelf into the northern Benguela via the Angola Current, or, more precisely, via its southward continuation in the form of a poleward undercurrent penetrating through the Angola-Benguela Front (ABF). As regards the maximum southward reach of the undercurrent, 27°S is considered a good estimate (Mohrholz et al., 2008). Owing to its low oxygen content, SACW is held partly responsible for the sub- to anoxic condition above the shelf (Chapman and Shannon, 1987; Shannon and Nelson, 1996).

The second water mass, ESACW, is formed in the Agulhas Retroflection area in the south. It represents a mixture of central water from the subtropical gyre and varying amounts of warm Indian Ocean Central (Agulhas) Water injected into the South Atlantic through the Agulhas Current (Gordon, 1986; Shannon and O'Toole, 2003; Mohrholz et al., 2008). ESACW is carried northward along the upper continental slope and edge of the shelf by the Benguela current itself (Gordon, 1986; Mohrholz et al., 2008).
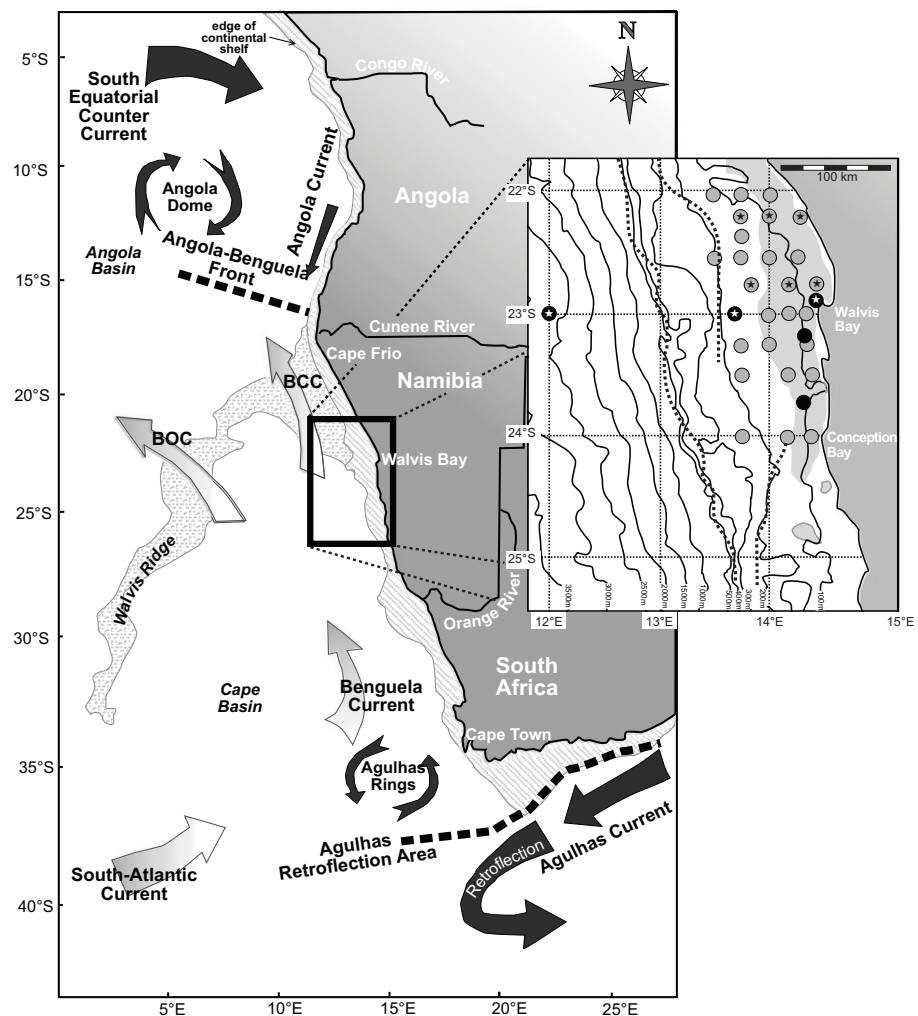
Fig. 1. The Benguela Upwelling is bordered by highly dynamic warm water regimes at both of its ends, i.e. the Angola-Benguela Front (ABF) in the north and the Agulhas Retroflection area in the south. The warm South Equatorial Counter Current (SECC) flows southeastward towards the Angola Basin at subsurface depths. It reaches the surface at around 10°S where it continues southward as the Angola Current (Moroshkin et al., 1970). The Benguela Current splits into the Benguela Oceanic Current (BOC) and the Benguela Coastal Current (BCC) at approximately 28°S. The BOC is separated from the SECC by the Angola Dome, a large cyclonic gyre, which is considered the remote source of hypoxic, nutrient-rich SACW (Mohrholz et al., 2008). The BCC travels parallel to the coast and turns west at the ABF (Stramma and Peterson, 1989). The ABF migrates seasonally between about 14 and 17°S and separates the oligotrophic tropical ecosystem in the north from the nutrient-rich Benguela upwelling system in the south (Summerhayes et al., 1995). Still, it is no strong barrier and allows the injection of SACW into the northern Benguala via a poleward undercurrent (Mohrholz et al., 2008). Light arrows denote cold surface currents, the darker arrows denote warm surface currents (map modified after Holmes et al. (1999)).
The small chart zooms in on the area under investigation and shows where water column profiles for the collection of SPM and hydrographic data were taken (black dots M57-3 expedition; grey dots AHAB 05 cruise). Fig. 3 provides details about the locations highlighted. The diatomaceous muds, coating the inner shelf up to approximately 150 m depth, are shaded grey. The dotted lines denote the double shelf break, which characterises much of the central Namibian region (after Bremner and Willis, 1993).

The northward flowing ESACW and southward flowing SACW meet in the large transition area between the ABF and the Lüderitz Upwelling, being mixed by cross-shelf circulation (see above). As with cross-shelf circulation, Mohrholz et al. (2008) reported a clear seasonal variability in the intensity of the longshore current components and the proportions of ESACW and SACW off Walvis Bay. In austral winter, northward advected ESACW shifts the frontal zone between both water masses equatorward and most of the SACW is removed. During summer, when upwelling slackens and the ABF moves southward and weakens, the percentage of hypoxic SACW on the northern Benguela shelf rises.

2.2. Shelf anoxia

The adverse influence of SACW on the local oxygen status is evidenced by the strong inverse correlation between SACW fraction and oxygen concentration over the entire northern Benguela shelf (Mohrholz et al., 2008). Still, SACW is not the sole reason for the lack of oxygen. The extent of the oxygen deficiency also depends on local oxygen consumption associated with remineralisation of sinking organic detritus. High primary production induces great oxygen demand down in the water column and often brings about severe anoxia over large areas of the southwest African shelf (Chapman and Shannon, 1985; Codispoti and Christensen, 1985; Shannon and O'Toole, 1999; Tyrrell and Lucas, 2002; Gaye-Haake et al., 2005). The subsurface transport of oxygen-rich ESACW from the shelf edge onto the shelf theoretically balances the oxygen consumption below the surface mixed layer. During summer, when upwelling-favourable winds weaken, however, the Ekman compensation flow is restricted to intermediate depths with the bottom layer being excluded. Weaker advection of oxygenated ESACW in combination with pronounced intrusions of hypoxic SACW (section 2.1.) and continuing oxygen demand due to respiration makes the summer ventilation less effective than in winter (Mohrholz et al., 2008). In fact, the occurrence of widespread shelf anoxia is a seasonally recurrent feature.

3. Material and methods

The investigation is based on an extensive compilation of (i) hydrographic measurements, (ii) suspended particulate matter and (iii) surface sediments. (i) and (ii) include data from the sea surface and the water column. See Table 2 for a clear listing of the respective parameters analysed.

Table 1
Water mass definitions for South Atlantic Central Water (SACW) in the Angola Gyre and Eastern South Atlantic Central Water (ESACW).

	SACW *Mohrholz et al. (2008)*	ESACW *Poole and Tomczak (1999)*
temperature (°C)	8.0 - 16.0	6.0 - 14.4
oxygen (µmol/l)	22.4 - 68.4	249.3 - 300.1
nitrate (µmol/l)	21.9 - 37.9	0 - 11.8

3.1. Water sampling (hydrographic data and suspended particulate matter)

Samples and measurements were taken during METEOR cruise M57-3 (15/03/2003 to 08/04/2003) and the AHAB 05-expedition (RV Alexander von Humboldt; Angola-Benguela; 17/03/2004 to 05/04/2004) in late austral summer. At that time of the year, upwelling typically slackens (section 2.1.). Most of the data derive from the shelf between 22 and 25°S and only few reach up to 250 km offshore (Table 2).

The investigation is based on suspended particulate matter (SPM) collected along with hydrographic data (temperature, oxygen, chlorophyll) at 31 water column profiles (Fig. 1). Double in amount are SPM-samples from the surface waters (Fig. 4a) and measurements of the sea surface temperature (SST) (Fig. 2a).

Water sampling and hydrographic measurements were done by means of a CTD (conductivity-temperature-depth)-Rosette-water-sampling-system equipped with an oxygen sensor (Sea-Bird Electronics, Bellevue, WA) and a Haardt Chlorophyll detector (Lavik et al., 2004). The sensor was calibrated by manual Winkler titration. CTD-measurements were taken at roughly 1 m-intervals.

Water samples were taken at various depths with SPM being obtained by filtration of 0.2 to 2 litres of seawater through pre-combusted glass fibre filters (Whatman GFF 0.8 µm) (NB: The term 'suspended particulate matter' includes both sinking and suspended matter.). Carbonate-carbon was removed in a vapour of concentrated hydrochloric acid. Prior to measurement the filters were wrapped in tin-foil vessels. The isotopic composition of nitrogen ($\delta^{15}N$) and the total weight percent (wt%) of organic carbon (C_{org}) and nitrogen were determined in a Thermo NC2500 Elemental Analyser connected to an isotope-ratio mass-spectrometer (Finnigan, Delta Plus). The reference gas was pure N_2 calibrated against IAEA-standards N-1 and N-2. In replication measurements, the standard deviation of the lab standard (peptone) did not exceed ±0.2‰. Nitrogen isotope

ratios are reported in the conventional δ-notation in per mil (‰) with respect to the atmospheric N_2-standard (AIR) (Mariotti et al., 1981).

3.2. Surface sediment samples

The term 'surface sediment' denotes the upper 1 cm of sediment. In the diatomaceous muds (see below), where sedimentation rates average 1 mm/a (Bremner and Willis, 1993), 1 cm of sediment corresponds to the last 10 years.

The sediment samples span a broader coastal section (latitude 19 to 30°S) than the surface ocean SPM-data and reach far beyond the edge of the shelf. Most sediment data has already been published by various authors (see Table 2). The compilation in one single set of data provides the hitherto most comprehensive spatial image of the central Namibian shelf and slope. Besides, from the comparison with $\delta^{15}N_{SPM}$ we expect novel insights into the transfer of pelagic δ¹⁵N-signals to the sea floor.

Delta¹⁵N$_{sediment}$ analyses were made on untreated sedimentary material (Pichevin, 2005; Emeis et al., 2009 and ref. therein). SSTs were reconstructed by means of the alkenone palaeo-temperature index UK′37 (Emeis et al., 2009 and ref. therein). TOC (wt%) from Mollenhauer et al. (2002) is complemented by hitherto unpublished data from METEOR cruise M48-2 (05/08/2000 to 23/08/2000) and RV POSEIDON cruise 250 (06/04/1999 to 28/04/1999).

As a result of the high primary production rates, the shelf sediments are predominantly of biogenic nature. The majority of the samples derive from the organic-rich diatomaceous muds (average opal 54wt%; average OM 10wt%; Bremner and Willis, 1993) running parallel to the coast (Fig. 1). The mud belt coats the inner shelf up to 150 m depth and thickens to more than 10 m in coastal vicinity (Struck et al.,

2002; Brüchert et al., 2004; Emeis et al., 2004). The outer shelf and upper slope are covered by a calcareous facies (> 50wt% $CaCO_3$) (Bremner and Willis, 1993). Towards the shelf break, strong bottom currents impede the deposition of sediments and the sea bottom often consists of hard ground (Brüchert et al., 2004).

4. Results

4.1. Hydrographic data

The SST contour plot is based on 63 CTD-measurements (Fig. 2a). The sampling depths rarely exceed 5 m. SSTs range from roughly 12.5 to 19°C, with increasing temperatures towards the open ocean. The fact that the gradient along latitude 23°S is that weak is consistent with slackened upwelling at that time of the year. Towards the Lüderitz Cell (27°S) in the south, where upwelling occurs throughout the year, the SST-gradient is much more pronounced indicating upwelling of cold subsurface waters (±12.5°C) in the immediate vicinity of the coast.

Fig. 3 displays a selection of 9 water column profiles analysed in this study. Their locations are marked with a star in Fig. 1. The profiles lie on three east-west-oriented transects and provide an insight in the water column properties at various distances to the coast. If existing, the thermocline is situated between 10 and 30 m depth (Figs. 3b and 3c). In the shallow coastal waters, however, stratification is usually rather weak and offsets between surface and bottom water temperatures rarely exceed 2°C (Figs. 3d and 3g). Further offshore, the temperature offsets and the thermocline are generally more pronounced. Oxygen declines more or less abruptly below the thermocline and comes close to zero above the ground (Fig. 3).

Table 2

Compilation of the sample material and proxies. The number of measurements, or rather, samples is also shown (= n). Origin of the data: [a] Most of the data derive from the shelf between 22 and 25°S. Only few reach up to 250 km offshore. [b] The profiles derive nearly exclusively from the inner shelf area between 22 und 24°S. [c] The sediments span a broader coastal section than the surface ocean SPM-data, reaching from latitude 19 to 30°S. At the same time they reach far beyond the edge of the shelf (TOC up to 230 km, SST and δ¹⁵N$_{sediment}$ up to ±1000 km offshore). Source studies of previously published data are mentioned.

hydrographic measurements		SPM		surface sediments [c]	
surface water [a] (n = 63)	water column profile [b] (n = 28)	surface water [a] (n = 62)	water column profile [b] (n = 31)		
temperature	temperature (°C)	$\delta^{15}N_{SPM}$ (‰)	$\delta^{15}N_{SPM}$ (‰)	δ¹⁵N$_{sediment}$ (‰) *Emeis et al. (2009); Pichevin et al. (2005)*	(n = 98)
	oxygen (ml/l)	PN (mg/l)	PN (mg/l)	SST (UK-37) (°C) *Emeis et al. (2009)*	(n = 123)
	chlorophyll *a* (mg/l)	POC (mg/l)	C_{org}/N (molar)	TOC (%) *Mollenhauer et al. (2002)*	(n = 68; 43 yet unpubl.)
	C_{org}/N (molar)				
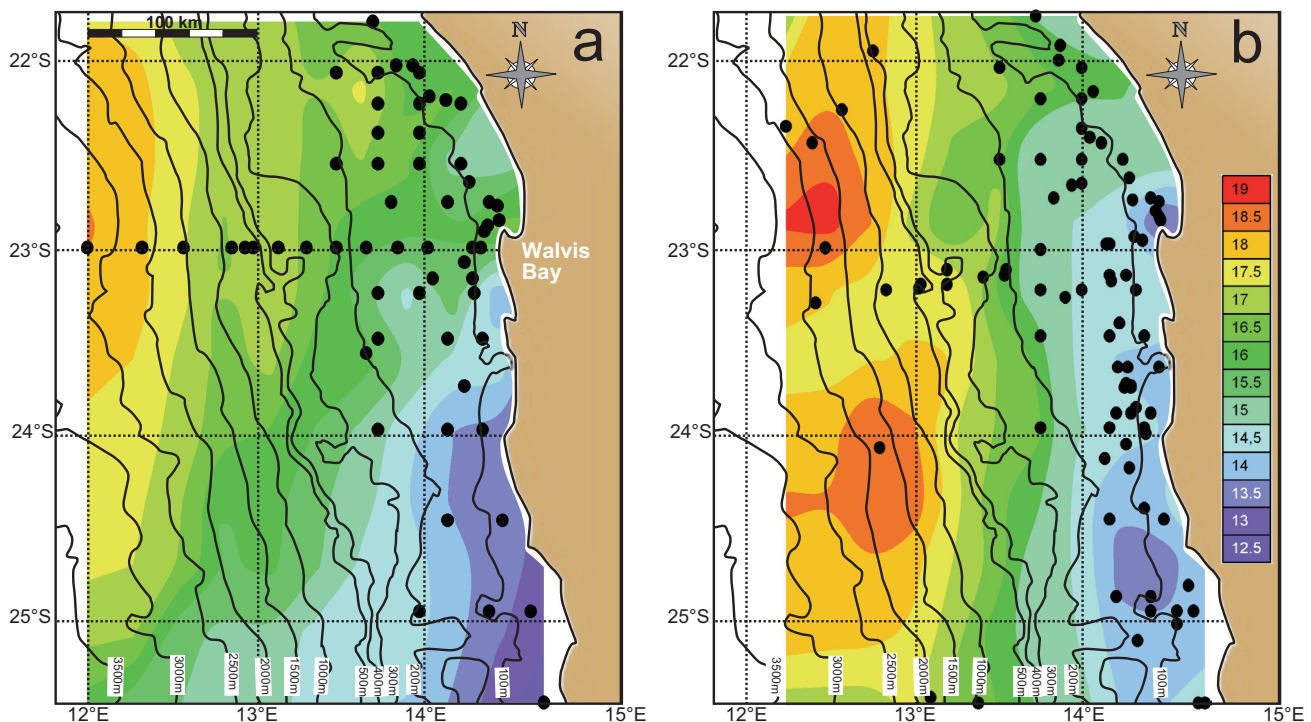
Fig. 2. Spatial distribution of SST (°C) reconstructed by means of (a) CTD-measurements and (b) sedimentary alkenone (UK′37) data. The UK'37-record mirrors two centres of upwelling: the seasonally active Central Namibian Cell, located between 22.7 and 24.5°S, and the Lüderitz Cell further south (Shannon and Nelson, 1996). The CTD-data bear only witness to the latter.

4.2. Suspended particulate matter (SPM)

Concentrations: Due to the absence of terrestrial material (see section 5.1.) variations in the amount of particulate nitrogen (PN) and particulate organic carbon (POC) are regarded as an indication of varying primary production rates.

[POC] (particulate organic carbon) in the surface waters ranges from 0.1 to 2.8 mg/l and [PN] (particulate nitrogen) from 0.01 to 0.34 mg/l (Fig. 4a). The oceanward decline in [PN] and [POC] in the upper water layers is clearly visible in Fig. 4a and 5.

Both chlorophyll (chl *a*) and [PN] decrease with depth. The CTD-measurements show that the decline in chlorophyll tends to be bound to the thermocline (Figs. 3a and 3e). Around longitude 13.75°E, however, there is a deep chlorophyll maximum (DCM) at the depth of the thermocline (Figs. 3c, 3f and 3h). DCM are a common feature in many regions of the tropical Atlantic (Ravelo and Fairbanks, 1992). The phenomenon was observed during both METEOR cruise M57-3 and the AHAB 05-expedition and vanishes south of 23°S.

$δ¹⁵N_{SPM}$: Surface water $δ¹⁵N_{SPM}$ ranges from roughly 1 to 16‰ and decreases with increasing distance to the coast (Figs. 6a and 7) (NB: The $δ¹⁵N_{SPM}$-range is more or less comparable to values from the Peru Upwelling (Libes and Deuser, 1988).). Highest values are found in the coastal waters at 23.5°S (Fig. 6a).

With increasing depth, SPM generally exhibits increasing $δ¹⁵N$-signatures. Different mechanisms seem to operate in close proximity to the coast, where $δ¹⁵N_{SPM}$ often declines with depth (Figs. 3a and 3d).

4.3. Surface sediments

$δ¹⁵N_{sediment}$: The spatial distribution of $δ¹⁵N_{sediment}$ was extrapolated from nearly one hundred measurements taken between latitude 19 and 30°S as far as 1°E (Figs. 7 and 8). Highest $δ¹⁵N_{sediment}$-values (±10‰) are situated about one degree latitude further north

Fig. 3. The locations of the profiles and corresponding transects (22.21°S; 22.75°S; 23.00°S) are highlighted in Fig. 1. With each transect, the distance to the coast increases from top to bottom. Characteristics of filtration-derived SPM ($δ¹⁵N_{SPM}$, [PN], C_{org}/N) in the left chart are shown along with the CTD-derived hydrographic measurements (temperature, oxygen and chlorophyll content) in the right chart.

Profiles (a) – (f) were taken during the AHAB 05-cruise, profiles (g) – (i) during the M57-3 expedition. Oxygen and chlorophyll were many times higher during Meteor cruise M57-3 than during AHAB 05 (note the larger scale for oxygen and chlorophyll in the 23°S-transect). Such variability is not unusual and testifies to the highly dynamic nature of the region. (a) 14.25°E / 22.21°S; water depth 27 m; (b) 14.00°E / 22.21°S; w.d. 89 m; (c) 13.75°E / 22.21°S; w.d. 120 m; (d) 14.42°E / 22.75°S; w.d. 51 m; (e) 14.17°E / 22.75°S; w.d. 108 m; (f) 13.83°E / 22.75°S; w.d. 134 m; (g) 14.39°E / 22.91°S; w.d. 59 m; (h) 13.68°E / 22.99°S; w.d. 151 m; (i) 12.00°E / 23.00°S w.d. not mentioned.
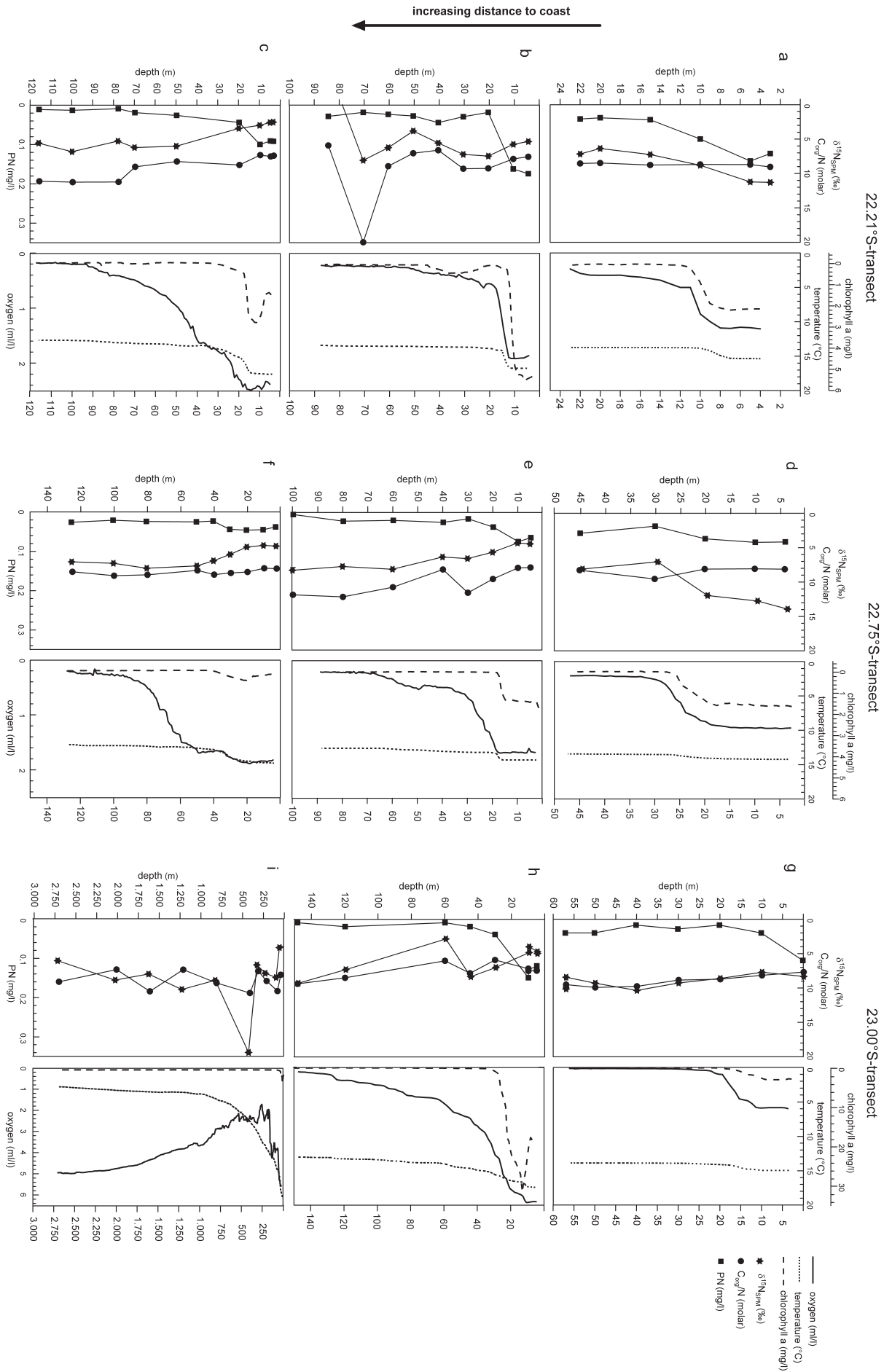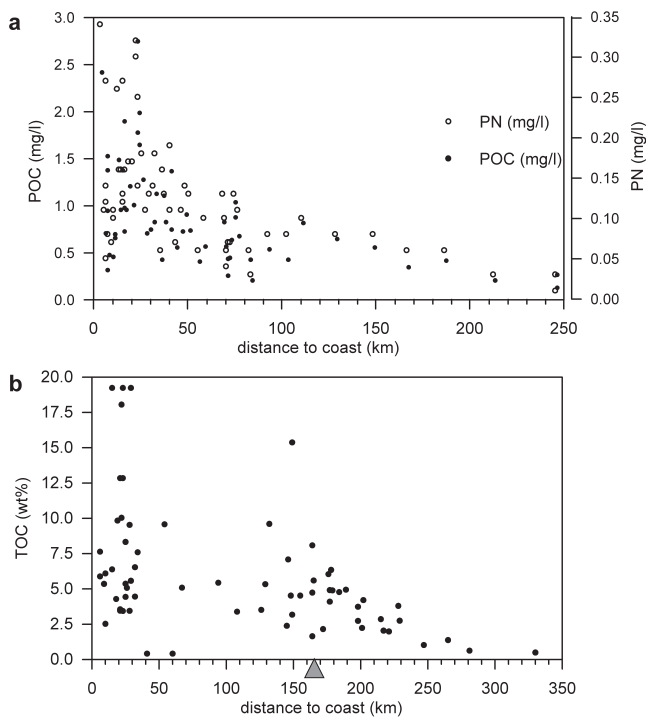
Fig. 4. (a) [PON] and [PN] in the surface water layer (between latitude 22 and 25.5°S) vs. distance to coast. (b) [TOC] in the surface sediments (between latitude 19 and 28°S) vs. distance to coast. Above the lower shelf break (see triangle), [TOC] exhibits a minor peak. Note that the sediment data reach slightly further offshore than the data in (a).
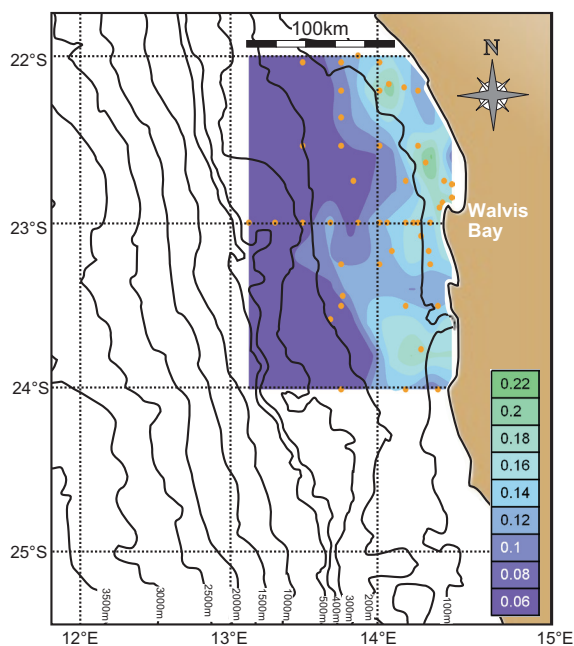
Fig. 5. Spatial distribution of [PN] in surface water layer in mg/l. Concentrations are highest in vicinity to the coast and decrease towards the open ocean.

(22.5°S) than maximum surface ocean $\delta^{15}N_{SPM}$ (Fig. 6). Overall, however, $\delta^{15}N_{sediment}$ imitates the oceanward decline in $\delta^{15}N_{SPM}$, reaching a minimum (±6‰) approximately 160 km off the coast (Fig. 7). Interestingly, this distance coincides perfectly with the lower shelf break, situated at an approximate depth of 400 m (Fig. 1 right chart; Shannon, 1985; Bremner and Willis, 1993). West of the shelf break, the trend of $\delta^{15}N_{sediment}$ is being reversed. Above the continental slope and toward the mesopelagic ocean $\delta^{15}N_{sediment}$ rises continuously (reaching 12‰ 1500 km off the coast). Unfortunately, we lack $\delta^{15}N_{SPM}$-data for comparison (Figs. 7 and 8) (NB: The $\delta^{15}N_{sediment}$-range is more or less comparable to values from the Peru Upwelling (Libes and Deuser, 1988).).

UK'37-temperature: As expected, UK'37-derived SST-records reflect the seasonal upwelling in the vicinity of Walvis Bay (corresponding to the Central Namibian Cell) much better than the CTD-measurements, which were taken during slackened upwelling (Fig. 2). The UK'37-derived SST-range shown in Fig. 2 (~12.5 to 20°C) is markedly similar to the SST-range observed through direct measurements (~12.5 to 19°C; section 4.1.).

Total organic carbon: [TOC] ranges from less than 0.1 to 19% by weight (Fig. 4b). Coastal sediments exhibit particularly variable concentrations and above the middle shelf, data are sparse. Contrary to surface water SPM (Fig. 4a), the oceanward decline in organic matter is not clearly obvious in sedimentary [TOC]. It is only beyond the shelf break, i.e. above the upper slope, that [TOC] displays a clear oceanward decline.

Varying amounts of diluents such as carbonate, siliceous matter, etc. may account for the great range of [TOC] above the inner shelf and contribute to the lacking trend (Fig. 4a). The fuzziness of coastal [TOC] nonetheless, UK'37-temperatures and [TOC] perform a rather clear inverse correlation (Fig. 9).

5. Discussion

5.1. Vertical variation of $\delta^{15}N_{SPM}$ and comparing surface ocean $\delta^{15}N_{SPM}$ with $\delta^{15}N_{sediment}$

The comparison of $\delta^{15}N$-signatures in SPM with the underlying sediment shows if, or the extent to which, secondary processes blur the original pelagic signal. The better we understand such processes, the more valuable our interpretation of isotopic variations in ancient sediments.
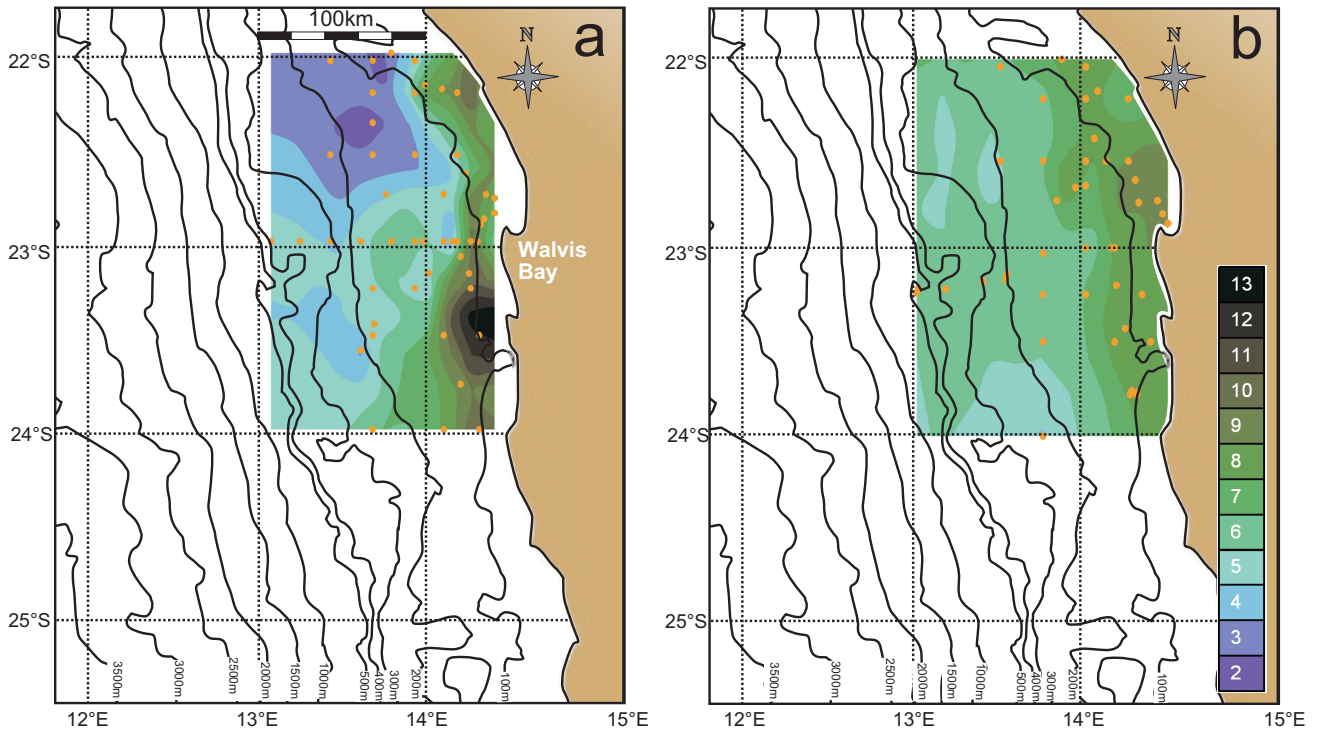
Fig. 6. Spatial distribution of surface ocean $\delta^{15}N_{SPM}$ (a) and $\delta^{15}N_{sediment}$ (b). Note that $\delta^{15}N_{SPM}$ and $\delta^{15}N_{sediment}$ (in ‰) decrease in tandem with increasing distance offshore. The sediment exhibits a smaller isotopic range (4.8 to 11.6‰) than SPM (0.8 to 16.1‰).

Unaltered $\delta^{15}N_{SPM}$- and $\delta^{15}N_{sediment}$-signals are anticipated to reflect the isotopic signatures of the first trophic level. Given the excess of phytoplankton biomass, the influence of higher trophic levels (i.e. zooplankton) is considered negligible. This is particularly true for the inner shelf, where the large quantity of primary producers dilutes any other isotopic influence. The same argument applies to the influence of terrestrial material introduced by winds as dust. Due to the absence of a major river draining into the ocean, significant fluvial input can be ruled out a priori (Holmes et al., 1998; Tyrrell and Lucas, 2002). Molar C_{org}/N ratios in surface water SPM (spanning 6.6 to 13.6; see Fig. 3 although only a selection of surface ocean C_{org}/N ratios are shown there) further support the primarily marine nature of the particles (Redfield, 1934; Schubert and Calvert, 2001).

Admittedly, the comparison of $\delta^{15}N_{sediment}$ with $\delta^{15}N_{SPM}$ is not ideal. Delta$^{15}N_{sediment}$ represents a time-integrated signal while $\delta^{15}N_{SPM}$ has a rather instantaneous character. Outliers and the strong seasonal imprint account for the larger isotopic range of the latter (Libes and Deuser, 1988; Montoya, 1994). Long-term sediment trap studies integrate seasonal fluctuations signals and would be more appropriate than filtration-based SPM. As a matter of fact, intense fishing activities inhibit an area-wide deployment of

moorings, which is why we have to content ourselves with the filtration-based "snapshot" signal.

Given the extremely dynamic nature of the system including the interaction of longshore and cross-shelf water movements, this "snapshot" character of $\delta^{15}N_{SPM}$ should definitely be kept in mind. Rapid changes are common to the system (e.g. Shannon, 1985; Shannon and O'Toole, 1999; Brüchert et al., 2004) and samples taken in one year certainly cannot be generalised to the next or even other seasons. In the shallow inner shelf region, short-term variability is particularly pronounced due to strong vertical water movements associated with the coastal upwelling (section 4.1.).

Also note that the samples were taken off the main upwelling season, when $\delta^{15}N$ is expected to already have shifted towards higher values as a result of advanced nutrient depletion. Within 20 km off the coast, this 'end-of-bloom' sampling tends to manifests itself in a negative offset between $\delta^{15}N_{sediment}$ and surface ocean $\delta^{15}N_{SPM}$, i.e. $\delta^{15}N_{SPM}$ exceeding $\delta^{15}N_{sediment}$ (Fig. 10). The recent addition of denitrified ^{15}N-enriched nitrate to the surface water masses represents an alternative explanation (section 5.2.1.).

Nearshore stations often exhibit declining $\delta^{15}N_{SPM}$-values with increasing depth (Fig. 3a and 3d). This contradicts the idea of remineralisation in the
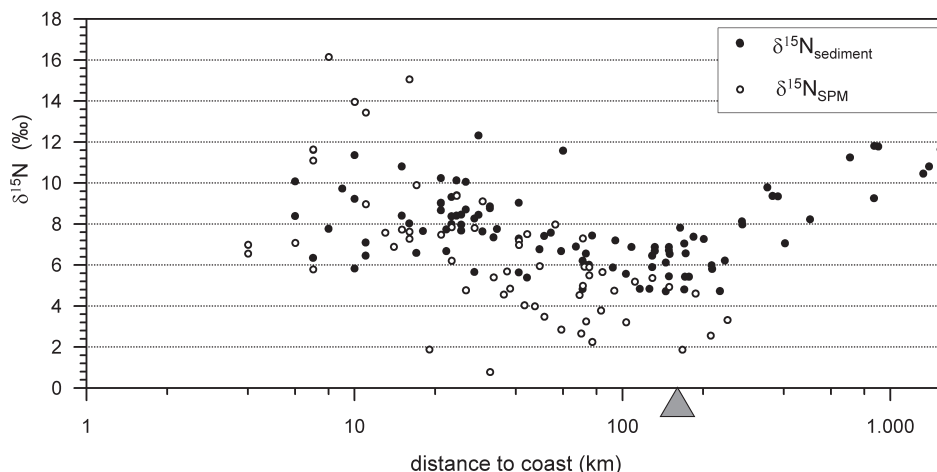
Fig. 7. Surface water $\delta^{15}N_{SPM}$ and $\delta^{15}N_{sediment}$ vs. distance to coast. Note the logarithmic scale. The $\delta^{15}N_{SPM}$-records are basically restricted to the shelf between latitude 22 and 25.5°S. Delta$^{15}N_{sediment}$ covers a much broader coastal section (19 to 30°S) and reach far over the continental slope more than 1000 km offshore (for a map view see Fig. 8). Note the reversal of trend above the lower shelf break, marked by the triangle, in approximately 160 km distance to the coast.

water column. It is a popular belief that microbial degradation produces elevated $\delta^{15}N$-signatures in the residual OM as a result of discrimination against ^{15}N during metabolic reactions [a] (e.g. Melander, 1960; Gaebler et al., 1966; Saino and Hattori, 1980; Altabet and McCarthy, 1985; Schäfer and Ittekkot, 1993; Altabet and Francois, 1994; Montoya, 1994; Ostrom et al., 1997; Sachs and Repeta, 1999). Still, the

Fig. 8. Spatial distribution of $\delta^{15}N_{sediment}$ (in ‰). The larger scale shows that the previously observed oceanward decrease in $\delta^{15}N_{sediment}$ (Fig. 6b) is restricted to the shelf. Beyond the shelf edge (marked by the dotted line), the sediments exhibit continuously rising $\delta^{15}N_{sediment}$-values (see also Fig. 7).

observation that the $\delta^{15}N$-signature of OM may also decline is not new (e.g. Altabet et al., 1991; Gaye-Haake et al., 2005). Some authors mention the ingrowth of bacteria (containing low $\delta^{15}N$) as a potential candidate capable of efficiently counteracting the effects of remineralisation (Libes and Deuser, 1988; Holmes et al., 1999; Lehmann et al., 2002).

Another possible explanation for the depth-related decline in $\delta^{15}N_{SPM}$ is based on the 'end-of-bloom' sampling: Assuming that the particles do not undergo any $\delta^{15}N$-relevant alteration while sinking, the downward gradient would simply mirror the typical course of a phytoplankton bloom, i.e. the progressive ^{15}N-enrichment of surface ocean organic matter, with subsurface $\delta^{15}N_{SPM}$-signals corresponding to older surface signals. In other words, if the transfer of SPM to the ocean floor is too fast for biochemical processes to leave an imprint, low $\delta^{15}N_{SPM}$ in deeper waters reflect surface water conditions at an earlier, i.e. less nutrient-depleted state.

How is it, however, that the material only escapes degradation in coastal vicinity? Both the depth-related decline in $\delta^{15}N$ and the negative offsets between $\delta^{15}N_{sediment}$ and $\delta^{15}N_{SPM}$ are predominantly found within 20 km off the coast. Further offshore, $\delta^{15}N_{SPM}$ rises with depth (Figs. 3c, 3e and 3f) and sediments are nearly universally ^{15}N-enriched compared to surface ocean suspended matter (Fig. 10). Here, remineralisation, or rather, NH_3-outgassing [a] seems to effectively influence the $\delta^{15}N_{SPM}$-signal.

---

[a] Contrary to popular belief, recent studies have shown that the shift towards higher $\delta^{15}N$ is only indirectly related to OM decay and truly results from kinetic isotope fractionation during the drying process, when NH_4^+ transforms to gaseous NH_3 (Meisel and Struck, 2011). Sediments and particulate matter contain varying amounts of NH_4^+ generated during OM decayal. During ammonia volatilisation ^{14}N accumulates in the gaseous phase, thus leaving ^{15}N-enriched NH_4^+ behind. Rinsing, irrespective of whether acidification is included or not, eliminates the decomposition-, or more precisely, outgassing-derived increase of $\delta^{15}N$ and restores the original pelagic signal.

In the shallow inner shelf waters, a combination of several aspects seems to promote the preservation of the original signal. High primary production and correspondingly high particle concentrations induce the formation of bigger and fast sinking aggregates (Figs. 4 and 5). Both the short transit to the bottom as well as rapid burial after deposition contributes to the preservation of the original signal (Libes and Deuser, 1988; Altabet et al., 1991; Montoya, 1994; Ostrom et al., 1997; Altabet et al., 1999; Holmes et al., 2002). The lack of oxygen moreover inhibits diagenetic alteration (e.g. Altabet et al., 1999; Sachs and Repeta, 1999). Note that sampling took place during austral summer, when the O_2-deficiency above the inner shelf is particularly pronounced due to the higher percentage of hypoxic SACW (section 2.1.). In fact, during Meteor cruise M57-3 the inner shelf bottom waters exhibited zero oxygen (Brüchert et al., 2004). Other studies conducted at that time of the year report similar circumstances (e.g. Lavik et al., 2009).

Above the outer shelf, OM is much more liable to degradation for several reasons. Due to greater depths and lower sedimentation rates, the residence time in the water column increases. This fact greatly enhances the particulates' exposure and suscepti-
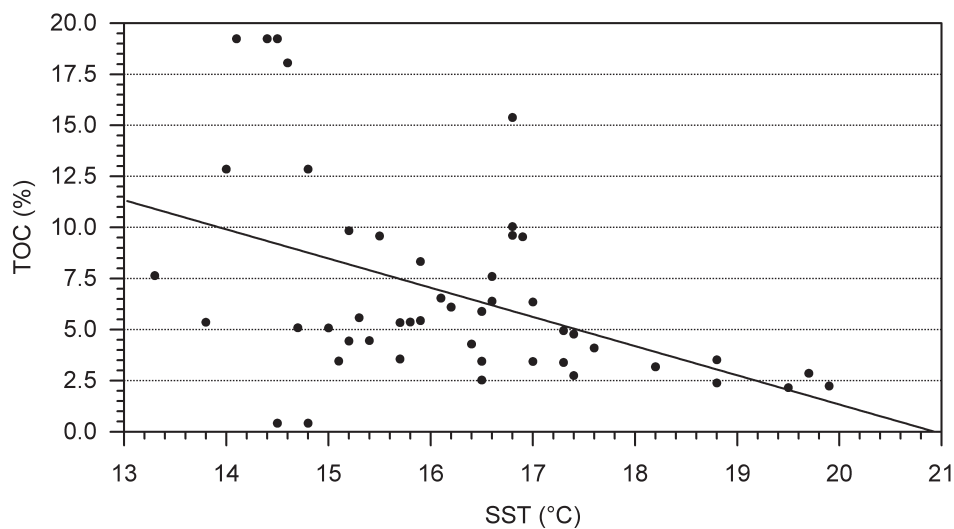
Fig. 9. SST (alkenone-based) vs. sedimentary [TOC] : The inverse correlation (r^2 = 0.21; p = 0.141%) agrees with highest primary production in coastal proximity where the pristine pool of cold and nutrient-rich waters upwells. The majority of data pairs derives from the shelf.
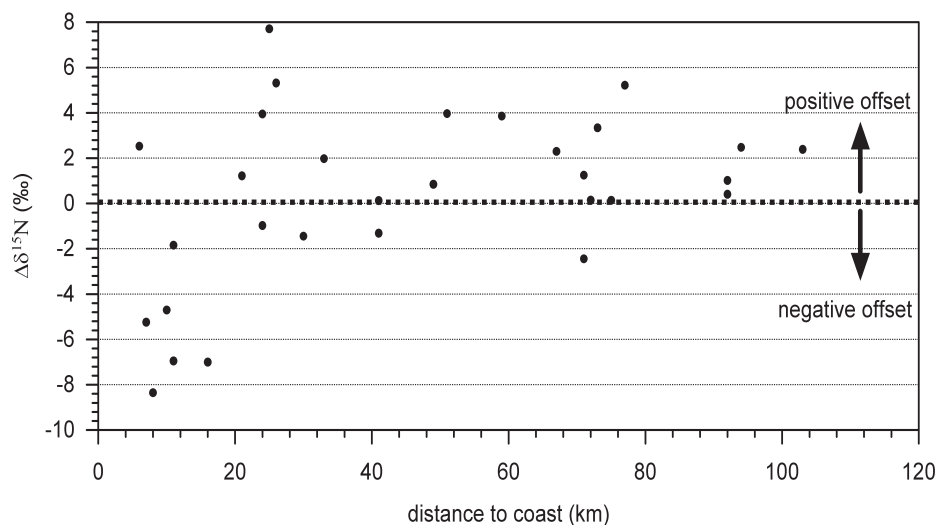
Fig. 10. Offset between $\delta^{15}N_{sediment}$ and surface ocean $\delta^{15}N_{SPM}$ ($\Delta\delta^{15}N = \delta^{15}N_{sediment} - \delta^{15}N_{SPM}$) vs. distance to coast. Samples of the data pairs are restricted to the region between latitude 22 and 25.5°S. Above the innermost shelf, the sediments tend to contain lower $\delta^{15}N$-signatures than surface water SPM, hence the negative $\Delta\delta^{15}N$-values. This observation might be ascribed to the 'end-of bloom' sampling and / or the recent upwelling of denitrified nitrate.

bility to microbial activity (e.g. Holmes et al., 1999). Besides that, little vertical flux comes along with lower local oxygen consumption (see also section 2.2.). The greater influence of oxygen-rich ESACW towards the west further contributes to the better ventilation above the outer shelf (Brüchert et al., 2004; Lavik et al., 2009). As a matter of fact, the rising susceptibility to diagenesis with increasing distance to the coast (as inferred from the $\delta^{15}N_{SPM}$-profiles) agrees well with the zonal bottom O_2-gradient.

5.2. Spatial trends and relationships between proxy indicators

A number of studies conducted in the northern Benguela reported decreasing $[NO_3^-]$ and concomitantly increasing $\delta^{15}N$-signatures with increasing distance to the coast (e.g. Conkright et al., 1998; Holmes et al., 1998, 1999, 2002). These observations are consistent with the idea of nutrient-rich waters coming to the surface along the coast, being dragged offshore by Ekman transport and, according to the concept of Rayleigh fractionation kinetics, becoming more and more depleted in ^{14}N-NO_3^- along the way (section 1.1.). Until now, however, the majority of studies (including the ones mentioned above) has dealt with the continental slope and only minor attention has been paid to the shelf. Here, $\delta^{15}N$-values behave precisely opposite to the expected pattern. Both sediments and suspended particles exhibit a westward decline in $\delta^{15}N$, reaching a minimum above the edge of the shelf (Fig. 7).

The coastal $\delta^{15}N$-maximum has already been mentioned by Pichevin et al. (2005) and Emeis et al. (2009). Comparing two multicores, one from the inner and one from the outer shelf, Struck et al. (2002) found the former exhibiting higher $\delta^{15}N$-values. As a matter of fact, the mechanisms are still far from being understood. In the following we are going to propose a model that might account for the unexpected spatial pattern of $\delta^{15}N$. At the same time, the applicability of $\delta^{15}N_{sediment}$ as a proxy of past nitrogen cycling in the northern Benguela is reassessed.

5.2.1. Denitrification and the $\delta^{15}N$-maximum along the coast

When oxygen consumption exceeds the oxygen concentration of the source water, anaerobic decomposition starts in the form of denitrification (Mohrholz et al., 2008). Denitrifying microbes use nitrate instead of oxygen in order to oxidise OM and are observed to become dominant only when oxygen drops below 0.2 ml/l (Bubnov, 1972; Cline and Kaplan, 1975; Knowles, 1982; Packard et al., 1983). The oxygen deficiency results from a combination of high remineralisation supported by the initially O_2-rich ESACW on its pathway up the shelf as well as high fractions of O_2-poor SACW. Local oxygen consumption due to high organic particle flux further contributes to the high O_2-demand and O_2-depletion in the bottom waters (section 2.2.). In fact, denitrification tends to be associated with high primary production rates (e.g. Tyrrell and Lucas, 2002).

Denitrifying bacteria discriminate against ^{15}N. As a consequence, the residual NO_3^--pool becomes progressively enriched in ^{15}N by several per mil. Once this ^{15}N-enriched nitrate is carried to the photic zone, it is assimilated by the plankton, thus initiating a shift towards higher $\delta^{15}N$-signals in the primary products (Cline and Kaplan, 1975; Montoya, 1994; Holmes et al., 1996). As a consequence, denitrification not only brings about immense nitrogen loss but also strongly interferes with the isotopic record.

In actual fact, coastal $\delta^{15}N_{SPM}$ and $\delta^{15}N_{sediment}$ exhibit values exclusively higher than 5.5‰ (Fig. 7), which is the average isotopic signature of the source water nitrate (Sigman et al., 1997, 2000; Ren et al., 2009). Given the proximity to the nutrient source and upwelling, prior consumption can hardly be held responsible for this ^{15}N-enrichment (section 1.1.). Second, the central Namibian shelf exhibits pronounced nitrate deficits [b] in coastal proximity (Tyrrell and Lucas, 2002; Kuypers et al., 2005). The nitrate deficits (i) in combination with the coastal-parallel belt of high $\delta^{15}N_{SPM}$ and $\delta^{15}N_{sediment}$ (ii) (Figs. 6 and 7), high flux rates (iii) (Figs. 4a and 5), and the oxygen depletion in the bottom waters (iv), unanimously support the influence of denitrification in the source waters (see also Pichevin et al., 2005; Emeis et al., 2009; Lavik et al., 2009). Based on a number of nutrient profiles taken at selected stations during Meteor cruise M57-3, Brüchert et al. (2004) were able to locate the zones of denitrification along the water column.

We shall mention that Kuypers et al. (2005) believe in anammox (anaerobic ammonium oxidation by nitrate and / or nitrite to yield N_2) rather than denitrification as the main process behind the observed nitrogen deficit in the shelf waters. As far as we know, no study has yet examined whether or not annamox is associated with nitrogen isotope fractionation. Without this knowledge, the ultimate reason for the coastal ^{15}N-enrichment remains open to discussion and the influence of a process other than denitrification cannot be ruled out.

---

[b] 'Nitrate deficit' implies that nitrate is depleted relative to phosphate with regard to the Redfield ratio. Low nitrate concentrations are not necessarily equivalent to a nitrate deficit (Tyrrell and Lucas, 2002).

5.2.2. Delta^{15}N vs. [TOC] and $\delta^{15}N$ vs. SST

Given the contemporaneous westward decrease in primary production and shelf $\delta^{15}N$-values (Figs. 4 and 6), we expected [TOC] and $\delta^{15}N_{sediment}$ to be positively correlated within 170 km off the coast. In fact, the great range of coastal [TOC] (Fig. 4b) largely obliterates the anticipated relationship. The remaining correlation is nearly negligible (Fig. 11), but still corroborates the presence of denitrified source waters.

Above the continental slope, the relationship is being reversed and lower $\delta^{15}N$-signals correlate with higher [TOC] (Holmes et al., 1998). The coincidence of minimum $\delta^{15}N$ (Fig. 7) and elevated [TOC] right above the edge of the shelf (Fig. 4b) supports these findings. Holmes et al. (1998) interpreted the negative correlation as the direct response to relative nitrate consumption and Rayleigh fractionation kinetics.

This interpretation, however, is valid on two assumptions only: Firstly, relative nitrate utilisation represents the only significant process acting on the $\delta^{15}N$-signature of nitrate ($\delta^{15}N_{nitrate}$). Secondly, nitrate is not in limited supply as phytoplankton only discriminates between the heavy and light isotopes as long as nutrients are abundant (Ostrom et al., 1997). Both prerequisites turn out problematic where denitrification plays a prominent role (denitrification acts as a nitrate sink and enriches the remaining pool in ^{15}N at the same time) and thus hardly apply to the inner shelf region, where photic zone [NO_3^-] often approximates near-zero levels (Tyrrell and Lucas, 2002; Lavik et al., 2009).

As with [TOC] and $\delta^{15}N_{sediment}$, the relationship between SST and $\delta^{15}N_{sediment}$ reverses west of the shelf break (Fig. 12). In coastal proximity, low SSTs and concomitantly high $\delta^{15}N_{sediment}$-values testify to the upwelling of cold and denitrified source waters (Emeis et al., 2009). The negative correlation between SST and $\delta^{15}N_{sediment}$ only concerns the continental shelf though. Beyond 170 km offshore, both parameters increase in tandem. Even though the latter finding is only supported by a limited data set herein, it agrees well with the results presented by Holmes et al. (1999).

5.2.3. Potential reasons for the $\delta^{15}N$-minimum at the shelf break

Potential reasons for low $\delta^{15}N$-signals in the primary product include (i) nitrogen fixation by cyanobacteria, (ii) diatom-mediated, vertical nutrient transport (Villareal et al., 1993) and (iii), according to the concept of Rayleigh fractionation kinetics, abundant nitrate supply. To our knowledge, no evidence has yet been found that nitrogen fixation plays an important role in the area investigated (see also Emeis et al., 2009). The same applies to vertically migrating diatoms.

The fact that minimum $\delta^{15}N$ coincides that well with the edge of the shelf (Fig. 7) strongly suggests a topographically controlled scenario. Shelf edge upwelling represents a highly promising explanation. Hart and Currie (1960) were the first to advance the idea of two-celled circulation in the northern Benguela region. Since then, various authors have put the hypothesis of shelf edge upwelling further forward (e.g. Bang, 1971; Barange and Pillar, 1992; Brüchert et al., 2004; Pichevin et al., 2005; Summerhayes et al., 2005; Emeis et al. 2009).

Emeis et al. (2009) reported a narrow band of elevated nitrate concentrations situated above the shelf break between latitude 22 and 24°S. Nutrient
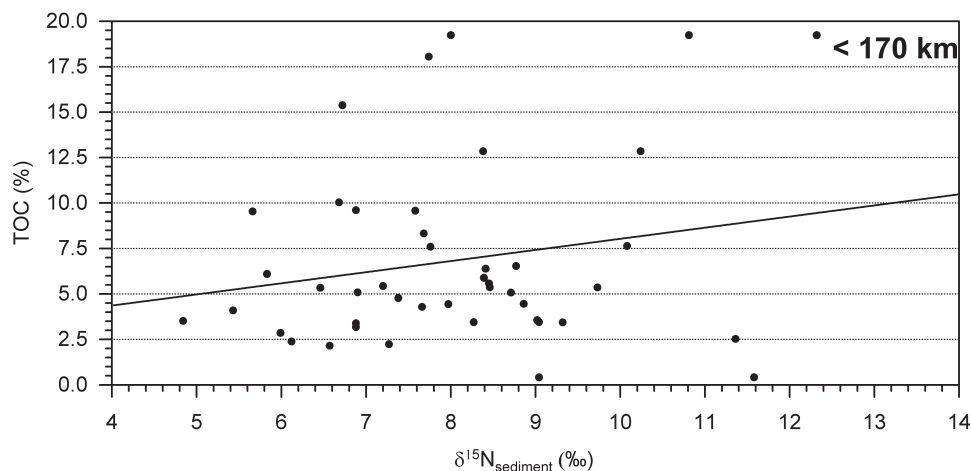
Fig. 11. Delta$^{15}N_{sediment}$ vs. [TOC]. Data pairs are restricted to the continental shelf (< 170 km distance to the coast) between latitude 19.0 and 25.5°S. High primary production, as indicated by high [TOC], tends to be associated with high $\delta^{15}N$-values. The observed relation of $\delta^{15}N_{sediment}$ and [TOC] is neither pronounced nor statistically significant ($r^2 = 0.04$; $p = 18.10\%$). However, it does not strictly follow Rayleigh fractionation kinetics either but rather suggests the influence of denitrification.

a

b
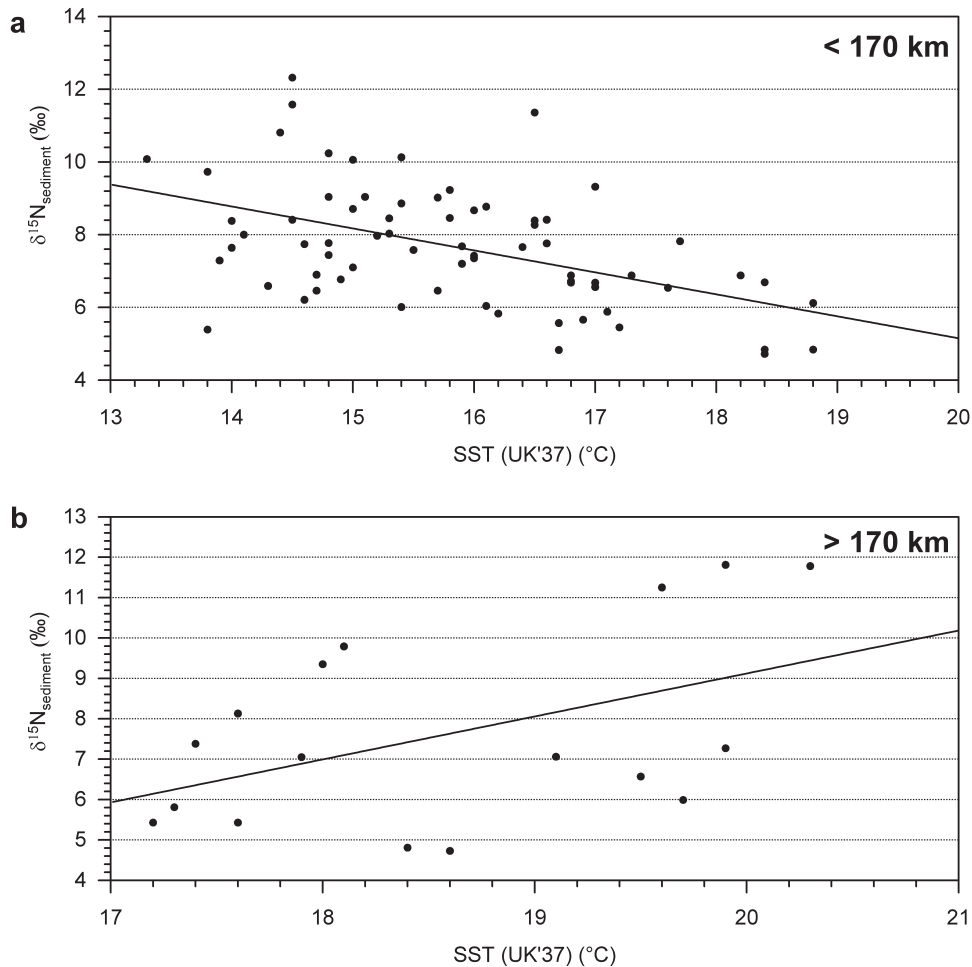
Fig. 12. SST (alkenone-based) vs. $\delta^{15}N_{sediment}$ between latitude 19 and 26.5°S. (a) The negative correlation above the continental shelf (< 170 km off the coast) corresponds to the upwelling of cold and denitrified (i.e. ^{15}N-enriched) source waters ($r^2 = 0.23$; $p = 0.01\%$). (b) Beyond the shelf edge, the trend reverses ($r^2 = 0.22$; $p = 5.2\%$).

replenishment via shelf edge upwelling not only accounts for reduced relative nitrate consumption and a corresponding decline in $\delta^{15}N$ in the primary product, but also fits the increase in primary production, as inferred from the minor peak in [TOC] above the outer shelf and upper continental slope (Fig. 4b). Summerhayes et al. (1995) argue that high concentrations of nutrients and organic particles make shelf edge upwelling a reasonable scenario.

The theory of a two-celled circulation scheme fits our findings reasonably well. The fact that the UK'37-record (Fig. 2b) indicates no shelf break cooling is not automatically considered a counter-argument. Upwelled waters do not necessarily reach the uppermost water layer where the UK'37-record is generated (the UK'37-record derives from phytoplankton dwelling between 0 and 2 m depth; see Emeis et al., 2009). Besides that, shelf edge upwelling does not bring as cold waters to the surface ocean as the coastal upwelling does (Summerhayes et al., 1995).

5.3. Potential interplay of oceanographic and nutrient-relevant processes and their control on the local nutrient dynamics

Before going into details we would like to emphasise that the model proposed here is intended to be valid for the area investigated only. So far, we have discussed the coastal $\delta^{15}N$-maximum (section 5.2.1.) as well as the shelf break minimum (section 5.2.3.). However, the reason for the actual decline in $\delta^{15}N_{sediment}$ and $\delta^{15}N_{SPM}$ within ±160 km to the coast is still open. The combination of the following two mechanisms provides a reasonable explanation:

(i) As bottom waters travel up the shelf they get more and more anoxic due to decomposition reactions they are supporting on their way. The proceeding exhaustion of O_2 is accompanied by rising $\delta^{15}N_{nitrate}$-values because denitrification gets increasingly important as oxygen is gradually used up. Interestingly, the oceanward decline in surface water $\delta^{15}N_{SPM}$ (Fig. 6a) represents an exact copy of the trend bottom $\delta^{15}N_{nitrate}$

is expected to perform. Apparently, bottom nitrate somehow supports primary production in the photic zone over large areas of the continental shelf. An obvious explanation is that the penetration of wind- and wave-induced mixing is so deep as to tap the varyingly denitrified, subsurface waters (Fig. 13).

The fact remains, however, that the vertical mixing is not so pronounced as to erase the east-west temperature gradient of the surface waters (Fig. 2b). Coldest SSTs concentrate to a narrow band right at the coast and temperatures increase slightly above the middle shelf. The actual process of upwelling only occurs when the cold bottom waters hit the coast.

(ii) The second feature considered capable of outweighing the ^{15}N-enrichment of surface nitrate as the water masses are dragged offshore is related to shelf edge upwelling. Shelf edge upwelling involves the formation of large eddies and swirls, whose interaction with the westward flowing surface currents is believed to create a zone of turbulence and mixing spreading across the middle shelf (Fig. 13). In this zone, situated roughly between 20 and 170 km off the coast, denitrified ^{15}N-enriched water from the coastal upwelling encounters and mixes with nutrient-rich waters introduced at the shelf edge.

The scenario of eddy-induced, cross-shelf mixing corresponds well with the random distribution of [NO_3^-] across the shelf, shown by Tyrrell and Lucas (2002). The fact is, however, that their compilation combines [NO_3^-]-data from a wide range of depths and the question arises whether the trend would still be lacking if only surface [NO_3^-] be considered.

So far, there is no adequate set of [NO_3^-]-data to test our hypotheses against. On the basis of the available facts we incline to the view that the westward decrease in $\delta^{15}N_{sediment}$ and surface ocean $\delta^{15}N_{SPM}$ results from decreasing relative nitrate consumption, based on a combination of less primary production (the vertical flux declines; Fig. 4) and replenished nutrient supplies. The replenishment with nutrients occurs via shelf edge upwelling (hypothesis ii) as well as the mixing of subsurface nitrate into the surface layer over large areas of the shelf (hypothesis i), with both mechanisms working against the expected nutrient drawdown as surface waters travel offshore.

As outlined above (section 5.1.), terrestrial material has no measurable effect. Some might argue nonetheless that, with increasing distance to the coast and concomitantly declining primary production rates (Fig. 4), terrigenous nitrogen (i.e. ammonium bound in clays; Bremner and Willis, 1993) could gain proportionally enough importance to lower the bulk $\delta^{15}N$-signal. Dust from southern Africa
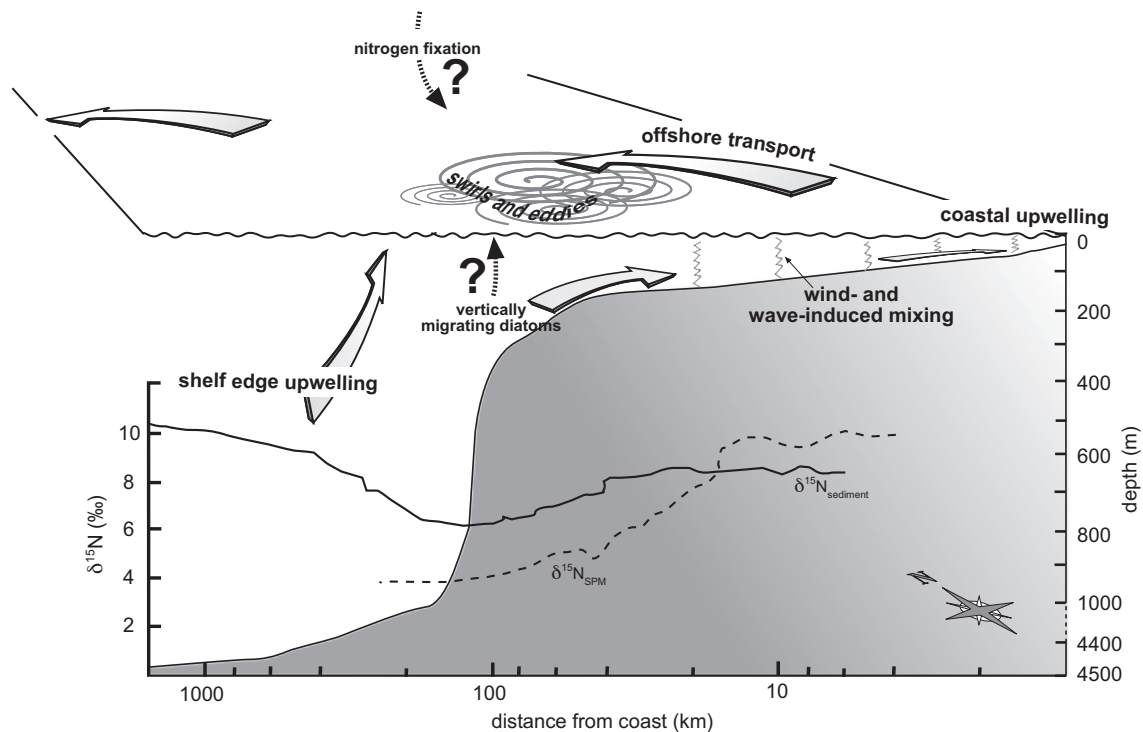
Fig. 13. Model showing the potential factors controlling the nutrient dynamics above the shelf. The decline in $\delta^{15}N$ toward the outer shelf (see Fig. 7) may partially be ascribed to shelf edge upwelling and the formation of large eddies and swirls creating a zone of mixing spreading across the shelf. In this zone, westward propagating waters from the coastal upwelling (denitrified, i.e. ^{15}N-enriched) encounter and mix with nutrient-rich waters introduced via shelf edge upwelling. Vigorous wind- and wave-induced mixing and the resultant introduction of denitrified bottom waters to the photic zone represents an alternative scenario that might account for the $\delta^{15}N$-gradient. Indirect nutrient supply, mediated by organisms such as vertically migrating diatoms or nitrogen-fixing cyanobacteria, may contribute to the $\delta^{15}N$ minimum above the shelf edge.

exhibits comparably low $\delta^{15}N$-values (ca. 5‰; Holmes et al., 2002) and could contribute, therefore, to the observed decline in $\delta^{15}N$. However, C_{org}/N of surface ocean suspended matter argues against this hypothesis. C_{org}/N values are a widely used instrument in distinguishing between marine and terrestrial organic matter (Schubert and Calvert, 2001). If terrestrial matter would increase relative to marine material, C_{org}/N should increase. In fact, C_{org}/N ratios are randomly distributed (not shown).

The rise in $\delta^{15}N_{sediment}$ beyond the shelf agrees with earlier studies and is usually ascribed to the steady ^{15}N-enrichment of the nitrate pool as it is drawn down by phytoplankton growth (Holmes et al., 1996, 1998, 1999; Pichevin et al., 2005). Still, the translation of $\delta^{15}N_{sediment}$-values into nitrate consumption remains debatable. As microbial impact increases along with depth (section 5.1.), the oceanward rise in $\delta^{15}N_{sediment}$ may also be ascribed to the increasing influence of organic matter decay, or rather, NH_3-outgassing [a].

As long as we lack surface ocean $\delta^{15}N_{SPM}$-data from the continental slope, the topic remains open to discussion. In case that surface water $\delta^{15}N_{SPM}$ copies the rise performed by $\delta^{15}N_{sediment}$, the development of $\delta^{15}N_{sediment}$ might primarily be Rayleigh-controlled. An increasing offset between surface water and sedimentary $\delta^{15}N$ would rather account for degradation-controlled $\delta^{15}N_{sediment}$, instead. Analysing $\delta^{15}N$ on rinsed sediment represents an alternative in order to detect the influence of microbial impact (Meisel and Struck, 2011). Rinsing prior to measurement seems capable of restoring the original pelagic signal, wiping out decayal-related $\delta^{15}N$-shifts [a].

6. Conclusions and outlook

Surface ocean $\delta^{15}N_{SPM}$-data substantiate the previously observed $\delta^{15}N_{sediment}$-gradient above the central Namibian shelf (i.e. decreasing $\delta^{15}N$-signals towards the shelf edge). On the evidence of the strikingly parallel trend of $\delta^{15}N_{sediment}$ and $\delta^{15}N_{SPM}$, secondary processes such as microbial activity are apparently not so pronounced as to obliterate the surface-generated signal. The downward transfer of unaltered surface production seems to work particularly well in the shallow coastal waters where the flux is high and fast. However, in order that $\delta^{15}N_{sediment}$ can be a reliable tool in the study of palaeo-oceanography, it is not only the link between the surface production and the sedimentary record that needs to be demonstrated. In fact, the parameter only becomes useful if the processes producing the surface signal are known. Main uncertainties stem from the potential influence of denitrified waters as well as the apparent, yet

unsubstantiated, introduction of nutrient-rich water at the shelf edge and its mixing into the original pool along its flow path. The deep penetration of wind- and wave-induced mixing and the tapping of varyingly denitrified bottom waters appear to be additional characteristics of the shallow shelf. All these factors complicate the local nitrogen budget and should be kept in mind when interpreting $\delta^{15}N$-fluctuations in sediment cores retrieved from this area.

The apparent lack of any relationship between $\delta^{15}N$ and $[NO_3^-]$ casts doubt on the applicability of $\delta^{15}N$ as a reliable proxy of relative nutrient utilisation above the central Namibian shelf. Much effort is currently being put in the data mining of large amounts of surface $[NO_3^-]$-measurements and shelf-wide $[NO_3^-]$-profiles, including isotopic analysis ($\delta^{15}N_{nitrate}$). This will help to identify the sources contributing to today's nutrient regime and will highly improve the interpretation of the $\delta^{15}N_{sediment}$-pattern as well as advance our understanding of the single processes involved (i.e. shelf edge upwelling, nitrogen fixation, etc.).

References

Altabet, M.A., McCarthy, J.J., (1985) Temporal and spatial variations in the natural abundance of ^{15}N in PON from a warm-core ring. *Deep-Sea Research*, 32, 755-772.

Altabet, M., Deuser, W.G., Honjo, S., Stienen, C., (1991) Seasonal and depth-related changes in the source of sinking particles in the North Atlantic. *Nature*, 354, 136-139.

Altabet, M.A., Francois, R., (1994) Sedimentary nitrogen isotopic ratio as a recorder for surface ocean nitrate utilization. *Global Biogeochemical Cycles*, 8, 103-116.

Altabet, M.A., Pilskaln, C., Thunnel, R., Pride, C., Sigman, D., Chavez, F., Francois, R., (1999) The nitrogen isotope biogeochemistry of sinking particles from the margin of the Eastern North Pacific. *Deep Sea Research I*, 46, 655-679.

Bakun, A., Weeks, S.J., (2004) Greenhouse gas buildup, sardines, submarine eruptions and the possibility of abrupt degradation of intense marine upwelling ecosystems. *Ecology Letters*, 7, 1015-1023.

Bang, N.D., (1971) The southern Benguela current region in February, 1966: Part II. Bathythermography and air-sea interactions. *Deep-Sea Research*, 18, 209-224.

Barange, M., Pillar, S.C., (1992) Cross-shelf circulation, zonation and maintenance mechanisms of *Nyctiphanes capensis* and *Euphausia hanseni* (Euphausiacea) in the northern Benguela upwelling system. *Continental Shelf Research*, 12(9), 1027-1042.

Berger, W.H., Smetacek, V.S., Wefer, G., (1989) Productivity of the ocean: present and past, pp. 471. John Wiley and Sons, Chichester.

Berger, W.H., Wefer, G., (2002) On the reconstruction of upwelling history: Namibia upwelling in context. *Marine Geology*, 180, 3-28.

Boebel, O., Lutjeharms, J., Schmid, C., Zenk, W., Rossby, T., Barron, C., (2003) The Cape Cauldron: a regime of turbulent inter-ocean exchange. *Deep-Sea Research*, II(50), 57-86.

Bremner, J.M., Willis, J.P., (1993) Mineralogy and geochemistry of the clay fraction of sediments from the Namibian continental margin and the adjacent hinterland. *Marine Geology*, 115, 85-116.

Brüchert, V., Altenbach, A.V., Bening, G., Bockelmann, F., Currie, B., Donath, J., Dübecke, J., Endler, R., Erdmann, S., Ertan, T., Fuchs, B., Klockgether, G., Krüger, S., Kuypers, M.M.M., Lass, H.U., Lavik, G., Lilienthal, S., Leipe, T., Nickel, G., Noli-Peard, K., Ohde, T., Schulz, B., Schulz, H., Siegel, H., Struck, U., Wulf, J., Zitzmann, S., Zonneveld, K., (2004) The Benguela Upwelling System 2003, Part 3, Cruise No. 57, Leg 3, March 15 – April 13, 2003, Walvis Bay, Namibia - Dakar. In: *Meteor Berichte*, *4*, pp. 53.

Bubnov, V.A., (1972) Structure and characteristics of the oxygen minimum layer in the southeast Atlantic Ocean. *Oceanology*, 12, 193-201.

Calvert, S.E., Price, N.B., (1971) Upwelling and nutrient regeneration in the Benguela Current, October, 1968. *Deep-Sea Research*, 18, 505-523.

Chapman, P., Shannon, L., (1985) The Benguela ecosystem Part II. Chemistry and related processes. *Oceanography and Marine Biology Annual Review* 23, 183-251.

Chapman, P., Shannon, L., (1987) Seasonality in the oxygen minimum layers at the extremities of the Benguela system. *South African Journal of Marine Science*, 5, 51-62.

Cline, J.D., Kaplan, I.R., (1975) Isotopic fractionation of dissolved nitrate during denitrification in the eastern tropical North Pacific Ocean. *Marine Chemistry*, 3, 271-299.

Codispoti, L., Christensen, J.P., (1985) Nitrification, denitrification and nitrous oxide cycling in the eastern tropical South Pacific Ocean. *Marine Chemistry*, 16, 277-300.

Conkright, M., Levitus, S., O`Brien, T., Boyer, T.P., Antonov, J., Stephens, C., (1998) World Ocean Atlas 1998. CD-ROM Data Set Documentation. In: *Tech. Rep.15, NODC Internal Report, Silver Spring, MD*.

Emeis, K.-C., Brüchert, V., Currie, B., Endler, R., Ferdelman, T., Kiessling, A., Leipe, T., Noli-Peard, K., Struck, U., Vogt, T., (2004) Shallow gas in shelf sediments of the Namibian coastal upwelling ecosystem. *Continental Shelf Research*, 24(6), 627-642.

Emeis, K.-C., Struck, U., Leipe, T., Ferdelman, T.G., (2009) Variability in upwelling intensity and nutrient regime in the coastal upwelling system offshore Namibia: results from sediment archives. *International Journal of Earth Sciences* 98, 309-326.

Francois, R., Altabet, M.A., Burckle, L.H., (1992) Glacial to interglacial changes in surface nitrate utilization in the Indian sector of the southern ocean as recorded by sediment δ¹⁵N. *Paleoceanography*, 7, 589-606.

Gaebler, O.H., Vitti, T.G., Vukmirovich, R., (1966) Isotope effects in metabolism of ¹⁴N and ¹⁵N from unlabeled dietary proteins. *Canadian Journal of Biochemistry*, 44, 1249-1257.

Gaye-Haake, B., Lahajnar, N., Emeis, K.-C., Unger, D., Rixen, T., Suthhof, A., Ramaswamy, V., Schulz, H., Paropkari, A.L., Guptha, M.V.S., Ittekkot, V., (2005) Stable nitrogen isotopic ratios of sinking particles and sediments from the northern Indian Ocean. *Marine Chemistry*, 96, 243-255.

Gordon, A.L., (1986) Interocean Exchange of Thermocline Water. *Journal of Geophysical Research*, 91(C4), 5037-5046.

Hart, T.J., Currie, R.I., (1960) The Benguela Current. *Discovery Report*, 31, 123-127.

Holmes, M.E., Müller, P.J., Schneider, R.R., Segl, M., Pätzold, J., Wefer, G., (1996) Stable nitrogen isotopes in Angola Basin surface sediments. *Marine Geology*, 134, 1-12.

Holmes, M.E., Müller, P.J., Schneider, R.R., Segl, M., Wefer, G., (1998) Spatial variations in euphotic zone nitrate utilization based on δ¹⁵N in surface sediments. *Geo-Marine Letters*, 18(1), 58-65.

Holmes, B., Eichner, C., Struck, U., Wefer, G., (1999) Reconstructions of surface ocean nitrate utilization using stable nitrogen isotopes in sinking particles and sediments. In: *Use of Proxies in Paleoceanography: Examples from the South Atlantic* (Ed. by G. Fischer, G. Wefer), pp. 447-468. Springer, Berlin.

Holmes, E., Lavik, G., Fischer, G., Segl, M., Ruhland, G., Wefer, G., (2002) Seasonal variability of δ¹⁵N in sinking particles in the Benguela upwelling region. *Deep-Sea Research I*, 49, 377-394.

Knowles, R., (1982) Denitrification. *Microbiological Reviews*, 46(1), 43-70.

Kuypers, M.M.M., Lavik, G., Woebken, D., Schmid, M., Fuchs, B.M., Amann, R., Jørgensen, B.B., Jetten, M.S.M., (2005) Massive nitrogen loss from the Benguela upwelling system through anaerobic ammonium oxidation. *PNAS*, 102(18), 6478-6483.

Lavik, G., Krüger, S., Leipe, T., (2004) CTD Profiling of Nutrients in the Water Column. In: *The Benguela Upwelling System 2003, Part 3, Cruise No. 57, Leg 3, March 15 – April 13, 2003, Walvis Bay, Namibia - Dakar, Meteor Berichte, 4* (Ed. by V. Brüchert, A.V. Altenbach, G. Bening, F. Bockelmann, B. Currie, J. Donath, J. Dübecke, R. Endler, S. Erdmann, T. Ertan, B. Fuchs, G. Klockgether, S. Krüger, M.M.M. Kuypers, H.U. Lass, G. Lavik, S. Lilienthal, T. Leipe, G. Nickel, K. Noli-Peard, T. Ohde, H. Schulz, H.D. Schulz, H. Siegel, U. Struck, J. Wulf, S. Zitzmann, K. Zonneveld), pp. 20-20.

Lavik, G., Stührmann, T., Brüchert, V., van der Plas, A., Mohrholz, V., Lam, P., Mußmann, M., Fuchs, B.M., Amann, R., Lass, U., Kuypers, M.M.M., (2009) Detoxification of sulphidic African shelf waters by blooming chemolithotrophs. *Nature*, 459, 581-585.

Lehmann, M.F., Bernasconi, S.M., Barbieri, A., McKenzie, J.A., (2002) Preservation of organic matter and alteration of its carbon and nitrogen isotope composition during simulated and in situ early sedimentary diagenesis. *Geochimica et Cosmochimica Acta*, 66, 3573-3584.

Libes, S.M., Deuser, W.G., (1988) The isotope geochemistry of particulate nitrogen in the Peru Upwelling Area and the Gulf of Maine. *Deep-Sea Research*, 35(4), 517-533.

Lutjeharms, J.R.E., Meeuwis, J.M., (1987) The extent and variability of southeast Atlantic upwelling. *South African Journal of Marine Science*, 5, 85-94.

Mariotti, A., Germon, J.C., Hubert, P., Kaiser, P., Letolle, R., Tardieux, A., Tardieux, P., (1981) Experimental determination of nitrogen kinetic isotope fractionation: Some principles; illustration for the denitrification and nitrification processes. *Plant and Soil*, 62, 413-430.

Meisel, S., Struck, U., (2011) The potential distortion of sedimentary δ¹⁵N and C_{org}/N ratios by NH_4^+ and the effects of pre-analysis sample treatment. *Fossil Record,* 14(2), 141-152.

Meisel, S., Emeis, K.-C., Struck, U., Kristen, I., (2011) Nutrient regime and upwelling in the northern Benguela since the middle Holocene in a global context – a multi-proxy approach. *Fossil Record,* 14(2), 171-193.

Melander, L., (1960) *Isotope effects on reaction rates.* Ronald Press, New York.

Mohrholz, V., Bartholomae, C.H., van der Plas, A.K., Lass, H.U., (2008) The seasonal variability of the northern Benguela undercurrent and its relation to the oxygen budget on the shelf. *Continental Shelf Research*, 28(3), 424-441.

Mollenhauer, G., Schneider, R.R., Müller, P.J., Spieß, V., Wefer, G., (2002) Glacial/interglacial variability in the Benguela upwelling system: Spatial distribution and budgets of organic carbon accumulation. *Global Biogeochemical Cycles*, 16(4), 1134.

Montoya, J.P., (1994) Nitrogen isotope fractionation in the modern ocean: Implications for the sedimentary record. In: *Carbon Cycling in the Glacial Ocean: Constraints on the Ocean´s Role in Global Change.*, 17, *NATO ASI Series* (Ed. by R. Zahn, T.F. Pedersen, M.A. Kaminski, L. Labeyrie), pp. 259-279. Springer-Verlag, Berlin.

Montoya, J.P., McCarthy, J.J., (1995) Isotopic fractionation during nitrate uptake by phytoplankton growth in continuous culture. *Journal of Plankton Research*, 17, 439-464.

Moroshkin, K.V., Bubnov, V.A., Bulatov, R.P., (1970) Water circulation in the eastern South Atlantic Ocean. *Oceanology*, 10(1), 27-34.

Nelson, G., Hutchings, L., (1983) The Benguela upwelling area. *Progress in Oceanography*, 12, 333-356.

Ostrom, N.E., Macko, S.A., Deibel, D., Thompson, R.J., (1997) Seasonal variation in the stable carbon and nitrogen isotope biogeochemistry of coastal cold ocean environment. *Geochimica et Cosmochimica Acta*, 61(14), 2929-2942.

Packard, T.T., Garfield, P.C., Codispoti, L.A., (1983) Oxygen consumption and denitrification below the Peruvian upwelling. In: *Coastal Upwelling: Its Sediment Record* (Ed. by E. Suess, J. Thiede), pp. 147-173. Plenum Press, New York.

Pichevin, L., Martinez, P., Bertrand, P., Schneider, R., Giraudeau, J., Emeis, K., (2005) Nitrogen cycling on the Namibian shelf and slope over the last two climatic cycles: Local and global forcings. *Paleoceanography*, 20.

Poole, R., Tomczak, M., (1999) Optimum multiparameter analysis of the water mass structure in the Atlantic Ocean thermocline. *Deep-Sea Research I*, 46, 1895-1921.

Ravelo, A.C., Fairbanks, R.G., (1992) Oxygen Isotopic Composition of Multiple Species of Planktonic Foraminifera: Recorders of the Modern Photic Zone Temperature Gradient. *Paleoceanography*, 7(6), 815-831.

Redfield, A.C., (1934) On the proportions of organic derivatives in sea water and their relation to the composition of plankton, *James Johnston Memorial Volume*, pp. 176-192. University Press of Liverpool, UK.

Ren, H., Sigman, D.M., Meckler, A.N., Plessen, B., Robinson, R.S., Rosenthal, Y., Haug, G.H., (2009) Foraminiferal Isotope Evidence of Reduced Nitrogen Fixation in the Ice Age Atlantic Ocean. *Science*, 323, 244-248.

Sachs, J.P., Repeta, D.J., (1999) Oligotrophy and nitrogen fixation during eastern Mediterranean sapropel events. *Science*, 286, 2485-2488.

Saino, T., Hattori, A., (1980) ^{15}N natural abundance in oceanic suspended particulate matter. *Nature*, 283, 752-754.

Schäfer, P., Ittekkot, V., (1993) Seasonal variability of $\delta^{15}N$ in settling particles in the Arabian Sea and its paleogeochemical significance. *Naturwissenschaften*, 80, 511-513.

Schubert, C.J., Calvert, S.E., (2001) Nitrogen and carbon isotopic composition of marine and terrestrial organic matter in Arctic Ocean sediments: implications for nutrient utilization and organic matter composition. *Deep-Sea Research I*, 48, 789-810.

Shannon, L.V., (1985) The Benguela ecosystem. Part I. Evolution of the Benguela, physical features and processes. *Oceanography and Marine Biology Annual Review*, 23, 105-182.

Shannon, L.V., Boyd, A.J., Brundrit, G.B., Taunton-Clark, J., (1986) On the existence of an El Niño-type phenomenon in the Benguela system. *Journal of Marine Research*, 44(3), 495-520.

Shannon, L.V., Nelson, G., (1996) The Benguela: Large Scale Features and Processes and System Variability. In: *The South Atlantic: Present and Past Circulation* (Ed. by G. Wefer, W.H. Berger, G. Siedler, D. Webb), pp. 163-210. Springer, Berlin, Heidelberg.

Shannon, L.V., O'Toole, M.J., (1999) Integrated Overview of the Oceanography and Environmental Variability of the Benguela Current Region - Thematic Report NO.2. In: *Synthesis and Assessment of Information on the Benguela Current Large Marine Ecosystem (BCLME)*, Windhoek, Namibia.

Shannon, L.V., O'Toole, M.J., (2003) Sustainability of the Benguela: ex Africa semper aliquid novi. In: *Large marine ecosystems of the world: trends in exploitation, protection and research* (Ed. by G. Hempel, K. Sherman), pp. 227-253. Elsevier B.V., Amsterdam.

Sigman, D.M., Altabet, M.A., Michener, R., McCorkle, D.C., Fry, B., Holmes, R.M., (1997) Natural abundance-level measurement of the nitrogen isotopic composition of oceanic nitrate: an adaption of the ammonia diffusion method. *Marine Chemistry*, 57(3-4), 227-242.

Sigman, D.M., Altabet, M.A., McCorkle, D.C., Francois, R., Fischer, G., (2000) The $\delta^{15}N$ of nitrate in the Southern Ocean: nitrogen cycling and circulation in the ocean interior. *Journal of Geophysical Research*, 105(C8), 599-614.

Stander, G.H., (1964) The Benguela Current off South West Africa. *Investigational Report of the Marine Research Laboratory of South West Africa*, 12, 1-43.

Stramma, L., Peterson, R.G., (1989) Geostrophic Transport in the Benguela Current region. *Journal of Physical Oceanography*, 19, 1440-1448.

Struck, U., Emeis, K.-C., Alheit, J., Schneider, R., Eichner, C., Altenbach, A.-V., (2002) Changes of the upwelling rates of nitrate preserved in the $\delta^{15}N$-signature of sediments and fish scales from the diatomaceous mud belt off Namibia. *GeoBios*, 35(EPA-special issue), 3-11.

Summerhayes, C.P., Kroon, D., Rosell-Mele, A., Jordan, R.W., Schrader, H.-J., Hearn, R., Villanueva, J., Grimalt, J.O., Eglington, G., (1995) Variability in the Benguela Current upwelling system over the past 70,000 years. *Progress in Oceanography*, 35, 207-251.

Tomczak, M., Godfrey, J.S., (2003) *Regional Oceanography: An Introduction*. Daya Publishing House.

Tyrrell, T., Lucas, M.I., (2002) Geochemical evidence of denitrification in the Benguela upwelling system. *Continental Shelf Research*, 22, 2497-2511.

Villareal, T.A., Altabet, M.A., Culver-Rymsza, K., (1993) Nitrogen transport by vertically migrating diatom mats in the North Pacific Ocean. *Nature*, 363, 709-712.

Voss, M., Altabet, M., von Bodungen, B., (1996) $\delta^{15}N$ in sedimenting particles as indicator for euphotic zone processes. *Deep-Sea Research*, 43, 33-47.

Wada, E., Hattori, A., (1978) Nitrogen isotope effects in the assimilation of inorganic nitrogenous compounds by marine diatoms. *Geomicrobiology Journal*, 1, 85-101.

Wada, E., (1980) Nitrogen isotope fractionation and its significance in biogeochemical processes occurring in marine environments. In: *Isotope Marine Chemistry* (Ed. by E.D. Goldberg, Y. Horibe, K. Saruhashi), pp. 375-398. Uchida Rokakuho, Japan.

Waser, N.A.D., Turpin, D.H., Harrison, P.J., Nielsen, B., Calvert, S.E., (1998) Nitrogen isotope fractionation during uptake and assimilation of nitrate, nitrite, ammonium and urea by a marine diatom. *Limnology and Oceanography*, 43, 215-224.

Weeks, S.J., Currie, B., Bakun, A., Peard, K.R., (2004) Hydrogen sulphide eruptions in the Atlantic Ocean off southern Africa: implications of a new view based on SeaWiFS satellite imagery. *Deep-Sea Research I*, 51, 153-172.

Nutrient regime and upwelling in the northern Benguela since the middle Holocene in a global context – a multi-proxy approach

Sandra Meisel [a], Kay-Christian Emeis [b], Ulrich Struck [a,*], Iris Kristen [c]

[a] *Museum für Naturkunde, Leibniz-Institut für Evolutions- und Biodiversitätsforschung an der Humboldt-Universität zu Berlin, Invalidenstraße 43, 10115 Berlin, Germany*

[b] *Institut für Biogeochemie und Meereschemie, Universität Hamburg, Bundesstr. 55, 20146 Hamburg, Germany*

[c] *Walaboda 69B, 7063 Praden, Switzerland*

ABSTRACT

The last 5500 years of climate change and environmental response in the northern Benguela Coastal Upwelling are reconstructed by means of three sediment cores from the inner shelf off central Namibia. The study is based on nutrient (δ^{15}N, δ^{13}C) and productivity proxies (accumulation rates of total organic carbon; AR_{TOC}). Reconstructed sea surface temperatures (alkenone-derived SST) and temperatures at subsurface depths ($T_{\delta180}$; based on tests of planktonic foraminifers) reflect the physical boundary conditions. The selection of proxy indicators proved a valuable basis for robust palaeo-climatic reconstructions, with the resolution ranging from multi-decadal (NAM1) over centennial (core 178) to millennial scale (core 226620).

The northern Benguela experienced pronounced and rapid perturbation during the middle and late Holocene, and apparently, not all are purely local in character. In fact, numerous correlations with records from the adjacent South African subcontinent and the northern hemisphere testify to global climatic teleconnections. The Holocene Hypsithermal, for instance, is just as evident as the Little Ice Age (LIA) and the Roman Warm Period. The marked SST-rise associated with the latter is substantiated by other marine and terrestrial data from the South African realm. The LIA (at least its early stages) manifests itself in intensified winds and upwelling, which accords with increased rainfall receipts above the continental interior.

It appears that climate signals are transferred both via the atmosphere and ocean. The combined analysis of SST and $T_{\delta180}$ proved a useful tool in order to differentiate between both pathways. SSTs are primarily controlled by the intensity of atmospheric circulation features, reflecting changes of upwelling-favourable winds. $T_{\delta180}$ records the temperature of the source water and often correlates with global ocean conveyor speed due to varying inputs of warm Agulhas Water. It seems as though conveyor slowdown or acceleration not only affected the temperature of the source water but also its nutrient content. This relationship between source water quality and conveyor speed is already known from glacial times.

1. Introduction

The Benguela Coastal Upwelling is one of the most productive ecosystems on Earth, holding a considerable amount of the world's living marine resources. After mining, the fisheries sector represents the second largest export earner in the Namibian economy (van Zyl, 2010). Over the last decades, conditions have been rapidly deteriorating due to overfishing, habitat degradation, excessive nutrient loading, pollution effects, etc. The imminent threat of greenhouse warming raises additional concern (Shannon and O'Toole, 2003; Cochrane et al., 2007). By means of climate models, it has already been tried to evaluate the potential impact of global climate change on the coastal upwelling. However, predictions have been inconclusive and remain to be tested against additional palaeo-records (Cohen and Tyson, 1995).

We investigate the variability of the northern Benguela Upwelling since the middle Holocene and try to examine the impact of past climate fluctuations on the system. This is in order to assess its vulnerability to external climate forcing and to gain a better understanding of what the system may await in the future. In this regard, it is necessary to distinguish global and

* Corresponding author. Tel.: +49 (0)30 2093-8552;
  Fax: +49 (0)30 2093-8565.

  E-mail address: Ulrich.Struck@mfn-berlin.de (U. Struck).

regional perturbations from those that are purely local in character.

Much effort has already been put in a better understanding of glacial-interglacial fluctuations in the Benguela system. Owing to several ODP-expeditions on the continental slope off southwest Africa, the Pleistocene evolution of upwelling is relatively well known, (e.g. Diester-Haas et al., 1988; Oberhänsli, 1991; Summerhayes et al., 1995; Kirst et al., 1999; Berger and Wefer, 2002; Kim et al., 2002). In contrast, only few studies (e.g. Emeis et al., 2009) have so far availed themselves of the high-resolution shelf sediments. Terrestrial-based geoarchives from the adjacent subcontinent are also scarce, usually poorly resolved and dated (Heine, 2005). As a consequence, the hitherto documented history of Holocene climate variability is still fragmentary.

Compared to glacial-interglacial cycles, the Holocene is considered relatively stable. Nonetheless, palaeo-climate records from the North Atlantic show that periods comparable to the Little Ice Age and the Medieval Warming are recurrent features of the last millennia (Kreutz et al., 1997; Bianchi and McCave, 1999).

The Benguela is a highly dynamic system on both temporal and spatial scales, and the question is whether global perturbations are pronounced and far-reaching enough to leave clear marks in the central Namibian shelf environment, that is, to outweigh the immanent heterogeneity of the system. Our investigation is based on three sediment cores from the central Namibian inner shelf. Their N-S alignment allows us to explore shifts of upwelling through time and to study local inhomogeneities. Palaeo-temperature estimates (alkenone unsaturation index UK'37 and $\delta^{18}O$ from foraminiferal calite) hold clues to the intensity of upwelling and varying
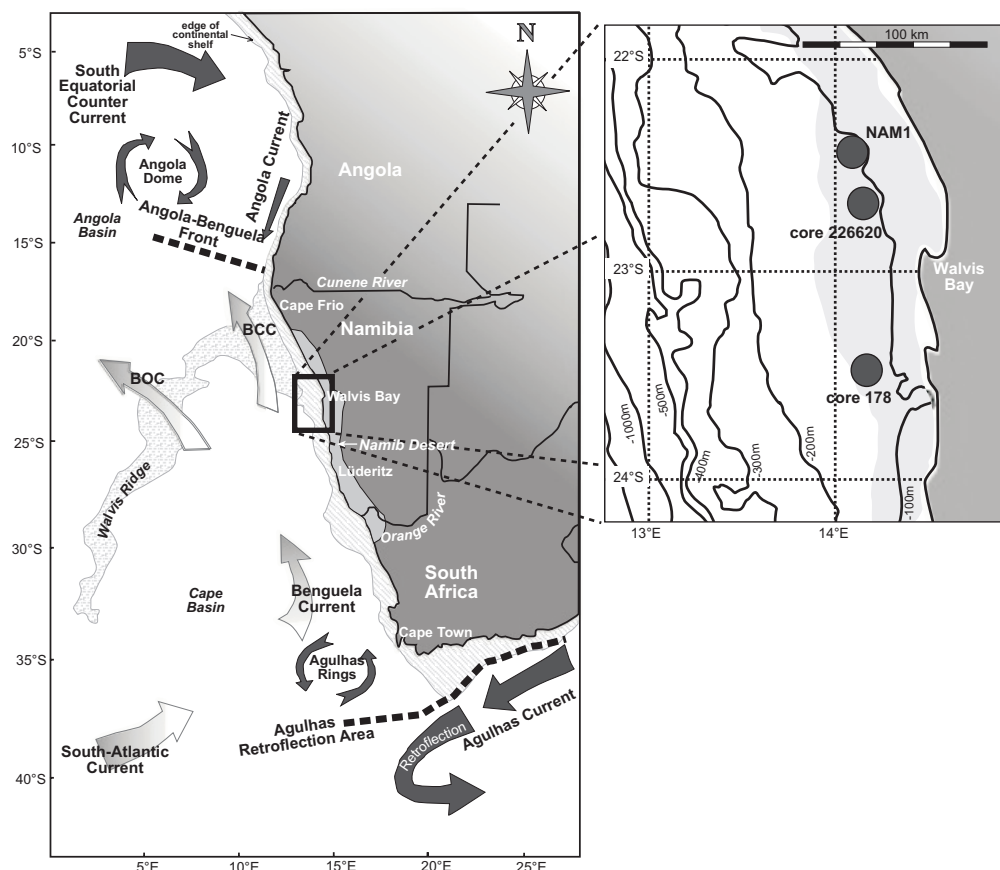
Fig. 1. Oceanographic setting and area of investigation. The Benguela Coastal Upwelling extends from southern Angola along the west coast of Namibia and South Africa. At its northern and southern ends, the system is bordered by highly dynamic warm water regimes, the Angola-Benguela Front and the Agulhas Retroflection area respectively. The warm and nutrient-poor South Equatorial Counter Current (SECC) flows south-eastward towards the Angola Basin at subsurface depths until it reaches the surface at around 10°S where it continues southward as the Angola Current (Moroshkin et al., 1970). The equatorward flowing Benguela Current splits into the Benguela Oceanic Current (BOC) and the Benguela Coastal Current (BCC) at about 28°S (Stramma and Peterson, 1989). The BOC flows towards the northwest and is separated from the eastward flowing SECC by a large cyclonic gyre, the Angola Dome. BCC continues its coastal-parallel journey until meeting the Angola Current at the Angola-Benguela Front situated between 14 and 17°S, depending on the season. Cold surface currents are lightly coloured, darker arrows denote warm surface currents (map modified after Holmes et al., 1999). The small chart zooms in on the area under investigation showing the locations of the three cores investigated herein. The diatomaceous muds are shaded grey.

types of source waters. Isotopic abundance ratios of nitrogen ($\delta^{15}N$) and organic carbon ($\delta^{13}C_{org}$), accumulation rates (AR) and total organic carbon (TOC) are used to reconstruct the nutrient regime and biological response at the time of deposition.

1.1. Setting

The Benguela Current represents the eastern boundary current of the South Atlantic anticyclonic gyre. A coastal upwelling system is situated at its eastern periphery. Coastal upwelling extends seaward about 150 to 200 km, but upwelling filaments have been observed as far offshore as 1000 km (Shannon, 1985; Lutjeharms and Stockton, 1987). Upwelling generally concentrates on seven cells located along the southwest African coast (Shannon and Nelson, 1996). The principal centre is in the vicinity of Lüderitz (27°S) where strong upwelling occurs throughout the year. The Lüderitz Upwelling represents an environmental boundary between the northern and southern Benguela, creating two quasi-independent subsystems (Shannon and Nelson, 1996; Shannon and O'Toole, 2003; Mohrholz et al., 2008). Fig. 1 provides an insight in the main oceanographic features and modern flow pattern.

The trade wind-driven upwelling taps water from up to 200 m depths (Mohrholz et al., 2008). The upwelled water represents a mélange of two upper central water masses, namely nutrient-rich and oxygen-poor South Atlantic Central Water (SACW) and well-oxygenated and nutrient-poor Eastern SACW (ESACW) (Mohrholz et al., 2008).

SACW originates from the Brazil-Malvinas Confluence region of the Subtropical Convergence in the SW-Atlantic and is transported within the subtropical gyre and the equatorial current system into the Angola Dome region. From there it is eventually advected along the shelf into the northern Benguela via the Angola Current, or, more precisely, via its southward continuation in the form of a poleward undercurrent penetrating through the Angola-Benguela Front. Its maximum southward reach is estimated at 27°S (Mohrholz et al., 2008). Owing to its low oxygen content, SACW is partly held responsible for the sub- to anoxic condition above the shelf (Chapman and Shannon, 1987; Shannon and Nelson, 1996). The second water mass, ESACW, is formed in the Agulhas Retroflection area in the south. It is a mixture of central water from the subtropical gyre and varying amounts of warm Indian Ocean Central (Agulhas) Water injected into the South Atlantic through the Agulhas Current (Gordon, 1986; Mohrholz et al., 2008). The Agulhas Retroflection area and southern Cape Basin are referred to as

the 'Cape Cauldron', a zone of turbulent inter-ocean exchange where Indian and South Atlantic waters are thoroughly stirred and mixed (Boebel et al., 2003). The enhanced introduction of warm Agulhas Water is a recurrent event on (inter-) annual scales. On such occasions the Agulhas Water takes a more northerly path than usual, impacting on subsurface currents along the edge of the continental shelf (Shannon and O'Toole, 2003). On larger time scales, the amount of Indian Ocean Water injected into the South Atlantic is conjectured to depend on the intensity of the global thermohaline overturn (Gordon, 1986). We will expatiate on this phenomenon below, when placing the northern Benguela in the context of global climate variability (section 3.3.1.1.).

ESACW is carried northward along the upper continental slope and edge of the shelf by the Benguela Current itself (Gordon, 1986; Mohrholz et al., 2008). The mixing of the northward flowing ESACW and southward flowing SACW occurs in the large transition area between the Angola-Benguela Front and the Lüderitz Upwelling. There is a clear seasonal variability in the proportion of well-oxygenated ESACW and oxygen-poor SACW on the shelf off Walvis Bay; this results in seasonally alternating oxygenation of the bottom waters. The interaction of the alongshore and Ekman-induced cross-shelf current components makes the flow regime extremely complex (Mohrholz et al., 2008). For detailed insight in today's nutrient dynamics and oceanographic features of the central Namibian shelf see Mohrholz et al. (2008) and Meisel et al. (2011). Comprehensive reviews of the physical processes, chemistry and biology of the area are given by Chapman and Shannon (1985), Shannon (1985), Shannon and Pillar (1986), Shannon and O'Toole (2003) and Shannon and Nelson (1996).

2. Material and methods

2.1. Sediment cores

We investigated two gravity cores (178 and 226620) and one giant-kastencore (NAM1) lying on a N-S-oriented transect off central Namibia. Some data have already been published previously (see clear listing in Table 1), however, in combination with hitherto unpublished data it is certainly worth showing it again.

General core properties are summarised in Table 1. The cores originate from the coastal parallel belt of organic-rich, diatomaceous ooze coating the inner shelf up to more or less 150 m water depth (Fig. 1). The thickness of the mud depends on the morphology of the basement transgressed in the course of

Table 1
General core characteristics (a), details about sample preparation and listing of parameters (b). Source studies of previously published data are mentioned. For information about pre-analysis sample preparation methods see Meisel and Struck (2011). [*] Delta[15]N-data from untreated sample splits have already been published by Emeis et al. (2009).

a) general characteristics	NAM1	178	226620
cruise	Petr-Kottsov (04/04/1997)	Meteor Cruise M57-3 (18/03/2003)	Meteor Cruise M48-2 (05/08/2000)
latitude / longitude (dez)	22.67°S / 14.02°E	23.76°S / 14.27°E	22.75°S / 14.31°E
water depth	125 m	114 m	81 m
core length	545 cm	561 cm	380 cm
age	62 to 3036 BP	1757 to 3585 BP	860 to 5610 BP
b) core preparation and proxies	**NAM1**	**178**	**226620**
syringe samples	at 1 cm-intervals ($\varnothing$ 5.5 a)	at 5 cm-intervals ($\varnothing$ 16.5 a)	at 5 cm-intervals ($\varnothing$ 62.5 a)
TOC (wt%)	in-situ acidified sediment *Struck et al. (2002)*	in-situ acidified sediment	in-situ acidified sediment
$\delta^{13}C_{org}$ (‰)	in-situ acidified sediment *Struck et al. (2002)*	acidified plus rinsed sediment	acidified plus rinsed sediment
$\delta^{15}N$ (‰)	in-situ acidified sediment *Struck et al. (2002)*	acidified plus rinsed sediment	acidified plus rinsed sediment [*]
SST (°C)	UK'37	UK'37	UK'37 *Emeis et al. (2009)*
sediment slices	upper 50 cm (~330 BP) cut in 5 cm thick slices; then 1 cm-slices	5 cm thick slices	2 cm thick slices were taken at 4 cm-intervals
$T_{\delta18O}$ (°C)	foraminiferal calcite	foraminiferal calcite	foraminiferal calcite

the early Holocene (Bremner and Willis, 1993; Vogt, 2002; Emeis et al., 2004). From today's perspective, core 178 is situated in the centre of the Central Namibian Upwelling Cell (extending from 22.7 and 24.5°S; Shannon and Nelson, 1996) while NAM1 and core 226620 are situated below its northern fringes. In the shallow coastal waters primary production is particularly high (Meisel et al., 2011). High biogenic particle flux induces great oxygen demand in subsurface depths and contributes to the oxygen deficiency in bottom waters and sediments (Copenhagen, 1953; Bakun and Weeks, 2004, Brüchert et al., 2004; Emeis et al., 2004). The lack of oxygen prevents bioturbation, often resulting in a continuously laminated sediment sequence.

2.2. Sample processing

Syringe samples were taken at 1 cm-intervals from NAM1 (corresponding to an average sampling resolution of 5.5 a) and 5 cm-intervals from core 178 (16.5 a) and 226620 (62.5 a) (Table 1). The sediment was desiccated, homogenised by grinding and split for isotope and alkenone measurements (sections 2.3.1 and 2.4.2.). After that, the cores were cut into slices, out of which the foraminiferal tests (*O.universa*) were picked. The carbonate shells are used for $\delta^{18}O$-temperature reconstructions and ^{14}C-dating (sections 2.4.1. and 2.5.). Table 1 provides details about the pre-analysis processing and a compilation of the parameters.

2.3. Isotopic measurements

2.3.1. Sediments

As to core 178 and 226620, $\delta^{13}C_{org}$ and $\delta^{15}N$ were determined on acidified plus rinsed material. With NAM1 the isotopic measurements are based on in-situ acidified sediment instead (published in Struck et al., 2002). The same applies to the analysis of TOC. Details about pre-analysis sample preparation (such as acidification plus rinsing and in-situ acidification) and implications for $\delta^{15}N$ are given in Meisel and Struck (2011). Isotope abundance ratios are reported in the conventional δ-notation in per mil (‰) with respect to atmospheric N_2 (AIR; concerning $\delta^{15}N$) and the VPDB-standard (concerning $\delta^{13}C_{org}$). Analytical precision was ±0.2‰, respectively (1σ standard deviation). The reproducibility of [TOC] (in wt%) is ±3% of the real amount present.

2.3.2. Foraminiferal calcite

The samples contained between 5 and 30 tests of the planktonic, symbiont-bearing foraminifer *O. universa*. Prior to analysis, the tests were soaked in methyl alcohol and cleansed of contaminants in an ultrasonic bath. Excess alcohol was removed with a pipette. The volatile residual was allowed to evaporate in the heating oven at 40°C. During measurement, the carbonate dissolves in orthophosphoric acid at constant 72°C. The $\delta^{18}O$-values in the calcite ($\delta^{18}O_{calcite}$) are related to the VPDB-standard (reported in ‰). Reproducibility of replicates was generally below ±0.1‰, which corresponds to ±0.5°C.

Carbon isotopes in foraminiferal calcite are much more susceptible to disequilibrium effects than oxygen isotopes. So-called "vital effects", processes such as foraminiferal metabolism and photosynthetic activity of symbionts are capable of changing the isotopic composition of the CO_2 available for calcification (Spero and Deniro, 1987; Wefer and Berger, 1991; Mulitza et al., 1999;). We decided therefore to do without the $\delta^{13}C_{calcite}$-signals as they provide rather unclear insights in the nutrient regime, only.

2.4. Temperature reconstruction

2.4.1. Subsurface depths ($\delta^{18}O_{calcite}$)

The $\delta^{18}O_{calcite}$-signals are a function of the temperature and oxygen isotope composition of the water (δ_w) during shell accretion (Niebler et al., 1999). According to the global ocean isotope curve of Fairbanks (1989), variations in δ_w are negligible for the period of investigation. During the last 5000 years the decline in δ_w due to meltwater discharge was actually lower than the precision of the method. This is why isotopic fluctuations are interpreted solely in terms of fluctuating water temperature. Disequilibrium effects (offset between the $\delta^{18}O_{calcite}$-value and the isotopic signature of calcite formed in thermodynamic equilibrium) are likewise negligible (Niebler et al., 1999). The palaeo-temperature equation applied describes low-light conditions where symbiont activity is moderate (Bemis et al., 1998).

$$T_{\delta 18O}\ (°C) = 16.5 - 4.8 \cdot (\delta_c - \delta_w) \qquad \text{with } \delta_w = -0.22\ ^{a)}$$

O. universa is a tropical to subpolar species. Generally, planktonic foraminifera do rarely have a preferred depth habitat but adapt to the respective hydrological conditions (Ravelo and Fairbanks, 1992; Hemleben and Bijma, 1994; Tedesco et al., 2007). To our knowledge there are yet no details about *O. universa* population dynamics in the Benguela Upwelling. Despite its algal symbionts, it is not necessarily bound to the photic zone. By and large, *O. universa* is considered an intermediate dweller. Its depth habitat extends from subthermocline depth into the mixed layer, varying with season, ontogeny, lunar cyclicity, availability of nutrients, etc. (Murray, 1991; Hemleben and Bijma, 1994; Tedesco et al., 2007). These changes in calcification depth are considered the reason for the typical fuzziness of the $T_{\delta 18O}$-signal.

Note that a sediment assemblage represents an integration of species growing at different seasons and depths. We anticipate that the range of $\delta^{18}O_{calcite}$-signals of the assemblage approximates the total temperature range through the depth habitat. Tedesco et al. (2007) have shown that the flux-weighted $\delta^{18}O_{calcite}$-means for *O. universa* are close to their respective unweighted annual $\delta^{18}O_{calcite}$-means, indicating that the $\delta^{18}O_{calcite}$-signals are not biased towards any season.

2.4.2. Sea surface temperature (SST)

Sea surface temperatures (SST) are determined by means of alkenone UK'37-records in phytoplankton dwelling in the uppermost surface layers up to 2 m water depth. The analytical error estimated for the method is < 0.4°C in repeated determinations of individual samples (Emeis et al., 2009). The method is described in detail by Blanz et al. (2005).

Photosynthetic activity (i.e. alkenone production) is controlled by insolation and nutrient supply. Both are not constant throughout the year. Equatorward of the two tropics, insolation reaches its maximum twice a year (Lorenz et al., 2006). Upwelling (and thus nutrient supply) is most intense from winter to early spring (September to November) in the northern Benguela (Hart and Currie, 1960; Stander, 1964; Nelson and Hutchings, 1983; Shannon, 1985; Lutjeharms and Meeuwis, 1987). Despite the seasonality of insolation and nutrient supply, sediment trap studies above Walvis Ridge have shown that alkenone records approximate the mean annual temperature signal (Kirst et al., 1999 and ref. therein) (NB: This is different from high latitudes where alkenone-derived SSTs clearly reflect summer temperatures (Lorenz et al., 2006).). Holocene orbital forcing and associated changes in the seasonal cycle of solar irradiance (Lorenz et al., 2006) are not expected, therefore, to create a seasonal fingerprint in the alkenone data.

2.5. Age determination

Age determinations were made on calcite from snails, shells and foraminiferal tests (*O. universa*), fish bone material or acid residual (Table 2; Fig. 2). The conversion of conventional radiocarbon ages (^{14}C-ages) into calendar years (BP; before present) was done by means of the calibration program CALIB 5.0 by Stuiver et al. (2005). Marine ^{14}C-ages generally appear several hundred years older than their terrestrial counterparts. The *Marine04* curve accom-

---

[a)] δ_w is corrected by -0.22‰ in order to adjust the oxygen isotope values in H_2O (measured in VSMOW) to the VPDB-scale (Erez and Luz, 1983).

Table 2

Age conversion via CALIB 5.0 (Stuiver et al., 2005), applying the calibration dataset *Marine04*. Programme settings: ΔR = 0; lab error = 1; age span = 0; lab error treated as multiplier. All BP-ages refer to AD 1950. ^{14}C-ages of acid residual (see *) required a correction of +152 years prior to their transformation into calendar years (Kristen, 2003). The core top of 226620 (core depth = 0 cm) was dated by means of the associated MUC (Emeis et al., 2009). The uppermost age determination of NAM1 (core depth = 7.5 cm) is based on Pb-dating and derives from the associated MUC 226870 (Kristen, 2003). Accelerated mass spectrometry (AMS) ^{14}C-dating was done at the Leibniz dating facility, Kiel, FRG. Pb-dating was conducted by the Gamma Dating Centre, Copenhagen by Dr. H. Kunzendorf.

	core depth (cm)	material used for age determination	^{14}C-ages (BP)	cal age (BP)
NAM1	7.5	Pb-dating	-	101
	47.5	collagen (fish bone)	680 ± 25	325
	149.5	collagen (fish bone)	1025 ± 30	600
	200.5	acid remains	1502 ± 30 *	1051
	250.5	acid remains	1587 ± 40 *	1150
	299.5	acid remains	1647 ± 30 *	1213
	324.5	carbonate (snail, shells)	1705 ± 25	1264
	343.0	acid remains	2222 ± 35 *	1824
	347.5	collagen (fish bone)	2315 ± 25	1927
	363.5	carbonate (snail, shells)	2515 ± 25	2191
	393.5	carbonate (snail, shells)	3005 ± 30	2773
	539.5	acid remains	3217 ± 45 *	3031
core 178	52.5	O. universa	2310 ± 30	1922
	97.5	O. universa	2445 ± 30	2086
	197.5	O. universa	2710 ± 30	2403
	296.5	O. universa	3005 + 40	2776
	393.5	O. universa	3215 ± 35	3028
	515.5	O. universa	3550 ± 35	3435
core 226620	0	O. universa	1315 ± 25	860
	126.0	O. universa	3430 ± 30	3311
	165.0	O. universa	3785 ± 25	3729
	206.5	O. universa	4135 ± 25	4197
	312.0	O. universa	4785 ± 35	5056

modates this age difference and includes a mean global ocean reservoir correction of 400 years. Usually, however, the correction varies slightly with location. ΔR takes account of the region-specific offset from the global reservoir correction (Stuiver and Braziunas, 1993; Stuiver et al., 2005). To our knowledge, no ΔR-values for the Benguela Upwelling have yet been published, hence the lacking consideration of a potential offset in our calculations (ΔR = 0). Since upwelling typically introduces "old", viz. ^{14}C-deficient waters to the surface ocean, the ages might be slightly overestimated (Kim et al., 2002). As the core top of NAM1 was dated by means of the ^{210}Pb-method, we were able to evaluate the potential bias. This is because the risk of overestimation is eliminated with ^{210}Pb-dating (Christiansen and Kunzendorf, 1998). Given the reasonable age difference between the upper two age control points, the overestimation is considered negligible.

Note that most age determinations of core 226620 and NAM1 have already previously been published (Struck et al., 2002; Kristen, 2003; Emeis et al., 2009). However, as uniform programme settings highly improve the temporal comparability of the cores, we decided to do our own conversion of ^{14}C-ages into calendar years (Table 2). This is why the calendar years shown here deviate slightly from the ones already published.

3. Results and discussion

3.1. Applicability of the proxy records

Before going into the interpretation we look at the applicability of the proxies in use (see Table 3), paying particular attention to the characteristics and features that are specific to the coastal upwelling environment.

3.1.1. Temperature records (SST, $T_{\delta 18O}$, ΔT)

From today's perspective, core 178 lies in the centre of upwelling where modern SSTs are lowest. NAM1 and core 226620 are situated below the northern fringes of the cell where modern SSTs are slightly higher. For the time frame overlapping (3036 to 1757 BP; Table 1) median SST recorded by the cores agree with
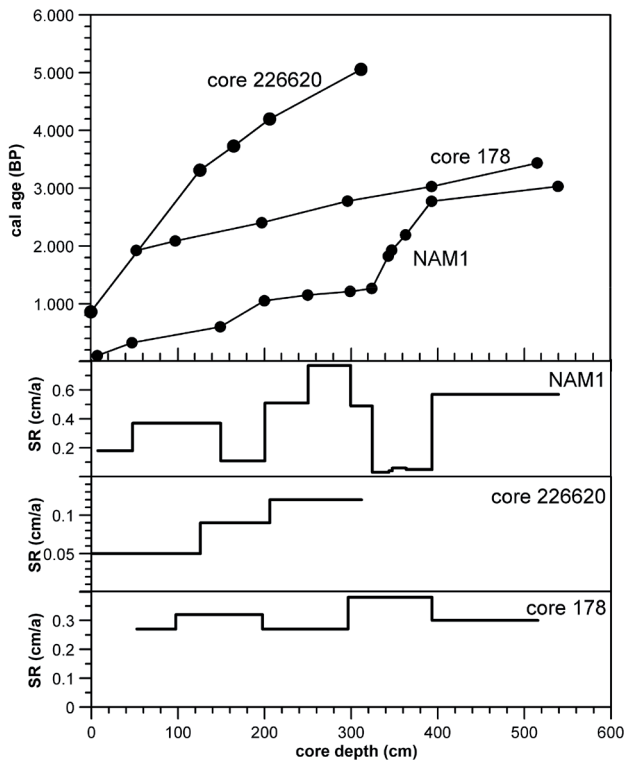
Fig. 2. Core depth vs. calendar years. The age model is based on linear extrapolation through the age control points (based on BP-dates shown in Table 2).
Corresponding sedimentation rates (SRs) are shown below. Core 178 exhibits the most constant SRs. In core 226620 the SRs and, as a consequence, the temporal resolution, are lowest. At the same time, however, it covers the largest time span. Note that NAM1 and core 178 are exclusively post-transgressive.

today's conditions concerning both the N-S-gradient and absolute values (NAM1: 16.0°C; core 226620: 15.1°C; core 178: 15.0°C) (see Meisel et al., 2011).

CTD-measurements on the central Namibian inner shelf have shown that water column stratification is poor. The seasonal thermocline situated between 10 and 20 m depth is weak and even though measurements were taken off the main upwelling season, the temperature offsets between surface and bottom waters rarely exceed 2°C (Meisel et al., 2011). Reconstructed temperature offsets much higher than that (ΔT up to 8°C; Fig. 3c), as recorded by the difference between SST and $T_{\delta 18O}$, suggest the semi-allochthonous nature of the foraminiferal tests. It is plausible to anticipate that the foraminifers are advected from the middle and outer shelf areas where subsurface temperatures between 10 and 12°C (corresponding to the main temperature range $T_{\delta 18O}$ straddles in between) are common. The lateral transport of the species further adds to the fuzziness of the $T_{\delta 18O}$-record (section 2.4.1.). As $T_{\delta 18O}$ may not be purely in-situ in nature, ΔT does not exactly monitor

vertical but rather diagonal temperature gradients. Leaving aside such biases, increasing or decreasing $T_{\delta 18O}$-values are ascribed to deeper or shallower penetration of wind- and wave-induced mixing and a corresponding weakening or strengthening of the thermocline. Moreover, the interpretation of $T_{\delta 18O}$ needs to take account of possible variations in the temperature of the source water. Obviously, variations in the temperature of the source water also imprint themselves on SST. As a consequence, SST-changes cannot be simply ascribed to variably intense upwelling of cold subsurface waters. As we will see, it is sometimes not easy to clearly differentiate between upwelling-related or source water-related SST-changes.

Although being valid with reservation only, ΔT gives an immediate idea of how well the upper water column is mixed. Declining ΔT based on rising $T_{\delta 18O}$, suggests a deeper penetration of wind- and wave-induced mixing. By contrast, declining ΔT based on falling SST, rather suggests intensified upwelling. Slackened upwelling manifests itself in rising SSTs, instead. As the winds weaken, the water column stratifies and the surface layer responds more sensitively to insolation.

3.1.2. Accumulation and sedimentation rates (AR, SR)

Average [TOC] amounts to 4wt% in core 226620 and 7wt% in NAM1 and core 178. This roughly corresponds to the mean organic carbon content typically found in sediments below coastal upwelling regions (Berger and Wefer, 2002). [TOC] tends to be diluted by varying amounts of other constituents like carbonate, siliceous matter, etc. By considering accumulation rates (AR_{TOC}) such biases are circumvented.

Variations in AR_{TOC} reflect changes in biological production and provide, therefore, indirect information about nutrient supply, upwelling and the local wind conditions. In core 178, AR_{TOC} appears to work particularly well as such proxy indicator: Elevated AR_{TOC} generally comes along with intensified mixing (ΔT low) and correspondingly sound nutrient supply (around 2900 and 2200 BP; Fig. 3c). In contrast, low AR_{TOC} coincides with a short-term increase in ΔT (approx. 2600 BP).

Note, however, that sedimentary archives tend to exaggerate variations in organic matter (OM) (Berger and Wefer, 2002): High flux promotes the preservation of organic material due to rapid burial and the lack of oxygen (Libes and Deuser, 1988; Montoya, 1994; Ostrom et al., 1997; Sachs and Repeta, 1999; Holmes et al., 2002). During periods of low flux, ventilation improves and a much smaller proportion of OM escapes degradation. NAM1 documents these mechanisms perfectly well: As shown by the

Table 3
A listing of the proxy indicators used and their application.

proxy indicators		information and use
AR_{TOC} (mg/cm^2/a)	accumulation rates of total organic carbon	primary production rates
$\delta^{13}C_{org}$ (‰)	isotope ratios of organic carbon in the sediment	relative CO_2-consumption
$\delta^{15}N$ (‰)	isotope ratios of sedimentary nitrogen	denitrification (i.e. O_2 in source waters), relative NO_3^--consumption
SST (°C)	sea surface temperature (UK'37-based)	upwelling and wind intensity
$T_{\delta 18O}$ (°C)	temperature reconstructions based on oxygen isotope ratios in calcite from planktic foraminifers	temperature of the source water
ΔT (°C)	temperature difference between SST and $T_{\delta 18O}$	mixing of the upper water column

simplified sketch in Fig. 3a, high ARs are generally accompanied by a densely laminated sediment sequence. The apparent absence of bioturbating organisms suggests scarce amounts of bottom oxygen. By contrast, at low ARs laminae are usually rare or completely lacking.

Note that the rapid alternations of production rates are due to the fact that age determinations are preferentially conducted at the bottom and top of a laminated sequence.

The sedimentation rates of core 226620 are consistent with the mean SR of the diatomaceous muds, which is estimated at 1 mm/a (Bremner and Willis, 1993). SR and AR in NAM1 and core 178 are manifold higher (Fig. 3). It seems as though NAM1 and core 178 originate from some natural sediment trap, i.e. a morphological depression such as a submarine canyon for instance, where sediments are protected against erosion and accumulation rates greatly enhanced for gravitational reasons. This circumstance poses no problem as our interpretation is not concerned about absolute values but relative fluctuations instead.

Above all this, however, the usefulness of ARs as a meaningful proxy strongly depends on regular age determinations. The longer the time interval between two age control points, the bigger the risk that fluctuations are obliterated and smoothed out. Unfortunately, this applies to the upper half of core 226620 (3311 to 860 BP) where age control points are scarce and ARs and SRs, by inference, poorly significant.

3.1.3. Isotopic records ($\delta^{15}N$, $\delta^{13}C_{org}$)

The combined study of $\delta^{15}N$ and $\delta^{13}C_{org}$ is a valuable tool in the reconstruction of past nutrient regimes. The assimilation of NO_3^- and CO_2 by phytoplankton is accompanied by isotope fractionation, with ^{15}N and ^{13}C being preferentially left behind (only as long as nutrients are abundant though). The remaining nutrient pool becomes progressively "heavier" and with it the phytoplankton that grows within that pool (e.g. Wada and Hattori, 1978; Wada, 1980; Montoya,

1994; Ostrom et al., 1997; Waser et al., 1998).

Fluctuations in $\delta^{15}N$ and $\delta^{13}C_{org}$ can be related to varying degrees of relative nutrient consumption ("relative" refers to the initial amount present) (e.g. Francois et al., 1992; Altabet and Francois, 1994; Montoya and McCarthy, 1995; Voss et al., 1996; Ostrom et al. 1997; Holmes et al., 2002). Relative consumption changes along with biological production and / or the nutrient supply. The nutrient supply, in turn, not only depends on the intensity of upwelling and mixing of the upper water column, but also depends on the type of source water.

The $\delta^{13}C_{org}$-core signals reach up to -18‰, dropping only rarely below -21‰. According to Rau (1994), values that high are usually associated with SST above 25°C (NB: The higher the temperature, the less CO_2 dissolves in the water, at the same time driving acqueous $\delta^{13}C_{CO2}$- and, as a consequence, $\delta^{13}C_{org}$-signals towards higher values). The significant ^{13}C-enrichment of the diatomaceous muds at surface ocean temperatures of ±16°C results from high primary production and high relative consumption.

Average $\delta^{15}N$ of the source water nitrate ($\delta^{15}N_{nitrate}$) is estimated at 5.5‰ (Sigman et al., 1997, 2000; Ren et al., 2009). Sedimentary $\delta^{15}N$-signals below that suggest a surplus in nitrate and comparably low relative consumption. Our cores, however, mostly exhibit higher values. Given the proximity to the nutrient source and upwelling, prior consumption can hardly be held responsible for the ^{15}N-enrichment. Instead, shifts beyond 5.5‰ are taken as an indication of denitrification in the source waters (see dashed line in Fig. 3).

During denitrification, anaerobic prokaryotes use nitrate instead of oxygen in order to oxidise OM. Due to the preference of denitrifying bacteria for ^{14}N-NO_3^-, the NO_3^--pool gets progressively enriched in ^{15}N (Cline and Kaplan, 1975; Montoya, 1994; Holmes et al., 1996). Denitrification sets in as soon as oxygen drops below 0.2 ml/l (Bubnov, 1972; Knowles, 1982; Packard et al., 1983). In the modern central Namibian shelf environment, bottom O_2 is frequently below detection level and denitrification strongly influences
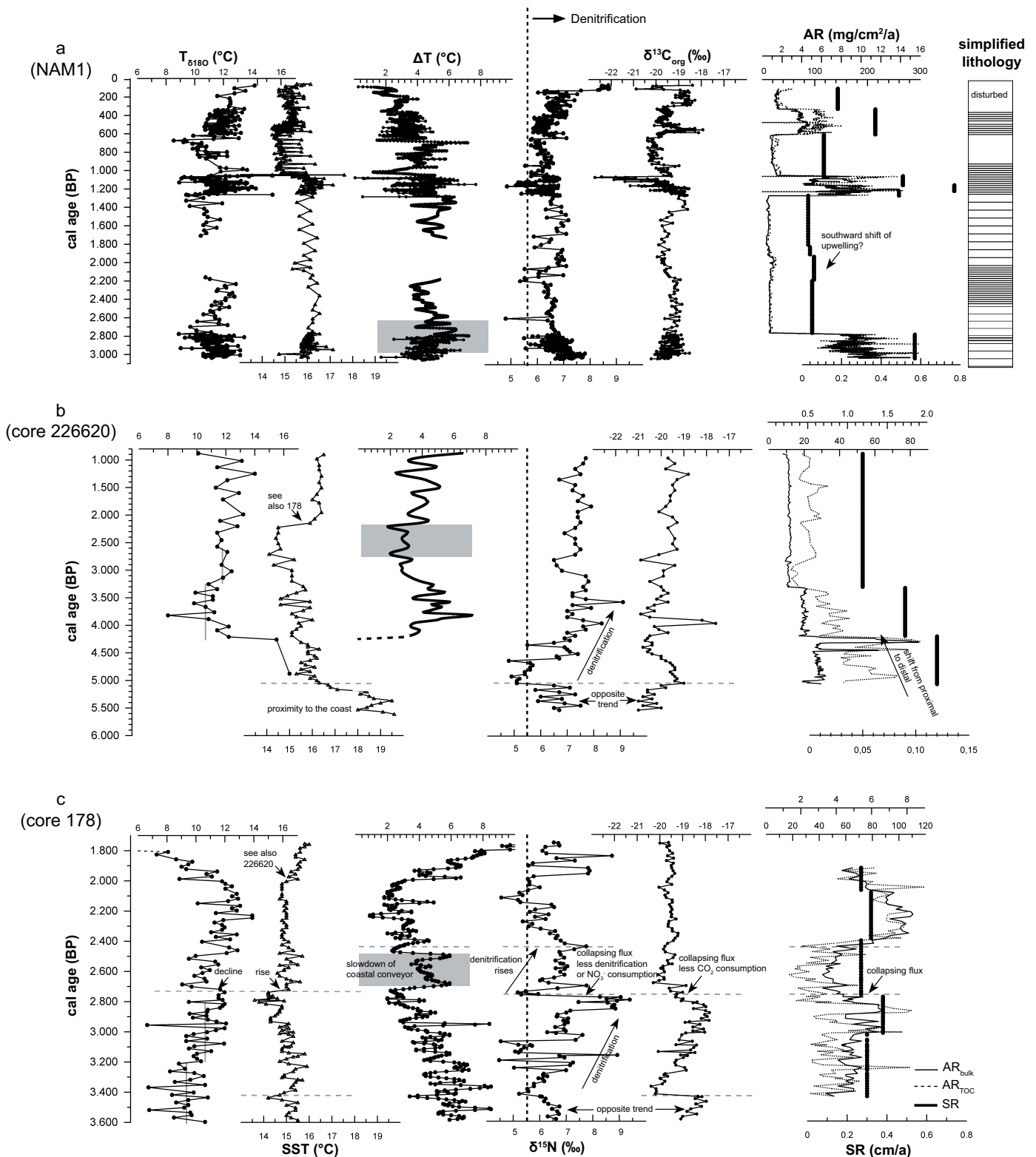
Fig. 3. Proxy indicators vs. calendar years. From north to south (a) NAM1, (b) core 226620 and (c) core 178. Data that are already published elsewhere are clearly listed in Table 1. Significant co-variations of the proxies are marked. Please note that it is only for SR, AR$_{bulk}$ and AR$_{TOC}$ that the scales differ. The simplified lamination of NAM1 is based on an X-Ray (modified after Struck et al., 2002). No X-rays are available for core 178 and 226620. ΔT-records are based on the offsets between SST and T$_{δ18O}$. The interpolation of the SST- and T$_{δ18O}$-data was computed by the akima method with 5 years-intervals. ΔT-records older than 4100 BP in (b) (dashed line) are regarded poorly significant because of lacking T$_{δ18O}$-data compared to SST-records. The pronounced decline in T$_{δ18O}$ (dashed line) at the top of core 178 (c) should not be overinterpreted due to the possibly allochthonous nature of the T$_{δ18O}$-signals (see text).

the δ^{15}N-signal of the primary product (Brüchert et al., 2004; Lavik et al., 2009; Meisel et al., 2011).

The oxygen deficiency itself results from a combination of several factors: The varying poleward advection of hypoxic SACW plays a major role in the oxygen dynamics of the shelf (section 1.1.) (Chapman and Shannon, 1987; Shannon and Nelson, 1996; Mohrholz et al., 2008). High primary production and vertical flux enhance the local oxygen consumption due to respiration and often contribute to deteriorated O_2-supply in subsurface depths (Libes and Deuser, 1988; Tyrrell and Lucas, 2002; Gaye-Haake et al., 2005). Nowadays, the subsurface transport of oxygen-rich ESACW from the shelf edge onto the shelf seasonally balances the oxygen consumption below the surface mixed layer (Mohrholz et al., 2008). However, the more time it takes for the Ekman compensation current to travel up the shelf, the more organic matter decay it is supporting on its way and the greater the O_2-consumption due to respiration. During periods of slackened upwelling, the cross-shelf conveyor system slows down and the Ekman-induced O_2-replenishment is less effective.

Diagenesis often limits the use of δ^{15}N as a palaeo-proxy. However, recent investigations have shown that pre-analysis acidification plus rinsing is capable of eliminating decomposition-derived influences in the diatomaceous muds (Meisel and Struck, 2011). As regards core 226620 and 178, we therefore expect related δ^{15}N-shifts to be erased. This does not apply to NAM1 where measurements are based on in-situ acidified sediment instead (published in Struck et al., 2002; Table 1). Although the lack of oxygen in the shallow coastal waters promotes the preservation of the original signal (Meisel et al., 2011), the potential influence of OM decomposition has to be kept in mind with the δ^{15}N-signals in NAM1 (Meisel and Struck, 2011).

This restriction aside, δ^{15}N-signals are predominantly to be interpreted in terms of relative nutrient consumption, denitrification or a combination of both. Declining δ^{15}N-values, for instance, do not necessarily result from reduced relative consumption but could equally be due to less denitrification in the bottom waters travelling up the shelf [b]. This allochthonous influence on δ^{15}N$_{nitrate}$ is why δ^{15}N sometimes not co-varies with δ^{13}C$_{org}$ or the other proxies. The δ^{13}C$_{org}$-records are easier to handle than δ^{15}N as they are mainly controlled by relative CO_2-consumption; there is no such process that compares to denitrification.

Note that OM is primarily of marine origin. Neither is there a major river draining into the ocean nor can terrestrial material introduced by winds as dust exert enough influence to outweigh the excess of phytoplankton biomass and bias the isotopic signal (Holmes et al., 1998; Tyrrell and Lucas, 2002). Molar C_{org}/N ratios of suspended particulate matter confirm the primarily marine nature of the material (Meisel et al., 2011).

Note that most trends and peaks discussed below significantly exceed the precision of the methods. Still, there are some fluctuations that deserve a mention notwithstanding being only subtle and smaller than the precision. This is when co-variations amongst the proxies substantiate the credibility and significance of the fluctuation.

3.2. Climatic reconstructions

This section relates exclusively to own data, describing and discussing co-variances between the proxy indicators and between the cores. The interpretation is rather "local-minded" and it is only in the following section that the core data are compared to other palaeo-archives and placed in a regional and global context.

With core 226620, our data set in around 5600 BP (Fig. 3b). This is about 1000 years before the sea level rise has come to an end and the modern shelf circulation pattern is established (Emeis et al., 2009). The sedimentation is characterised by a sand-sized quartz minerals with various shell remains imbedded. This and concomitantly high SSTs (> 19°C) fit the proximity to the shore at that time.

The beginning sedimentation of silt and muds around 5200 BP testifies to the flooding of the shelf and the resultant shift from proximal to distal depositional settings. The simultaneous drop in SST by almost 5°C suggests an increasing influence of cold, upwelled waters. At first, δ^{13}C$_{org}$ and δ^{15}N respond with a sudden rise and drop respectively (Fig. 3b). Their opposite development results from the different availability of CO_2 and NO_3^- (Ostrom and Macko, 1991). Contrary to CO_2, NO_3^- is often in limited supply. With the onset of upwelling, however, the photic zone experiences an instant and hitherto unknown abundance of nitrate. Relative consumption declines driving the system towards lower δ^{15}N-signatures in the nitrate pool and primary product (Ostrom and Macko, 1991; Altabet and Francois, 1994; Holmes et al., 1996, 1999). As

---

[b] Anammox (anaerobic ammonium oxidation by nitrate and / or nitrite to yield N_2) is an additional process strongly interfering with the nitrogen cycle above the central Nambian shelf (Kuypers et al., 2005). As far as we know, however, no study has yet examined whether or not annamox is associated with nitrogen isotope fractionation. It cannot be ruled out that anammox also impinges on the nutrient's δ^{15}N-signature.

primary production flourishes, CO_2-utilisation and $\delta^{13}C_{org}$ rise in tandem (Hollander and McKenzie, 1991; Schelske and Hodell, 1991; Rau, 1994; Fry, 1996). 5100 BP the trends are being reversed (Fig. 3b; dotted line). The decline in $\delta^{13}C_{org}$ (from around -19 to -20.5‰) suggests increasing supply of CO_2, as the coastal upwelling system is about to develop (note that SSTs continue falling). The growing $\delta^{15}N$-offset between sediments and marine nitrate (5.5‰) testifies to increasing O_2-depletion and denitrification. Around 4000 BP sedimentary $\delta^{15}N$ has attained ±7.5‰, which approximates today's level at that site (Meisel et al., 2011). The concomitant decline in ARs and SRs should not be mistaken as slackened productivity. It rather reflects the shift and transition from littoral to subtidal facies characteristics as the site moves offshore.

From 3600 BP on, core 226620 is complemented by core 178 (Fig. 3c). Its higher resolution provides insight in decadal-scale variability. Between 3600 and 3400 BP, core 178 records an opposite development of $\delta^{13}C_{org}$ and $\delta^{15}N$ at contemporaneously declining SSTs. A comparable situation already occurred 5200 BP (core 226620; q.v.).
The sudden collapse of $\delta^{13}C_{org}$ at 3400 BP is accompanied by a slight increase in SST (Fig. 3c; dotted line) while $\delta^{15}N$ continuous its previously initiated decline. CO_2-consumption seems to drop as a response to slackened upwelling and scarce nutrient supply. The lacking reaction of $\delta^{15}N$ is somewhat intriguing.

Despite their different temporal resolution, the temperature records of core 226620 and 178 bear marked resemblances. On close examination, it is found that $T_{\delta18O}$ performs a slight but simultaneous jump (±1°C) at approx. 3200 BP in both cores. Before and after, $T_{\delta18O}$ oscillates around constant values (indicated by the vertical lines in Figs. 3b and 3c). In the meanwhile, SST decreases more or less gradually in both cores. By 2800 BP, ΔT has fallen to 2°C. According to core 178, primary production seems to benefit from increased nutrient supplies (Fig. 3c): AR_{TOC} increases (note the concomitant peak in NAM1; Fig. 3a), rising $\delta^{13}C_{org}$-values testify to high CO_2-consumption. Rising $\delta^{15}N$ hints at increasingly denitrified and oxygen-deficient bottom waters. The rising flux of organic detritus might contribute to the lack of oxygen at the site of deposition. Intense $\delta^{15}N$-fluctuations superimposed on the upward $\delta^{15}N$-trend suggest intermittently reduced O_2-consumption in the source waters and may indicate varying fractions of hypoxic SACW and well-oxygenated ESACW. Variation in the composition of the source waters and associated alternating oxygenation stages is a seasonal phenomenon (section 1.1.), which,

however, may also act on larger time scales. Interestingly, the highest-amplitude variability coincides with the shift towards warmer $T_{\delta18O}$ around 3200 BP.

The period around 2700 BP (slight age discrepancies are ascribed to dating uncertainties) marks significant and area-wide perturbations. All three cores register rising ΔT (Fig. 3; grey bars). Considering the proxy indicators as a whole, core 178 (Fig. 3c) provides the most conclusive insight. The divergence of SST and $T_{\delta18O}$ (see dotted line) suggests increased water column stratification. Rising SSTs imply slackened upwelling and a more sensitive response to insolation while falling $T_{\delta18O}$ suggest a shallower penetration of wind-induced mixing. A potential cause might be a shift of the cyclonic wind stress and upwelling. The adverse effect on the replenishment with nutrients manifests itself in collapsing growth rates (see also NAM1; Fig. 3a). Diminished CO_2-consumption, as evidenced by concomitantly falling $\delta^{13}C_{org}$-values, fits the decline in photosynthetic activity. $\delta^{15}N$ declines drastically (from ±9.5 to 5.0‰) and although less distinct, NAM1 (Fig. 3a) exhibits a comparable development. Lower $\delta^{15}N$-signals may indicate less denitrification (i.e. rising oxygen in the bottom waters as the biogenic flux decreases), reduced relative nitrate utilisation or a combination of both.
Stratified conditions and reduced primary production persist for a couple of centuries (~2700 to 2500 BP). This fact notwithstanding, $\delta^{15}N$-values rise again almost immediately after their pronounced drop around 2700 BP (Fig. 3c), suggesting that denitrification again dominates the signal. ARs remain low (Fig. 3c), implying that the lack of oxygen is hardly due to enhanced in-situ respiration. Slackened upwelling - as proposed before - and a slowdown of the coastal conveyor system offer a likely explanation (section 3.1.3.). The more time it takes for the bottom water to travel up the shelf, the greater the O_2-consumption and the bigger the shift towards higher $\delta^{15}N_{nitrate}$-signals.
Around 2500 BP ΔT drops due to increasing $T_{\delta18O}$ (Fig. 3c). Note that the warming of the source waters does not imprint itself back on SST. SST remains constant, which makes only sense if upwelling intensifies at the same time. An intensification of upwelling might account for the concomitantly increasing primary production and declining $\delta^{15}N$-values (Fig. 3c; dotted lines). The faster the cross-shelf conveyor, the less the time for denitrification to take effect.
The decline in ARs after 2200 BP in core 178 (Fig. 3c) is difficult to interpret. SST remains constant and neither $\delta^{13}C_{org}$ nor $\delta^{15}N$ provides any evidence of deteriorated nutrient supply.
The reaction of NAM1 compares rather poorly with
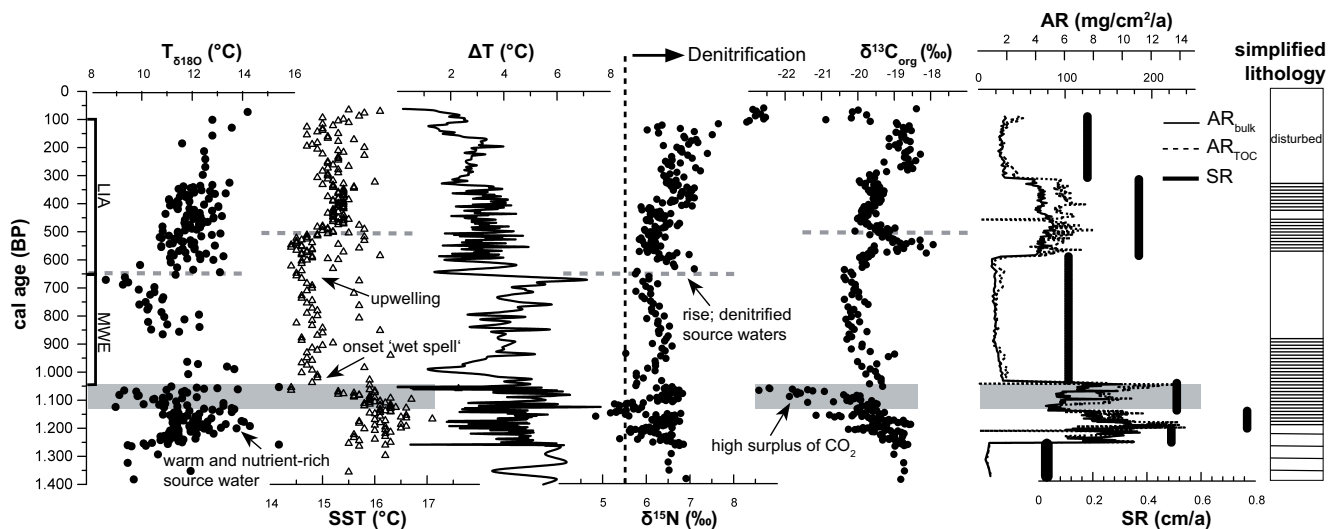
Fig. 4. Proxy indicators of NAM1 vs. calendar years (see Fig. 3), zoomed in on the last 1400 years for the sake of higher resolution. Note the parallel developing of the temperature and ARs.

the distinct trends in core 178. The rise in ARs and SRs centred around 2200 BP is almost negligible and the downward trend of $\delta^{15}N$ is noticeable but much less pronounced (Figs. 3a and 3c). Like today, NAM1 seemingly lay outside the high-productivity area, thus receiving attenuated signals only. This is further substantiated by the higher SSTs (±16°C) compared to both other cores (±15°C) around that time.

2200 BP core 226620 experiences a pronounced warming (Fig. 3b) in the course of which SST attains values similar to those recorded by NAM1. A possible explanation might be that upwelling has shifted further south. Core 178 is also affected. Unfortunately, the extent of the warming at site 178 remains in the dark as the record ends around 1800 BP already (Fig. 3c). The slightly latter onset compared to core 226620 might either be real (relating to the southward shift of upwelling) or result from interpolation uncertainties. Anyway, NAM1 and later also core 226620 seem to have been beyond the direct influence of upwelling for nearly two millennia. Throughout the second and third millennium, productivity was scarce with mean SR amounting to 0.5 mm/a only (Figs. 3a and 3b); this is merely half of the average SR reported for the diatomaceous muds (Bremner and Willis, 1993). Actually, the scenario resembles modern conditions according to which NAM1 and core 226620 are situated slightly north of the principal centre of upwelling.

In core 178 the rise in SST from 2000 BP on is accompanied by a sharp decline in subsurface temperatures. Within two centuries, $T_{\delta18O}$ drops from 12 to nearly 3°C (Fig. 3c). No such trend is recorded by core 226620 and as regards NAM1 the samples covering 2150 to 1700 BP are unfortunately lost. The other proxies hold no further clues to the nature of the event either. The possibility that the foraminiferal

tests are advected from colder subsurface waters further offshore cannot be excluded.

The reconstruction of the last millennium is exclusively based on NAM1 (Fig. 4). Its high-resolution data set is certainly special, although often not easy to interpret. The biggest surprise was the parallel up and down of temperature and productivity. According to theory, temperature and productivity are inversely correlated as intensified (or slackened) upwelling usually brings about high (or low) nutrient supplies and low (or high) SSTs (e.g. Holmes et al., 1999). In fact, Quaternary-age sediment cores from the continental slope off Walvis Bay display a close negative correlation between AR_{TOC} and SST (Kirst et al., 1999; Summerhayes et al., 1995).

On the shelf, different mechanisms seem to operate. Fig. 4 zooms in on the last 1400 years and shows that the relationship between AR_{TOC} and SST is precisely opposite. Still, the marked co-variations amongst both proxy indicators definitely substantiate the credibility of the data.

The markedly high ARs between 1250 and 1000 BP are presumably due in part to improved preservation; oxygen seems to be lacking at the site of deposition, as inferred from the dense laminae. The simultaneous trend towards lower $\delta^{15}N$-signatures indicates that primary production benefits from increased nutrient supply. Compared to $\delta^{13}C_{org}$, however, the fluctuation is comparably small and should not be over-interpreted.

In fact, the $\delta^{13}C_{org}$-record deserves particular attention as it is in conflict with our hitherto applied way of interpretation. Different from NO_3^-, CO_2 is usually abundant which is why increasing photosynthetic rates and CO_2-consumption are normally accompa-

nied by rising $\delta^{13}C_{org}$-signatures. The fact that $\delta^{13}C_{org}$ drops to values as low as -22‰ during times of enhanced biological production suggests an unusually high surplus of isotopically light CO_2. What are the reasons for this exceptionally high CO_2-supply? 'Nutrient trapping' associated with continuous remineralisation reactions as the subsurface waters travel up the shelf, might partly account for this surplus [c] (Tyrrell and Lucas, 2002).

The grey band in Fig. 4 marks a significant change in the properties of the system. Within only one century, the surface ocean cools by 1.5°C. On closer examination SST appears tied to the developing of $T_{\delta 18O}$. The cooling is accompanied by collapsing ARs. As SST drops, $\delta^{13}C_{org}$ at first continues its steep decline but then suddenly jumps by nearly 4‰ back to former levels. The leap of $\delta^{13}C_{org}$ as ARs collapse is as unusual as the above outlined decline at rising ARs. Again it shows that our hitherto applied line of reasoning does not bear the circumstances.

The abruptness of events shows that the properties of the system are able to flip in an instant. On the basis of the available evidence it seems like temperature and nutrient content of the source water are liable to pronounced changes through time. Contemporaneously high temperature and ARs in combination with relatively low $\delta^{13}C_{org}$ ("relatively" because $\delta^{13}C_{org}$-signal are still comparably ^{13}C-enriched; see section 3.1.3.) around 1200 BP are best explained by the presence of "warm" and nutrient-rich source waters (with 'nutrient trapping' potentially contributing to the surplus in CO_2). The subsequent collapse in AR and SST accompanied by the leap in $\delta^{13}C_{org}$ altogether suggests reduced influence of this warm and nutrient-rich water mass.

The presence of warm and nutrient-rich source water including its potential to imprint itself back on SST offers a reasonable explanation for the direct (instead of invers) correlation between SST and AR_{TOC}. Further notions concerning this water mass are addressed in section 3.3.2. when it comes to external forcing and inter-hemispheric climate teleconnections.

Between 1050 and 900 BP, $T_{\delta 18O}$-data are too scarce to be reasonably interpreted (Fig. 4). The image gets clearer after 900 BP; then $T_{\delta 18O}$ starts a steep decline and apparently imprints itself back on SST. Low primary production might again be due to reduced inflow of warm and nutrient-rich source water. Apart from that, high OM-decomposition (as inferred from the absence of laminae) may have contributed to the low ARs.

The dotted line at 650 BP marks a pronounced jump in $T_{\delta 18O}$ (Fig. 4). At the same time SSTs remain more or less constant. Enhanced wind-induced mixing immediately comes to mind, although this scenario provides no adequate explanation for the contemporaneous increase in $\delta^{15}N$. The simultaneous jump in $T_{\delta 18O}$ and $\delta^{15}N$ is hardly coincident and suggests the introduction of warmer and more denitrified source waters. Their high nutrient content manifests itself in rising productivity, i.e. ARs; the small temporal offset is attributed to the "later" position of the age control point. The fact that SSTs remain constant while source waters are getting warmer testifies to a contemporaneous intensification of upwelling, which further contributes to the sound nutrient supply.

The nutrient surplus seems to outweigh the denitrification-induced shift towards higher $\delta^{15}N$-values, forcing $\delta^{15}N$ to slightly decline again. The $\delta^{13}C_{org}$-values perform an opposite development and peak at -18‰. Rising $\delta^{13}C_{org}$ complies with the rising CO_2-consumption as the biological production increases. The $\delta^{13}C_{org}$-signals do not remain high for long, though. Their subsequent decline coincides with a rapid increase in SST by roughly 1°C at 500 BP (Fig. 4; dotted line). In the meanwhile, $T_{\delta 18O}$ remain more or less the same. The warming of the surface ocean suggests slackened upwelling and an increasing influence of insolation. The decline in $\delta^{13}C_{org}$ may indicate less CO_2-consumption and biological production. However, neither $\delta^{15}N$ nor the ARs show any corresponding reaction. Taken overall, the short-lived peak of $\delta^{13}C_{org}$ is not entirely conclusive.

During the past 100 years both $\delta^{18}O_{calcite}$- and UK'37-records denote rising temperatures. The $\delta^{15}N$-values exceed 8.5‰, the pool is highly denitrified. Concomitantly low $\delta^{13}C_{org}$ suggests comparably low primary production rates, which might result from enhanced denitrification and corresponding nitrate deficits (Cline and Kaplan, 1975; Montoya, 1994; Tyrrell and Lucas, 2002).

3.3. The northern Benguela in the context of Holocene climate variability

In this section we attempt to place our observations in the context of Holocene climate variability. In order to differentiate between local perturbations, regional- or global-scale events, we examine our findings alongside existing palaeo-climatic records.

---

[c] Note that 'nutrient trapping' does not necessarily hold to the same extent for nitrate as for dissolved inorganic carbon. Where denitrification inhibits the parallel "supercharge" with NO_3^-, the source waters exhibit continuously rising CO_2/NO_3^- ratios (Tyrrell and Lucas, 2002).

3.3.1. The global propagation of climate signals

First of all, however, we shortly present the potential pathways of global climate signals and how they may impact on the northern Benguela system. In fact, the role of the ocean and atmosphere as transmission agents is highly debated (e.g. Vidal et al., 1999). It is pre-empted that climate signals seem to reach the northern Benguela both through the ocean, i.e. the thermohaline circulation system, and the atmosphere. For a better comprehension of the following please consult Fig. 5.

3.3.1.1. Pathway ocean

Countless studies provide convincing evidence of a link between the intensity of thermohaline circulation and Holocene climate variability (e.g. Bianchi and McCave, 1999 and ref. therein; Marshall et al., 2001). As regards the Benguela region, the role of the ocean in the transfer of climate signals is controversially discussed. To our knowledge, there are two contrasting theories circulating on that issue:

Gordon (1986) suggests a link between North Atlantic Deep Water (NADW) production and the amount of warm, intermediate Indian Ocean Water introduced into the Benguela region. The stronger or weaker the global thermohaline overturn, the stronger or weaker the Agulhas Current gets and with it the heat transfer around the southern Cape (Fig. 1). Following this assumption, the cooling of the southern Benguela during the Younger Dryas and oxygen isotope stages 2 - 4 has been ascribed to slackened thermohaline overturn and a correspondingly reduced input of warm Agulhas Water (Cohen et al., 1992; Summerhayes et al., 1995).

Only strong Agulhas-signals are expected to weather the 1500 km long equatorward journey to the northern Benguela without being wiped out on the way. In order to assess the influence of thermohaline circulation on the temperature of central Namibian source waters (recorded by $T_{\delta18O}$; section 3.1.1.), we compare fluctuations in NADW-production (Bianchi and McCave, 1999), with the $T_{\delta18O}$-record. As shown below, there are indeed a number of $T_{\delta18O}$-fluctuations that are significantly correlated with NADW-production.

Contrary to our findings, sedimentary records from the continental slope off Namibia register temperature trends opposite to the ones in high northern latitudes. Kim et al. (2002) and Vidal et al. (1999) report rising temperatures during 'Heinrich Event 1', a period when the North Atlantic experienced prominent cooling (~15000 BP). This inter-hemispheric asynchrony is attributed to decreased (or increased)
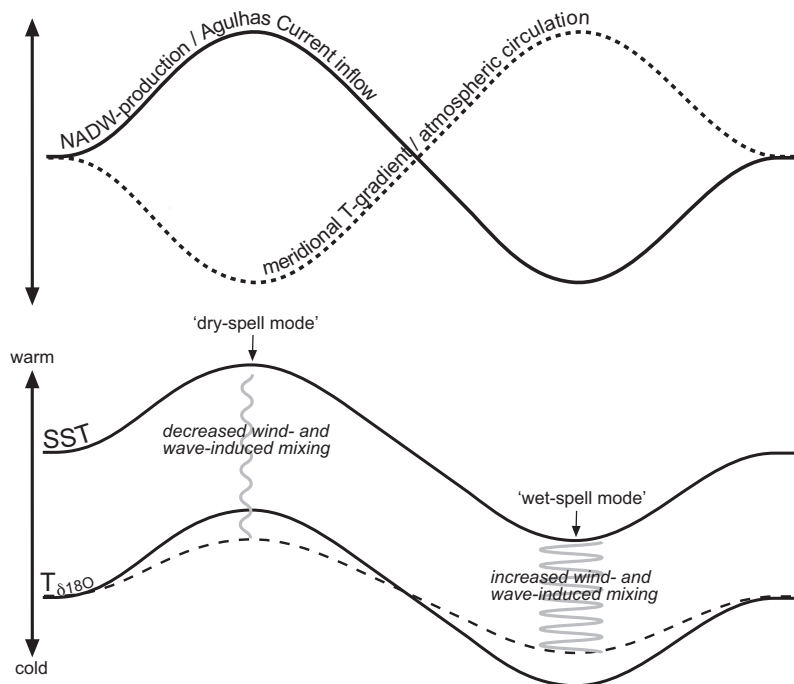
Fig. 5. Simplified scheme showing the connection between atmospheric and oceanic forcing (above) and possible implications for surface (SST) and subsurface temperatures ($T_{\delta18O}$) in the Benguela region (below). High NADW-production rates bring about warmer conditions in high northern latitudes (e.g. Bianchi and McCave, 1999). The meridional temperature gradient consequently declines and atmospheric circulation weakens (for details see section 3.3.1.2.); upwelling slackens and SSTs rise. The simultaneous increase in $T_{\delta18O}$ is due to the enhanced inflow of warm Agulhas Water as the ocean conveyor accelerates. The opposite holds true during times of reduced NADW-production. Note, however, that wind- and wave-induced mixing may attenuate the development of $T_{\delta18O}$ (dashed line).

heat transport from the South into the North Atlantic when the conveyor slows down (or accelerates) (Stuiver et al., 1995; Rühlemann et al., 1999; Kim et al., 2002). The anti-phase developing of isotope records from both polar ice sheets is the most prominent supporting evidence for the inter-hemispheric "seesaw" pattern (Blunier et al., 1998). Our data bear hardly any witness to such asynchrony. It seems like varying fractions of Agulhas Water in ESACW is the single most important factor on the shelf. It could be argued that beyond the shelf, its influence is overcompensated by cross-equatorial heat transfer.

3.3.1.2. Pathway atmosphere

At present the southern hemisphere, in comparison to the northern, is much cooler and its temperature gradient between high and low latitudes much bigger. This is predominantly due to the fact that the Antarctic continent is much colder than the Arctic Ocean. Owing to the steeper temperature gradient, atmospheric circulation is more vigorous in the southern hemisphere (Nicholson and Flohn, 1980).

When the high northern latitudes cool (as a result of decreased NADW-production for instance), the thermal contrast between both hemispheres is minimised. This results in an equatorward displacement of the ITCZ (Nicholson and Flohn, 1980), which further increases the southern hemisphere's temperature gradient (Tyson, 1999) leading to an acceleration of the South Atlantic anticyclone in tandem with a strengthening of the eastern trade wind system (Rühlemann et al., 1999; Berger and Wefer, 2002). Enhanced zonal circulation brings about upwelling-related cooling in eastern boundary current regions (e.g. Hsieh and Boer, 1992; Kim et al., 2002). Indeed, northern Benguela SSTs were lower during glacial than interglacial stages (Kirst et al., 1999). SST-records from the eastern Walvis Ridge and the upper continental slope off Walvis Bay also support the notion that upwelling was generally more intense during glacials (Oberhänsli, 1991; Summerhayes et al., 1995).

Cohen and Tyson (1995) propose a valuable model, which predicts the response of coastal SSTs around South Africa to the displacement and intensification of the atmospheric circulation features associated with extended, i.e. decadal- to centennial-scale, wet and dry periods over the South African subcontinent (see also Cockcroft et al., 1987; Tyson, 1999). Rainfall is generally derived from moisture transport in the tropical easterlies. The stronger the winds, the wetter the subcontinent becomes (Tyson and Lindesay, 1992). In more detail, over the continental interior - referred to as the 'summer rainfall region' - rainfall increases. Over the 'winter rainfall region', the south-western part of South Africa, average rainfall declines instead. Still, the net result is an increase in precipitation receipts.

Note that the Namib Desert, notwithstanding lying in the summer rainfall region (Brook et al., 1999), does not necessarily receive more rainfall at times that the easterlies strengthen. This is because invigorated upwelling and the resultant cooling of coastal SSTs have a countervailing effect on the moisture availability along the west coast. Cold SSTs lower the evaporation and stabilise offshore high-pressure centres, which hamper moist marine air from entering the adjacent land (Berger and Wefer, 2002). As a consequence, imprints of climatic fluctuations in Namib-based records might often be rather ambiguous and less clear than in the better-watered parts of the summer rainfall zone to the east.

Taken together, SST and continental rainfall records are potentially able to provide significant information about surface wind conditions and large-scale atmospheric circulation pattern. The conceptual model by Cohen and Tyson (1995) posits that anomalously cool SST are likely to have been associated with invigorated tropical easterlies, increased rainfall in the summer rainfall region, drier conditions in the winter rainfall region as well as distinct droughts in the Namib Desert (hereafter referred to as the 'wet-spell mode'). Overall, the precipitation receipts of South Africa increase and average continental temperatures rise (note the opposite trend of SST and terrestrial temperatures). In contrast, increasing SSTs, decreasing mean continental temperatures, reversed precipitation pattern including slightly more rainfall over the Namib are associated with the 'dry-spell mode' when winds and upwelling slacken.

For the sake of completeness, it must be mentioned that terrestrial and marine temperature trends do not necessarily take opposite directions. The model represents a generalisation but does not preclude 'wet-spell modes' to be associated with continental cooling and 'dry-spell modes' to bring about higher terrestrial temperatures (Holmgren et al., 2003).

In order to evaluate the regional significance of northern Benguela SST-changes, we compare our data against records from the adjacent mainland and ocean areas.

Given the potential control of NADW-production on atmospheric forcing (see Fig. 5) we also cross-check the northern Benguela SST-record against fluctuations in the conveyor speed. In this regard, we need to add that Fig. 5 shows only part of the truth. In reality, the ocean-atmosphere feedback mechanism are much more complex than illustrated. As a matter of fact, the
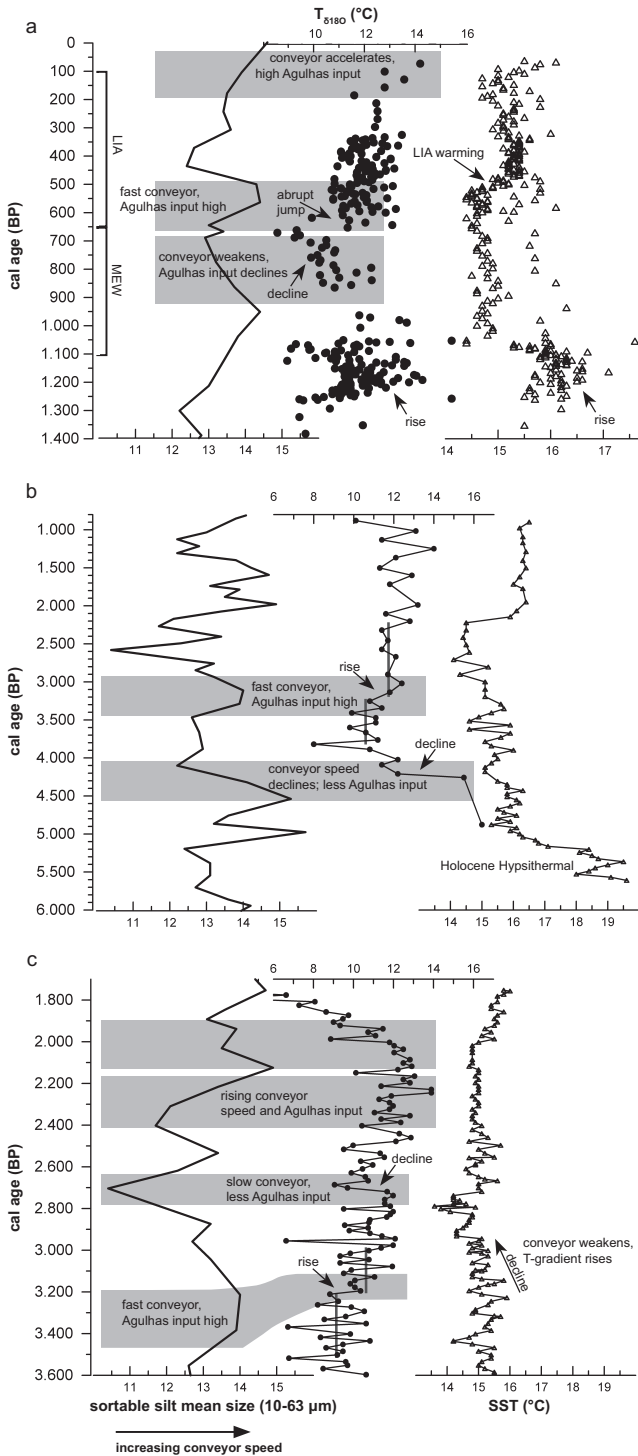
Fig. 6. NADW-production rates along with temperature records from NAM1 (a), core 226620 (b) and core 178 (c). Flow speed fluctuations are inferred from sediment grain-size data from the Iceland Basin (redrawn after Bianchi and McCave, 1999). Bigger grain-size implies faster deep-water masses and increased pole-ward flux of warm Atlantic waters. Variations in the conveyor speed are believed to influence the introduction of warm Agulhas Water, resulting in a synchronous temperature evolution of the Nordic Seas and the central Namibian source waters (recorded by $T_{\delta 18O}$). SST is partly tied to the developing of $T_{\delta 18O}$. Apart from that, SST directly reacts to changes in the atmospheric circulation, which is, in turn, linked to changes in NADW-formation (Fig. 5). Grey bars highlight potential links. MWE = Medieval Warm Epoch; approx. 1050 – 650 BP. LIA = Little Ice Age; approx. 650 – 100 BP (Tyson and Lindesay, 1992).

ocean does not only control the atmosphere, it is also the other way round. Unlike the atmosphere, however, the ocean is a fairly inert system. The oceanic transport of climate perturbations not only takes longer, the ocean integrates the high-frequency atmospheric forcing acting on it (Marshall et al., 2001). So despite the control of NADW-production on atmospheric forcing it is inadequate, therefore, to expect a one-to-one correspondence between NADW-production and the Benguela SST-record. Obvious connections between the conveyor speed and global temperature gradient are anticipated to predominantly appear in the form of major and long-term trends (section 3.3.2.2.).

3.3.2. Regional- and global-scale events

With the knowledge about how global climate signals may reach the Benguela Upwelling we now compare the core records with already existing palaeo-archives, zooming in on fluctuations in our data that may be linked to larger-scale climatic events.

3.3.2.1. Multi-decadal to centennial variability

The immediate vicinity of the coast seems not be the only reason for the high SSTs around 5500 BP (Fig. 3b). In fact, the Holocene Hypsithermal is centred around that time. Records from the South African subcontinent indicate an average temperature increase of 2°C (Cohen and Tyson, 1995). Concomitantly rising surface ocean temperatures have already been reported by Cohen and Tyson (1995), Shi et al. (2000) and Kim et al. (2002). Warmer SSTs suggest a weakening of upwelling-favourable winds, which agrees with the dramatic reduction of Namib dust transported into the Benguela and the reduction of rainfall over the South African interior (Cockroft et al., 1987; Cohen and Tyson, 1995 and ref. therein; Brook et al., 1999). In addition to this, higher SSTs are in accordance with wetter conditions in the coastal area as inferred from pollen records (Shi et al., 2000) (see section 3.3.1.2.).

The drop of $T_{\delta 18O}$ at 4200 BP is markedly equivalent in timing to a slowdown of NADW-production (Fig. 6b) supporting the idea of reduced inflow of warm Agulhas Water as the conveyor decelerates (section 3.3.1.1.). Apparently, the impulse of conveyor slowdown or acceleration propagates so fast as to provoke a more or less "immediate" inter-hemispheric response. Similarly, the slight increase in $T_{\delta 18O}$ at 3200 BP might be linked to the short-term acceleration of NADW-formation (Figs. 6b and 6c) and enhanced Agulhas heat input.

The lacking response of $T_{\delta180}$ to the subsequent slow-down in ocean conveyor speed (Fig. 6c) might be due to strengthened winds and enhanced vertical mixing; the presumed capacity of atmospheric forcing to attenuate or even outweigh the remote influence of the global ocean conveyor is illustrated in Fig. 5. In fact, falling SSTs suggest an intensification of upwelling-favourable winds and fit the invigorated atmospheric circulation and rising meridional temperature gradient associated with the global glacier expansion, occurring in many parts of the world around that time (Cohen and Tyson, 1995 and ref. therein); more about the 'mid Holocene cooling' in the following section when it comes to millennial-scale trends.

The fact that all three cores register an increase in ΔT around 2700 BP (Fig. 3) marks a significant change in the hydrology of the shelf environment. The comparison with NADW-production reveals that the findings are not necessarily purely local in character (shift of the cyclonic wind stress) as outlined in section 3.2.. In fact, the slight decline in $T_{\delta180}$ at 2700 BP coincides with minimum NADW-production (Fig. 6c) and may result, therefore, from a diminished fraction of warm Agulhas Water in ESACW. The conveyor slowdown at that time is also emphasised by Oppo et al. (2003). The subsequent trend towards higher $T_{\delta180}$ (shortly interrupted at 2400 / 2500 BP) might in turn be related to the increasing speed of the global ocean conveyor and a greater fraction of Agulhas Water (Fig. 6c).

Around 2000 BP, terrestrial and marine records display striking parallels. Oxygen isotope data ($\delta^{18}O$) of stalagmites from the Cango Cave (transition between summer and winter rainfall region) and the Cold Air Cave (summer rainfall region) in southern and north-eastern South Africa (Talma and Vogel, 1992; Holmgren et al., 2003), $\delta^{18}O$-signals of mollusc shells in the southern Benguela region (Cohen et al., 1992) and SST-records of core 226620 and core 178 (Figs. 3b and 3c) all testify to a pronounced event of warming around 2000 BP. This marked concurrence of marine and terrestrial records can hardly be coincident. It appears as if major climatic changes affect the South African region at that time. Interestingly, the warming coincides with the Roman Warm Period, a comparatively short spell of higher temperatures in Europe (Bianchi and McCave, 1999). Rising SST might indicate a stronger response to insolation as the global temperature gradient declines and the winds attenuate. Considering our above reasoning in section 3.2., the coincidence of larger-scale forcing and local perturbation (southward shift of upwelling) cannot be ruled out; again, more in the following

section when it comes to millennial trends.

The sharp decline in $T_{\delta180}$ after 2000 BP (Fig. 6c) raises intriguing questions. Although NADW-production declines somewhat between 2100 and 1900 BP, the cooling is certainly too pronounced to be solely attributed to less Agulhas Water. Previous studies already reported colder subsurface temperatures off Walvis Bay, thus offering some support for our data (Tyson and Lindesay, 1992 and ref. therein). According to our above reasoning (section 3.2.) the extent of the cooling may result from the allochthonous nature of the $T_{\delta180}$-signals. However, a satisfying explanation is admittedly lacking and without additional data the mechanisms remain unclear.

Valuable compilations of terrestrial records covering the last two millennia of South African climate including the Medieval Warm Epoch (MWE) and the Little Ice Age (LIA) are found in Tyson and Lindesay (1992) and Holmgren et al. (1999) [d].

The Medieval Warm Epoch (approx. 1050 to 650 BP) is characterised by approximately four centuries of variable but generally warmer conditions. It is proposed that the state of the atmosphere is analogous to the state associated with the wet-spell mode (section 3.3.1.2.; Cohen and Tyson, 1995; Tyson 1999). Corroborating evidence from stalagmite-based terrestrial rainfall records is given by Holmgren et al. (1999; 2003). The development of a forest along the Hoanib River in the northern Namib Desert (Vogel and Rust, 1990; Tyson and Lindesay, 1992) further testifies to increased rainfall receipts in the summer rainfall region. The parallel strengthening of the coastal high-pressure centre is apparently outweighed by the greater moisture availability in the river catchment to the east.

Our data substantiate the wet-mode functioning around that time. The abrupt decline in SST by nearly 2°C at the onset of the MWE (Fig. 4) corroborates the invigoration of upwelling-favourable winds as proposed by the conceptual model outlined in section 3.3.1.2. Its low chronological resolution notwithstanding, SST-data from GeoB1023-5 offshore Cape Frio in the north (Kim et al., 2002) record a simultaneous drop in temperature at the beginning of the last millennium. Mayewski et al. (2004) refer to the onset of the MWE as a short-lived RCC (rapid climate change) -event that coincides with the drought-related fall of the Maya civilization and the collapse of Greenland's colonies as the polar region cooled. The influence of varying NADW-production is again well worth considering. Fig. 6a highlights the parallel decline in NADW-production and $T_{\delta180}$ from

---

[d] Note that there are no universally accepted definitions as regards the duration and timing of the LIA and the MWE. Here, we stick to the dates proposed by Tyson and Lindesay (1992).

900 to 650 BP, a concurrency that seems too obvious to be ignored.

The Little Ice Age (approx. 650 to 100 BP) is the most extensive cool period since the Younger Dryas (Tyson and Lindesay, 1992). Despite being a phenomenon experienced in many parts of the world, it is not a centennial-long period of continuous cold. The LIA is characterised by considerable variability and instability, including substantial fluctuations in the atmospheric circulation strength. Distinct LIA-signals are not necessarily found and its local expression varies with region. As regards the southern African continental interior, the Tyson model (Tyson, 1986, 1999) posits a cool and dry LIA, accompanied by weakened tropical easterlies and slackened upwelling along the southwest African coast (Cohen and Tyson, 1995). Several terrestrial datasets assembled by Tyson and Lindesay (1992) as well as a high-resolution stalagmite record from the Cold Air Cave in NE-South Africa (summer rainfall region) confirm these model results (Holmgren et al., 1999; 2003).

Other studies draw reverse conclusions instead. Geomorphological, palynological and micro-mammalian evidence (sum. in Cohen and Tyson, 1995) indicate trends towards wetter conditions in the continental interior including intensified eastern trades and coastal upwelling. Corresponding SST-cooling has been found in sediments collected off Walvis Bay (Herbert, 1987; Johnson, 1988; both from Tyson and Lindesay, 1992), in the southern Benguela (Cohen et al., 1992) and on the Agulhas Bank (Cohen and Tyson, 1995).

As regards the early stage of the LIA (650 to 500 BP), our data support the scenario of intensified upwelling, thus corroborating the wet-mode functioning around that time (Fig. 4). The transition from the MEW to the LIA is considered the globally most distributed RCC of the late Holocene with pronounced and rapid changes in global-scale atmospheric circulation pattern (Mayewski et al. 2004; Maasch et al., 2005). A LIA-bound strengthening of the atmospheric circulation and resulting intensification of coastal upwelling has also been observed in other parts of the world (Cohen and Tyson, 1995).

Also note the contemporaneous increase in NADW-formation and $T_{\delta 180}$ at 650 BP, i.e. the onset of the LIA (Fig. 6a), again confirming the influence of the thermohaline overturn on the temperature of the source water.

The marked increase in SST at 500 BP (Fig. 4) coincides with period of sudden warming ubiquitously interrupting the LIA in southern Africa (see Tyson and Lindesay, 1992 and ref. therein). Following our above reasoning (section 3.2.) the pronounced rise results from a short-term weakening of upwelling-favourable winds. By inference, the continental interior should have been drier at these times. However, conclusions reached by terrestrial-based records are contradictory (Cockkroft et al., 1987; Tyson and Lindesay, 1992; Cohen and Tyson, 1995; Holmgren et al., 1999). Disparities may be due to differences in the nature and timing of climatic events as well as the varying susceptibility of different environments to climatic fluctuations. Differences in the records' continuity, the large variety of methods applied (Heine, 2005) and vast room for interpretation pose further discrepancies. In addition to this, imprecision due to dating is particularly problematic when it comes to comparatively short spells, such as the LIA. More high-resolution data are needed in order to resolve these ambiguities.

The post-LIA SST-rise may be in part linked to the $T_{\delta 180}$-increase. The warming of the source water might again result from rising NADW-formation or, more precisely, elevated Agulhas heat transfer (Fig. 6a). The SST-rise is corroborated by records from several adjacent multicores (MUC) originating from 22 to 24°S (Emeis et al., 2009). Slightly further south, towards the Lüderitz Upwelling, SSTs decline instead. It shows that spatial SST-variations on the Namibian shelf were markedly heterogeneous during the last couple of centuries. When it comes to the most recent past, i.e. AD 1850 to present, inhomogeneities in SST further increase (Emeis et al., 2009). The findings are ascribed to local perturbations, such as changes in the wind stress curl and accompanied shifts in the position of upwelling. Unfortunately, age determinations of the available MUCs are insufficient to enable any deeper comparison with NAM1.

Irrespective of the sense and magnitude of SST-changes, all MUCs registered increasing $\delta^{15}N$-signals in the youngest sediments. This corresponds with our record (Fig. 4) and implies a higher degree of denitrification in the source waters.

3.3.2.1.1. The thermohaline overturn and the availability of nutrients

The direct correlation between the temperature records and AR_{TOC} in NAM 1 (Fig. 4) has already been an issue in section 3.2.. Apparently, warmer source waters tend to contain higher amounts of nutrients. Taking this observation to its logical conclusion, it follows that NADW-formation not only affects temperature but also controls the amount of nutrients and primary production rates. On closer examination, core 178 lends support to this hypothesis. The rise in $T_{\delta 180}$ at 3200 BP and from 2400 BP on is accompanied by rising AR_{TOC} and NADW-formation. On the other hand, the sudden cooling at 2700 BP is paralleled by collapsing ARs and minimum NADW-formation (Figs.

3c and 6c).

The direct relationship between NADW-production and nutrient content has already previously been observed. Hay and Brock (1992) suggest that northern Benguela source waters were less nutrient-rich during stadials, i.e. at times when NADW-production slowed down considerably. Data from the continental slope off southwest Africa further confirms the diminished nutrient supply during stadials (Berger and Wefer, 2002).

The question is, what are the reasons for the decline in both nutrients and temperature as the conveyor decelerates? Much of the nutrients are brought in by the poleward transport of nutrient-rich SACW from the Angola Dome region. ESACW from the Agulhas Retroflection area in the south (section 1.1.) is the second water mass of interest. If NADW-formation slackens, the conveyor decelerates as a whole. A weakening of all associated currents may induce decreased heat input via the Agulhas Retroflection and reduced nutrient supply from the Angola Dome region (see also Berger and Wefer, 2002). Although being merely speculative at the present stage, this scenario offers a reasonable explanation for the simultaneous decrease of temperature and primary production (Fig. 4).

Despite diminished nutrient supply, productivity proxies all along the SW-African coast testify to enhanced primary production during stadial times. It is suggested that strongly intensified winds and upwelling compensated for the nutrient deficiency in the upwelled waters (Berger and Wefer, 2002). This does not apply to the middle and late Holocene when upwelling rarely makes up for the lack of nutrients in the source water. On most occasions it appears as though the availability of nutrients would be primarily controlled by the type of source water rather than by the intensity of upwelling. Still, this certainly not excludes fluctuations in upwelling to either improve or deteriorate the nutrient situation. For instance, slackened upwelling at 2700 BP (as inferred from rising SST; Fig. 3c) probably further aggravated the nutrient deficiency, while enhanced upwelling after 2400 BP and at 600 BP (as inferred from constant SST at rising $T_{\delta 180}$; Figs. 3c and 4) may have contributed to a sound nutrient supply.

3.3.2.2. Millennial-scale variability

When it comes to millennial scales, orbital forcing is often considered one of the major causes of Holocene climate variance (Tyson, 1999; Lorenz et al., 2006). Over the course of the middle and late Holocene, changes in precession and obliquity induce the continuous displacement of the perihelion towards austral summer. The resultant shift in the seasonal cycle of solar irradiance causes the thermal equator to

strengthen (Tyson, 1999; Lorenz et al., 2006) and the high northern latitudes to cool (Kim and Schneider, 2004). As a consequence, the ITCZ moves southward (Nicholson and Flohn, 1980; Tyson, 1999) and the trade wind system intensifies (section 3.3.1.2.). Sediments from the upper continental slope off Walvis Bay (Summerhayes et al., 1995) as well as different sites on the South African continent testify to the southward movement of the ITCZ over the last millennia (Tyson, 1999; Scott and Woodborne, 2007 and ref. therein). The decline in SST between 5000 and 2200 BP recorded by core 226620 (Fig. 6b) fits the invigoration of the eastern trades also reasonably well.

However, according to Lorenz et al. (2006) orbitally-driven insolation changes exert only a minor influence in the SE-Atlantic realm. They report discrepancies between model simulations and reconstructed SSTs off Namibia concluding that millennial-scale SST-shifts tend to be dominated by processes related to thermohaline and atmospheric forcing.

In fact, an apparent dependence of millennial-scale SST-variance on NADW-production changes can be inferred from Fig. 7a. The parallel evolution of SST and NADW-production fits the theory outlined in Fig. 5, substantiating the influence of the thermohaline overturn on atmospheric circulation and the atmosphere-controlled teleconnection between both hemispheres (see section 3.3.1.2.). The decline in SST between 5000 and 2200 BP is referred to as the mid Holocene cooling (Holmgren et al., 2003) and accords with the steepened meridional temperature gradient and strengthening of upwelling-favourable winds as the conveyor decelerates. Further evidence of cooling in the Benguela has been found in GeoB1023-5 retrieved offshore Cape Frio; (Kim et al., 2002), as well as in mollusc shells from the Agulhas Bank (Cohen and Tyson, 1995) and the southern Benguela region (Cohen et al., 1992). By inference, the continental interior should have been wetter at these times but terrestrial rainfall records are again highly contradictory (Brook et al., 1999; Tyson, 1999; Holmgren et al., 2003; Scott and Woodborne, 2007 and ref. therein).

The marked increase in SST at 2200 BP coincides with the Roman Warm Period and is markedly equivalent in timing with a reversal of the conveyor speed (Fig. 7a). As NADW-production reaccelerates and the high latitudes warm, both winds and upwelling slacken and SST rises (Fig. 5). Admittedly, if the smoothing curves in Fig. 7a were lacking, there would be no immediate visual agreement between both data sets. The observation deserves a mention nonetheless but needs to be verified by additional data.

The concurrences shown in Fig. 7b are much clearer. The temperatures in the northern Benguela Upwelling and the Cold Air Cave located in NE-South Africa (Holmgren et al., 2003) follow markedly similar millennial trends. According to Holmgren et al. (2003) the millennial- and centennial-scale
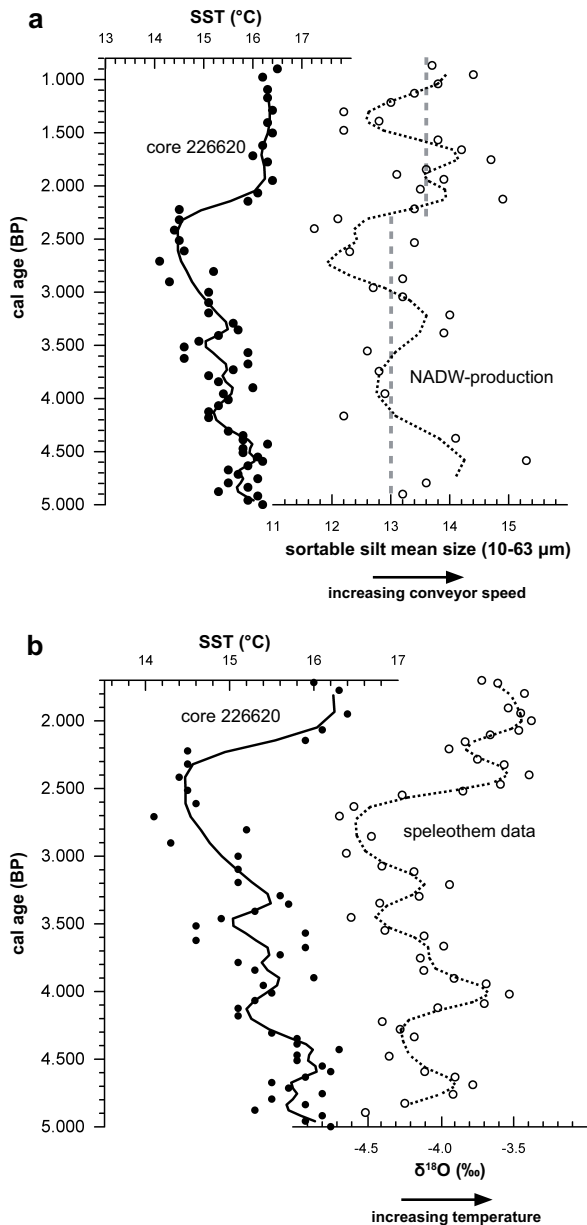
Fig. 7. (a) Millennial-scale SST-evolution recorded by core 226620 alongside NADW-production (redrawn after Bianchi and McCave, 1999), both smoothed with a 3 point running mean. The dashed lines show average grain sizes before and after the 2200 BP-event (Roman Warm Period). The millennial view reveals the possibility of upwelling being indirectly controlled by NADW-production. This observation fits the theory illustrated in Fig. 5 implying that atmospheric forcing, being triggered by changes in NADW-production, may be capable of producing responses in the Benguela Upwelling. (b) Millennial-scale SST-evolution (core 226620) alongside high-resolution speleothem $\delta^{18}O$-records from the Cold Air Cave in NE-South Africa (3 point running mean; redrawn after Holmgren et al., 2003). Note the markedly similar evolution of the marine and terrestrial records.

variability in the $T_{\delta 180}$-data is due to atmospheric circulation changes associated with displacements of southern hemisphere circulation features. In fact, the large distance between both sites suggests perturbations operating on a large spatial scale.

The comparison of SST-trends in the coastal upwelling regions off NW- and SW-Africa (Fig. 8) bears further evidence of large-scale atmospheric forcing. Both GeoB 2007-2 (Kim et al., 2007) and NAM1 exhibit markedly similar SST-variability during the total of the last 1500 years. Here also, the synchrony appears too pronounced to be coincident although the ultimate causes of the parallels are still to be established.

It appears that external climate forcing leaves its marks on a large spectrum of time scales. Contrary to centennial-scale variance (section 3.3.2.1.), however, we found no correlation between NADW-formation and the quality of the source water (in terms of $T_{\delta 180}$ or nutrient content) when it comes to millennial scales. On millennial scales we only found some correlation between NADW-production and SST-records (Fig. 7a) and it seems as though climate signals reaching the northern Benguela - nonetheless being triggered by changes in NADW-production - are rather transferred by the atmosphere than the ocean. This, however, is still to be substantiated by other data.

The common idea of orbital forcing being the ultimate trigger behind millennial-scale climate variance does not entirely fit the circumstances; although applicable to the decline in SST between 5000 and 2200 BP (see above), it fails to explain the pronounced warming at 2200 BP. Our findings agree with Lorenz et al. (2006) who suggest the overriding influence of oceanic and atmospheric forcing in the SE-Atlantic realm.

3.4. Outlook and future scenarios

Eastern boundary upwelling regions strongly affect the global carbon cycle and heat balance of the planet and their role in the global climate system should not be underestimated. As regards the Benguela Current and the associated upwelling, the heat transfer into the North Atlantic is of special interest, with the equatorward heat transport being globally unique (Berger et al., 1989; Berger and Wefer, 2002). Not only plays the Benguela an active role in the global climate system, but it is also considered extremely vulnerable to climate change (Shannon and O'Toole, 2003). Potential implications are still highly speculative though.

Recent monitoring programs have shown that North Atlantic SSTs have increased in the course of the last decades (Marshall et al., 2001 and ref. therein;

Schubert et al., 2006). Still, in the long run and with continued climate warming, most projections anticipate severe and rapid cooling in the high northern latitudes. Although such changes do not seem to be imminent, worst-case scenarios even expect a total cessation of deep-water formation (Schubert et al., 2006). Whether the larger global temperature gradient and intensified upwelling would then compensate for the nutrient deficiency in the source water as it happened in glacial times (Berger and Wefer, 2002) remains to be seen.

4. Conclusions

[1] The three cores document climate variability in the northern Benguela Upwelling back to 5500 BP. The resolution of the data ranges from multi-decadal (NAM1) over centennial (core 178) to millennial scale (core 226620). The selection of proxy indicators provides a valuable basis for robust palaeo-climatic and -environmental reconstructions of the region. The proxies often correlate well with one another, which substantiates the credibility of the data also where fluctuations are only subtle.

Usually, studies are based on one palaeo-thermometer only. The combined analysis of SST and $T_{\delta 18O}$ proved a useful tool in order to differentiate between climate signals transferred by the ocean or the atmosphere. Our results provide convincing evidence that properties and functioning of the northern Benguela system are intimately linked, on a large spectrum of time scales, to changes in both atmospheric circulation features and the thermohaline overturn.

[2] The δ^{15}N-records indicate that denitrification seems to have prevailed since the modern shelf circulation system has established. Average SST-records agree with today's temperature distribution suggesting that the location of upwelling did not substantially change through time.

Although the median values of the proxy indicators lie within today's range, the northern Benguela experienced pronounced and rapid perturbations during the middle and late Holocene, and apparently, not all are purely local in character. We have thoroughly compared our data with other palaeo-environmental records. Unfortunately a meaningful comparison with archives from the adjacent mainland is often hampered due to the insufficiently fine resolution and poor age determinations of terrestrial geoarchives. Besides, continental temperature and rainfall records are not unambiguous (Cohen and Tyson, 1995; Heine, 2005). Moreover it is often difficult to clearly differentiate between local-, regional- and global-scale events.
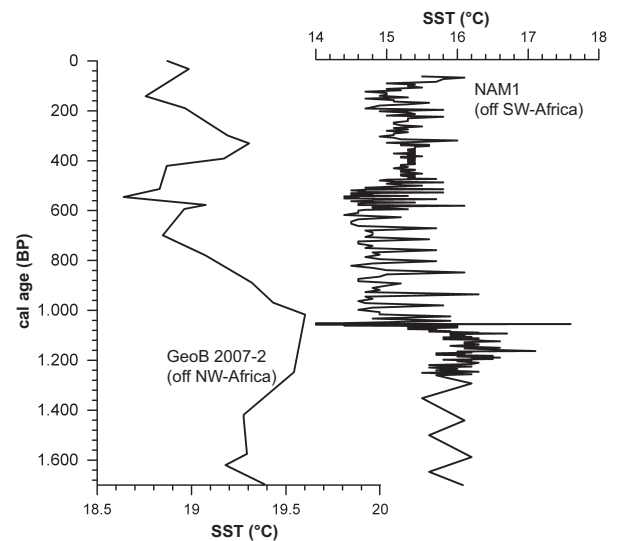
Fig. 8. Comparison of the SST-evolution in the northern Benguela (NAM1) and off NW-Africa (GeoB 2007-2; redrawn after Kim et al., 2007). Both coastal upwelling areas exhibit strikingly contemporaneous reversals and trends in SST during the last one and a half millennia. This includes the slight warming around 1200 BP and the subsequent cooling associated with the MWE. The warming around 500 BP is also markedly synchronous.

Despite all this, the northern Benguela exhibits some strong correlations with both temperature and rainfall records from various sites across the South African subcontinent. Significant parallels with data from high northern latitudes provide evidence for inter-hemispheric climatic teleconnections. We were rather surprised at the frequent evidence of links between the core records and global climate variability (Holocene Hypsithermal, Roman Warm Period, LIA, etc.). Given the extremely heterogeneous and dynamic nature of the Benguela Upwelling, we anticipated global climate signals to be largely obliterated. Irrespective of whether or not some of the observed concurrences are pure coincidence, it definitively seems like the Holocene global climate history did not go by the northern Benguela without trace.

[3] One of the key findings is that the source waters are liable to substantial changes in the nutrient content and temperature. Available information supports the hypothesis that these changes are, at least partly, caused by varying rates of NADW-production. During periods of slackened NADW-formation, $T_{\delta 18O}$ declines and primary production diminishes. The latter is taken as an indication of decreased nutrient supply, the former agrees with reduced introduction of warm Agulhas Water as the global conveyor decelerates. With increased NADW-formation the conditions reverse.

On the basis of the available evidence, we incline to the view that fluctuations in primary production reflect the dynamics of currents and source water masses rather than the dynamics of the atmosphere and upwelling. This is exactly opposite to glacial times when atmospheric forcing outweighed the nutrient deficiency of the source waters (Berger and Wefer, 2002).

Although definite conclusions are conditional upon further investigation, our findings substantiate the previously observed control of Agulhas Water on the quality of ESACW (e.g. Gordon, 1986). Apparently, its influence reaches higher up north than hitherto discovered (NB: The variability of inter-ocean exchange in the Agulhas Retroflection area is currently being investigated by a project called ASTTEX [e)], Agulhas-South Atlantic Thermohaline Transport Experiment).

[4] Predictions about the future stability of the global ocean conveyor vary substantially and region-specific consequences of abrupt changes in NADW-production are also highly speculative. As regards the Benguela system, a severe slowdown of the ocean conveyor may have adverse effects on primary production and the ecosystem as a whole due to deteriorating amounts of nutrients in the source waters. If, however, the system switches back to the glacial mode, increased upwelling may be able to compensate for that nutrient deficiency.

There is no single dominant factor controlling variability in the northern Benguela system. Apart from local perturbations, the influence of both atmospheric and oceanic forcing seems beyond all question. Still, the full array of feedback mechanisms, ocean-atmosphere interactions and causal links including the implications for the Benguela upwelling are not entirely understood yet.

All remaining uncertainites notwithstanding, our data yield novel information on how external forcing acted on the northern Benguela Upwelling in the past. The study and thorough comparison of three highly resolved cores from the northern Benguela shelf is hitherto unique. When worked into numerical and conceptual models the data will contribute to the refinement of future climate predictions for the South African realm and the development of a long-term sustainable fisheries management plan.

References

Altabet, M.A., Francois, R., (1994) The use of nitrogen isotopic ratio for reconstruction of past changes in surface ocean nutrient utilization. In: *Carbon Cycling in the Glacial Ocean: Constraints on the Ocean´s Role in Global Change.*, *Vol. 17*, *NATO ASI Series* (Ed. by R. Zahn, T.F. Pedersen, M.A. Kaminski, L. Labeyrie). Springer-Verlag, Heidelberg.

Bakun, A., Weeks, S.J., (2004) Greenhouse gas buildup, sardines, submarine eruptions and the possibility of abrupt degradation of intense marine upwelling ecosystems. *Ecology Letters*, 7, 1015-1023.

Bemis, B.E., Spero, H.J., Bijma, J., Lea, D.W., (1998) Reevaluation of the oxygen isotopic composition of planktonic foraminifera: experimental results and revised paleotemperature equations. *Paleoceanography*, 13, 150-160.

Berger, W.H., Smetacek, V.S., Wefer, G., (1989) Productivity of the ocean: present and past, pp. 471. John Wiley and Sons, Chichester.

Berger, W.H., Wefer, G., (2002) On the reconstruction of upwelling history: Namibia upwelling in context. *Marine Geology*, 180, 3-28.

Bianchi, G.G., McCave, N., (1999) Holocene periodicity in North Atlantic climate and deep-ocean flow south of Iceland. *Nature*, 397, 515-517.

Blanz, T., Emeis, K.-C., Siegel, H., (2005) Controls on alkenone unsaturation ratios along the salinity gradient between the open ocean and the Baltic Sea. *Geochimica et Cosmochimica Acta*, 69(14), 3589-3600.

Blunier, T., Chappellaz, J., Schwander, J., Dällenbach, A., Stauffer, B., Stocker, T.F., Raynaud, D., Jouzel, J., Clausen, H.B., Hammer, C.U., Johnsen, S.J., (1998) Asynchrony of Antarctic and Greenland climate change during the last glacial period. *Nature*, 394, 739-743.

Boebel, O., Lutjeharms, J., Schmid, C., Zenk, W., Rossby, T., Barron, C., (2003) The Cape Cauldron: a regime of turbulent inter-ocean exchange. *Deep-Sea Research*, II(50), 57-86.

Bremner, J.M., Willis, J.P., (1993) Mineralogy and geochemistry of the clay fraction of sediments from the Namibian continental margin and the adjacent hinterland. *Marine Geology*, 115, 85-116.

Brook, A.B., Marais, E., Cowart, J.B., (1999) Evidence of wetter and drier conditions in Namibia from tufas and submerged speleothems. *Cimbebasia*, 15, 29-39.

Brüchert, V., Altenbach, A.V., Bening, G., Bockelmann, F., Currie, B., Donath, J., Dübecke, J., Endler, R., Erdmann, S., Ertan, T., Fuchs, B., Klockgether, G., Krüger, S., Kuypers, M.M.M., Lass, H.U., Lavik, G., Lilienthal, S., Leipe, T., Nickel, G., Noli-Peard, K., Ohde, T., Schulz, B., Schulz, H., Siegel, H., Struck, U., Wulf, J., Zitzmann, S., Zonneveld, K., (2004) The Benguela Upwelling System 2003, Part 3, Cruise No. 57, Leg 3, March 15 – April 13, 2003, Walvis Bay, Namibia - Dakar. In: *Meteor Berichte*, *4*, pp. 53.

Bubnov, V.A., (1972) Structure and characteristics of the oxygen minimum layer in the southeast Atlantic Ocean. *Oceanology*, 12, 193-201.

[e)] Project homepage: http://gyre.umeoce.maine.edu/ASTTEX/. The project is conducted against the background that inter-ocean communication plays an important role in global climate change.

Chapman, P., Shannon, L., (1985) The Benguela ecosystem Part II. Chemistry and related processes. *Oceanography and Marine Biology Annual Review* 23, 183-251.

Chapman, P., Shannon, L., (1987) Seasonality in the oxygen minimum layers at the extremities of the Benguela system. *South African Journal of Marine Science*, 5, 51-62.

Christiansen, C.C., Kunzendorf, H., (1998) Datings and sedimentation rate estimations during GOBEX. A summary. *Meereswissenschaftliche Berichte*, 34, 55-76.

Cline, J.D., Kaplan, I.R., (1975) Isotopic fractionation of dissolved nitrate during denitrification in the eastern tropical North Pacific Ocean. *Marine Chemistry*, 3, 271-299.

Cochrane, K.L., Augustyn, C.J., Bianchi, G., De Barros, P., Fairweather, T., Iitembu, J., Japp, D., Kanandjembo, A., Kilongo, K., Moroff, N., Nel, D., Roux, J.-P., Shannon, L.J., Van Zyl, B., Vaz Velho, F., (2007) Results and conclusions of the project „Ecosystem approaches for fisheries management in the Benguela Current Large Marine Ecosystem". *FAO Fisheries Circular No. 1026*, 166.

Cockcroft, M.J., Wilkinson, M.J., Tyson, P.D., (1987) The application of a present-day climate model to the late quaternary in southern Africa. *Climate Change*, 10(161-181).

Cohen, A.L., Parkington, J.E., Brundrit, G.B., van der Merwe, N.J., (1992) A Holocene Marine Climate Record in Mollusc Shells from the Southwest African Coast. *Quaternary Research*, 38, 379-385.

Cohen, A.L., Tyson, P.D., (1995) Sea-surface temperature fluctuations during the Holocene off the south coast of Africa: implications for terrestrial climate and rainfall. *Holocene*, 5(3), 304-312.

Copenhagen, W.J., (1953) The periodic mortality of fish in the Walvis region — a phenomenon within the Benguela Current. *Investigational Report Division of Fisheries-Union of South Africa*, 14, 1-35.

Diester-Haass, L., Heine, K., Rothe, P., Schrader, H., (1988) Late Quaternary history of continental climate and the Benguela Current off South West Africa. *Palaeogeography, Palaeoclimatology, Palaeoecology*, 65, 81-91.

Emeis, K.-C., Brüchert, V., Currie, B., Endler, R., Ferdelman, T., Kiessling, A., Leipe, T., Noli-Peard, K., Struck, U., Vogt, T., (2004) Shallow gas in shelf sediments of the Namibian coastal upwelling ecosystem. *Continental Shelf Research*, 24(6), 627-642.

Emeis, K.-C., Struck, U., Leipe, T., Ferdelman, T.G., (2009) Variability in upwelling intensity and nutrient regime in the coastal upwelling system offshore Namibia: results from sediment archives. *International Journal of Earth Sciences* 98, 309-326.

Erez, J., Luz, B., (1983) Experimental paleotemperature equation for planktonic foraminifera. *Geochimica et Cosmochimica Acta*, 47, 1025-1031.

Fairbanks, R.G., (1989) A 17,000-year glacio-eustatic sea level record: influence of glacial melting rates on the Younger Dryas event and deep-ocean circulation. *Nature*, 342, 637-642.

Francois, R., Altabet, M.A., Burckle, L.H., (1992) Glacial to interglacial changes in surface nitrate utilization in the Indian sector of the southern ocean as recorded by sediment $\delta^{15}N$. *Paleoceanography*, 7, 589-606.

Fry, B., (1996) $^{13}C/^{12}C$ fractionation by marine diatoms. *Marine Ecology Progress Series*, 134, 283-294.

Gaye-Haake, B., Lahajnar, N., Emeis, K.-C., Unger, D., Rixen, T., Suthhof, A., Ramaswamy, V., Schulz, H., Paropkari, A.L., Guptha, M.V.S., Ittekkot, V., (2005) Stable nitrogen isotopic ratios of sinking particles and sediments from the northern Indian Ocean. *Marine Chemistry*, 96, 243-255.

Gordon, A.L., (1986) Interocean Exchange of Thermocline Water. *Journal of Geophysical Research*, 91(C4), 5037-5046.

Hart, T.J., Currie, R.I., (1960) The Benguela Current. *Discovery Report*, 31, 123-127.

Hay, W.W., Brook, J.C., (1992) Temporal variation in intensity of upwelling off Southwest Africa. In: *Upwelling Systems: Evolution since the Early Miocene*, *64* (Ed. by C.P. Summerhayes, W.L. Prell, K.C. Emeis), pp. 463-497. Geological Society Special Publication.

Heine, K., (2005) Holocene climate of Namibia: a review based on geoarchives. *African Study Monographs*, Suppl. 30, 119-133.

Hemleben, C., Bijma, J., (1994) Foraminiferal population dynamics and stable carbon isotopes In: *Carbon Cycling in the Glacial Ocean: Constraints on the Ocean´s Role in Global Change*, *17* (Ed. by R. Zahn, T.F. Pedersen, M.A. Kaminski, L. Labeyrie), pp. 145-166. Springer-Verlag.

Hollander, D.J., McKenzie, J.A., (1991) CO_2 control on carbon-isotope fractionation during aqueous photosynthesis: A paleo-pCO_2 barometer. *Geology*, 19(9), 929-932.

Holmes, M.E., Müller, P.J., Schneider, R.R., Segl, M., Pätzold, J., Wefer, G., (1996) Stable nitrogen isotopes in Angola Basin surface sediments. *Marine Geology*, 134, 1-12.

Holmes, M.E., Müller, P.J., Schneider, R.R., Segl, M., Wefer, G., (1998) Spatial variations in euphotic zone nitrate utilization based on $\delta^{15}N$ in surface sediments. *Geo-Marine Letters*, 18(1), 58-65.

Holmes, B., Eichner, C., Struck, U., Wefer, G., (1999) Reconstructions of surface ocean nitrate utilization using stable nitrogen isotopes in sinking particles and sediments. In: *Use of Proxies in Paleoceanography: Examples from the South Atlantic* (Ed. by G. Fischer, G. Wefer), pp. 447-468. Springer, Berlin.

Holmes, E., Lavik, G., Fischer, G., Segl, M., Ruhland, G., Wefer, G., (2002) Seasonal variability of $\delta^{15}N$ in sinking particles in the Benguela upwelling region. *Deep-Sea Research I*, 49, 377-394.

Holmgren, K., Karlén, W., Lauritzen, S.E., Lee-Thorp, J.A., Partridge, T.C., Piketh, S., Repinski, P., Stevenson, C., Svanered, O., Tyson, P.D., (1999) A 3000-year high-resolution stalagmitebased record of palaeoclimate for northeastern South Africa. *The Holocene*, 9(3), 295-309.

Holmgren, K., Lee-Thorp, J.A., Cooper, G.R.J., Lundblad, K., Partridge, T.C., Scott, L., Sithaldeen, R., Talma, A.S., Tyson, P.D., (2003) Persistent millennial-scale climatic variability over the past 25,000 years in Southern Africa. *Quaternary Science Research*, 22, 2311-2326.

Hsieh, W.W., Boer, G.J., (1992) Global climate change and ocean upwelling. *Fisheries Oceanography*, 1(333-338).

Kim, J.-H., Schneider, R.R., Müller, P.J., Wefer, G., (2002) Interhemispheric comparison of deglacial sea-surface temperature patterns in Atlantic eastern boundary currents. *Earth and Planetary Science Letters*, 1994, 383-393.

Kim, J.-H., Schneider, R.R., (2004) GHOST global database for alkenone-derived 6ka sea-surface temperatures.

Kim, J.-H., Meggers, H., Rimbu, N., Lohmann, G., Freudenthal, T., Müller, P.J., Schneider, R.R., (2007) Impacts of the North Atlantic gyre circulation on Holocene climate off northwest Africa. *Geology*, 35(5), 387-390.

Kirst, G.J., Schneider, R.R., Müller, P.J., von Storch, I., Wefer, G., (1999) Late Quaternary Temperature Variability in the Benguela Current System Derived from Alkenones. *Quaternary Research*, 52, 92-103.

Knowles, R., (1982) Denitrification. *Microbiological Reviews*, 46(1), 43-70.

Kreutz, K.J., Mayewski, P.A., Meeker, L.D., Twickler, M.S., Whitlow, S.I., Pittalwala, I.I., (1997) Bipolar Changes in Atmospheric Circulation During the Little Ice Age. *Science*, 277, 1294-1296.

Kristen, I., (2003) Paläoklimatologische Untersuchungen im Auftriebsgebiet vor Namibia. In: *Department für Geo- und Umweltwissenschaften*, pp. 48. Ludwig Maximilians Universität, München.

Kuypers, M.M.M., Lavik, G., Woebken, D., Schmid, M., Fuchs, B.M., Amann, R., Jørgensen, B.B., Jetten, M.S.M., (2005) Massive nitrogen loss from the Benguela upwelling system through anaerobic ammonium oxidation. *PNAS*, 102(18), 6478-6483.

Lavik, G., Stührmann, T., Brüchert, V., van der Plas, A., Mohrholz, V., Lam, P., Mußmann, M., Fuchs, B.M., Amann, R., Lass, U., Kuypers, M.M.M., (2009) Detoxification of sulphidic African shelf waters by blooming chemolithotrophs. *Nature*, 459, 581-585.

Libes, S.M., Deuser, W.G., (1988) The isotope geochemistry of particulate nitrogen in the Peru Upwelling Area and the Gulf of Maine. *Deep-Sea Research*, 35(4), 517-533.

Lorenz, S.J., Kim, J.-H., Rimbu, N., Schneider, R.R., Lohmann, G., (2006) Orbitally driven insolation forcing on Holocene climate trends: Evidence from alkenone data and climate modeling. *Paleoceanograohy*, 21, 14pp.

Lutjeharms, J.R.E., Meeuwis, J.M., (1987) The extent and variability of southeast Atlantic upwelling. *South African Journal of Marine Science*, 5, 85-94.

Lutjeharms, J.R.E., Stockton, P.L., (1987) Kinematics of the upwelling front off southern Africa. *South African Journal of Marine Science*, 5, 35-49.

Maasch, K.A., Mayewski, P.A., Rohling, E.J., Stager, J.C., Karlén, W., Meeker, L.D., Meyerson, E.A., (2005) A 2000-year context for modern climate change. *Geografiska Annaler*, A(1), 7-15.

Marshall, J., Kushnir, Y., Battisti, D., Chang, P., Czaja, A., Dickson, R., Hurrell, J., McCartney, M., Saravanan, R., Visbeck, M., (2001) North Atlantic climate variability: phenomena, impacts and mechanisms. *International Journal of Climatology*, 21, 1863-1898.

Mayewski, P.A., Rohling, E.E., Stager, J.C., Karlén, W., Maasch, K.A., Meeker, L.D., Meyerson, E.A., Gasse, F., van Kreveld, S., Holmgren, K., Lee-Thorph, J., Rosqvist, G., Rack, F., Staubwasser, M., Schneider, R.R., Steig, E.J., (2004) Holocene climate variability. *Quaternary Research*, 62, 243-255.

Meisel, S., Struck, U., (2011) The potential distortion of sedimentary $\delta^{15}N$ and C_{org}/N ratios by NH_4^+ and the effects of pre-analysis sample treatment. *Fossil Record,* 14(2), 141-152.

Meisel, S., Struck, U., Emeis, K.-C., (2011) Nutrient dynamics and oceanographic features in the central Namibian upwelling region as reflected in $\delta^{15}N$-signals of suspended matter and surface sediments. *Fossil Record,* 14(2), 153-169.

Mohrholz, V., Bartholomae, C.H., van der Plas, A.K., Lass, H.U., (2008) The seasonal variability of the northern Benguela undercurrent and its relation to the oxygen budget on the shelf. *Continental Shelf Research*, 28(3), 424-441.

Montoya, J.P., (1994) Nitrogen isotope fractionation in the modern ocean: Implications for the sedimentary record. In: *Carbon Cycling in the Glacial Ocean: Constraints on the Ocean´s Role in Global Change.*, *17*, *NATO ASI Series* (Ed. by R. Zahn, T.F. Pedersen, M.A. Kaminski, L. Labeyrie), pp. 259-279. Springer-Verlag, Berlin.

Montoya, J.P., McCarthy, J.J., (1995) Isotopic fractionation during nitrate uptake by phytoplankton growth in continuous culture. *Journal of Plankton Research*, 17, 439-464.

Moroshkin, K.V., Bubnov, V.A., Bulatov, R.P., (1970) Water circulation in the eastern South Atlantic Ocean. *Oceanology*, 10(1), 27-34.

Murray, J.W., (1991) Ecology and distribution of planktonic foraminifera In: *Biology of Foraminifera* (Ed. by J.J. Lee, O.R. Anderson), pp. 255-284. Academic Press.

Nelson, G., Hutchings, L., (1983) The Benguela upwelling area. *Progress in Oceanography*, 12, 333-356.

Nicholson, S.E., Flohn, H., (1980) African environmental and climatic changes and the general atmospheric circulation in late Pleistocene and Holocene. *Climatic Change*, 2, 313-348.

Niebler, H.-S., Huberten, H.-W., Gersonde, R., (1999) Oxygen Isotope Values of Planktic Foraminifera: A Tool for the Reconstruction of Surface Water Stratification In: *Use of Proxies in Paleoceanography: Examples from the South Atlantic* (Ed. by G. Fischer, G. Wefer), pp. 165-189. Springer-Verlag, Berlin Heidelberg.

Oberhänsli, H., (1991) Upwelling signals at the northeastern Walvis Ridge during the past 500,000 years. *Paleoceanography*, 6, 53-71.

Oppo, D.W., McManus, J.F., Cullen, J.L., (2003) Deepwater variability in the Holocene epoch. *Nature*, 422, 277-278.

Ostrom, N.E., Macko, S.A., (1991) Late Wisconsinan to present sedimentation of organic matter off northern Newfoundland in response to climatological events. *Continental Shelf Research*, 11, 1285-1296.

Ostrom, N.E., Macko, S.A., Deibel, D., Thompson, R.J., (1997) Seasonal variation in the stable carbon and nitrogen isotope biogeochemistry of a coastal cold ocean environment. *Geochimica et Cosmochimica Acta*, 61(14), 2929-2942.

Packard, T.T., Garfield, P.C., Codispoti, L.A., (1983) Oxygen consumption and denitrification below the Peruvian upwelling. In: *Coastal Upwelling: Its Sediment Record* (Ed. by E. Suess, J. Thiede), pp. 147-173. Plenum Press, New York.

Rau, G.H., (1994) Variations in sedimentary $\delta^{13}C$ as a proxy for past changes in ocean and atmospheric CO^2 concentrations. In: *Carbon Cycling in the Glacial Ocean: Constraints on the Ocean´s Role in Global Change*, *17*, *NATO ASI Series* (Ed. by R. Zahn, T.F. Pedersen, M.A. Kaminski, L. Labeyrie), pp. 307-321. Springer-Verlag, Berlin.

Ravelo, A.C., Fairbanks, R.G., (1992) Oxygen Isotopic Composition of Multiple Species of Planktonic Foraminifera: Recorders of the Modern Photic Zone Temperature Gradient. *Paleoceanography*, 7(6), 815-831.

Ren, H., Sigman, D.M., Meckler, A.N., Plessen, B., Robinson, R.S., Rosenthal, Y., Haug, G.H., (2009) Foraminiferal Isotope Evidence of Reduced Nitrogen Fixation in the Ice Age Atlantic Ocean. *Science*, 323, 244-248.

Rühlemann, C., Mulitza, S., Müller, P.J., Wefer, G., Zahn, R., (1999) Warming of the tropical Atlantic Ocean and slowdown of thermohaline circulation during the last deglaciation. *Nature*, 402, 511-514.

Sachs, J.P., Repeta, D.J., (1999) Oligotrophy and nitrogen fixation during eastern Mediterranean sapropel events. *Science*, 286, 2485-2488.

Schelske, C.L., Hodell, D.A., (1991) Recent changes in productivity and climate of Lake Ontario detected by isotopic analysis of sediments. *Limnology and Oceanography*, 36, 961-975.

Schubert, R., Schellnhuber, H.-J., Buchmann, N., Epiney, A., Grießhammer, R., Kulessa, M., Messner, D., Rahmstorf, S., Schmid, J., (2006) The Future Oceans - Warming Up, Rising High, Turning Sour, *Special Report*. German Advisory Council on Global Change (WBGU).

Scott, L., Woodborne, S., (2007) Vegetation history inferred from pollen in Late Quaternary faecal deposits (hyraceum) in the Cape winter-rain region and its bearing on past climates in South Africa. *Quaternary Science Reviews*, 26, 941-953.

Shannon, L.V., (1985) The Benguela ecosystem. Part I. Evolution of the Benguela, physical features and processes. *Oceanography and Marine Biology Annual Review*, 23, 105-182.

Shannon, L.V., Boyd, A.J., Brundrit, G.B., Taunton-Clark, J., (1986) On the existence of an El Niño-type phenomenon in the Benguela system. *Journal of Marine Research*, 44(3), 495-520.

Shannon, L.V., Pillar, S.C., (1986) The Benguela Ecosystem. Part III: Plankton. *Oceanography and Marine Biology Annual Review* 24, 65-170.

Shannon, L.V., Nelson, G., (1996) The Benguela: Large Scale Features and Processes and System Variability. In: *The South Atlantic: Present and Past Circulation* (Ed. by G. Wefer, W.H. Berger, G. Siedler, D. Webb), pp. 163-210. Springer, Berlin, Heidelberg.

Shannon, L.V., O'Toole, M.J., (2003) Sustainability of the Benguela: ex Africa semper aliquid novi. In: *Large marine ecosystems of the world: trends in exploitation, protection and research* (Ed. by G. Hempel, K. Sherman), pp. 227-253. Elsevier B.V., Amsterdam.

Shi, N., Dupont, L.M., Beug, H.-J., Schneider, R., (2000) Correlation between Vegetation in Southwestern Africa and Oceanic Upwelling in the Past 21,000 Years. *Quaternary Research*, 54, 72-80.

Sigman, D.M., Altabet, M.A., Michener, R., McCorkle, D.C., Fry, B., Holmes, R.M., (1997) Natural abundance-level measurement of the nitrogen isotopic composition of oceanic nitrate: an adaption of the ammonia diffusion method. *Marine Chemistry*, 57(3-4), 227-242.

Sigman, D.M., Altabet, M.A., McCorkle, D.C., Francois, R., Fischer, G., (2000) The $\delta^{15}N$ of nitrate in the Southern Ocean: nitrogen cycling and circulation in the ocean interior. *Journal of Geophysical Research*, 105(C8), 599-614.

Stander, G.H., (1964) The Benguela Current off South West Africa. *Investigational Report of the Marine Research Laboratory of South West Africa*, 12, 1-43.

Stramma, L., Peterson, R.G., (1989) Geostrophic Transport in the Benguela Current region. *Journal of Physical Oceanography*, 19, 1440-1448.

Struck, U., Emeis, K.-C., Alheit, J., Schneider, R., Eichner, C., Altenbach, A.-V., (2002) Changes of the upwelling rates of nitrate preserved in the $\delta^{15}N$-signature of sediments and fish scales from the diatomaceous mud belt off Namibia. *GeoBios*, 35(EPA-special issue), 3-11.

Stuiver, M., Braziunas, T.F., (1993) Modeling atmospheric ^{14}C influences and ^{14}C ages of marine samples to 10,000 BC. *Radiocarbon*, 35(1), 137-189.

Stuiver, M., Grootes, P.M., Braziunas, T.F., (1995) The GISP2 $\delta^{18}O$ Climate Record of the Past 16,500 Years and the Role of the Sun, Ocean, and Volcanoes. *Quaternary Research*, 44, 341-354.

Stuiver, M., Reimer, P.J., Reimer, R.W., (2005) CALIB 5.0. [WWW program and documentation].

Summerhayes, C.P., Kroon, D., Rosell-Mele, A., Jordan, R.W., Schrader, H.-J., Hearn, R., Villanueva, J., Grimalt, J.O., Eglington, G., (1995) Variability in the Benguela Current upwelling system over the past 70,000 years. *Progress in Oceanography*, 35, 207-251.

Talma, S.A., Vogel, J.C., (1992) Late Quaternary Paleotemperatures Derived from a Speleothem from Cango Caves, Cape Province, South Africa. *Quaternary Research*, 37, 203-213.

Tedesco, K., Thunell, R., Astor, Y., Muller-Karger, F., (2007) The oxygen isotope composition of planktonic foraminifera from the Cariaco Basin, Venezuela: Seasonal and interannual variations. *Marine Micropaleontology*, 62, 180-193.

Tyrrell, T., Lucas, M.I., (2002) Geochemical evidence of denitrification in the Benguela upwelling system. *Continental Shelf Research*, 22, 2497-2511.

Tyson, P.D., (1986) Climatic Change and Variability in Southern Africa, Oxford University Press, Cape Town.

Tyson, P.D., (1999) Atmospheric circulation changes and palaeoclimates of southern Africa. *South African Journal of Science*, 95, 194-201.

Tyson, P.D., Lindesay, J.A., (1992) The climate of the last 2000 years in southern Africa. *The Holocene*, 2(3), 271-278.

van Zyl, B.J., (2010) A Decade of Namibian Fisheries and Biodiversity Management. *www.unep.org/bpsp/Fisheries/Fisheries%20 Case%20Studies/VANZYL.pdf*, Access date April 2010.

Vidal, L., Schneider, R.R., Marchal, O., Bickert, T., Stocker, T.F., Wefer, G., (1999) Link between the North and South Atlantic during the Heinrich events of the last glacial period. *Climate Dynamics*, 15, 909-119.

Vogel, J.C., Rust, U., (1990) Ein in der Kleinen Eiszeit (Little Ice Age) begrabener Wald in der nördlichen Namib. *Berliner Geographische Studien*, 30, 15-34.

Vogt, T., (2002) Akustische Fazies auf dem Schelf und oberen Kontinentalrand vor Namibia - Auswertung von PARASOUND-Ergebnissen der Reise METEOR 48-2, *M.Sc. Thesis*, pp. 80. University of Greifswald, Greifswald.

Voss, M., Altabet, M., von Bodungen, B., (1996) $\delta^{15}N$ in sedimenting particles as indicator for euphotic zone processes. *Deep-Sea Research*, 43, 33-47.

Wada, E., Hattori, A., (1978) Nitrogen isotope effects in the assimilation of inorganic nitrogenous compounds by marine diatoms. *Geomicrobiology Journal*, 1, 85-101.

Wada, E., (1980) Nitrogen isotope fractionation and its significance in biogeochemical processes occurring in marine environments. In: *Isotope Marine Chemistry* (Ed. by E.D. Goldberg, Y. Horibe, K. Saruhashi), pp. 375-398. Uchida Rokakuho, Japan.

Waser, N.A.D., Turpin, D.H., Harrison, P.J., Nielsen, B., Calvert, S.E., (1998) Nitrogen isotope fractionation during uptake and assimilation of nitrate, nitrite, ammonium and urea by a marine diatom. *Limnology and Oceanography*, 43, 215-224.

Danksagung

Stavanger, 20. Mai 2011

Curriculum Vitae

Appendices

Appendix 1.1.

core depth (cm)	N (%) [1] MS-1	N (%) [2] MS-2	N (%) [3] MS-3	N (%) [4] MS-4	TC (%) [1] MS-1	TC (%) [2] MS-2	C_{org} (%) [5] MS-2	C_{org} (%) [3] MS-3	C_{org} (%) [4] MS-4	C_{inorg} (%) [6]	$CaCO_3$ (%) [7]	C_{org}/N (molar) [8] MS-1	C_{org}/N (molar) MS-2	C_{org}/N (molar) MS-3	C_{org}/N (molar) MS-4	$\delta^{15}N$ (‰) MS-1	$\delta^{15}N$ (‰) MS-2	$\delta^{15}N$ (‰) MS-3	$\delta^{15}N$ (‰) MS-4
2.5	0.76	0.82	0.88	0.73	7.17	7.47	6.78	7.76	6.48	0.69	5.79	7.31	7.11	7.57	7.58	8.25	8.16	8.00	9.30
7.5	0.65		0.85	0.60	6.11			7.43	5.09	1.02	8.50	6.67		7.48	7.31	9.32		8.13	10.61
12.5	0.63		0.74	0.64	6.02			6.43	5.51	0.50	4.19	7.55		7.48	7.41	8.43		7.87	9.50
17.5	0.67	0.69	0.74	0.63	6.36	6.22	5.35	6.40	5.49	0.87	7.21	7.03	6.68	7.46	7.50	8.67	8.14	8.11	9.57
22.5	0.63		0.83	0.61	5.78			7.27	5.19	0.59	4.89	7.02		7.54	7.26	10.29		7.94	10.85
27.5	0.65		0.75	0.63	6.24			6.55	5.58	0.66	5.54	7.31		7.48	7.60	8.32		7.95	9.45
32.5	0.70	0.71	0.81	0.69	6.66	6.36	5.79	7.13	6.09	0.57	4.74	7.50	6.96	7.52	7.61	8.25	8.37	7.98	9.28
37.5	0.59		0.80	0.60	5.47			6.91	5.17	0.30	2.47	7.55		7.44	7.38	10.02		8.07	10.93
42.5	0.62		0.84	0.61	5.81			7.36	5.25	0.57	4.73	7.21		7.51	7.38	9.45		7.85	10.79
47.5	0.60		0.83	0.63	5.48			7.23	5.32	0.15	1.28	7.56		7.43	7.28	10.97		7.85	10.86
52.5	0.65	0.78	0.86	0.64	5.91	6.94	6.53	7.56	5.50	0.41	3.40	7.27	7.22	7.51	7.42	10.58	8.15	7.93	10.82
57.5	0.62		0.83	0.61	5.79			7.43	5.38	0.40	3.36	7.41		7.65	7.53	9.59		7.97	11.09
62.5	0.60		0.74	0.63	5.54			7.30	5.59	-0.05		8.01		8.46	7.54	9.89		7.95	10.80
67.5	0.63		0.79	0.66	5.84			7.72	5.73	0.11	0.93	7.75		8.33	7.44	10.20		7.92	10.83
72.5	0.61	0.77	0.77	0.63	5.64	7.22	7.04	7.48	5.46	0.18	1.48	7.67	7.80	8.36	7.46	10.08	8.02	7.99	10.76
77.5			0.76	0.71	7.07			7.49						8.40		8.15		7.83	8.96
82.5	0.74		0.83	0.71	7.07			7.30	6.78	0.29	2.44	7.87		7.58	8.18	7.85		8.33	9.14
87.5	0.63	0.79	0.87	0.63	5.75	6.86	6.73	7.59	5.61	0.13	1.11	7.61	7.30	7.52	7.64	10.41	8.16	8.28	11.11
92.5	0.80		0.92	0.72	7.60			8.11						7.58		8.09		8.17	11.08
97.5	0.70		1.02	0.76	6.54			9.11	7.28	-0.74		8.86		7.68	8.25	9.28		8.25	8.76
102.5	0.68	0.74	0.81	0.57	6.41	6.49	4.76	7.02	4.68	1.74	14.48	5.86	5.54	7.39	7.08	9.49	8.22	8.16	10.70
107.5	0.68		0.82	0.58	6.16			7.05	4.67	1.49	12.42	5.89		7.38	6.86	10.87		8.07	11.37
112.5	0.68		0.84	0.59	6.24			7.13	4.79	1.45	12.04	6.00		7.31	6.99	10.69		8.01	11.29
117.5	0.73		0.83	0.65	6.98			7.11	5.63	1.36	11.31	6.61		7.34	7.45	8.53		8.09	10.13
122.5	0.72	0.69	0.86	0.66	6.87	6.06	5.05	7.33	5.86	1.01	8.38	6.93	6.30	7.34	7.55	8.77	8.39	7.96	9.36
127.5	0.61		0.84	0.61	2.79			7.22	5.01	-2.22		7.03		7.35	7.08	10.24		8.80	12.10
132.5	0.71		0.86	0.65	6.60			7.26	5.77	0.83	6.91	6.98		7.20	7.59	8.77		8.38	10.29
137.5	0.58		0.82	0.55	5.22			7.03	5.64	-0.42		8.32		7.32	8.74	10.95		8.39	11.51
142.5	0.58		0.80	0.58	5.00			6.77	4.63	0.38	3.14	6.83		7.23	6.79	12.54		8.65	12.64
147.5	0.56		0.77	0.56	5.03			6.45	4.51	0.51	4.27	6.88		7.17	6.87	10.63		8.58	12.59
152.5	0.53		0.77	0.58	4.79			6.47	4.70	0.08	0.70	7.60		7.17	7.01	10.18		8.54	12.25
157.5	0.61		0.78	0.57	5.30			6.52	4.49	0.81	6.76	6.35		7.20	6.70	11.37		8.46	12.55
162.5	0.60	0.68	0.79	0.60	5.34	6.02	5.45	6.67	4.76	0.57	4.78	6.85	6.91	7.25	6.77	11.11	8.65	8.24	12.60
167.5	0.61		0.77	0.58	5.42			6.41	4.85	0.57	4.76	6.83		7.15	7.22	10.54		8.26	11.43
172.5	0.57		0.78	0.59	5.16			6.54	4.79	0.37	3.11	7.16		7.14	6.98	11.37		8.30	12.18
177.5	0.61		0.78	0.58	5.60			6.62	4.88	0.72	5.98	6.85		7.27	7.22	10.69		8.47	12.22
182.5	0.58		0.82	0.61	5.24			6.93	4.59	0.64	5.36	6.83		7.25	6.46	10.68		8.29	12.46
187.5	0.66		0.78	0.66	6.19			6.65	5.34	0.85	7.10	6.92		7.27	6.97	8.69		8.37	10.53
192.5	0.66		0.80	0.64	6.23			6.84	5.44	0.78	6.53	7.10		7.31	7.25	8.76		8.29	10.04
197.5	0.66		0.80	0.65	6.20			6.76	5.47	0.73	6.12	7.11		7.25	7.23	8.54		8.28	10.27
203.5	0.68	0.68	0.77	0.67	6.27	6.01	5.48	6.59	5.74	0.53	4.39	7.19	6.86	7.32	7.33	9.45	8.52	8.60	9.93
208.5	0.69		0.79	0.70	6.37			6.86	5.98	0.38	3.19	7.43		7.45	7.38	9.73		8.47	9.88
213.5	0.62		0.77	0.60	5.37			6.52	4.86	0.51	4.23	6.72		7.30	6.91	12.51		8.56	12.08

Appendix 1.1. continued

core depth (cm)	N (%) [1] MS-1	N (%) [2] MS-2	N (%) [3] MS-3	N (%) [4] MS-4	TC (%) [1] MS-1	TC (%) [2] MS-2	C_{org} (%) [5] MS-2	C_{org} (%) [3] MS-3	C_{org} (%) [4] MS-4	C_{inorg} (%) [6]	$CaCO_3$ (%) [7]	C_{org}/N (molar) [8] MS-1	C_{org}/N (molar) MS-2	C_{org}/N (molar) MS-3	C_{org}/N (molar) MS-4	$\delta^{15}N$ (‰) MS-1	$\delta^{15}N$ (‰) MS-2	$\delta^{15}N$ (‰) MS-3	$\delta^{15}N$ (‰) MS-4
218.5	0.67		0.76	0.66	6.24			6.60	5.69	0.56	4.63	7.24		7.40	7.37	9.40		8.59	10.00
223.5	0.56	0.64	0.75	0.60	4.92	5.68	5.56	6.36	4.80	0.12	0.98	7.32	7.40	7.31	6.87	12.69	8.56	8.78	13.09
228.5	0.66		0.74	0.67	6.13			6.34	5.78	0.35	2.93	7.56		7.40	7.38	9.64		8.49	10.32
233.5	0.68		0.77	0.70	6.33			6.70	6.14	0.19	1.58	7.78		7.47	7.46	9.25		8.63	10.23
238.5	0.61		0.77	0.63	5.51			6.55	5.22	0.30	2.49	7.29		7.34	7.13	11.46		8.58	12.02
243.5	0.56	0.67	0.80	0.64	4.88	5.90	6.28	6.82	5.26	-0.38		8.03	8.01	7.33	7.07	12.81	8.47	8.43	12.20
248.5	0.66		0.77	0.68	6.20			6.61	5.89	0.31	2.55	7.63		7.51	7.48	9.25		8.35	10.34
253.5	0.62		0.78	0.64	5.40			6.83	4.26	1.14	9.48	5.92		7.56	5.70	12.53		8.49	12.80
258.5	0.70		0.79	0.66	6.56			6.93	5.04	1.52	12.63	6.14		7.57	6.49	9.51		8.46	9.78
263.5	0.68	0.69	0.75	0.66	6.37	6.15	4.78	6.62	5.00	1.37	11.42	6.26	5.94	7.49	6.48	9.90	8.39	8.41	10.23
268.5	0.61		0.78	0.63	5.67			6.79	4.59	1.08	8.97	6.42		7.54	6.28	10.98		8.44	11.80
273.5	0.62		0.81	0.62	5.65			7.13	4.53	1.11	9.26	6.31		7.61	6.32	9.12		8.47	11.81
278.5	0.68		0.76	0.69	6.49			6.77	5.67	0.82	6.85	7.10		7.53	6.99	8.82		8.44	9.68
283.5		0.69	0.78	0.59	11.11	6.05		6.82	4.91	6.19				7.52	7.13	8.29	8.35	8.84	11.65
288.5	0.64		0.78	0.62	5.72			6.81	5.03	0.68	5.68	6.71		7.59	6.96	11.61		8.97	12.92
293.5	0.68		0.76	0.66	6.46			6.76	5.59	0.87	7.24	7.07		7.52	7.28	9.62		8.71	9.99
298.5	0.64		0.81	0.62	5.54			7.10	4.94	0.60	4.98	6.65		7.56	6.84	12.70		8.78	12.94
304.5	0.62	0.69	0.80	0.69	5.36	6.37	6.31	7.01	5.30	0.06	0.54	7.34	7.85	7.54	6.62	13.29	8.62	8.94	13.95
309.5	0.61		0.80	0.67	5.26			7.03	5.20	0.06	0.50	7.36		7.60	6.66	12.89		8.92	13.87
314.5	0.64		0.83	0.68	5.54			7.37	5.45	0.10	0.79	7.24		7.63	6.86	13.24		8.79	13.84
319.5	0.65		0.81	0.69	5.76			7.18	5.63	0.13	1.09	7.47		7.66	7.00	12.24		8.70	12.30
324.5	0.69	0.72	0.79	0.71	6.49	6.31	5.99	7.04	6.18	0.31	2.62	7.71	7.13	7.65	7.42	9.39	8.41	8.58	11.70
329.5	0.67		0.79	0.70	6.32			7.04	5.91	0.40	3.35	7.55		7.65	7.24	10.60		8.55	12.21
334.5	0.59		0.80	0.64	4.86			7.16	5.00	-0.13		7.23		7.76	6.66	14.83		8.45	14.77
339.5	0.68		0.75	0.70	6.41			6.81	5.99	0.42	3.47	7.51		7.77	7.32	11.07		8.67	12.15
344.5	0.67	0.70	0.77	0.68	6.40	6.59	6.23	6.95	6.04	0.36	2.98	7.72	7.60	7.73	7.60	9.51	8.52	8.60	11.16
349.5	0.69		0.79	0.71	6.57			7.08	6.30	0.27	2.25	7.81		7.68	7.62	9.45		8.57	11.10
354.5	0.70		0.77	0.66	6.35			6.91	5.83	0.51	4.28	7.16		7.76	7.56	9.59		8.67	11.38
359.5	0.67		0.78	0.66	6.23			7.10	6.05	0.18	1.49	7.72		7.67	7.83	10.44		8.52	10.40
364.5	0.62	0.72	0.81	0.58	5.31	6.61	6.23	7.29	4.93	0.38	3.18	6.84	7.46	7.76	7.23	12.69	8.45	8.62	12.63
369.5	0.67		0.76	0.65	6.45			6.90	5.92	0.53	4.40	7.56		7.76	7.85	9.15		8.47	10.63
374.5	0.56		0.76	0.62	4.78			6.87	5.33	-0.54		8.15		7.75	7.35	13.07		8.73	12.04
379.5	0.61		0.80	0.59	5.41			7.27	4.91	0.50	4.15	6.85		7.28	7.09	13.07		8.67	14.47
384.5	0.55	0.69	0.79	0.63	4.68	6.34	6.89	6.73	5.23	-0.55		8.15	8.61	7.59	7.09	14.06	8.46	9.93	13.64
389.5	0.67		0.76	0.64	6.36			6.76	5.95	0.41	3.40	7.58		7.66	7.97	9.86		8.95	11.20
394.5	0.64		0.76	0.65	5.42			6.76	5.27	0.15	1.26	7.10		7.70	6.96	13.96		8.94	13.68
399.5	0.72		0.76	0.66	6.88			6.87	6.04	0.84	6.99	7.19		7.57	7.87	9.44		8.61	11.06
402.5	0.68	0.68	0.79	0.69	6.55	6.38	5.99	6.96	6.16	0.39	3.25	7.75	7.51	7.64	7.68	9.75	8.62	8.75	11.31
407.5	0.68		0.77	0.71	6.53			6.87	6.23	0.30	2.53	7.87		7.59	7.52	9.51		8.73	11.82
412.5	0.67		0.77	0.68	6.59			6.78	6.21	0.38	3.21	7.90		7.59	7.84	8.95		8.67	9.56
417.5	0.66		0.79	0.68	5.97			7.03	5.73	0.24	1.96	7.47		7.59	7.20	12.84		8.79	12.97
422.5	0.64	0.67	0.78	0.64	5.83	6.39	5.82	6.91	5.26	0.57	4.74	7.03	7.40	7.56	6.98	11.66	8.27	8.69	13.64
427.5	0.68		0.78	0.64	6.55			6.89	5.36	1.19	9.94	6.75		7.54	7.20	9.52		8.70	11.29

Appendix 1.1. continued

core depth (cm)	N (%)[1] MS-1	N (%)[2] MS-2	N (%)[3] MS-3	N (%)[4] MS-4	TC (%)[1] MS-1	TC (%)[2] MS-2	C_{org} (%)[5] MS-2	C_{org} (%)[3] MS-3	C_{org} (%)[4] MS-4	C_{inorg} (%)[6]	$CaCO_3$ (%)[7]	C_{org}/N (molar)[8] MS-1	C_{org}/N (molar) MS-2	C_{org}/N (molar) MS-3	C_{org}/N (molar) MS-4	$\delta^{15}N$ (‰) MS-1	$\delta^{15}N$ (‰) MS-2	$\delta^{15}N$ (‰) MS-3	$\delta^{15}N$ (‰) MS-4
432.5	0.67		0.76	0.65	6.59			6.77	5.54	1.04	8.68	7.09		7.66	7.33	9.00		8.83	11.24
437.5	0.62		0.79	0.61	5.71			6.98	4.92	0.79	6.61	6.78		7.59	6.92	12.40		8.82	13.40
442.5	0.67		0.76	0.67	6.58			6.70	5.76	0.82	6.81	7.39		7.54	7.37	9.16		8.65	11.67
447.5	0.65		0.78	0.68	6.31			6.93	5.82	0.49	4.10	7.63		7.59	7.31	10.98		8.56	11.84
452.5	0.61		0.79	0.63	5.34			6.99	5.12	0.22	1.84	7.21		7.55	7.01	11.64		8.49	13.39
457.5	0.63		0.79	0.63	6.11			6.92	5.40	0.72	5.99	7.29		7.56	7.29	10.33		8.56	13.04
462.5	0.62	0.73	0.82	0.63	5.73	6.83	6.32	6.89	5.22	0.51	4.25	7.21	7.45	7.24	7.10	12.12	8.43	8.65	13.57
467.5	0.64		0.80	0.66	5.95			6.92	5.62	0.32	2.68	7.53		7.41	7.33	11.68		9.01	12.96
472.5	0.66		0.80	0.68	5.83			7.19	5.90	-0.06		7.65		7.66	7.47	12.66		8.64	12.42
477.5	0.68		0.82	0.68	6.43			7.21	5.96	0.47	3.91	7.48		7.58	7.48	11.28		9.07	13.00
482.5	0.66		0.81	0.69	6.27			7.19	5.86	0.42	3.46	7.56		7.60	7.25	10.70		8.97	13.55
487.5	0.71		0.82	0.72	6.95			7.34	6.48	0.47	3.89	7.87		7.71	7.73	9.28		8.70	11.77
492.5	0.96		0.80	0.73	8.39			7.09	6.01	2.38	19.81	5.35		7.59	7.05	13.03		8.99	13.55
496.0	0.72		0.83	0.77	6.05			7.51	5.87	0.18	1.49	6.96		7.71	6.53	14.82		8.30	13.88

MS-1: untreated sediment; MS-2: rinsing; MS-3: acidification plus rinsing; MS-4: in-situ acidification

[1] referring to the bulk sediment volume

[2] referring to the sediment volume remaining after rinsing

[3] referring to the sediment volume remaining after acidification plus rinsing

[4] referring to the bulk sediment volume because samples are decalcified after being weighed

[5] $[C_{org}]_{MS-2} = [TC]_{MS-2} - [C_{inorg}]$

[6] $[C_{inorg}] = [TC]_{MS-1} - [C_{org}]_{MS-4}$

[7] $[CaCO_3] = [C_{inorg}] \times 8.33$; according to the molar relationships in $CaCO_3$; cleansed of outliers and negative values

[8] C_{org} is taken from MS-4, N is taken from MS-1; both refer to the bulk sediment volume

Appendix 1.2.

core depth (cm)	N (%) in MS-1 (untreated)	MS-2 (rinsing)				MS-3 (acidification plus rinsing)				delta N lost (%) [1]
		sample weight (mg)	N (mg) in sample before treatment	N lost (mg)	N lost (%)	sample weight (mg)	N (mg) in sample before treatment	N lost (mg)	N lost (%)	
2.5	0.76	197.0	1.50	0.01	0.45	200.8	1.53	0.05	2.99	2.54
17.5	0.67	196.2	1.31	0.01	0.91	202.3	1.35	0.04	2.64	1.72
32.5	0.70	167.4	1.17	0.01	0.75	196.3	1.37	0.02	1.12	0.37
52.5	0.65	189.6	1.23	0.05	3.80	186.6	1.21	0.11	9.09	5.28
72.5	0.61	196.3	1.20	0.04	3.15	199.8	1.22	0.08	6.40	3.25
87.5	0.63	123.0	0.78	0.05	5.88	137.3	0.87	0.05	6.04	0.17
102.5	0.68	199.4	1.36	0.06	4.47	197.7	1.35	0.08	6.22	1.75
122.5	0.72	177.5	1.29	0.01	1.00	153.0	1.11	0.04	3.81	2.81
162.5	0.60	198.4	1.18	0.08	6.38	198.8	1.18	0.14	12.08	5.70
203.5	0.68	200.1	1.37	0.02	1.42	200.3	1.37	0.07	5.45	4.03
223.5	0.56	197.6	1.11	0.09	7.78	199.3	1.12	0.09	8.11	0.33
243.5	0.56	198.7	1.11	0.08	7.49	198.5	1.11	0.08	7.22	-0.27
263.5	0.68	186.5	1.28	0.02	1.71	121.4	0.83	0.07	7.83	6.13
283.5	1.93	198.4	3.83	0.06	1.45	197.0	3.80	0.05	1.35	-0.10
304.5	0.62	196.3	1.21	0.13	10.78	201.4	1.25	0.17	14.04	3.25
324.5	0.69	196.9	1.35	0.03	2.22	197.6	1.36	0.06	4.44	2.22
344.5	0.67	195.5	1.31	0.02	1.74	202.3	1.36	0.03	2.23	0.49
364.5	0.62	198.4	1.23	0.09	7.63	194.1	1.20	0.10	7.96	0.33
384.5	0.55	196.8	1.08	0.11	10.34	199.1	1.10	0.12	11.38	1.04
402.5	0.68	196.8	1.34	0.01	1.10	198.1	1.35	0.03	2.18	1.08
422.5	0.64	198.6	1.27	0.11	8.84	198.2	1.27	0.12	9.51	0.67
462.5	0.62	198.6	1.23	0.07	5.96	200.8	1.25	0.12	9.44	3.47

MS-1: untreated sediment; MS-2: rinsing; MS-3: acidification plus rinsing
[1] N lost (MS-3) - N lost (MS-2)

Appendix 2.1. (Fig. 2a)

	station-ID	longitude E (dez)	latitude S (dez)	sampling depth (m)	SST (°C)
AHAB 05	266210	13.50	22.04	4.0	17.29
17/03/2004	266220	13.75	22.04	4.0	18.07
to 05/04/2004	266230	14.00	22.04	4.0	15.50
	266250	14.25	22.21	4.0	15.37
	266260	14.00	22.21	3.0	16.68
	266270	13.75	22.21	4.0	17.81
	266300	13.75	22.37	2.0	17.35
	266310	14.00	22.37	3.0	17.16
	266360	14.25	22.54	3.0	15.09
	266370	14.00	22.54	4.0	15.77
	266380	13.75	22.54	5.0	17.09
	266390	13.50	22.54	5.0	16.48
	266450	13.83	22.75	4.0	15.09
	266470	14.17	22.75	2.0	14.52
	266480	13.75	23.25	3.0	15.04
	266500	14.00	23.25	4.0	14.77
	266520	14.33	23.25	3.0	13.79
	266550	14.42	22.75	3.0	14.37
	266590	14.17	23.50	4.0	14.22
	266600	13.75	23.50	4.0	15.58
	266630	14.38	23.50	3.0	13.68
	266640	13.75	24.00	3.0	15.44
	266650	14.17	24.00	4.0	14.13
	266660	14.38	24.00	3.0	13.48
	266680	14.17	24.50	3.0	14.12
	266690	14.50	24.50	3.0	13.58
	266700	14.00	25.00	3.0	14.97
	266710	14.42	25.00	4.0	13.91
	266720	14.67	25.00	3.0	13.37
	266750	14.75	25.50	3.0	12.64
Meteor Cruise	168	13.86	23.00	2.4	16.56
M57-3	178	14.27	23.76	2.8	16.63
15/03/2003	179	14.32	23.17	2.8	16.65
to 08/04/2003	180	14.41	22.88	2.2	17.48
	181	14.39	22.91	2.4	18.10
	182	14.08	23.17	4.2	17.20
	183	14.27	23.08	2.8	17.29
	184	14.37	23.00	1.2	17.56
	185	14.32	23.00	2.1	17.27
	186	14.22	23.00	4.2	17.41
	187	14.05	23.00	5.1	17.29
	188	13.87	23.00	1.5	16.89
	189	13.68	23.00	2.2	16.52
	190	13.50	23.00	8.3	16.52
	191	13.31	23.00	9.3	16.67
	192	13.15	23.00	9.9	16.73
	193	12.95	23.00	14.3	16.93
	194	12.78	23.00	6.0	17.49
	195	12.58	23.00	7.8	17.58
	196	12.33	23.00	8.2	18.08
	197	12.00	23.00	14.0	18.81
	198	13.72	21.76	4.2	16.11
	199	13.96	22.00	3.5	16.25
	200	14.48	22.85	3.1	16.00
	201	14.47	22.77	2.5	16.65
	202 [a]	14.30	22.64	4.3	16.10
	203	14.06	22.17	2.2	17.27
	204	14.16	22.19	6.4	17.65
	210	12.87	23.00	6.2	16.81
	211	13.75	23.50	2.0	16.72
	214	13.32	23.00	3.1	16.97
	220	13.00	23.00	9.1	18.64
	221	13.68	23.58	3.1	16.32

Appendix 2.2. (Figs. 2b, 4b, 6b, 7, 8, 9, 11, 12)

			Fig. 4b (all) Fig. 9 (see compilation in appendix 2.3.) Fig. 11 * (< 170 km distance to coast)	Fig. 2b Fig. 9 (see compilation in appendix 2.3.) Fig. 12 (see compilation in appendix 2.4.)	Fig. 6b Fig. 7, 8 (all) Fig. 11 * (< 170 km distance to coast) Fig. 12 (see compilation in appendix 2.4.)
longitude E (dez)	**latitude S (dez)**	**distance to coast (km)**	**TOC (%)**	**SST (°C) (UK'37)**	**δ¹⁵N$_{sediment}$ (‰)**
			M48-2 (05/08 to 23/08/2000); unpublished data	Emeis et al. (2009) and ref. therein	Emeis et al. (2009); Pichevin et al. (2005) and ref. therein
14.31	22.76	32	4.46*	15.4	8.86*
14.15	23.00	26	5.08*	15.0	8.71*
14.18	23.20	29	5.58*	15.3	8.45*
13.08	25.47	177	4.10	17.6	5.43
12.77	24.11	172	2.16	19.5	6.57
14.30	23.77	21	3.56*	15.7	9.02*
14.30	23.78	21	3.46*	15.1	9.04*
14.26	23.78	25	4.44*	15.2	7.97*
12.44	23.02	201	2.24	19.9	7.27
12.73	21.95	145	2.39*	18.8	6.12*
14.07	22.17	23	3.44*	17.0	9.32*
13.86	22.00	32	6.54*	16.1	8.77*
13.87	21.92	25	5.37*	15.8	8.46*
13.72	21.76	25	8.33*	15.9	7.68*
13.67	21.38	10	6.10*	16.2	5.83*
13.37	21.00	15	6.39*	16.6	8.41*
12.87	19.78	6	5.89*	16.5	8.39*
12.77	19.81	18	4.29*	16.4	7.66*
12.68	19.84	28	9.54*	16.9	5.66*
11.87	20.10	126	3.52*	18.8	4.84*
13.88	21.73	10	2.53*	16.5	11.36*
14.12	22.45	34	7.60*	16.6	7.76*
14.00	22.67	54	9.58*	15.5	7.58*
12.34	19.07	22	10.04*	16.8	6.68*
12.23	19.02	28	3.45*	16.5	8.27*
12.36	22.45	215	2.86	19.7	5.99
			POS 250 (06/04 to 28/04/1999); unpublished data		
14.48	22.87	6	7.64*	13.3	10.08*
14.45	22.82	9	5.36*	13.8	9.73*
14.29	22.64	24		15.4	10.13
14.05	22.42	41	0.42*	14.8	9.04*
13.94	22.68	60	0.42*	14.5	11.58*
13.75	23.03	67	5.09*	14.7	6.90*
13.53	23.17	94	5.44*	15.9	7.20*
13.40	23.18	108	3.39*	17.3	6.88*
13.18	23.22	132		18.4	6.69
13.01	23.24	149	3.18*	18.2	6.88*
12.81	23.25	170		17.9	7.05
13.03	25.51	184	4.78	17.4	7.38
13.37	25.50	149	15.38*	16.8	6.72*
13.56	25.52	132	9.61*	16.8	6.88*
14.71	25.50	15	19.24*	14.4	10.81*
14.58	25.07	29	19.24*	14.5	12.32*
14.38	24.44	23	19.24*	14.1	8.00*
14.29	24.22	22	18.06*	14.6	7.74*
14.27	23.76	23	12.85*	14.0	8.38*
14.23	23.43	21	12.85*	14.8	10.24*

Appendix 2.2. continued (Figs. 2b, 4b, 6b, 7, 8, 9, 11, 12)

longitude E (dez)	latitude S (dez)	distance to coast (km)	TOC (%)	SST (°C) (UK'37)	δ15Nsediment (‰)
			Mollenhauer et al. (2002)		
13.18	23.14	129	5.34*	15.7	6.46*
12.54	22.27	189	4.95	17.3	
13.08	25.47	178	6.35	17.0	
14.33	23.89	19	9.84	15.2	
12.20	22.36	229	2.75	17.4	
14.01	27.95	164	1.65		
13.46	26.79	164	4.74		
13.23	25.52	164	8.09		
13.08	25.47	176	6.05		
13.00	24.30	155	4.53		
12.60	22.72	198	3.74		
12.19	21.63	177	4.92		
11.83	21.09	179	4.9		
11.26	21.48	265	1.38		
11.40	20.66	202	4.21		
10.77	19.84	228	3.8		
11.06	18.96	148	4.53		
13.35	24.83	146	7.09		
13.16	24.90	165	5.6		
12.87	25.00	198	2.74		
12.67	25.07	221	1.99		
12.40	25.15	247	1.03		
12.02	25.25	281	0.63		
11.53	25.40	330	0.5		
12.37	23.32	217	2.05		
9.18	20.10	404		19.1	7.06
7.10	21.89	707		19.6	11.25
11.61	19.41	116		18.4	4.84
11.38	19.50	145		18.4	4.72
11.18	19.56	170		18.4	4.81
10.66	19.70	231		18.6	4.73
10.76	23.59	380		18.0	9.35
11.70	23.43	279		17.6	8.13
12.38	23.32	216		17.3	5.81
12.80	23.26	171		17.2	5.43
13.02	23.22	149		17.2	5.45
13.54	23.14	92		17.1	5.88
11.64	26.48	347		18.1	9.79
14.01	27.96	164		17.7	7.82
14.42	28.21	150		17.6	6.54
15.21	28.71	129			5.9
14.17	28.93	241			6.22
13.83	29.00	280			7.98
13.09	29.18	363			9.37
11.75	29.45	501			8.23
8.04	29.97	869			9.26
3.26	30.27	1327			10.46
2.41	29.84	1395			10.81
1.00	28.89	1540			11.64
6.03	22.91	871		19.9	11.81
5.03	21.60	902		20.3	11.78
13.50	22.04	73		17.0	6.56
14.00	22.04	21		16.0	8.67
14.25	22.21	7			6.35
14.00	22.21	33		16.0	7.35
13.75	22.21	59		17.0	6.68
14.00	22.37	44		16.0	
14.25	22.54	26		15.0	10.06

Appendix 2.2. continued (Figs. 2b, 4b, 6b, 7, 8, 9, 11, 12)

longitude E (dez)	latitude S (dez)	distance to coast (km)	TOC (%)	SST (°C) (UK'37)	$\delta^{15}N_{sediment}$ (‰)
14.00	22.54	51		16.0	7.42
13.75	22.54	77		14.8	7.44
13.50	22.54	103		16.7	5.57
13.83	22.75	71		14.6	6.21
13.75	23.25	75		15.4	6.01
14.00	23.25	49		14.9	6.77
14.33	23.25	16		15.3	8.03
14.42	22.75	10		15.8	9.23
14.17	23.50	30		14.0	7.64
13.75	23.50	72		16.1	6.04
14.38	23.50	8		14.8	7.77
13.75	24.00	71		16.7	4.83
14.17	24.00	28		14.4	
14.38	24.00	7		14.0	
14.17	24.50	44		13.8	5.39
14.50	24.50	11		14.7	6.46
14.42	25.00	41		13.9	7.29
14.67	25.00	17		14.3	6.59
14.75	25.50	11		15.0	7.10
14.17	23.00	24		14.5	8.41
14.00	23.00	41			5.64
14.32	22.96	9		14.1	
14.47	22.85	7		16.5	
14.47	22.77	6		15.1	
14.68	25.00	16		13.5	
14.42	23.92	9		14.2	
14.30	23.92	21		15.2	
14.21	23.92	30		14.8	
14.14	24.17	35		14.1	
14.27	24.09	19		14.6	
14.39	24.03	6		14.7	
14.34	25.16	51		13.8	
14.65	24.86	14		14.2	
14.42	24.92	38		12.4	
14.21	24.92	59		14.5	
14.47	23.67	3		14.1	
14.28	23.67	23		14.6	
14.22	23.67	29		14.4	
14.37	22.98	4		14.6	
14.27	23.17	19		14.8	
14.17	23.17	29		15.0	
13.90	23.29	61		14.8	
14.58	25.00	26		13.5	

Appendix 2.3. (Fig. 9)

longitude E (dez)	latitude S (dez)	distance to coast (km)	SST (°C) (UK'37)	TOC (%)
12.87	19.78	6	16.5	5.89
14.48	22.87	6	13.3	7.64
14.45	22.82	9	13.8	5.36
13.67	21.38	10	16.2	6.10
13.88	21.73	10	16.5	2.53
13.37	21.00	15	16.6	6.39
14.71	25.50	15	14.4	19.24
12.77	19.81	18	16.4	4.29
14.33	23.89	19	15.2	9.84
14.30	23.77	21	15.7	3.56
14.30	23.78	21	15.1	3.46
14.23	23.43	21	14.8	12.85
12.34	19.07	22	16.8	10.04
14.29	24.22	22	14.6	18.06
14.07	22.17	23	17.0	3.44
14.38	24.44	23	14.1	19.24
14.27	23.76	23	14.0	12.85
14.26	23.78	25	15.2	4.44
13.87	21.92	25	15.8	5.37
13.72	21.76	25	15.9	8.33
14.15	23.00	26	15.0	5.08
12.68	19.84	28	16.9	9.54
12.23	19.02	28	16.5	3.45
14.18	23.20	29	15.3	5.58
14.58	25.07	29	14.5	19.24
14.31	22.76	32	15.4	4.46
13.86	22.00	32	16.1	6.54
14.12	22.45	34	16.6	7.60
14.05	22.42	41	14.8	0.42
14.00	22.67	54	15.5	9.58
13.94	22.68	60	14.5	0.42
13.75	23.03	67	14.7	5.09
13.53	23.17	94	15.9	5.44
13.40	23.18	108	17.3	3.39
11.87	20.10	126	18.8	3.52
13.18	23.14	129	15.7	5.34
13.56	25.52	132	16.8	9.61
12.73	21.95	145	18.8	2.39
13.01	23.24	149	18.2	3.18
13.37	25.50	149	16.8	15.38
12.77	24.11	172	19.5	2.16
13.08	25.47	177	17.6	4.10
13.08	25.47	178	17.0	6.35
13.03	25.51	184	17.4	4.78
12.54	22.27	189	17.3	4.95
12.44	23.02	201	19.9	2.24
12.36	22.45	215	19.7	2.86
12.20	22.36	229	17.4	2.75

Appendix 2.4. (Fig. 12)

longitude E (dez)	latitude S (dez)	distance to coast (km)	SST (°C) (UK'37)	$\delta^{15}N_{sediment}$ (‰)
12.87	19.78	6	16.5	8.39
14.48	22.87	6	13.3	10.08
14.38	23.50	8	14.8	7.77
14.45	22.82	9	13.8	9.73
13.67	21.38	10	16.2	5.83
13.88	21.73	10	16.5	11.36
14.42	22.75	10	15.8	9.23
14.50	24.50	11	14.7	6.46
14.75	25.50	11	15.0	7.10
13.37	21.00	15	16.6	8.41
14.71	25.50	15	14.4	10.81
14.33	23.25	16	15.3	8.03
14.67	25.00	17	14.3	6.59
12.77	19.81	18	16.4	7.66
14.30	23.77	21	15.7	9.02
14.30	23.78	21	15.1	9.04
14.23	23.43	21	14.8	10.24
14.00	22.04	21	16.0	8.67
12.34	19.07	22	16.8	6.68
14.29	24.22	22	14.6	7.74
14.07	22.17	23	17.0	9.32
14.38	24.44	23	14.1	8.00
14.27	23.76	23	14.0	8.38
14.29	22.64	24	15.4	10.13
14.17	23.00	24	14.5	8.41
14.26	23.78	25	15.2	7.97
13.87	21.92	25	15.8	8.46
13.72	21.76	25	15.9	7.68
14.15	23.00	26	15.0	8.71
14.25	22.54	26	15.0	10.06
12.68	19.84	28	16.9	5.66
12.23	19.02	28	16.5	8.27
14.18	23.20	29	15.3	8.45
14.58	25.07	29	14.5	12.32
14.17	23.50	30	14.0	7.64
14.31	22.76	32	15.4	8.86
13.86	22.00	32	16.1	8.77
14.00	22.21	33	16.1	7.35
14.12	22.45	34	16.6	7.76
14.05	22.42	41	14.8	9.04
14.42	25.00	41	13.9	7.29
14.17	24.50	44	13.8	5.39
14.00	23.25	49	14.9	6.77
14.00	22.54	51	16.1	7.42
14.00	22.67	54	15.5	7.58
13.75	22.21	59	17.1	6.68
13.94	22.68	60	14.5	11.58
13.75	23.03	67	14.7	6.90
13.83	22.75	71	14.6	6.21
13.75	24.00	71	16.7	4.83
13.75	23.50	72	16.1	6.04
13.50	22.04	73	17.0	6.56
13.75	23.25	75	15.4	6.01
13.75	22.54	77	14.8	7.44
13.54	23.14	92	17.1	5.88
13.53	23.17	94	15.9	7.20
13.50	22.54	103	16.7	5.57
13.40	23.18	108	17.3	6.88
11.61	19.41	116	18.4	4.84
11.87	20.10	126	18.8	4.84
13.18	23.14	129	15.7	6.46
13.18	23.22	132	18.4	6.69
13.56	25.52	132	16.8	6.88
12.73	21.95	145	18.8	6.12
11.38	19.50	145	18.4	4.72
13.01	23.24	149	18.2	6.88
13.37	25.50	149	16.8	6.72

Appendix 2.4. continued (Fig. 12)

longitude E (dez)	latitude S (dez)	distance to coast (km)	SST (°C) (UK'37)	$\delta^{15}N_{sediment}$ (‰)
13.02	23.22	149	17.2	5.45
14.42	28.21	150	17.6	6.54
14.01	27.96	164	17.7	7.82
12.81	23.25	170	17.9	7.05
11.18	19.56	170	18.4	4.81
12.80	23.26	171	17.2	5.43
12.77	24.11	172	19.5	6.57
13.08	25.47	177	17.6	5.43
13.03	25.51	184	17.4	7.38
12.44	23.02	201	19.9	7.27
12.36	22.45	215	19.7	5.99
12.38	23.32	216	17.3	5.81
10.66	19.70	231	18.6	4.73
11.70	23.43	279	17.6	8.13
11.64	26.48	347	18.1	9.79
10.76	23.59	380	18.0	9.35
9.18	20.10	404	19.1	7.06
7.10	21.89	707	19.6	11.25
6.03	22.91	871	19.9	11.81
5.03	21.60	902	20.3	11.78

Appendix 2.5. (Figs. 4a, 5, 6a, 7)

	station-ID	longitude E (dez)	latitude S (dez)	distance to coast (km)	sampling depth (m)	Fig. 5 / Fig. 4a (all) PN (mg/l)	Fig. 4a (all) POC (mg/l)	Fig. 6a / Fig. 7 (all) $\delta^{15}N_{SPM}$ (‰)	C_{org}/N (molar)
AHAB 05	266210	13.50	22.04	73	5	0.07	0.65	3.22	10.36
17/03/2004	266220	13.75	22.04	47	4	0.11	0.74	3.96	7.69
to 05/04/2004	266230	14.00	22.04	21	4	0.17	1.02	7.45	7.06
	266250	14.25	22.21	7	3	0.12	0.96	11.59	9.04
	266260	14.00	22.21	33	4	0.18	1.14	5.37	7.51
	266270	13.75	22.21	59	4	0.10	0.58	2.82	7.12
	266300	13.75	22.37	70	3	0.10	0.58	2.63	6.95
	266360	14.25	22.54	26	4	0.18	1.29	4.74	8.13
	266370	14.00	22.54	51	4	0.13	0.75	3.45	6.88
	266380	13.75	22.54	77	5	0.11	0.69	2.22	7.08
	266390	13.50	22.54	103	3	0.08	0.44	3.18	6.69
	266450	13.83	22.75	71	3	0.04	0.27	4.96	8.16
	266470	14.17	22.75	36	5	0.06	0.44	4.53	7.95
	266480	13.75	23.25	75	4	0.13	1.05	5.87	9.18
	266500	14.00	23.25	49	3	0.14	0.92	5.92	7.81
	266520	14.33	23.25	16	3	0.12	0.74	15.03	7.36
	266550	14.42	22.75	10	4	0.07	0.47	13.93	7.97
	266590	14.17	23.50	30	4	0.13	0.76	9.08	6.86
	266600	13.75	23.50	72	4	0.07	0.46	5.89	7.67
	266630	14.38	23.50	8	2	0.08	0.49	16.12	6.99
	266640	13.75	24.00	71	3	0.06	0.45	7.27	8.73
	266650	14.17	24.00	28	4	0.11	0.72	7.78	7.87
	266660	14.38	24.00	7	3	0.05	0.33	11.61	7.71
	266680	14.17	24.50	44	3	0.07	0.57	7.48	10.08
	266690	14.50	24.50	11	3	0.10	0.67	13.41	7.80
	266700	14.00	25.00	84	4	0.03	0.22	5.63	8.24
	266710	14.42	25.00	41	4	0.11	0.76	7.16	8.06
	266720	14.67	25.00	17	3	0.16	0.97	9.87	7.12
	266750	14.75	25.50	11	4	0.11	0.71	8.94	7.42
	266920	14.33	23.00	7	5	0.14	1.39	11.07	11.38
	266930	14.17	23.00	24	3	0.14	1.66	9.38	13.62
	266940	14.00	23.00	41	4	0.19	1.38	6.95	8.46

Appendix 2.5. continued (Figs. 4a, 5, 6a, 7)

	station-ID	longitude E (dez)	latitude S (dez)	distance to coast (km)	sampling depth (m)	PN (mg/l)	POC (mg/l)	$\delta^{15}N_{SPM}$ (‰)	C_{org}/N (molar)
Meteor Cruise M57-3									
15/03/2003	164	14.37	23.00	4	0	0.13	0.99	6.53	9.00
to 08/04/2003	165	14.25	23.00	16	0	0.17	1.22	7.60	8.23
	166	14.22	23.00	19	0	0.06	0.42	1.85	8.38
	168	13.86	23.00	56	0	0.13	0.89	7.95	8.00
	169	13.68	23.00	75	0	0.08	0.55	5.47	8.53
	170	13.50	23.00	93	0	0.10	0.83	4.72	9.29
	171	13.32	23.00	111	0	0.08	0.66	5.16	9.69
	172	13.15	23.00	129	0	0.08	0.57	5.34	8.70
	173	12.95	23.00	149	0	0.06	0.36	4.90	7.38
	174	12.78	23.00	167	0	0.03	0.22	1.84	7.48
	176	12.33	23.00	213	0	0.03	0.28	2.53	10.67
	177	12.00	23.00	246	0	0.32	1.79	3.29	6.57
	178	14.27	23.76	23	2	0.16	0.97	7.82	7.16
	179	14.32	23.17	14	0	0.26	1.50	6.86	6.77
	180	14.41	22.88	13	0	0.34	2.43	7.55	8.42
	181	14.39	22.91	4	0	0.13	0.84	6.96	7.64
	182	14.08	23.17	38	0	0.27	1.91	4.82	8.25
	183	14.27	23.08	16	0	0.06	0.43	7.25	8.84
	195	12.58	23.00	187	0			4.58	
	198	13.72	21.76	43	0			4.01	
	199	13.86	22.00	32	0	0.14	0.84	0.75	7.13
	200	14.47	22.85	7	0	0.27	1.54	5.76	6.75
	201	14.47	22.77	6	0	0.11	0.72	7.05	7.9
	202	14.30	22.64	23	0	0.30	2.76	6.18	10.94
	203	14.06	22.17	24	0	0.25	2.00	9.35	9.63
	204	14.16	22.19	15	0	0.16	1.39	7.70	10.13
	209	14.05	23.00	37	0	0.16	0.16	5.66	8.26
	211	13.76	23.44	69	0	0.13	0.13	4.51	7.58
	220	12.00	23.00	246	30	0.01	0.01	4.28	8.07
	221	13.68	23.58	83	0	0.06	0.06	3.75	8.29

Appendix 2.6. (Fig. 3 [1])

	station-ID	longitude E (dez)	latitude S (dez)	sampling depth (m)	C_{org}/N (molar)	$\delta^{15}N_{SPM}$ (‰)	PN (mg/l)
AHAB 05 17/03/2004 to 05/04/2004	266250 (Fig. 3a)	14.25	22.21	3	9.04	11.59	0.12
				5	8.70	11.52	0.14
				10	8.69	9.10	0.09
				15	8.76	7.54	0.04
				20	8.48	6.66	0.03
				22	8.54	7.46	0.04
	266260 (Fig. 3b)	14.00	22.21	4	7.51	5.37	0.18
				10	7.83	5.78	0.17
				20	9.20	7.49	0.02
				30	9.25	7.24	0.03
				40	6.57	5.59	0.05
				50	7.00	3.84	0.03
				60	8.89	6.27	0.03
				70	19.95	8.10	0.02
				84	5.87	-5.38	0.03
	266270 (Fig. 3c)	13.75	22.21	4	7.12	2.82	0.10
				5	7.24	2.88	0.09
				10	7.04	3.29	0.10
				20	8.47	3.73	0.05
				50	7.96	6.32	0.03
				70	8.74	6.51	0.02
				78	10.94	5.58	0.01
				100	10.97	7.12	0.02
				116	10.84	5.87	0.01
	266550 (Fig. 3d)	14.42	22.75	4	7.97	13.93	0.07
				10	7.91	12.75	0.07
				20	7.95	11.95	0.06
				30	9.39	7.05	0.03
				45	8.12	8.10	0.05
	266470 (Fig. 3e)	14.17	22.75	5	7.95	4.53	0.06
				10	8.01	4.40	0.07
				20	9.63	5.76	0.04
				30	11.63	6.67	0.02
				40	8.24	6.44	0.03
				60	10.82	8.22	0.02
				80	12.23	7.82	0.02
				100	11.93	8.37	0.01
	266450 (Fig. 3f)	13.83	22.75	3	8.16	4.96	0.04
				10	8.12	4.87	0.05
				20	8.66	5.10	0.05
				30	8.80	6.18	0.05
				40	9.04	7.10	0.02
				50	8.42	7.84	0.03
				80	9.07	8.18	0.03
				100	9.20	7.46	0.02
				125	8.63	7.25	0.03
Meteor Cruise M57-3 15/03/2003 to 08/04/2003	205 (Fig. 3g)	14.39	22.91	0	7.65	8.24	0.12
				10	8.12	7.63	0.05
				20	8.69	8.53	0.03
				30	8.81	9.19	0.04
				40	9.72	10.27	0.03
				50	9.89	9.22	0.05
				57	9.48	8.35	0.05
				57	9.91	10.05	0.05
	212 (Fig. 3h)	13.68	23.00	5	7.52	4.86	0.12
				5	7.57	4.60	0.12
				10	7.61	3.88	0.13
				10	7.28	4.72	0.15
				30	6.02	6.89	0.04
				45	7.95	8.23	0.02
				60	6.14	2.74	0.01
				120	8.61	7.20	0.02
				149	9.48	9.18	0.01
	220 (Fig. 3i)	12.00	23.00	30	8.07	4.28	0.01
				70	10.44	8.63	0.01
				200	8.97	8.01	0.01
				300	7.54	6.80	0.01
				400	10.72	19.53	0.01
				800	9.27	9.04	0.01
				1200	7.33	10.37	0.01
				1600	10.48	8.13	0.01
				2000	7.31	9.00	0.01
				2690	9.09	6.19	0.01

[1] Table shows only SPM-data (Fig. 3 left charts). The CTD-data are too many to be printed. They are available digitally including the data of all water column profiles shown in Fig. 1.

Appendix 2.7. (Fig. 10)

latitude S (dez) [1]	longitude E (dez) [1]	distance to coast (km) [2]	$\delta^{15}N_{sediment}$ (‰)	$\delta^{15}N_{SPM}$ (‰)	$\Delta\delta^{15}N$ (‰)
22.87 / 22.88	14.48 / 14.41	**6** / 13	10.08	7.55	2.53
22.21	14.25	7	6.35	11.59	-5.24
23.50	14.38	8	7.77	16.12	-8.35
22.75	14.42	10	9.23	13.93	-4.70
24.50	14.50	11	6.46	13.41	-6.95
25.50	14.75	11	7.10	8.94	-1.84
23.25	14.33	16	8.03	15.03	-7.00
22.04	14.00	21	8.67	7.45	1.22
22.00	14.17	24	8.41	9.38	-0.97
22.64	14.30	**24** / 23	10.13	6.18	3.95
21.92 / 22.00	13.87 / 13.86	**25** / 32	8.46	0.75	7.71
22.54	14.25	26	10.06	4.74	5.32
23.50	14.17	30	7.64	9.08	-1.44
22.21	14.00	33	7.35	5.37	1.98
25.00	14.42	41	7.29	7.16	0.13
22.00	14.00	41	5.64	6.95	-1.31
23.25	14.00	49	6.77	5.92	0.85
22.54	14.00	51	7.42	3.45	3.97
22.21	13.75	59	6.68	2.82	3.86
23.03 / 23.00	13.75 / 13.68	**67** / 74	6.90	4.6	2.30
22.75	13.83	71	6.21	4.96	1.25
23.00	13.75	71	4.83	7.27	-2.44
23.50	13.75	72	6.04	5.89	0.15
22.04	13.50	73	6.56	3.22	3.34
23.25	13.75	75	6.01	5.87	0.14
22.54	13.75	77	7.44	2.22	5.22
23.14 / 23.00	13.54 / 13.68	**92** / 75	5.88	5.47	0.41
23.17 / 23.00	13.53 / 13.50	**94** / 93	7.20	4.72	2.48
22.54	13.50	103	5.57	3.18	2.39

[1] Not all $\delta^{15}N_{sediment}$- and surface ocean $\delta^{15}N_{SPM}$-values building a data pair derive from the exactly same location. In this case, the first figure refers to the sediment, the second figure to SPM.
[2] In the figure, the distance of the sediment samples are used (shown bold).

Appendix 3.1.

Core 226620				
core depth (cm)	cal age (BP) [1]	SR (cm/a)	dry bulk density (g/cm³)	AR_{bulk} (mg/cm²/a) [2]
0	**860**	0.05		
1	879	0.05	0.16	8.0
2	899	0.05	0.20	10.3
3	918	0.05	0.20	10.2
4	938	0.05	0.19	9.9
5	957	0.05	0.20	10.5
6	977	0.05	0.21	11.0
7	996	0.05	0.22	11.4
8	1016	0.05	0.22	11.1
9	1035	0.05	0.21	10.8
10	1055	0.05	0.22	11.2
11	1074	0.05	0.22	11.4
12	1093	0.05	0.22	11.4
13	1113	0.05	0.22	11.4
14	1132	0.05	0.22	11.3
15	1152	0.05	0.22	11.5
16	1171	0.05	0.22	11.4
17	1191	0.05	0.21	11.0
18	1210	0.05	0.22	11.1
19	1230	0.05	0.21	10.8
20	1249	0.05	0.22	11.5
21	1269	0.05	0.22	11.4
22	1288	0.05	0.22	11.3
23	1307	0.05	0.22	11.1
24	1327	0.05	0.22	11.1
25	1346	0.05	0.22	11.3
26	1366	0.05	0.22	11.3
27	1385	0.05	0.23	11.7
28	1405	0.05	0.22	11.5
29	1424	0.05	0.22	11.5
30	1444	0.05	0.22	11.2
31	1463	0.05	0.25	12.7
32	1482	0.05	0.22	11.4
33	1502	0.05	0.22	11.6
34	1521	0.05	0.23	11.7
35	1541	0.05	0.22	11.5
36	1560	0.05	0.22	11.2
37	1580	0.05	0.22	11.1
38	1599	0.05	0.23	11.6
39	1619	0.05	0.22	11.4
40	1638	0.05	0.22	11.3
41	1658	0.05	0.21	10.9
42	1677	0.05	0.22	11.2
43	1696	0.05	0.23	11.7
44	1716	0.05	0.22	11.1
45	1735	0.05	0.22	11.1
46	1755	0.05	0.24	12.1
47	1774	0.05	0.23	11.6
48	1794	0.05	0.21	11.0
49	1813	0.05	0.21	11.0
50	1833	0.05	0.21	11.0
51	1852	0.05	0.22	11.1
52	1872	0.05	0.21	11.0
53	1891	0.05	0.23	11.6
54	1910	0.05	0.22	11.4
55	1930	0.05	0.23	11.6
56	1949	0.05	0.23	11.8
57	1969	0.05	0.21	11.0
58	1988	0.05	0.21	10.9
59	2008	0.05	0.21	10.8
60	2027	0.05	0.23	11.6
61	2047	0.05	0.23	11.9
62	2066	0.05	0.24	12.4
63	2085	0.05	0.24	12.2
64	2105	0.05	0.23	12.0
65	2124	0.05	0.24	12.1
66	2144	0.05	0.24	12.1
67	2163	0.05	0.23	11.9
68	2183	0.05	0.22	11.2
69	2202	0.05	0.24	12.4
70	2222	0.05	0.23	12.0
71	2241	0.05	0.23	11.7
72	2261	0.05	0.23	11.9
73	2280	0.05	0.23	11.9
74	2299	0.05	0.23	12.1
75	2319	0.05	0.23	11.9
76	2338	0.05	0.24	12.5
77	2358	0.05	0.23	12.1
78	2377	0.05	0.24	12.5

Appendix 3.1. continued

core depth (cm)	cal age (BP) [1]	SR (cm/a)	dry bulk density (g/cm³)	AR$_{bulk}$ (mg/cm²/a) [2]
79	2397	0.05	0.25	12.7
80	2416	0.05	0.24	12.1
81	2436	0.05	0.24	12.5
82	2455	0.05	0.24	12.4
83	2475	0.05	0.23	12.0
84	2494	0.05	0.23	11.7
85	2513	0.05	0.23	11.9
86	2533	0.05	0.24	12.2
87	2552	0.05	0.23	11.8
88	2572	0.05	0.23	11.7
89	2591	0.05	0.23	11.8
90	2611	0.05	0.23	12.0
91	2630	0.05	0.24	12.4
92	2650	0.05	0.24	12.6
93	2669	0.05	0.24	12.5
94	2689	0.05	0.24	12.1
95	2708	0.05	0.24	12.5
96	2727	0.05	0.23	12.1
97	2747	0.05	0.21	11.0
98	2766	0.05	0.20	10.3
99	2786	0.05		
100	2805	0.05	—	—
101	2825	0.05	0.18	9.2
102	2844	0.05	0.25	12.7
103	2864	0.05	0.23	11.8
104	2883	0.05	0.20	10.5
105	2902	0.05	0.20	10.3
106	2922	0.05	0.22	11.2
107	2941	0.05	0.22	11.1
108	2961	0.05	0.21	10.7
109	2980	0.05	0.21	10.8
110	3000	0.05	0.22	11.1
111	3019	0.05	0.21	10.6
112	3039	0.05	0.21	10.8
113	3058	0.05	0.21	10.9
114	3078	0.05	0.21	11.0
115	3097	0.05	0.23	11.6
116	3116	0.05	0.22	11.4
117	3136	0.05	0.23	11.6
118	3155	0.05	0.22	11.5
119	3175	0.05	0.23	11.7
120	3194	0.05	0.23	12.0
121	3214	0.05	0.21	10.7
122	3233	0.05	0.21	10.7
123	3253	0.05	0.20	10.2
124	3272	0.05	0.22	11.4
125	3292	0.05	0.21	10.5
126	**3311**	0.09	0.22	20.4
127	3322	0.09	0.22	20.7
128	3332	0.09	0.23	21.7
129	3343	0.09	0.23	21.1
130	3354	0.09	0.22	20.3
131	3365	0.09	0.22	20.7
132	3375	0.09	0.21	19.8
133	3386	0.09	0.22	20.6
134	3397	0.09	0.21	19.8
135	3407	0.09	0.23	21.3
136	3418	0.09	0.22	20.1
137	3429	0.09	0.22	20.2
138	3440	0.09	0.21	19.5
139	3450	0.09	0.20	18.3
140	3461	0.09	0.19	17.9
141	3472	0.09	0.19	18.0
142	3482	0.09	0.20	18.3
143	3493	0.09	0.20	18.3
144	3504	0.09	0.20	18.6
145	3515	0.09	0.20	18.9
146	3525	0.09	0.20	18.3
147	3536	0.09	0.22	20.1
148	3547	0.09	0.21	19.6
149	3558	0.09	0.21	19.9
150	3568	0.09	0.21	19.4
151	3579	0.09	0.20	18.9
152	3590	0.09	0.22	20.2
153	3600	0.09	0.21	19.8
154	3611	0.09	0.20	18.9
155	3622	0.09	0.20	18.7
156	3633	0.09	0.21	19.1
157	3643	0.09	0.20	18.3
158	3654	0.09	0.20	18.9
159	3665	0.09	0.20	18.7

Appendix 3.1. continued

core depth (cm)	cal age (BP) [1]	SR (cm/a)	dry bulk density (g/cm³)	AR$_{bulk}$ (mg/cm²/a) [2]
160	3675	0.09	0.22	20.5
161	3686	0.09	0.22	20.6
162	3697	0.09	0.22	20.9
163	3708	0.09	0.22	20.8
164	3718	0.09	0.22	20.8
165	**3729**	0.09	0.23	20.0
166	3740	0.09	0.25	22.4
167	3752	0.09	0.23	20.7
168	3763	0.09	0.21	18.7
169	3774	0.09	0.22	19.5
170	3785	0.09	0.22	19.6
171	3797	0.09	0.23	20.1
172	3808	0.09	0.22	19.9
173	3819	0.09	0.23	20.5
174	3830	0.09	0.25	22.0
175	3842	0.09	0.23	20.4
176	3853	0.09	0.21	19.0
177	3864	0.09	0.24	21.0
178	3876	0.09	0.24	21.0
179	3887	0.09	0.23	20.6
180	3898	0.09	0.22	19.2
181	3909	0.09	0.22	19.9
182	3921	0.09	0.21	18.4
183	3932	0.09	0.21	18.6
184	3943	0.09	0.23	20.6
185	3955	0.09	0.22	19.4
186	3966	0.09	0.21	19.0
187	3977	0.09	0.22	19.4
188	3988	0.09	0.22	19.9
189	4000	0.09	0.21	18.5
190	4011	0.09	0.21	18.7
191	4022	0.09	0.21	18.7
192	4033	0.09	0.21	19.0
193	4045	0.09	0.20	17.8
194	4056	0.09	0.22	19.1
195	4067	0.09	0.20	18.1
196	4079	0.09	0.26	23.0
197	4090	0.09	0.26	22.6
198	4101	0.09	0.22	19.8
199	4112	0.09		
200	4124	0.09		
201	4135	0.09		
202	4146	0.09	0.24	21.4
203	4158	0.09	0.24	21.0
204	4169	0.09	0.20	18.1
205	4180	0.09	0.19	17.0
206	4191	0.09	0.21	18.8
206.5	**4197**	0.12		
207	4201	0.12	0.23	28.4
208	4209	0.12	0.24	29.7
209	4217	0.12	0.35	43.1
210	4225	0.12	0.49	59.7
211	4234	0.12	0.49	60.5
212	4242	0.12	0.50	60.9
213	4250	0.12	0.51	62.7
214	4258	0.12	0.55	67.7
215	4266	0.12	0.61	75.4
216	4274	0.12	0.65	79.9
217	4282	0.12	0.66	80.9
218	4291	0.12	0.69	84.3
219	4299	0.12	0.69	84.8
220	4307	0.12	0.28	34.7
221	4315	0.12	0.23	28.6
222	4323	0.12	0.24	29.2
223	4331	0.12	0.23	28.4
224	4339	0.12	0.22	26.8
225	4348	0.12	0.23	28.4
226	4356	0.12	0.22	26.9
227	4364	0.12	0.22	27.4
228	4372	0.12	0.22	27.4
229	4380	0.12	0.22	27.6
230	4388	0.12	0.21	26.1
231	4396	0.12	0.22	27.6
232	4405	0.12	0.23	28.1
233	4413	0.12	0.24	29.5
234	4421	0.12	0.23	28.5
235	4429	0.12	0.32	38.9
236	4437	0.12	0.50	61.3
237	4445	0.12	0.51	62.2
238	4453	0.12	0.33	40.1
239	4462	0.12	0.20	25.1

Appendix 3.1. continued

core depth (cm)	cal age (BP) [1]	SR (cm/a)	dry bulk density (g/cm³)	AR$_{bulk}$ (mg/cm²/a) [2]
240	4470	0.12	0.20	24.8
241	4478	0.12	0.21	25.6
242	4486	0.12	0.21	25.7
243	4494	0.12	0.21	25.3
244	4502	0.12	0.21	26.1
245	4510	0.12	0.21	26.3
246	4519	0.12	0.23	28.0
247	4527	0.12	0.22	26.7
248	4535	0.12	0.22	26.7
249	4543	0.12	0.21	26.1
250	4551	0.12	0.21	25.8
251	4559	0.12	0.22	26.6
252	4567	0.12	0.22	27.4
253	4576	0.12	0.23	28.8
254	4584	0.12	0.23	27.9
255	4592	0.12	0.22	27.2
256	4600	0.12	0.24	29.2
257	4608	0.12	0.24	28.9
258	4616	0.12	0.22	27.2
259	4624	0.12	0.21	26.3
260	4633	0.12	0.22	27.2
261	4641	0.12	0.24	29.4
262	4649	0.12	0.24	29.3
263	4657	0.12	0.22	26.7
264	4665	0.12	0.23	27.7
265	4673	0.12	0.21	26.0
266	4681	0.12	0.22	27.4
267	4690	0.12	0.23	27.8
268	4698	0.12	0.22	26.9
269	4706	0.12	0.22	27.3
270	4714	0.12	0.22	27.3
271	4722	0.12	0.22	27.1
272	4730	0.12	0.23	28.1
273	4738	0.12	0.24	29.5
274	4747	0.12	0.24	29.6
275	4755	0.12	0.23	28.8
276	4763	0.12	0.22	27.4
277	4771	0.12	0.23	27.7
278	4779	0.12	0.25	30.8
279	4787	0.12	0.25	30.7
280	4795	0.12	0.23	28.6
281	4804	0.12	0.23	27.7
282	4812	0.12	0.25	30.7
283	4820	0.12	0.23	28.7
284	4828	0.12	0.23	27.8
285	4836	0.12	0.23	28.3
286	4844	0.12	0.23	28.5
287	4852	0.12	0.23	28.8
288	4861	0.12	0.23	28.0
289	4869	0.12	0.23	28.4
290	4877	0.12	0.23	27.8
291	4885	0.12	0.23	27.7
292	4893	0.12	0.26	31.7
293	4901	0.12	0.25	31.2
294	4909	0.12	0.26	32.2
295	4918	0.12	0.25	30.2
296	4926	0.12	0.21	26.0
297	4934	0.12	0.24	29.2
298	4942	0.12	0.25	30.5
299	4950	0.12	0.25	30.3
300	4958	0.12		
301	4966	0.12		
302	4975	0.12	0.26	31.5
303	4983	0.12	0.23	28.0
304	4991	0.12	0.23	27.6
305	4999	0.12	0.16	19.2
306	5007	0.12	0.16	19.9
307	5015	0.12	0.15	19.0
308	5023	0.12	0.19	23.1
309	5032	0.12	0.18	21.7
310	5040	0.12	0.21	25.6
311	5048	0.12	0.24	29.4
312	**5056**	0.12	0.24	29.1

---

[1] Bold figures denote age control points.
[2] AR$_{bulk}$ = SR × dry bulk density × 1000

Appendix 3.2.

Core 226620

core depth (cm)	cal age (BP)	TOC (%) [1]	AR$_{TOC}$ (mg/cm²/a) [2]
1	879	5.41	0.43
5	957	5.08	0.53
9	1035	4.84	0.52
13	1113	4.57	0.52
17	1191	4.08	0.45
21	1269	3.59	0.41
25	1346	3.43	0.39
29	1424	4.71	0.54
31	1463	5.95	0.75
33	1502	5.47	0.63
37	1580	5.55	0.62
41	1658	4.63	0.50
45	1735	4.61	0.51
49	1813	4.75	0.52
53	1891	4.65	0.54
57	1969	5.87	0.65
59	2008	5.42	0.58
61	2047	5.58	0.67
65	2124	3.32	0.40
73	2280	4.31	0.51
81	2436	4.21	0.53
85	2513	4.45	0.53
89	2591	4.85	0.57
93	2669	4.78	0.60
97	2747	5.43	0.60
105	2902	3.22	0.33
109	2980	2.66	0.29
111	3019	3.40	0.36
113	3058	3.50	0.38
117	3136	2.57	0.30
123	3253	3.67	0.37
125	3292	3.51	0.37
133	3386	3.54	0.73
137	3429	3.81	0.77
141	3472	3.32	0.60
145	3515	3.30	0.62
149	3558	3.28	0.65
153	3600	3.99	0.79
157	3643	3.32	0.61
161	3686	3.76	0.77
165	3729	4.98	1.00
169	3774	3.96	0.77
173	3819	3.82	0.78
177	3864	4.86	1.02
181	3909	3.87	0.77
185	3955	3.52	0.68
189	4000	4.90	0.90
193	4045	4.60	0.82
195	4067	5.08	0.92
197	4090	4.15	0.94
205	4180	3.81	0.65
209	4217	3.48	1.50
213	4250	2.87	1.80
217	4282	2.36	1.91
221	4315	5.16	1.48
225	4348	4.65	1.32
230	4388	4.19	1.10
235	4429	4.52	1.76
237	4445	2.00	1.24
240	4470	4.05	1.00
245	4510	3.66	0.96
249	4543	4.92	1.29
253	4576	3.20	0.92
257	4608	3.56	1.03
265	4673	3.60	0.94
269	4706	3.52	0.96
273	4738	4.21	1.24
277	4771	4.88	1.35
281	4804	4.60	1.27
289	4869	4.57	1.30
293	4901	5.18	1.62
297	4934	5.43	1.59
305	4999	4.99	0.96
309	5032	4.38	0.95

[1] Derives from in-situ acidified sediment.

[2] AR$_{TOC}$ = (AR$_{bulk}$ / 100) × TOC

Appendix 3.3.

Core 226620			
core depth (cm)	cal age (BP)	δ^{15}N (‰) [1]	δ^{13}C$_{org}$ (‰) [1]
5	957	7.75	-19.65
10	1055	7.56	-19.42
15	1152	7.34	-19.81
20	1249	7.55	-18.83
25	1346	6.70	-19.33
30	1444	7.29	-19.45
35	1541	7.24	-19.40
40	1638	7.60	-19.63
45	1735	7.37	-19.56
50	1833	7.95	-19.79
55	1930	7.44	-20.13
60	2027	7.43	-19.49
65	2124	7.48	-19.34
70	2222	7.33	-19.69
75	2319	6.88	-25.67
80	2416	7.28	-19.42
85	2513	7.35	-19.47
90	2611	7.46	-19.30
95	2708	7.34	-20.06
100	2805	6.53	-20.89
105	2902	6.55	-19.39
110	3000	6.84	-19.90
115	3097	7.67	-19.88
120	3194	7.81	-20.51
125	3292	7.65	-19.99
130	3354	7.70	-19.86
135	3407	7.19	-19.67
140	3461	7.24	-20.00
145	3515	7.74	-20.21
150	3568	9.12	-19.70
155	3622	7.24	-20.32
160	3675	7.85	-20.58
165	3729	7.00	-20.33
170	3785	7.17	-20.93
175	3842	7.05	-20.49
180	3898	7.64	-18.17
185	3955	8.26	-17.56
190	4011	7.65	-20.26
195	4067	7.68	-20.11
200	4124	7.01	-19.70
205	4180	7.33	-20.53
210	4225	6.91	-20.56
215	4266	7.12	-20.70
220	4307	6.45	-20.43
225	4348	5.52	-20.36
230	4388	6.86	-20.79
235	4429	6.96	-20.46
240	4470	7.09	-20.61
245	4510	7.38	-20.44
250	4551	6.59	-20.00
255	4592	6.70	-20.00
260	4633	4.78	-19.81
265	4673	5.58	-19.58
270	4714	5.65	-19.52
275	4755	5.64	-19.40
280	4795	5.55	-19.44
285	4836	5.41	-19.57
290	4877	5.37	-19.49
295	4918	4.90	-19.40
300	4958	5.25	-19.33
305	4999	5.07	-19.44
310	5040	5.07	-19.01
315	5080	6.55	-19.97
320	5121	7.11	-19.85
325	5162	5.83	-20.63
330	5203	6.75	-20.60
335	5243	7.32	-20.35
340	5284	5.97	-20.82
345	5325	6.78	-20.43
350	5365	5.94	-21.03
355	5406	6.86	-20.16
360	5447	7.52	-20.79
365	5488	6.51	-20.03
370	5528	6.68	-20.98

[1] Sediment acidified and rinsed prior to measurement.

Appendix 3.4.

Core 226620

core depth (cm)	cal age (BP)	SST (°C) (UK'37)	core depth (cm)	cal age (BP)	$\delta^{18}O_{calcite}$	$T_{\delta 18O}$ (°C) [1]
		Emeis et al. (2009)				
2	899	16.5	1	879	1.12	10.1
6	977	16.2	8	1016	0.48	13.1
12	1093	16.3	14	1132	0.85	11.4
16	1171	16.3	20	1249	0.31	14.0
22	1288	16.4	26	1366	0.69	12.1
28	1405	16.3	33	1502	0.86	11.3
33	1502	16.4	38	1599	0.54	12.9
39	1619	16.2	44	1716	0.77	11.8
44	1716	16.2	58	1988	0.48	13.2
47	1774	16.3	64	2105	0.81	11.6
56	1949	16.4	69	2202	0.55	12.8
62	2066	16.1	75	2319	0.84	11.4
66	2144	15.9	82	2455	0.78	11.7
70	2222	14.5	88	2572	0.84	11.4
75	2319	14.5	93	2669	0.69	12.1
80	2416	14.4	105	2902	0.78	11.7
85	2513	14.5	111	3019	0.64	12.4
90	2611	14.6	117	3136	0.77	11.8
95	2708	14.1	123	3253	0.97	10.8
100	2805	15.2	129	3343	0.84	11.4
105	2902	14.3	135	3407	1.16	9.9
110	3000	15.1	141	3472	0.91	11.1
115	3097	15.1	147	3536	0.91	11.1
120	3194	15.1	153	3600	1.18	9.8
125	3292	15.6	159	3665	1.02	10.6
130	3354	15.7	168	3763	0.87	11.2
135	3407	15.3	173	3819	1.54	8.0
140	3461	14.9	179	3887	0.97	10.8
145	3515	14.6	191	4022	0.68	12.2
150	3568	15.9	197	4090	0.85	11.4
155	3622	14.6	208	4209	0.67	12.2
160	3675	15.9	214	4258	-0.01	15.5
165	3729	15.6	290	4877	-0.19	16.4
170	3785	15.1				
175	3842	15.3				
180	3898	16.0				
185	3955	15.4				
190	4011	15.5				
195	4067	15.3				
200	4124	15.1				
205	4180	15.1				
220	4307	15.5				
225	4348	15.8				
230	4388	15.8				
235	4429	16.3				
240	4470	15.8				
245	4510	15.8				
250	4551	16.1				
255	4592	16.2				
260	4633	15.9				
265	4673	15.5				
270	4714	15.7				
275	4755	16.1				
280	4795	15.5				
285	4836	15.9				
290	4877	15.3				
295	4918	16.1				
300	4958	15.9				
305	4999	16.2				
310	5040	16.3				
315	5080	16.7				
320	5121	16.8				
325	5162	17.1				
330	5203	18.4				
335	5243	18.1				
340	5284	18.5				
345	5325	18.7				
350	5365	19.5				
355	5406	19.0				
360	5447	18.6				
365	5488	18.4				
370	5528	18.0				
375	5569	19.1				
380	5610	19.6				

[1] $T_{\delta 18O} = 16.5 - 4.8 \times (\delta^{18}O_{calcite} + 0.22)$

Appendix 3.5.

NAM1

core depth (cm)	cal age (BP) [1]	SR (cm/a)	dry bulk density (g/cm³)	AR_{bulk} (mg/cm²/a) [2]	TOC (%) [3] Struck et al. (2002)	AR_{TOC} (mg/cm²/a) [4]	$\delta^{15}N$ (‰) [3] Struck et al. (2002)	$\delta^{13}C_{org}$ (‰) [3] Struck et al. (2002)
0.5	62		0.26		6.70		8.69	-18.39
1.5	67		0.18		8.24		8.44	-19.99
2.5	73		0.15		8.54		8.52	-20.15
4.5	84		0.14		8.93		8.62	-19.76
5.5	90		0.16		8.64		8.50	
6.5	95		0.15		8.49		8.73	-20.18
7.5	**101**	0.18	0.17	30.2	8.54	2.58	8.69	-20.88
8.5	107	0.18	0.18	31.5	9.54	3.00	8.36	-19.66
9.5	112	0.18	0.17	30.1	7.30	2.19	8.30	-18.94
10.5	118	0.18	0.16	28.3	9.05	2.56	7.65	-18.91
11.5	123	0.18	0.16	28.6	5.84	1.67	6.36	-18.59
12.5	129	0.18	0.17	30.1	7.10	2.13	6.26	-18.75
13.5	135	0.18	0.15	27.4	5.62	1.54	6.78	-18.66
14.5	140	0.18	0.16	28.6	6.63	1.90	6.02	-18.53
15.5	146	0.18	0.15	27.4	5.32	1.46	7.10	-18.95
16.5	151	0.18	0.16	28.8	5.80	1.67	6.28	-18.82
17.5	157	0.18	0.14	25.4	5.01	1.27	7.51	-18.74
18.5	163	0.18	0.16	29.2	5.76	1.68	6.86	-18.79
19.5	168	0.18	0.15	27.2	5.69	1.55	6.88	-19.14
20.5	174	0.18	0.13	23.8	4.96	1.18	7.14	-18.66
21.5	179	0.18	0.14	24.9	5.54	1.38	7.03	-18.56
22.5	185	0.18	0.15	25.9	5.55	1.44	7.18	-18.86
23.5	191	0.18	0.15	27.2	5.62	1.53	6.97	-18.97
24.5	196	0.18	0.15	26.3	6.29	1.65	6.39	-19.14
25.5	202	0.18	0.15	26.5	5.10	1.35	6.70	-18.89
26.5	207	0.18	0.16	28.1	6.21	1.74	6.80	-18.56
27.5	213	0.18	0.15	27.4	5.91	1.62	6.78	-18.63
28.5	219	0.18	0.14	25.2	5.96	1.50	6.82	-18.71
29.5	224	0.18	0.13	22.7	5.80	1.32	7.40	-18.28
30.5	230	0.18	0.14	25.2	6.01	1.52	6.95	-18.70
31.5	235	0.18	0.14	25.4	5.67	1.44	6.58	-18.72
32.5	241	0.18	0.14	24.5	6.25	1.53	7.05	-18.62
33.5	247	0.18	0.15	26.7	6.30	1.68	6.59	-18.41
34.5	252	0.18	0.15	27.0	6.52	1.76	6.44	-19.28
35.5	258	0.18	0.16	29.0	6.59	1.91	6.78	-18.56
36.5	263	0.18	0.17	29.9	6.79	2.03	6.50	-18.72
37.5	269	0.18	0.16	28.3	6.59	1.86	6.58	-18.82
38.5	275	0.18	0.15	26.5	6.50	1.72	7.13	-18.49
39.5	280	0.18	0.17	31.1	7.12	2.22	6.34	-18.63
40.5	286	0.18	0.17	30.2	7.71	2.33	7.24	-19.21
41.5	291	0.18	0.16	28.8	7.84	2.26	6.70	-19.49
42.5	297	0.18	0.16	28.1	8.88	2.49	6.54	-19.68
43.5	303	0.18	0.18	32.2	8.03	2.59	6.40	-19.6
44.5	308	0.18	0.16	27.7	8.32	2.31	6.86	-19.54
45.5	314	0.18	0.16	29.0	8.24	2.39	6.46	-19.66
46.5	319	0.18	0.17	30.4	8.52	2.59	6.68	-19.96
47.5	**325**	0.37	0.18	65.0	8.04	5.23	6.56	-19.93
48.5	328	0.37	0.17	63.9	9.03	5.77	6.46	-19.79
49.5	330	0.37	0.17	64.2	8.76	5.63	6.68	-19.45
50.5	333	0.37	0.17	62.4	8.66	5.40	6.52	-19.56
51.5	336	0.37	0.18	65.7	8.34	5.48	6.73	-19.55
52.5	338	0.37	0.18	66.8	8.26	5.52	6.71	-19.80
53.5	341	0.37	0.15	55.0	9.48	5.21	6.57	-19.40
54.5	344	0.37	0.17	62.0	8.87	5.50	6.93	-19.49
55.5	347	0.37	0.17	63.1	8.25	5.21	7.10	-19.58
56.5	349	0.37	0.18	68.3	9.29	6.35	6.61	-19.43
57.5	352	0.37	0.19	71.7	7.41	5.31	6.99	-19.71
58.5	355	0.37	0.19	69.1	8.52	5.88	6.62	-19.28
59.5	357	0.37	0.19	69.1	7.31	5.05	7.04	-19.57
60.5	360	0.37	0.19	70.9	7.47	5.30	6.82	-19.66
61.5	363	0.37	0.20	74.6	7.59	5.66	6.83	-19.53
62.5	365	0.37	0.19	70.2	7.67	5.38	6.80	-19.30
63.5	368	0.37	0.21	76.5	7.76	5.94	6.97	-19.57
64.5	371	0.37	0.20	74.3	8.05	5.98	6.96	-19.40
65.5	374	0.37	0.19	70.9	8.94	6.34	6.79	-19.52
66.5	376	0.37	0.19	69.1	7.70	5.32	6.78	-19.54
67.5	379	0.37	0.21	76.1	7.59	5.78	7.02	-19.53
68.5	382	0.37	0.19	68.7	8.52	5.85	7.10	-19.58
69.5	384	0.37	0.20	73.9	7.50	5.54	6.98	-19.54
70.5	387	0.37	0.20	75.0	7.93	5.95	6.24	-19.36
71.5	390	0.37	0.19	69.4	8.24	5.72	6.59	-19.48
72.5	392	0.37	0.21	76.5	8.26	6.32	6.66	-19.42
73.5	395	0.37	0.20	73.2	7.91	5.79	6.62	-19.40
74.5	398	0.37	0.20	72.4	8.61	6.23	6.55	-19.52

Appendix 3.5. continued

core depth (cm)	cal age (BP) [1]	SR (cm/a)	dry bulk density (g/cm³)	AR$_{bulk}$ (mg/cm²/a) [2]	TOC (%) [3]	AR$_{TOC}$ (mg/cm²/a) [4]	δ¹⁵N (‰) [3]	δ¹³C$_{org}$ (‰) [3]
75.5	400	0.37	0.18	68.0	8.59	5.84	6.37	-19.56
76.5	403	0.37	0.19	72.0	8.55	6.16	6.93	-19.71
77.5	406	0.37	0.19	72.0	8.59	6.19	6.91	-19.65
78.5	409	0.37	0.21	78.7	8.29	6.53	6.81	-19.53
79.5	411	0.37	0.20	74.3	8.26	6.13	7.05	-19.83
80.5	414	0.37	0.20	73.2	9.92	7.26	5.88	
81.5	417	0.37	0.20	73.2	7.75	5.67	6.07	-19.85
82.5	419	0.37	0.20	75.4	7.57	5.71	6.10	-19.66
83.5	422	0.37	0.18	68.3	7.87	5.38	6.05	-19.88
84.5	425	0.37	0.19	71.7	8.07	5.78	5.90	-19.64
85.5	427	0.37	0.18	66.1	7.71	5.10	6.12	-19.90
86.5	430	0.37	0.19	70.6	7.57	5.34	6.31	-19.70
87.5	433	0.37	0.18	65.7	7.83	5.15	6.24	-19.76
88.5	436	0.37	0.19	71.7	7.80	5.59	6.33	-19.50
89.5	438	0.37	0.18	68.3	7.69	5.25	6.56	-19.73
90.5	441	0.37	0.18	68.3	7.56	5.17	6.09	-19.72
91.5	444	0.37	0.19	71.7	7.80	5.59	6.10	-19.91
92.5	446	0.37	0.19	72.0	8.11	5.84	6.43	-19.82
93.5	449	0.37	0.21	76.5	8.25	6.31	6.26	-19.79
94.5	452	0.37	0.21	78.7	8.24	6.49	6.28	-20.00
95.5	454	0.37	0.21	77.6	8.19	6.36	6.32	-20.01
96.5	457	0.37	0.23	84.3	7.69	6.48	6.40	-19.92
97.5	460	0.37	0.21	78.7	7.29	5.74	6.00	-19.86
98.5	463	0.37	0.21	77.2	7.43	5.74	6.01	-19.81
99.5	465	0.37	0.22	82.1	6.78	5.56	6.09	-19.92
100.5	468	0.37	0.22	81.7				
101.5	471	0.37	0.22	83.2	5.27	4.38	6.54	-19.73
102.5	473	0.37	0.23	86.1	5.33	4.59	6.76	-19.77
103.5	476	0.37	0.23	83.9	5.86	4.92	6.52	-19.37
104.5	479	0.37	0.23	85.4	7.15	6.11	6.45	-19.48
105.5	481	0.37	0.23	85.0	6.86	5.83	6.71	-19.67
106.5	484	0.37	0.23	86.1	6.32	5.44	6.20	-19.43
107.5	487	0.37	0.23	86.1	7.27	6.26	6.43	-18.98
108.5	489	0.37	0.23	86.1	8.28	7.13	6.38	-19.19
109.5	492	0.37	0.24	90.6	5.88	5.33	6.26	-19.52
110.5	495	0.37	0.22	81.7	8.00	6.54	5.96	-19.11
111.5	498	0.37	0.23	85.8	5.91	5.07	5.97	-20.08
112.5	500	0.37	0.22	82.1	7.38	6.06	5.99	-19.30
113.5	503	0.37	0.22	83.2	8.66	7.20	6.10	-19.43
114.5	506	0.37	0.24	88.7	8.99	7.98	6.20	-19.20
115.5	508	0.37	0.20	75.8	8.38	6.35	6.27	-19.17
116.5	511	0.37	0.21	78.0	6.58	5.13	6.29	-19.67
117.5	514	0.37	0.20	74.6	8.72	6.51	6.05	-19.19
118.5	516	0.37	0.22	80.9	7.22	5.84	6.24	-19.15
119.5	519	0.37	0.21	78.0	6.53	5.09	6.23	-19.33
120.5	522	0.37	0.22	83.2	7.64	6.35	6.43	-19.15
121.5	525	0.37	0.23	83.9	6.80	5.71	5.88	-19.05
122.5	527	0.37	0.21	79.5	6.48	5.15	6.12	-19.01
123.5	530	0.37	0.19	71.7	7.21	5.17	5.84	-18.29
124.5	533	0.37	0.20	74.3	6.53	4.85	6.13	-18.92
125.5	535	0.37	0.20	72.8	8.68	6.32	5.91	-18.52
126.5	538	0.37	0.19	70.9	5.94	4.21	6.11	-19.04
127.5	541	0.37	0.20	73.5	6.65	4.89	6.21	-18.83
128.5	543	0.37	0.20	75.8	7.74	5.86	6.18	-18.67
129.5	546	0.37	0.18	68.3	8.33	5.69	6.12	-17.93
130.5	549	0.37	0.21	77.2	7.71	5.95	5.96	-18.74
131.5	551	0.37	0.19	69.8	7.99	5.58	6.08	-19.55
132.5	554	0.37	0.18	68.0	8.02	5.45	6.33	-18.28
133.5	557	0.37	0.20	75.0	7.07	5.30	6.02	-18.76
134.5	560	0.37	0.20	73.9	7.02	5.19	6.19	-18.74
135.5	562	0.37	0.23	83.5	5.82	4.86	6.17	-18.94
136.5	565	0.37	0.19	68.7	5.16	3.54	6.21	-19.64
137.5	568	0.37	0.20	72.4	6.33	4.58	6.01	-19.53
138.5	570	0.37	0.20	74.6	7.14	5.33	6.17	-18.91
139.5	573	0.37	0.19	68.7	7.00	4.81	5.84	-19.20
140.5	576	0.37	0.19	70.6	9.89	6.98	6.03	-18.12
141.5	578	0.37	0.19	72.0	7.17	5.17	6.70	-19.72
142.5	581	0.37	0.18	67.6	8.95	6.05	6.29	-19.62
143.5	584	0.37	0.18	68.3	6.07	4.15	6.98	-19.86
144.5	587	0.37	0.18	68.3	7.70	5.26	6.52	-19.80
145.5	589	0.37	0.18	68.0	7.42	5.04	6.61	-19.70
146.5	592	0.37	0.18	67.2	6.25	4.20	6.54	-19.95
147.5	595	0.37	0.18	65.4	7.09	4.63	6.33	-19.78
148.5	597	0.37	0.14	53.1	7.84	4.16	6.48	-19.81
149.5	**600**	0.11	0.23	25.6	7.98	2.04	6.25	-19.82
150.5	609	0.11	0.14	15.6	8.14	1.27	6.46	-19.88
151.5	618	0.11	0.14	15.5	5.89	0.91	6.62	-19.77

Appendix 3.5. continued

core depth (cm)	cal age (BP) [1]	SR (cm/a)	dry bulk density (g/cm³)	AR_{bulk} (mg/cm²/a) [2]	TOC (%) [3]	AR_{TOC} (mg/cm²/a) [4]	$\delta^{15}N$ (‰) [3]	$\delta^{13}C_{org}$ (‰) [3]
152.5	627	0.11	0.14	15.8	6.37	1.01	6.65	-19.88
153.5	635	0.11	0.13	14.9	8.20	1.22	7.10	-20.37
154.5	644	0.11	0.16	17.8	8.03	1.43	5.79	-20.19
155.5	653	0.11	0.19	20.9	8.35	1.75	5.75	-20.14
156.5	662	0.11	0.17	18.8	8.41	1.58	6.06	-20.38
157.5	671	0.11	0.16	18.1	7.45	1.35	6.06	-20.34
158.5	680	0.11	0.17	19.2	8.24	1.58	5.92	-20.17
159.5	688	0.11	0.17	19.3	7.26	1.40	6.26	-20.07
160.5	697	0.11	0.17	18.8	8.11	1.52	5.99	-20.07
161.5	706	0.11	0.17	19.2	8.45	1.63	6.09	-20.11
162.5	715	0.11	0.16	17.8	8.26	1.47	5.76	-19.98
163.5	724	0.11	0.16	17.6	6.75	1.19	6.10	-20.16
164.5	733	0.11	0.17	19.2	6.20	1.19	5.90	-19.97
165.5	741	0.11	0.14	16.1	6.73	1.08	5.96	-20.37
166.5	750	0.11	0.16	18.4	6.69	1.23	6.10	-19.81
167.5	759	0.11	0.15	16.4	6.34	1.04	6.16	-19.72
168.5	768	0.11	0.16	18.3	5.95	1.09	6.30	-20.27
169.5	777	0.11	0.17	19.1	6.71	1.28	6.12	-20.11
170.5	786	0.11	0.17	19.3	5.51	1.07	6.13	-20.20
171.5	795	0.11	0.16	18.4	6.58	1.21	6.21	-20.00
172.5	803	0.11	0.17	19.7	5.64	1.11	6.41	-20.18
173.5	812	0.11	0.17	19.0	6.03	1.15	6.01	-20.33
174.5	821	0.11	0.16	18.3	6.57	1.20	6.27	-19.95
175.5	830	0.11	0.18	20.2	6.03	1.22	6.26	-20.26
176.5	839	0.11	0.17	19.6	5.56	1.09	6.53	-20.17
177.5	848	0.11	0.17	19.1	5.70	1.09	6.33	-20.10
178.5	856	0.11	0.18	20.5	6.32	1.29	6.28	-19.75
179.5	865	0.11	0.16	17.6	5.88	1.04	6.29	-20.24
180.5	874	0.11	0.18	20.0	5.45	1.09	6.50	-20.17
181.5	883	0.11	0.16	18.6	5.34	0.99	6.46	-20.30
182.5	892	0.11	0.16	18.2	6.09	1.11	6.42	
183.5	901	0.11	0.15	16.6	6.18	1.03	6.14	-19.88
184.5	910	0.11	0.17	19.6	5.82	1.14	6.59	-19.89
185.5	918	0.11	0.17	19.7	5.29	1.04	6.36	-20.18
186.5	927	0.11	0.18	20.8	7.31	1.52	6.43	-19.66
187.5	936	0.11	0.19	21.2	6.72	1.42	5.53	-18.99
188.5	945	0.11	0.20	22.9	6.43	1.47	6.33	-19.16
189.5	954	0.11	0.20	22.7	7.82	1.78	6.45	
190.5	963	0.11	0.21	23.2	7.41	1.72	6.20	-20.01
191.5	971	0.11	0.21	23.3	6.44	1.50	6.21	-19.48
192.5	980	0.11	0.23	25.8	5.27	1.36	6.21	-19.89
193.5	989	0.11	0.21	24.1	6.63	1.60	6.03	-19.66
194.5	998	0.11	0.23	25.7	7.69	1.97	6.20	-19.52
195.5	1007	0.11	0.22	25.3	6.64	1.68	5.77	-19.78
196.5	1016	0.11	0.25	27.7	7.15	1.98	5.77	-19.46
197.5	1024	0.11	0.23	25.9	6.07	1.57	5.93	-19.36
198.5	1033	0.11	0.25	27.8	7.10	1.98	6.35	-19.36
199.5	1042	0.11	0.25	28.1	6.65	1.87	5.78	-19.68
200.5	**1051**	0.51	0.26	131.8	6.81	8.98	5.76	-19.32
201.5	1053	0.51	0.27	134.9				
202.5	1055	0.51	0.33	165.7	8.02	13.29	6.59	
203.5	1057	0.51	0.25	128.3	10.66	13.68	6.45	-22.44
204.5	1059	0.51	0.24	119.7	8.95	10.71	6.23	-22.42
205.5	1061	0.51	0.28	141.4	8.74	12.36	6.41	-21.80
206.5	1063	0.51	0.24	120.2	9.35	11.24	6.58	-21.38
207.5	1065	0.51	0.23	113.9	8.41	9.58	6.65	-22.72
208.5	1067	0.51	0.25	126.8	9.27	11.75	6.75	-21.24
209.5	1069	0.51	0.24	120.2	8.67	10.42	6.46	-20.92
210.5	1071	0.51	0.24	122.2	8.20	10.02	6.51	-21.66
211.5	1073	0.51	0.23	113.7	8.83	10.04	6.73	-21.70
212.5	1075	0.51	0.24	119.7	8.76	10.49	6.60	-21.58
213.5	1077	0.51	0.23	114.7	8.48	9.72	6.67	-21.68
214.5	1079	0.51	0.32	160.6	5.69	9.15	6.83	-21.67
215.5	1081	0.51	0.19	97.0	8.16	7.91	6.49	-20.39
216.5	1083	0.51	0.20	101.5	8.39	8.52	6.50	-20.03
217.5	1085	0.51	0.19	95.5	8.43	8.05	6.36	-19.94
218.5	1087	0.51	0.19	94.5	8.67	8.19	6.44	-21.88
219.5	1089	0.51	0.18	89.4	10.11	9.04	6.43	-20.31
220.5	1091	0.51	0.19	98.0	8.50	8.33	6.52	-20.14
221.5	1093	0.51	0.19	94.5	9.07	8.57	6.24	-20.17
222.5	1095	0.51	0.18	89.9	9.47	8.52	6.08	-20.10
223.5	1097	0.51	0.21	105.6	7.87	8.31	6.73	-19.95
224.5	1099	0.51	0.18	90.4	9.94	8.98	6.36	-19.92
225.5	1101	0.51	0.19	94.0	9.51	8.93	6.41	-20.30
226.5	1102	0.51	0.21	104.6	8.79	9.19	6.64	-19.62
227.5	1104	0.51	0.21	104.6	8.21	8.58	6.45	-20.21
228.5	1106	0.51	0.21	107.6	9.79	10.54	6.26	-20.67

Appendix 3.5. continued

core depth (cm)	cal age (BP) [1]	SR (cm/a)	dry bulk density (g/cm³)	AR_{bulk} (mg/cm²/a) [2]	TOC (%) [3]	AR_{TOC} (mg/cm²/a) [4]	$\delta^{15}N$ (‰) [3]	$\delta^{13}C_{org}$ (‰) [3]
229.5	1108	0.51	0.29	146.5	5.93	8.68	6.60	-21.38
230.5	1110	0.51	0.20	99.0	9.70	9.60	5.68	-19.61
231.5	1112	0.51	0.19	95.0	9.62	9.14	5.93	-19.51
232.5	1114	0.51	0.20	99.5	9.12	9.08	5.57	-19.47
233.5	1116	0.51	0.20	100.0	9.14	9.14	5.27	-19.73
234.5	1118	0.51	0.19	94.0	9.19	8.63	5.53	-19.62
235.5	1120	0.51	0.20	100.0	9.24	9.24	5.36	-19.89
236.5	1122	0.51	0.19	95.5	9.19	8.77	5.39	-19.58
237.5	1124	0.51	0.19	97.0	6.75	6.55	5.70	
238.5	1126	0.51	0.19	95.0	7.63	7.25	5.73	-19.73
239.5	1128	0.51	0.18	88.4	6.48	5.73	5.89	-19.99
240.5	1130	0.51	0.16	81.3	6.34	5.16	5.71	-20.02
241.5	1132	0.51	0.15	77.8	6.28	4.89	5.73	-19.72
242.5	1134	0.51	0.17	83.9	6.46	5.42	5.71	-19.95
243.5	1136	0.51	0.18	91.9	6.05	5.56	5.82	-19.72
244.5	1138	0.51	0.17	87.9	6.07	5.34	5.54	-19.48
245.5	1140	0.51	0.17	84.4	5.73	4.83	5.39	-19.59
246.5	1142	0.51	0.19	98.0	5.87	5.75	5.34	-20.01
247.5	1144	0.51	0.18	88.9	7.01	6.23	5.30	-19.27
248.5	1146	0.51	0.16	80.8	7.05	5.70	5.31	-19.80
249.5	1148	0.51	0.16	80.3	8.00	6.43	5.18	-19.42
250.5	**1150**	0.77	0.17	130.8	7.67	10.04	6.79	-19.85
251.5	1151	0.77	0.16	121.5	7.34	8.92	6.48	-20.12
252.5	1153	0.77	0.18	139.4	5.78	8.05	5.52	-20.78
253.5	1154	0.77	0.17	130.1	4.47	5.81	5.99	-21.15
254.5	1155	0.77	0.17	134.7	7.57	10.20	6.22	-20.52
255.5	1156	0.77	0.17	130.8	7.11	9.30	6.65	-20.16
256.5	1158	0.77	0.18	137.8	7.90	10.89	6.59	-19.89
257.5	1159	0.77	0.17	130.1	8.66	11.26	5.60	-20.46
258.5	1160	0.77	0.16	123.1	6.50	8.00	4.84	-20.64
259.5	1162	0.77	0.17	130.1	7.74	10.07	6.48	-19.71
260.5	1163	0.77	0.16	123.1	8.45	10.40	6.65	-19.38
261.5	1164	0.77	0.17	130.8	6.65	8.71	6.41	-19.58
262.5	1165	0.77	0.15	119.2	7.70	9.19	6.56	-19.45
263.5	1167	0.77	0.18	140.9	6.83	9.62	6.66	-19.35
264.5	1168	0.77	0.16	124.6	7.33	9.13	6.51	-19.64
265.5	1169	0.77	0.18	142.5	6.85	9.76	6.55	-19.15
266.5	1171	0.77	0.18	139.4	7.07	9.85	6.28	-19.01
267.5	1172	0.77	0.18	142.5	6.80	9.69	6.13	-18.75
268.5	1173	0.77	0.18	136.3	6.44	8.78	6.15	-19.22
269.5	1174	0.77	0.18	141.7	7.02	9.94	6.14	-19.11
270.5	1176	0.77	0.18	135.5	7.37	9.98	6.21	-18.75
271.5	1177	0.77	0.16	121.5	6.25	7.59	6.37	-19.45
272.5	1178	0.77	0.18	140.1	6.67	9.34	6.76	-18.79
273.5	1180	0.77	0.18	136.3	6.74	9.19	6.64	-18.90
274.5	1181	0.77	0.18	138.6	6.52	9.03	6.38	-18.72
275.5	1182	0.77	0.22	169.5	6.07	10.29	6.64	-18.70
276.5	1183	0.77	0.17	130.8	6.88	9.00	6.52	-18.66
277.5	1185	0.77	0.17	133.9	6.47	8.67	6.29	-18.71
278.5	1186	0.77	0.17	131.6	6.69	8.80	6.36	-18.55
279.5	1187	0.77	0.18	140.9	7.60	10.71	6.51	-18.59
280.5	1189	0.77	0.18	137.0	6.47	8.86	6.38	-19.60
281.5	1190	0.77	0.22	171.9	8.03	13.81	6.42	-19.21
282.5	1191	0.77	0.20	157.9	8.01	12.65	6.36	-19.28
283.5	1192	0.77	0.22	171.9	7.84	13.47	6.42	-19.22
284.5	1194	0.77	0.22	167.2	6.99	11.69	6.38	-19.45
285.5	1195	0.77	0.23	175.7	7.35	12.91	6.26	-19.39
286.5	1196	0.77	0.22	169.5	7.20	12.21	6.22	-19.46
287.5	1198	0.77	0.23	175.0	6.55	11.46	6.25	-19.86
288.5	1199	0.77	0.23	175.7	6.38	11.21	6.07	-19.73
289.5	1200	0.77	0.23	178.8	7.70	13.78	5.99	-19.67
290.5	1201	0.77	0.26	200.5	5.96	11.96	6.59	-19.63
291.5	1203	0.77	0.22	167.2	6.35	10.61	6.08	-19.99
292.5	1204	0.77	0.29	222.2	4.17	9.26	5.91	-20.26
293.5	1205	0.77	0.21	164.9	4.12	6.79	5.64	-20.08
294.5	1207	0.77	0.22	168.0	6.28	10.56	5.75	-19.85
295.5	1208	0.77	0.20	151.7	6.79	10.30	5.94	-19.26
296.5	1209	0.77	0.27	209.8	6.77	14.19	6.09	-19.10
297.5	1210	0.77	0.21	164.9	7.54	12.43	5.87	-18.90
298.5	1212	0.77	0.23	179.6	5.32	9.55	5.61	-19.61
299.5	**1213**	0.49	0.22	108.7	6.09	6.62	5.95	-19.55
300.5	1215	0.49	0.28	139.1	6.58	9.15	6.09	-18.80
301.5	1217	0.49	0.21	100.9	7.61	7.68	5.64	-18.97
302.5	1219	0.49	0.32	154.3	6.81	10.51	6.19	-18.73
303.5	1221	0.49	0.23	112.2				
304.5	1223	0.49	0.37	182.2	6.01	10.96	6.27	-19.38
305.5	1225	0.49	0.34	166.0	6.23	10.34	6.56	-19.37

Appendix 3.5. continued

core depth (cm)	cal age (BP) [1]	SR (cm/a)	dry bulk density (g/cm³)	AR_{bulk} (mg/cm²/a) [2]	TOC (%) [3]	AR_{TOC} (mg/cm²/a) [4]	$\delta^{15}N$ (‰) [3]	$\delta^{13}C_{org}$ (‰) [3]
306.5	1227	0.49	0.38	186.1	5.78	10.75	6.59	-19.33
307.5	1229	0.49	0.29	143.5	6.38	9.16	5.88	-18.77
308.5	1231	0.49	0.29	139.6	5.70	7.96	6.46	-18.99
309.5	1233	0.49	0.34	166.0	5.34	8.87	6.41	-19.08
310.5	1235	0.49	0.33	159.7	5.62	8.97	6.55	-19.04
311.5	1237	0.49	0.34	167.5	4.48	7.50	6.51	-19.16
312.5	1240	0.49	0.32	155.8	3.72	5.79	5.39	-19.14
313.5	1242	0.49	0.31	151.8	4.00	6.07	5.80	-19.32
314.5	1244	0.49	0.29	139.6	5.15	7.19	6.34	-18.97
315.5	1246	0.49	0.22	107.3	6.02	6.45	6.32	-18.89
316.5	1248	0.49	0.22	105.3	5.79	6.10	6.47	-18.78
317.5	1250	0.49	0.27	131.3	6.40	8.40	6.56	-18.77
318.5	1252	0.49	0.30	146.4	5.07	7.42	6.15	-18.82
319.5	1254	0.49	0.32	158.2	4.91	7.77	6.74	-18.90
320.5	1256	0.49	0.25	120.5	6.36	7.67	6.65	-18.80
321.5	1258	0.49	0.33	161.6	6.62	10.70	6.78	-18.63
322.5	1260	0.49	0.37	179.3	5.69	10.20	6.85	-18.69
323.5	1262	0.49	0.29	142.0	7.45	10.58	6.66	-18.73
324.5	**1264**	0.03	0.37	12.4	5.34	0.66	6.76	-18.98
325.5	1293	0.03	0.32	10.9	5.87	0.64	6.57	-19.01
326.5	1323	0.03	0.24	8.0	6.44	0.51	6.50	-18.74
327.5	1352	0.03	0.35	11.7	5.47	0.64	6.52	-18.72
328.5	1382	0.03	0.40	13.6	6.01	0.82	6.91	-18.82
329.5	1411	0.03	0.24	8.1	7.12	0.58	6.32	-18.61
330.5	1441	0.03	0.37	12.5	5.84	0.73	6.90	-19.42
331.5	1470	0.03	0.35	12.0	6.39	0.77	7.08	-19.29
332.5	1500	0.03	0.32	10.9	6.71	0.73	6.36	-19.52
333.5	1529	0.03	0.36	12.2	6.91	0.84	7.17	-19.80
334.5	1559	0.03	0.35	12.0	6.69	0.80	6.91	-19.27
335.5	1588	0.03	0.37	12.6	6.65	0.84	6.98	-19.73
336.5	1618	0.03	0.36	12.3	6.77	0.83	6.72	
337.5	1647	0.03	0.34	11.5	6.96	0.80	6.75	-19.61
338.5	1677	0.03	0.35	11.7	6.41	0.75	7.09	-19.44
339.5	1706	0.03	0.24	8.1	7.27	0.59	5.86	-19.51
340.5	1736	0.03	0.25	8.3	6.92	0.58	6.52	-19.76
341.5	1765	0.03	0.24	8.1	7.44	0.60	6.45	-19.64
342.5	1795	0.03	0.24	8.2	5.65	0.47	6.14	-19.89
343.5	**1824**	0.04	0.35	13.6	5.27	0.71	5.89	
344.5	1850	0.04	0.25	9.9	6.68	0.66	6.95	-19.42
345.5	1876	0.04	0.37	14.4	6.24	0.90	6.90	-19.73
346.5	1901	0.04	0.26	10.0	7.21	0.72	6.77	-19.64
347.5	**1927**	0.06	0.25	14.9	6.89	1.03	6.93	-19.95
348.5	1944	0.06	0.35	21.2	7.06	1.50	6.71	-19.63
349.5	1960	0.06	0.35	21.0	6.46	1.36	7.01	-19.76
350.5	1977	0.06	0.39	23.7	5.01	1.19	6.83	-19.66
351.5	1993	0.06	0.24	14.6	6.95	1.02	6.76	-19.75
352.5	2010	0.06	0.34	20.7	6.69	1.39	6.80	-19.63
353.5	2026	0.06	0.33	20.1			7.09	
354.5	2043	0.06	0.36	21.7	5.30	1.15	6.42	-19.37
355.5	2059	0.06	0.25	15.3	6.62	1.01	5.51	-19.54
356.5	2076	0.06	0.27	16.0	6.56	1.05	6.32	-19.63
357.5	2092	0.06	0.27	16.1	4.66	0.75	6.07	-19.59
358.5	2109	0.06	0.27	16.2	6.31	1.02	6.04	-19.52
359.5	2125	0.06	0.28	17.0	4.99	0.85	6.98	-19.47
360.5	2142	0.06	0.27	16.4	6.63	1.09	6.04	-19.41
361.5	2158	0.06	0.27	16.4	6.50	0.90	5.51	-19.17
362.5	2175	0.06	0.29	17.2	6.32	1.09	5.56	-18.93
363.5	**2191**	0.05	0.28	14.1	6.35	0.90	5.34	-19.24
364.5	2210	0.05	0.27	13.6	6.01	0.82	6.24	-19.07
365.5	2230	0.05	0.27	13.7	5.95	0.81	6.50	-19.10
366.5	2249	0.05	0.27	13.7	5.88	0.81	6.32	-19.18
367.5	2269	0.05	0.27	13.7	5.69	0.78	6.39	-19.19
368.5	2288	0.05	0.27	13.6	5.95	0.81	6.41	-19.04
369.5	2307	0.05	0.28	13.9	5.63	0.78	6.25	-19.20
370.5	2327	0.05	0.29	14.4	6.71	0.97	6.41	-19.19
371.5	2346	0.05	0.27	13.6	5.30	0.72	6.39	-19.40
372.5	2366	0.05	0.29	14.6	5.99	0.87	6.34	-19.37
373.5	2385	0.05	0.29	14.4	5.99	0.86	6.64	-19.12
374.5	2404	0.05	0.29	14.3	5.18	0.74	6.70	-19.33
375.5	2424	0.05	0.28	14.1	5.28	0.74	6.55	-19.10
376.5	2443	0.05	0.29	14.4	6.54	0.94	6.60	-18.86
377.5	2463	0.05	0.29	14.5	5.20	0.75	6.65	-19.31
378.5	2482	0.05	0.28	14.2	5.39	0.76	6.56	-19.15
379.5	2501	0.05	0.28	14.2	6.43	0.91	6.53	-19.09
380.5	2521	0.05	0.28	14.1	6.07	0.85	6.42	-18.94
381.5	2540	0.05	0.29	14.5	5.38	0.78	6.35	-19.12
382.5	2560	0.05	0.28	13.9	5.07	0.70	6.49	-19.37

Appendix 3.5. continued

core depth (cm)	cal age (BP) [1]	SR (cm/a)	dry bulk density (g/cm³)	AR$_{bulk}$ (mg/cm²/a) [2]	TOC (%) [3]	AR$_{TOC}$ (mg/cm²/a) [4]	δ^{15}N (‰) [3]	δ^{13}C$_{org}$ (‰) [3]
383.5	2579	0.05	0.30	14.8	6.55	0.97	6.56	-18.98
384.5	2598	0.05	0.28	13.9	6.60	0.91	4.79	-19.62
385.5	2618	0.05	0.28	14.1	6.34	0.89	6.39	-18.98
386.5	2637	0.05	0.27	13.7	5.88	0.81	6.57	-19.20
387.5	2657	0.05	0.27	13.6	6.19	0.84	6.52	
388.5	2676	0.05	0.28	14.1	6.20	0.87	6.57	-19.07
389.5	2695	0.05	0.32	16.0	6.25	1.00	6.54	-19.31
390.5	2715	0.05	0.32	15.8	6.35	1.00	6.62	-19.64
391.5	2734	0.05	0.27	13.6	6.21	0.84	6.67	-19.14
392.5	2754	0.05	0.27	13.6	6.29	0.86	6.80	-19.51
393.5	**2773**	0.57	0.35	197.5	5.79	11.43	6.82	-19.16
394.5	2775	0.57	0.32	181.7	6.10	11.08	6.54	-18.89
395.5	2777	0.57	0.29	164.1	6.20	10.17	6.63	-19.18
396.5	2778	0.57	0.28	156.8	5.90	9.25	6.38	-19.37
397.5	2780	0.57	0.27	155.1	5.72	8.88	6.58	-19.54
398.5	2782	0.57	0.26	148.8	5.55	8.26	6.82	-19.19
399.5	2784	0.57	0.31	174.9	5.86	10.25	6.64	-19.16
400.5	2785	0.57	0.33	185.0	5.50	10.18	6.67	-19.07
401.5	2787	0.57	0.33	186.2	5.33	9.93	6.66	-19.40
402.5	2789	0.57	0.32	178.8	4.48	8.02	6.02	-19.56
403.5	2791	0.57	0.29	163.5	5.79	9.47	5.81	-19.36
404.5	2792	0.57	0.30	169.8	6.30	10.70	6.54	-19.70
405.5	2794	0.57	0.31	176.0	4.96	8.73	6.60	-19.55
406.5	2796	0.57	0.31	177.1	5.63	9.96	6.74	-19.21
407.5	2798	0.57	0.29	166.4	5.45	9.06	6.86	-19.24
408.5	2800	0.57	0.32	181.7	5.36	9.73	6.72	-19.03
409.5	2801	0.57	0.30	166.9	5.49	9.16	6.87	-19.09
410.5	2803	0.57	0.31	177.7	5.77	10.26	6.35	-19.34
411.5	2805	0.57	0.30	171.5	5.56	9.53	6.37	-19.50
412.5	2807	0.57	0.30	170.3	5.20	8.85	6.97	-19.41
413.5	2808	0.57	0.30	166.9	6.32	10.55	6.73	-19.42
414.5	2810	0.57	0.37	207.7	5.98	12.42	5.49	-19.62
415.5	2812	0.57	0.29	166.4	6.24	10.39	6.85	-19.17
416.5	2814	0.57	0.38	213.3	5.93	12.65	6.74	-19.70
417.5	2815	0.57	0.38	214.5	5.71	12.25	6.72	-19.38
418.5	2817	0.57	0.36	203.2	6.72	13.65	6.49	-19.20
419.5	2819	0.57	0.29	163.0	5.07	8.26	6.50	
420.5	2821	0.57	0.39	221.3	5.41	11.96	6.41	-18.84
421.5	2822	0.57	0.29	164.7	6.42	10.57	6.93	-19.20
422.5	2824	0.57	0.32	178.3	6.00	10.69	6.99	-18.98
423.5	2826	0.57	0.32	180.0	6.12	11.01	6.80	-19.21
424.5	2828	0.57	0.32	180.0	5.82	10.48	6.86	-19.23
425.5	2830	0.57	0.31	173.7	6.12	10.62	6.86	-19.27
426.5	2831	0.57	0.30	172.0	6.00	10.32	7.11	-19.25
427.5	2833	0.57	0.31	173.7	6.14	10.66	7.31	-19.14
428.5	2835	0.57	0.32	180.0	5.99	10.78	6.97	-19.20
429.5	2837	0.57	0.29	163.5	5.83	9.53	6.93	-19.01
430.5	2838	0.57	0.27	153.9	5.53	8.51	6.22	-19.45
431.5	2840	0.57	0.26	147.7	5.58	8.24	6.61	-19.32
432.5	2842	0.57	0.25	141.5	4.20	5.94	6.16	-19.49
433.5	2844	0.57	0.34	194.1	4.02	7.81	6.96	-19.49
434.5	2845	0.57	0.28	156.2	5.41	8.44	7.27	-19.08
435.5	2847	0.57	0.25	143.7	6.40	9.20	6.90	-19.06
436.5	2849	0.57	0.27	154.5	5.65	8.73	6.74	-19.61
437.5	2851	0.57	0.26	148.8	4.65	6.92	6.17	-19.77
438.5	2853	0.57	0.30	171.5	5.38	9.22	7.23	-19.60
439.5	2854	0.57	0.31	174.3	5.33	9.28	6.82	-19.65
440.5	2856	0.57	0.29	163.0	5.15	8.40	6.43	-19.80
441.5	2858	0.57	0.38	214.5	5.34	11.45	7.03	-19.84
442.5	2860	0.57	0.33	185.0	4.60	8.51	7.07	-19.60
443.5	2861	0.57	0.37	208.2	5.19	10.81	7.12	-19.53
444.5	2863	0.57	0.31	173.7	6.30	10.94	6.21	-19.03
445.5	2865	0.57	0.25	142.0	6.43	9.13	6.95	-19.22
446.5	2867	0.57	0.33	188.4	4.94	9.30	6.89	-19.29
447.5	2868	0.57	0.31	172.6	5.69	9.82	6.71	-19.13
448.5	2870	0.57	0.27	151.1	5.65	8.53	6.94	-19.13
449.5	2872	0.57	0.36	202.6	5.18	10.50	7.00	-19.07
450.5	2874	0.57	0.36	203.7	6.18	12.59	6.92	-19.12
451.5	2875	0.57	0.34	191.8	8.36	16.03	6.55	
452.5	2877	0.57	0.34	191.3	6.14	11.75	5.91	-18.80
453.5	2879	0.57	0.24	135.2	7.24	9.79	5.74	-19.27
454.5	2881	0.57	0.24	138.1	7.73	10.67	5.92	
455.5	2883	0.57	0.25	142.6	7.74	11.03	6.26	-19.05
456.5	2884	0.57	0.25	139.8	6.77	9.47	7.08	-19.17
457.5	2886	0.57	0.32	180.5	5.20	9.40	6.83	-19.19
458.5	2888	0.57	0.24	136.9	5.69	7.79	6.76	-19.12
459.5	2890	0.57	0.24	133.0	4.88	6.48	6.44	-19.75

Appendix 3.5. continued

core depth (cm)	cal age (BP) [1]	SR (cm/a)	dry bulk density (g/cm³)	AR$_{bulk}$ (mg/cm²/a) [2]	TOC (%) [3]	AR$_{TOC}$ (mg/cm²/a) [4]	δ^{15}N (‰) [3]	δ^{13}C$_{org}$ (‰) [3]
460.5	2891	0.57	0.24	134.1	5.41	7.25	6.52	-19.33
461.5	2893	0.57	0.31	172.6	3.73	6.43	7.00	-19.63
462.5	2895	0.57	0.23	131.3	5.12	6.72	6.44	-19.66
463.5	2897	0.57	0.30	169.8	4.06	6.90	6.07	-19.70
464.5	2898	0.57	0.27	154.5	6.03	9.31	6.72	-18.94
465.5	2900	0.57	0.26	148.3	6.71	9.95	6.98	-18.91
466.5	2902	0.57	0.22	124.5	6.88	8.57	6.79	-19.05
467.5	2904	0.57	0.26	144.3	5.57	8.04	7.12	-19.07
468.5	2906	0.57	0.26	144.3	6.02	8.68	6.49	-18.89
469.5	2907	0.57	0.24	136.9	6.80	9.31	6.62	-18.95
470.5	2909	0.57	0.25	139.2	6.87	9.57	6.70	-18.96
471.5	2911	0.57	0.20	112.6	5.80	6.54	6.81	-19.13
472.5	2913	0.57	0.28	158.4	7.01	11.10	7.06	-19.14
473.5	2914	0.57	0.25	140.9	6.13	8.63	6.70	-19.06
474.5	2916	0.57	0.25	143.2	7.79	11.15	6.92	-19.39
475.5	2918	0.57	0.28	158.4	6.99	11.07	7.23	-19.10
476.5	2920	0.57	0.24	135.2	7.00	9.46	6.75	-19.45
477.5	2921	0.57	0.27	155.1	3.57	5.53	5.55	-19.80
478.5	2923	0.57	0.24	137.5	6.15	8.45	6.31	-19.60
479.5	2925	0.57	0.29	161.3	7.61	12.28	6.95	-19.57
480.5	2927	0.57	0.23	131.9	7.80	10.29	6.79	-19.70
481.5	2929	0.57	0.28	159.6	7.30	11.65	6.45	-19.25
482.5	2930	0.57	0.38	216.2	5.23	11.32	6.94	-19.32
483.5	2932	0.57	0.36	200.9	4.84	9.73	6.74	-19.63
484.5	2934	0.57	0.31	173.2	5.44	9.42	7.10	-19.57
485.5	2936	0.57	0.36	204.3	5.41	11.05	6.49	-19.28
486.5	2937	0.57	0.30	166.9	5.43	9.06	6.99	-19.52
487.5	2939	0.57	0.26	148.3	6.81	10.09	6.33	-19.53
488.5	2941	0.57	0.31	177.1	4.63	8.20	6.80	-19.59
489.5	2943	0.57	0.32	181.1	6.17	11.17	7.14	-19.42
490.5	2944	0.57	0.26	147.7	6.16	9.09	6.42	-18.83
491.5	2946	0.57	0.25	138.6	7.58	10.51	6.91	-19.40
492.5	2948	0.57	0.23	131.9	6.73	8.87	6.59	-19.30
493.5	2950	0.57	0.25	141.5	4.74	6.71	6.58	-19.30
494.5	2951	0.57	0.32	181.1	6.03	10.92	7.26	-18.99
495.5	2953	0.57	0.26	148.8	5.40	8.04	6.90	-19.98
496.5	2955	0.57	0.31	177.7	5.14	9.13	6.99	-19.78
497.5	2957	0.57	0.36	203.2	4.94	10.03	7.22	-19.03
498.5	2959	0.57	0.30	170.3	4.76	8.10	6.61	-19.52
499.5	2960	0.57	0.30	169.2	6.00	10.16	7.21	-19.17
500.5	2962	0.57	0.29	162.4	4.11	6.68	7.02	-19.75
501.5	2964	0.57	0.31	173.2	6.71	11.62	7.16	-19.06
502.5	2966	0.57	0.31	177.7	4.43	7.88	7.20	-19.18
503.5	2967	0.57	0.30	167.5	5.82	9.75	7.18	-19.65
504.5	2969	0.57	0.35	199.8	4.66	9.30	7.29	-19.44
505.5	2971	0.57	0.36	205.4	7.48	15.37	7.07	-19.97
506.5	2973	0.57	0.34	193.0	6.42	12.40	7.06	-19.14
507.5	2974	0.57	0.35	200.3	5.26	10.53	7.35	-18.52
508.5	2976	0.57	0.44	246.2	6.42	15.81	7.18	-18.72
509.5	2978	0.57	0.37	211.1	6.50	13.71	7.80	-18.99
510.5	2980	0.57	0.38	216.2	6.73	14.54	7.61	-18.96
511.5	2982	0.57	0.39	218.4	5.81	12.70	7.51	-19.45
512.5	2983	0.57	0.37	207.1	6.11	12.65	7.38	-19.52
513.5	2985	0.57	0.29	163.0	6.78	11.04	6.77	-19.95
514.5	2987	0.57	0.32	178.3	6.16	10.98	7.60	-19.73
515.5	2989	0.57	0.36	203.7	5.08	10.35	7.38	-20.05
516.5	2990	0.57	0.37	210.5	5.10	10.73	7.59	-19.67
517.5	2992	0.57	0.34	193.5	5.94	11.49	7.31	-19.63
518.5	2994	0.57	0.36	202.6	6.16	12.47	7.27	-19.03
519.5	2996	0.57	0.40	224.7	5.44	12.22	7.68	-19.51
520.5	2997	0.57	0.37	208.8	4.90	10.24	7.47	-19.46
521.5	2999	0.57	0.35	196.9	5.57	10.98	6.77	-19.73
522.5	3001	0.57	0.38	216.2	5.08	10.98	6.89	-19.78
523.5	3003	0.57	0.37	208.8	4.82	10.07	7.73	-19.91
524.5	3004	0.57	0.35	200.3	6.04	12.10	7.18	-19.77
525.5	3006	0.57	0.36	203.7	5.83	11.89	7.06	-19.64
526.5	3008	0.57	0.37	209.9	4.51	9.47	7.72	-19.36
527.5	3010	0.57	0.31	173.7	6.19	10.75	7.29	-19.66
528.5	3012	0.57	0.34	189.6	5.98	11.33	7.37	-19.72
529.5	3013	0.57	0.32	181.1	5.76	10.43	7.42	-19.71
530.5	3015	0.57	0.37	208.2	5.52	11.49	7.20	-19.35
531.5	3017	0.57	0.29	161.8	6.42	10.39	6.80	-19.74
532.5	3019	0.57	0.39	218.4	4.71	10.29	7.71	-19.56
533.5	3020	0.57	0.38	216.7	5.85	12.67	7.29	-19.63
534.5	3022	0.57	0.50	280.7	4.15	11.65	7.68	-19.55
535.5	3024	0.57	0.36	201.5	5.75	11.59	7.37	-19.47
536.5	3026	0.57	0.37	211.1	5.86	12.38	7.20	-19.43

Appendix 3.5. continued

core depth (cm)	cal age (BP) [1]	SR (cm/a)	dry bulk density (g/cm³)	AR$_{bulk}$ (mg/cm²/a) [2]	TOC (%) [3]	AR$_{TOC}$ (mg/cm²/a) [4]	δ^{15}N (‰) [3]	δ^{13}C$_{org}$ (‰) [3]
537.5	3027	0.57	0.39	217.9	5.50	11.98	6.94	-19.68
538.5	3029	0.57	0.37	207.7	5.93	12.31	7.26	-19.59
539.5	**3031**	0.57	0.32	183.3	6.10	11.19	6.82	-19.63
540.5	3032		0.36		6.04		7.01	-19.61
541.5	3033		0.33		6.11		7.30	-19.47
542.5	3034		0.26		6.38		6.68	-19.84
543.5	3035		0.30		6.44		6.85	-19.94
544.5	3036		0.30		6.69		6.94	-20.22

[1] Bold figures denote age control points.

[2] AR$_{bulk}$ = SR × dry bulk density × 1000

[3] Derives from in-situ acidified sediment.

[4] AR$_{TOC}$ = (AR$_{bulk}$ / 100) × TOC

Appendix 3.6.

NAM1

core depth (cm)	cal age (BP)	SST (°C) (UK'37)	core depth (cm)	cal age (BP)	$\delta^{18}O_{calcite}$	$T_{\delta 18O}$ (°C) [1]
0.5	62	15.5	2.5	73	0.26	14.2
1.5	67	16.1	7.5	101	0.55	12.8
2.5	73	15.8	12.5	129	0.39	13.6
4.5	84	15.7	17.5	157	0.55	12.8
5.5	90	15.0	22.5	185	0.80	11.6
6.5	95	15.4	27.5	213	0.62	12.5
7.5	101	15.3	32.5	241	0.61	12.5
8.5	107	15.5	37.5	269	0.61	12.5
9.5	112	15.0	42.5	297	0.63	12.4
10.5	118	15.2	47.5	325	0.41	13.5
11.5	123	14.7	50.5	333	0.55	12.8
12.5	129	15.0	51.5	336	0.65	12.3
13.5	135	15.0	52.5	338	0.79	11.7
14.5	140	14.9	53.5	341	0.71	12.0
15.5	146	15.3	54.5	344	0.73	11.9
16.5	151	14.7	55.5	347	0.83	11.5
17.5	157	15.1	56.5	349	0.80	11.6
18.5	163	15.1	57.5	352	0.64	12.4
19.5	168	15.6	58.5	355	0.57	12.7
20.5	174	15.3	59.5	357	0.70	12.1
21.5	179	14.9	60.5	360	0.70	12.1
22.5	185	14.8	61.5	363	0.44	13.3
23.5	191	14.7	62.5	365	0.53	12.9
24.5	196	15.8	63.5	368	0.77	11.7
25.5	202	14.9	64.5	371	0.74	11.9
26.5	207	15.3	65.5	374	0.82	11.5
27.5	213	15.4	66.5	376	0.77	11.7
28.5	219	15.0	68.5	382	0.58	12.7
29.5	224	15.8	69.5	384	0.91	11.1
30.5	230	15.3	70.5	387	0.91	11.1
31.5	235	15.3	71.5	390	0.84	11.4
32.5	241	15.3	72.5	392	0.74	11.9
33.5	247	15.1	73.5	395	0.85	11.4
34.5	252	15.1	75.5	400	0.83	11.5
35.5	258	15.2	76.5	403	0.62	12.5
36.5	263	15.5	77.5	406	0.90	11.1
37.5	269	15.1	78.5	409	0.50	13.0
38.5	275	15.3	79.5	411	0.50	13.0
39.5	280	15.0	80.5	414	0.84	11.4
40.5	286	15.3	81.5	417	0.74	11.9
41.5	291	15.1	82.5	419	0.84	11.4
42.5	297	15.1	83.5	422	0.70	12.1
43.5	303	14.9	84.5	425	0.55	12.8
44.5	308	15.1	85.5	427	0.70	12.1
45.5	314	15.2	86.5	430	0.70	12.1
46.5	319	16.0	87.5	433	0.66	12.3
47.5	325	15.4	88.5	436	0.94	10.9
48.5	328	15.0	89.5	438	0.70	12.1
49.5	330	15.2	90.5	441	0.76	11.8
50.5	333	15.2	91.5	444	0.47	13.2
51.5	336	15.6	92.5	446	0.65	12.3
52.5	338	15.2	93.5	449	0.54	12.8
53.5	341	15.6	94.5	452	0.54	12.8
54.5	344	15.4	95.5	454	0.71	12.0
55.5	347	15.4	96.5	457	0.78	11.7
56.5	349	15.4	97.5	460	0.63	12.4
57.5	352	15.4	98.5	463	0.66	12.3
58.5	355	15.3	99.5	465	0.59	12.6
59.5	357	15.4	100.5	468	0.78	11.7
60.5	360	15.3	101.5	471	0.64	12.4
61.5	363	15.4	102.5	473	0.66	12.3
62.5	365	15.4	103.5	476	0.74	11.9
63.5	368	15.4	104.5	479	0.77	11.7
64.5	371	15.1	105.5	481	0.96	10.8
65.5	374	15.4	106.5	484	0.65	12.3
66.5	376	15.3	107.5	487	0.73	12.0
67.5	379	15.3	108.5	489	0.72	12.0
68.5	382	15.5	109.5	492	0.68	12.2
69.5	384	15.2	110.5	495	0.78	11.7
70.5	387	15.2	111.5	498	0.96	10.8
71.5	390	15.4	112.5	500	0.84	11.4
72.5	392	15.4	113.5	503	0.84	11.4
73.5	395	15.3	114.5	506	0.48	13.1
74.5	398	15.4	115.5	508	0.82	11.5
75.5	400	15.3	116.5	511	0.55	12.8

Appendix 3.6. continued

core depth (cm)	cal age (BP)	SST (°C) (UK'37)	core depth (cm)	cal age (BP)	$\delta^{18}O_{calcite}$	$T_{\delta18O}$ (°C) [1]
76.5	403	15.3	117.5	514	0.91	11.1
77.5	406	15.4	118.5	516	0.64	12.4
78.5	409	15.3	119.5	519	0.99	10.7
79.5	411	15.4	120.5	522	0.97	10.8
80.5	414	15.4	121.5	525	0.86	11.3
81.5	417	15.2	122.5	527	0.85	11.4
82.5	419	15.2	123.5	530	0.73	11.9
83.5	422	15.2	124.5	533	0.81	11.6
84.5	425	15.3	125.5	535	0.79	11.6
85.5	427	15.2	126.5	538	0.70	12.1
86.5	430	15.1	127.5	541	0.88	11.2
87.5	433	15.2	128.5	543	0.91	11.1
88.5	436	15.4	129.5	546	0.72	12.0
89.5	438	15.4	130.5	549	0.53	12.9
90.5	441	15.2	131.5	551	0.97	10.8
91.5	444	15.2	132.5	554	0.97	10.8
92.5	446	15.3	133.5	557	0.70	12.1
93.5	449	15.4	134.5	560	0.80	11.6
94.5	452	15.5	135.5	562	0.70	12.1
95.5	454	15.2	136.5	565	0.81	11.6
96.5	457	15.4	137.5	568	0.83	11.5
97.5	460	15.2	139.5	573	0.77	11.7
98.5	463	15.3	140.5	576	0.89	11.2
99.5	465	15.4	141.5	578	0.60	12.5
100.5	468	15.4	142.5	581	0.66	12.3
101.5	471	15.3	143.5	584	0.87	11.3
102.5	473	15.7	144.5	587	0.46	13.2
103.5	476	15.0	146.5	592	0.90	11.1
104.5	479	14.9	147.5	595	0.76	11.8
105.5	481	15.0	148.5	597	0.65	12.3
106.5	484	15.1	149.5	600	0.54	12.8
107.5	487	15.8	150.5	609	0.89	11.2
108.5	489	15.1	151.5	618	1.15	9.9
109.5	492	15.0	152.5	627	0.84	11.4
110.5	495	15.2	153.5	635	0.71	12.0
111.5	498	15.2	154.5	644	0.49	13.1
112.5	500	15.5	155.5	653	0.86	11.3
113.5	503	15.1	156.5	662	1.27	9.3
114.5	506	14.9	157.5	671	1.43	8.6
115.5	508	14.7	158.5	680	1.25	9.5
116.5	511	14.9	159.5	688	1.29	9.2
117.5	514	15.8	160.5	697	1.03	10.5
118.5	516	14.7	161.5	706	1.16	9.9
119.5	519	14.5	162.5	715	1.03	10.5
120.5	522	14.7	163.5	724	1.07	10.3
121.5	525	14.6	164.5	733	0.96	10.8
122.5	527	15.8	165.5	741	0.97	10.8
123.5	530	14.5	166.5	750	1.10	10.1
124.5	533	14.5	167.5	759	1.16	9.9
125.5	535	14.8	168.5	768	1.08	10.3
126.5	538	14.5	169.5	777	1.09	10.2
127.5	541	15.3	170.5	786	0.97	10.8
128.5	543	14.4	171.5	795	0.66	12.3
129.5	546	14.6	172.5	803	0.95	10.9
130.5	549	14.6	173.5	812	0.78	11.7
131.5	551	14.4	174.5	821	1.08	10.3
132.5	554	15.7	175.5	830	0.92	11.0
133.5	557	14.8	176.5	839	0.66	12.3
134.5	560	14.8	177.5	848	1.06	10.4
135.5	562	14.5	178.5	856	0.83	11.5
136.5	565	14.7	179.5	865	0.96	10.8
137.5	568	15.4	190.5	963	0.76	11.8
138.5	570	14.7	191.5	971	0.67	12.2
139.5	573	14.6	192.5	980	0.43	13.4
140.5	576	14.6	193.5	989	0.37	13.7
141.5	578	14.6	195.5	1007	0.75	11.8
142.5	581	16.1	200.5	1051	0.89	11.2
143.5	584	14.8	202.5	1055	0.68	12.2
144.5	587	14.8	203.5	1057	0.51	13.0
145.5	589	14.8	204.5	1059	0.62	12.5
146.5	592	15.1	205.5	1061	0.34	13.8
147.5	595	15.3	206.5	1063	0.93	11.0
148.5	597	14.7	207.5	1065	1.28	9.3
149.5	600	14.6	208.5	1067	0.78	11.7
150.5	609	14.6	209.5	1069	1.18	9.8
151.5	618	14.4	210.5	1071	0.80	11.6

Appendix 3.6. continued

core depth (cm)	cal age (BP)	SST (°C) (UK'37)	core depth (cm)	cal age (BP)	$\delta^{18}O_{calcite}$	$T_{\delta 18O}$ (°C) [1]
152.5	627	15.2	211.5	1073	0.76	11.8
153.5	635	14.6	215.5	1081	1.32	9.1
154.5	644	14.5	216.5	1083	1.16	9.9
155.5	653	14.5	217.5	1085	1.17	9.8
156.5	662	14.6	218.5	1087	0.91	11.1
157.5	671	15.7	219.5	1089	0.68	12.2
158.5	680	14.7	220.5	1091	0.96	10.8
159.5	688	14.8	221.5	1093	0.80	11.6
160.5	697	14.8	222.5	1095	1.03	10.5
161.5	706	14.7	223.5	1097	1.04	10.5
162.5	715	15.6	226.5	1102	0.96	10.8
163.5	724	14.6	227.5	1104	0.85	11.4
164.5	733	14.6	230.5	1110	0.46	13.2
165.5	741	14.8	231.5	1112	0.94	10.9
166.5	750	14.7	232.5	1114	1.12	10.1
167.5	759	15.7	233.5	1116	0.99	10.7
168.5	768	14.8	234.5	1118	0.76	11.8
169.5	777	14.9	235.5	1120	0.46	13.2
170.5	786	14.7	236.5	1122	0.84	11.4
171.5	795	14.9	237.5	1124	1.35	9.0
172.5	803	15.7	238.5	1126	0.95	10.9
173.5	812	14.8	239.5	1128	0.39	13.6
174.5	821	14.5	240.5	1130	0.62	12.5
175.5	830	14.8	241.5	1132	0.37	13.7
176.5	839	15.0	242.5	1134	0.55	12.8
177.5	848	16.1	243.5	1136	0.84	11.4
178.5	856	15.0	244.5	1138	0.74	11.9
179.5	865	14.9	245.5	1140	0.49	13.1
180.5	874	14.6	246.5	1142	0.39	13.6
181.5	883	14.6	247.5	1144	0.87	11.3
182.5	892	15.2	248.5	1146	0.83	11.5
183.5	901	15.0	249.5	1148	0.66	12.3
184.5	910	14.8	250.5	1150	0.86	11.3
185.5	918	14.9	251.5	1151	0.96	10.8
186.5	927	14.7	252.5	1153	0.90	11.1
187.5	936	16.3	253.5	1154	0.76	11.8
188.5	945	14.7	254.5	1155	0.76	11.8
189.5	954	14.8	255.5	1156	0.87	11.3
190.5	963	14.6	256.5	1158	0.69	12.1
191.5	971	14.7	257.5	1159	0.78	11.7
192.5	980	15.8	258.5	1160	0.79	11.7
193.5	989	14.8	259.5	1162	0.67	12.2
194.5	998	14.6	260.5	1163	0.68	12.2
195.5	1007	14.9	261.5	1164	0.56	12.8
196.5	1016	14.9	262.5	1165	0.67	12.2
197.5	1024	15.9	263.5	1167	0.88	11.2
198.5	1033	14.8	264.5	1168	0.80	11.6
199.5	1042	15.9	265.5	1169	0.85	11.4
200.5	1051	14.4	266.5	1171	0.79	11.7
201.5	1053	12.0	267.5	1172	0.79	11.7
202.5	1055	17.6	268.5	1173	0.71	12.0
203.5	1057	13.5	269.5	1174	0.31	14.0
204.5	1059	15.9	270.5	1176	0.59	12.6
205.5	1061	14.4	271.5	1177	0.29	14.1
206.5	1063	16.0	273.5	1180	0.88	11.2
207.5	1065	15.3	274.5	1181	0.69	12.1
208.5	1067	15.3	275.5	1182	0.71	12.0
209.5	1069	16.0	276.5	1183	0.84	11.4
210.5	1071	15.6	277.5	1185	0.44	13.3
211.5	1073	15.4	278.5	1186	0.63	12.4
212.5	1075	15.3	280.5	1189	0.60	12.6
213.5	1077	15.7	281.5	1190	0.74	11.9
214.5	1079	15.7	282.5	1191	0.70	12.1
215.5	1081	15.6	283.5	1192	0.24	14.3
216.5	1083	15.9	284.5	1194	0.74	11.9
217.5	1085	15.6	285.5	1195	0.65	12.3
218.5	1087	16.0	286.5	1196	0.84	11.4
219.5	1089	16.3	287.5	1198	0.48	13.1
220.5	1091	15.9	288.5	1199	0.58	12.7
221.5	1093	16.7	289.5	1200	0.35	13.8
222.5	1095	15.9	290.5	1201	0.62	12.5
223.5	1097	15.9	291.5	1203	0.88	11.2
224.5	1099	16.1	292.5	1204	0.72	12.0
225.5	1101	16.1	293.5	1205	0.83	11.5
226.5	1102	16.0	294.5	1207	0.58	12.7
227.5	1104	15.9	295.5	1208	0.90	11.1

Appendix 3.6. continued

core depth (cm)	cal age (BP)	SST (°C) (UK'37)	core depth (cm)	cal age (BP)	$\delta^{18}O_{calcite}$	$T_{\delta18O}$ (°C) [1]
228.5	1106	16.2	296.5	1209	0.73	11.9
229.5	1108	15.8	297.5	1210	0.83	11.5
230.5	1110	15.9	298.5	1212	0.73	11.9
231.5	1112	16.3	299.5	1213	0.70	12.1
232.5	1114	16.1	300.5	1215	0.91	11.1
233.5	1116	15.8	301.5	1217	0.86	11.3
234.5	1118	16.3	302.5	1219	0.54	12.9
235.5	1120	16.3	303.5	1221	0.68	12.2
236.5	1122	16.4	304.5	1223	0.83	11.5
237.5	1124	16.6	305.5	1225	0.83	11.5
238.5	1126	16.3	306.5	1227	0.95	10.9
239.5	1128	16.1	307.5	1229	0.98	10.7
240.5	1130	16.1	308.5	1231	0.90	11.1
241.5	1132	16.1	309.5	1233	0.88	11.2
242.5	1134	16.2	310.5	1235	0.91	11.1
243.5	1136	16.3	311.5	1237	0.69	12.1
244.5	1138	16.3	312.5	1240	0.79	11.7
245.5	1140	16.1	313.5	1242	0.98	10.7
246.5	1142	15.9	314.5	1244	0.91	11.1
247.5	1144	16.0	315.5	1246	0.83	11.5
250.5	1150	16.6	316.5	1248	0.92	11.0
252.5	1153	16.1	317.5	1250	0.80	11.6
255.5	1156	16.5	318.5	1252	1.05	10.4
257.5	1159	16.6	319.5	1254	1.12	10.1
260.5	1163	17.1	320.5	1256	0.92	11.0
262.5	1165	16.0	322.5	1260	1.25	9.4
265.5	1169	16.2	323.5	1262	1.10	10.2
267.5	1172	15.7	324.5	1264	1.22	9.6
270.5	1176	16.1	325.5	1293	1.00	10.6
272.5	1178	15.7	326.5	1323	1.25	9.4
275.5	1182	16.5	327.5	1352	0.73	11.9
277.5	1185	16.0	328.5	1382	1.20	9.7
280.5	1189	16.6	329.5	1411	0.99	10.7
282.5	1191	16.2	330.5	1441	0.95	10.9
285.5	1195	16.5	331.5	1470	0.99	10.7
287.5	1198	15.8	332.5	1500	0.94	10.9
290.5	1201	16.2	333.5	1529	0.76	11.8
292.5	1204	16.0	334.5	1559	0.96	10.8
297.5	1210	16.3	335.5	1588	1.00	10.6
300.5	1215	16.2	336.5	1618	0.81	11.6
302.5	1219	15.6	337.5	1647	0.99	10.7
305.5	1225	16.2	338.5	1677	0.96	10.8
307.5	1229	15.6	339.5	1706	1.04	10.5
310.5	1235	16.0	361.5	2158	0.97	10.8
312.5	1240	15.7	362.5	2175	0.91	11.1
315.5	1246	16.3	365.5	2230	0.53	12.9
317.5	1250	15.5	366.5	2249	0.69	12.1
320.5	1256	16.2	367.5	2269	0.67	12.2
322.5	1260	15.7	368.5	2288	0.79	11.7
325.5	1293	16.2	369.5	2307	0.81	11.6
327.5	1352	15.5	370.5	2327	0.58	12.7
330.5	1441	16.1	371.5	2346	0.63	12.4
332.5	1500	15.6	372.5	2366	0.55	12.8
335.5	1588	16.2	373.5	2385	0.68	12.2
337.5	1647	15.6	374.5	2404	0.68	12.2
340.5	1736	16.4	375.5	2424	0.83	11.5
342.5	1795	15.8	376.5	2443	0.74	11.9
345.5	1876	16.3	377.5	2463	0.88	11.2
347.5	1927	15.8	378.5	2482	0.63	12.4
350.5	1977	16.1	379.5	2501	0.77	11.7
352.5	2010	15.4	380.5	2521	0.90	11.1
355.5	2059	16.1	381.5	2540	0.86	11.3
356.5	2076	15.3	382.5	2560	1.00	10.6
357.5	2092	15.8	383.5	2579	0.83	11.5
360.5	2142	16.2	384.5	2598	0.83	11.5
362.5	2175	16.1	385.5	2618	0.77	11.7
365.5	2230	16.4	386.5	2637	1.09	10.2
367.5	2269	16.0	387.5	2657	0.78	11.7
372.5	2366	16.5	388.5	2676	0.65	12.3
377.5	2463	16.3	389.5	2695	1.19	9.7
380.5	2521	16.2	391.5	2734	1.10	10.2
382.5	2560	16.5	392.5	2754	0.89	11.2
385.5	2618	16.2	393.5	2773	1.36	8.9
387.5	2657	16.2	394.5	2775	0.99	10.7
390.5	2715	16.0	395.5	2777	0.87	11.3
392.5	2754	16.2	396.5	2778	1.07	10.3

Appendix 3.6. continued

core depth (cm)	cal age (BP)	SST (°C) (UK'37)	core depth (cm)	cal age (BP)	$\delta^{18}O_{calcite}$	$T_{\delta 18O}$ (°C) [1]
395.5	2777	16.0	397.5	2780	1.04	10.5
397.5	2780	16.5	398.5	2782	1.01	10.6
400.5	2785	16.3	399.5	2784	1.11	10.1
402.5	2789	16.1	400.5	2785	1.00	10.6
405.5	2794	16.0	401.5	2787	0.83	11.5
407.5	2798	16.0	402.5	2789	0.81	11.6
410.5	2803	16.0	403.5	2791	0.56	12.8
412.5	2807	15.9	404.5	2792	0.81	11.6
415.5	2812	16.2	405.5	2794	0.63	12.4
417.5	2815	16.2	406.5	2796	0.81	11.6
420.5	2821	16.0	407.5	2798	0.75	11.8
422.5	2824	16.0	408.5	2800	0.61	12.5
425.5	2830	16.2	409.5	2801	0.87	11.3
427.5	2833	16.0	410.5	2803	0.87	11.3
430.5	2838	15.8	411.5	2805	1.20	9.7
432.5	2842	15.9	412.5	2807	0.93	11.0
435.5	2847	16.2	413.5	2808	0.41	13.5
437.5	2851	16.1	414.5	2810	1.00	10.6
440.5	2856	16.1	415.5	2812	1.06	10.4
442.5	2860	15.8	416.5	2814	1.27	9.3
445.5	2865	16.0	417.5	2815	0.98	10.7
447.5	2868	15.8	418.5	2817	1.15	9.9
450.5	2874	16.0	419.5	2819	0.97	10.8
452.5	2877	15.9	420.5	2821	0.93	11.0
455.5	2883	16.4	422.5	2824	0.84	11.4
457.5	2886	15.7	423.5	2826	0.95	10.9
460.5	2891	15.8	424.5	2828	0.60	12.6
462.5	2895	16.1	425.5	2830	0.91	11.1
465.5	2900	15.9	426.5	2831	0.88	11.2
467.5	2904	16.3	427.5	2833	0.66	12.3
470.5	2909	15.7	428.5	2835	1.03	10.5
472.5	2913	15.7	429.5	2837	0.79	11.7
475.5	2918	16.2	430.5	2838	0.74	11.9
477.5	2921	16.8	431.5	2840	1.10	10.2
480.5	2927	15.7	432.5	2842	1.07	10.3
482.5	2930	16.1	433.5	2844	0.74	11.9
485.5	2936	16.3	434.5	2845	1.10	10.2
487.5	2939	15.8	435.5	2847	0.58	12.7
490.5	2944	16.2	437.5	2851	0.73	11.9
492.5	2948	16.0	438.5	2853	0.95	10.9
495.5	2953	17.1	439.5	2854	0.83	11.5
497.5	2957	16.4	442.5	2860	0.85	11.4
502.5	2966	15.7	443.5	2861	0.94	10.9
507.5	2974	15.8	444.5	2863	0.92	11.0
512.5	2983	16.1	445.5	2865	0.79	11.7
517.5	2992	16.0	446.5	2867	0.77	11.7
522.5	3001	14.7	447.5	2868	1.01	10.6
527.5	3010	15.8	448.5	2870	0.81	11.6
532.5	3019	15.9	449.5	2872	0.86	11.3
537.5	3027	15.7	452.5	2877	0.91	11.1
542.5	3034	15.7	455.5	2883	0.80	11.6
544.5	3036	16.0	457.5	2886	1.02	10.5
			458.5	2888	0.97	10.8
			459.5	2890	0.80	11.6
			464.5	2898	0.67	12.2
			465.5	2900	0.79	11.7
			466.5	2902	0.79	11.7
			467.5	2904	0.50	13.0
			468.5	2906	0.65	12.3
			469.5	2907	0.77	11.7
			470.5	2909	0.99	10.7
			471.5	2911	0.95	10.9
			472.5	2913	0.66	12.3
			474.5	2916	0.82	11.5
			475.5	2918	0.78	11.7
			476.5	2920	0.93	11.0
			477.5	2921	0.92	11.0
			478.5	2923	0.70	12.1
			480.5	2927	1.33	9.1
			481.5	2929	0.74	11.9
			482.5	2930	1.17	9.8
			485.5	2936	0.77	11.7
			486.5	2937	0.71	12.0
			487.5	2939	0.77	11.7
			488.5	2941	0.94	10.9
			489.5	2943	0.77	11.7

Appendix 3.6. continued

core depth (cm)	cal age (BP)	$\delta^{18}O_{calcite}$	$T_{\delta18O}$ (°C) [1]
490.5	2944	0.72	12.0
491.5	2946	0.68	12.2
492.5	2948	0.65	12.3
493.5	2950	0.47	13.2
494.5	2951	0.73	11.9
495.5	2953	0.85	11.4
496.5	2955	0.89	11.2
497.5	2957	0.74	11.9
498.5	2959	0.67	12.2
499.5	2960	0.69	12.1
500.5	2962	0.79	11.7
501.5	2964	0.80	11.6
502.5	2966	0.75	11.8
503.5	2967	0.56	12.8
504.5	2969	0.69	12.1
505.5	2971	0.73	11.9
506.5	2973	0.58	12.7
507.5	2974	0.79	11.7
508.5	2976	0.62	12.5
509.5	2978	0.87	11.3
510.5	2980	0.84	11.4
511.5	2982	0.82	11.5
512.5	2983	0.87	11.3
513.5	2985	0.85	11.4
514.5	2987	1.00	10.6
515.5	2989	0.64	12.4
516.5	2990	0.60	12.6
517.5	2992	0.88	11.2
518.5	2994	0.63	12.4
519.5	2996	0.65	12.3
520.5	2997	0.84	11.4
521.5	2999	0.94	10.9
522.5	3001	0.91	11.1
523.5	3003	0.47	13.2
524.5	3004	0.93	11.0
525.5	3006	0.81	11.6
526.5	3008	0.66	12.3
527.5	3010	0.96	10.8
528.5	3012	0.91	11.1
529.5	3013	1.00	10.6
530.5	3015	0.97	10.8
531.5	3017	0.85	11.4
532.5	3019	0.68	12.2
533.5	3020	0.71	12.0
534.5	3022	0.88	11.2
535.5	3024	0.97	10.8
536.5	3026	0.87	11.3
537.5	3027	0.88	11.2
539.5	3031	0.88	11.2

---

[1] $T_{\delta18O} = 16.5 - 4.8 \times (\delta^{18}O_{calcite} + 0.22)$

Appendix 3.7.

Core 178

core depth (cm)	cal age (BP) [1]	SR (cm/a)	dry bulk density (g/cm³)	AR$_{bulk}$ (mg/cm²/a) [2]	TOC (%) [3]	AR$_{TOC}$ (mg/cm²/a) [4]	δ^{15}N (‰) [5]	δ^{13}C$_{org}$ (‰) [5]
1.5	1757		0.23		8.91		6.70	-20.00
3.5	1753		0.24		11.15		6.53	-19.62
6.5	1773		0.24		9.84		6.74	-19.58
9.5	1782		0.23		11.55		6.21	-19.69
17.5	1808		0.23		8.29		6.10	-19.57
22.5	1825		0.22		9.43		6.25	-19.44
27.5	1841		0.26		7.63		8.72	-19.66
32.5	1857		0.22		7.71		6.63	-19.40
37.5	1873		0.24		9.25		7.32	-19.71
42.5	1890		0.21		9.14		5.74	-19.41
47.5	1906		0.19		7.96		5.57	-19.50
52.5	**1922**	0.27	0.24	65.1	9.46	6.16	7.82	-19.48
57.5	1940	0.27	0.21	57.0	7.81	4.45	7.88	-19.42
62.5	1958	0.27	0.25	67.8	9.24	6.26	7.82	-19.35
67.5	1977	0.27	0.26	70.5			5.77	-19.47
72.5	1995	0.27	0.23	62.4	6.57	4.10	5.55	-19.62
77.5	2013	0.27	0.28	74.6	8.19	6.11	5.61	-19.69
82.5	2031	0.27	0.28	76.0	7.69	5.84	5.61	-19.48
87.5	2050	0.27	0.28	74.6	12.04	8.99	6.00	-20.04
92.5	2068	0.27	0.29	77.3	7.59	5.87	5.56	-19.80
97.5	**2086**	0.32	0.31	96.3	7.00	6.74	5.23	-19.64
102.5	2102	0.32	0.30	93.2	7.52	7.01	5.35	-19.78
107.5	2118	0.32	0.29	90.0	7.08	6.37	4.55	-19.72
112.5	2134	0.32	0.29	91.6	6.69	6.12	5.18	-19.46
117.5	2149	0.32	0.29	90.0			5.27	-19.45
122.5	2165	0.32	0.29	91.6			6.44	-19.58
127.5	2181	0.32	0.33	102.7	7.38	7.58	6.54	-19.51
132.5	2197	0.32	0.31	97.9	7.78	7.61	5.83	-19.46
137.5	2213	0.32	0.35	109.0	7.42	8.09	5.62	-19.53
142.5	2229	0.32	0.35	110.6	6.33	7.00	6.33	-19.48
147.5	2245	0.32	0.34	108.8	6.36	6.92	5.82	-19.50
152.5	2260	0.32	0.30	93.2			6.22	-19.29
157.5	2276	0.32	0.32	101.8	6.75	6.87	5.36	-19.60
162.5	2292	0.32	0.33	105.3	7.47	7.87	5.72	-19.63
167.5	2308	0.32	0.32	101.8	7.81	7.95	5.58	-19.64
172.5	2324	0.32	0.32	101.1	7.70	7.78	6.03	-19.46
177.5	2340	0.32	0.33	102.7	6.77	6.95	6.58	-19.45
182.5	2355	0.32	0.34	107.4	6.88	7.39	6.38	-19.20
187.5	2371	0.32	0.30	93.2	6.31	5.88	6.67	-19.22
192.5	2387	0.32	0.29	90.0	8.51	7.66	6.60	-19.33
197.5	**2403**	0.27	0.30	79.6	6.64	5.29	6.79	-19.41
202.5	2422	0.27	0.31	81.0	4.93	3.99	6.94	-19.66
207.5	2441	0.27	0.20	53.1	4.04	2.14	7.75	-19.78
212.5	2460	0.27	0.26	67.8	5.41	3.67	7.30	-19.84
217.5	2478	0.27	0.19	50.4	5.27	2.66	6.74	-19.76
222.5	2497	0.27	0.22	57.1	9.98	5.70	6.79	-19.34
227.5	2516	0.27	0.20	51.8	5.08	2.63	6.92	-19.42
232.5	2535	0.27	0.20	53.1	6.76	3.59	6.59	-19.67
237.5	2554	0.27	0.19	49.1	4.62	2.27	6.78	-19.62
238.5	2557	0.27	0.21	55.8	6.90	3.85	6.89	-19.46
242.5	2573	0.27	0.17	45.1	3.94	1.78	7.04	-19.86
246.0	2586	0.27	0.19	50.4	3.99	2.01	6.60	-19.96
247.5	2591	0.27	0.17	45.1	3.75	1.69	6.94	-19.86
252.5	2610	0.27	0.18	47.8	5.17	2.47	6.77	-19.80
257.5	2629	0.27	0.16	42.5	3.19	1.36	6.93	-20.08
262.5	2648	0.27	0.17	45.1	3.72	1.68	6.54	-19.82
265.5	2659	0.27	0.19	50.4	5.68	2.87	6.10	-19.81
267.5	2667	0.27	0.19	50.4	4.48	2.26	6.01	-20.03
271.5	2682	0.27	0.19	50.4	6.40	3.23	6.33	-20.29
276.5	2701	0.27	0.23	61.1	8.70	5.31	7.76	-18.85
281.5	2719	0.27	0.16	42.5	4.42	1.88	6.67	-19.59
286.5	2738	0.27	0.20	53.1	4.63	2.46	5.47	-19.53
288.5	2746	0.27	0.21	55.8	5.44	3.03	5.17	-19.00
291.5	2757	0.27	0.20	53.1	6.61	3.51	5.94	-19.25
292.5	2761	0.27	0.22	58.4	5.86	3.42	5.30	-19.29
296.5	**2776**	0.38	0.15	57.7	3.94	2.27	8.27	-19.29
297.0	2777	0.38	0.19	73.0	4.29	3.13	9.05	-19.31
301.5	2789	0.38	0.16	61.5	4.37	2.69	8.52	-18.98
303.5	2794	0.38	0.17	65.4	3.30	2.16	9.39	-19.01
306.5	2802	0.38	0.15	57.7	3.15	1.81	8.91	-19.06
309.5	2810	0.38	0.17	65.4	5.80	3.79	7.46	-18.36
311.5	2815	0.38	0.17	65.4	4.39	2.87	8.56	-18.54
316.5	2828	0.38	0.22	84.6	7.50	6.34	8.81	-18.08
321.5	2841	0.38			7.03		8.72	-17.98
326.5	2854	0.38	0.22	84.6	8.66	7.33	8.85	-18.52

Appendix 3.7. continued

core depth (cm)	cal age (BP) [1]	SR (cm/a)	dry bulk density (g/cm³)	AR$_{bulk}$ (mg/cm²/a) [2]	TOC (%) [3]	AR$_{TOC}$ (mg/cm²/a) [4]	δ¹⁵N (‰) [5]	δ¹³C$_{org}$ (‰) [5]
331.5	2867	0.38	0.23	88.4	9.34	8.26	7.15	-17.99
336.5	2880	0.38	0.22	82.7	9.73	8.04	7.00	-17.82
341.5	2893	0.38	0.16	59.8	5.94	3.55	6.67	-18.03
346.5	2906	0.38	0.16	59.8	4.70	2.81	6.64	-17.92
351.5	2919	0.38	0.16	59.6	4.95	2.95	7.07	-18.18
356.5	2932	0.38	0.20	75.0	5.29	3.97	6.89	-17.84
359.5	2940	0.38	0.22	84.6	4.87	4.12	6.97	-18.70
361.5	2945	0.38	0.20	76.9	4.79	3.68	7.06	-18.89
366.5	2958	0.38	0.17	65.4	7.53	4.92	6.93	-18.24
373.5	2976	0.38	0.23	86.5	7.70	6.66	6.58	-18.55
378.5	2989	0.38	0.20	75.0	8.28	6.21	6.91	-18.08
383.5	3002	0.38	0.21	78.8	6.03	4.75	6.98	-18.55
386.5	3010	0.38	0.22	84.6	9.26	7.83	6.28	-18.03
388.5	3015	0.38	0.19	73.0	5.11	3.73	6.61	-18.86
393.5	**3028**	0.30	0.22	65.9	4.80	3.17	7.61	-19.04
403.5	3061	0.30	0.21	62.9	6.52	4.11	7.35	-19.15
406.0	3070	0.30	0.24	71.9	5.02	3.61	4.53	-18.57
413.0	3093	0.30	0.19	57.0	4.62	2.63	5.19	-19.29
413.5	3095	0.30	0.20	60.0	5.86	3.51	5.64	-18.39
415.0	3100	0.30	0.19	57.0	5.00	2.84	5.71	19.78
418.5	3111	0.30	0.21	62.9	6.27	3.95	5.41	-18.51
423.5	3128	0.30	0.22	65.9	6.88	4.54	5.29	-18.65
426.5	3138	0.30	0.19	57.0	5.34	3.04	5.07	-20.07
428.5	3145	0.30	0.22	65.9	5.85	3.86	5.20	-18.46
433.5	3161	0.30	0.21	62.9	5.13	3.23	8.92	-19.09
434.5	3165	0.30	0.22	65.9	5.29	3.49	6.74	-18.79
438.5	3178	0.30	0.24	71.9	6.92	4.98	6.93	-18.97
443.5	3195	0.30	0.18	54.0	5.04	2.72	4.47	-19.28
448.5	3211	0.30	0.19	57.0	4.79	2.73	7.25	-19.34
453.5	3228	0.30	0.20	60.0	5.46	3.27	7.14	-19.30
458.5	3245	0.30	0.24	71.9	11.46	8.25	5.03	-18.91
463.5	3262	0.30	0.22	65.9	5.73	3.78	6.99	-18.84
470.5	3285	0.30	0.23	68.9	5.76	3.97	6.15	-19.76
472.5	3292	0.30	0.20	60.0	5.14	3.08	6.12	-19.82
475.5	3302	0.30	0.20	60.0	5.51	3.31	6.28	-19.66
479.5	3315	0.30	0.22	65.9	6.62	4.37	5.95	-19.99
480.5	3318	0.30	0.22	65.9	6.09	4.02	6.10	-19.97
485.5	3335	0.30	0.20	60.0	8.94	5.36	6.17	-19.78
490.5	3352	0.30	0.22	65.9	6.78	4.47	5.78	-19.89
495.5	3368	0.30	0.18	54.0	5.22	2.81	5.78	-20.39
500.5	3385	0.30	0.22	65.9	5.73	3.78	5.53	-20.17
505.5	3402	0.30	0.22	65.9	7.92	5.22	5.57	-20.15
510.5	3418	0.30	0.15	45.0	5.83	2.62	5.22	-20.20
515.5	**3435**	0.30	0.17	51.0	7.74	3.94	6.01	-18.33
516.5	3437		0.18		8.27		6.08	-18.15
520.5	3450		0.17		4.27		6.22	-18.45
525.5	3468		0.22		16.96		6.16	-17.96
530.5	3485		0.17		7.60		6.32	-18.42
535.5	3502		0.18		5.56		6.74	-18.17
540.5	3518		0.21		4.54		6.46	-18.64
545.5	3535		0.23		5.42		6.66	-18.81
550.5	3552		0.20		6.71		6.72	-18.38
555.5	3568		0.22		4.97		6.30	-19.00
560.5	3585		0.22		5.05		6.61	-19.08

---

[1] Bold figures denote age control points.

[2] AR$_{bulk}$ = SR × dry bulk density × 1000

[3] Derives from in-situ acidified sediment.

[4] AR$_{TOC}$ = (AR$_{bulk}$ / 100) × TOC

[5] Sediments were acidified and rinsed prior to measurement.

Appendix 3.8.

Core 178

core depth (cm)	cal age (BP)	SST (°C) (UK'37)	core depth (cm)	cal age (BP)	$\delta^{18}O_{calcite}$	$T_{\delta 18O}$ (°C) [1]
1.5	1757	16	2.5	1760	2.45	3.69
3.5	1753	15.8	7.5	1776	1.84	6.63
6.5	1773	15.8	12.5	1792	2.49	3.51
9.5	1782	15.6	17.5	1808	1.54	8.07
17.5	1808	15.6	22.5	1825	1.70	7.28
22.5	1825	15.4	32.5	1857	1.42	8.63
27.5	1841	15.4	37.5	1873	1.19	9.75
32.5	1857	15.8	42.5	1890	1.24	9.47
37.5	1873	15.6	47.5	1906	1.34	9.00
42.5	1890	15.5	52.5	1922	1.27	9.33
47.5	1906	15.6	57.5	1938	0.83	11.47
52.5	1922	15.5	62.5	1954	0.98	10.73
57.5	1938	15.2	67.5	1971	0.91	11.10
62.5	1954	15.4	72.5	1987	1.37	8.86
67.5	1971	15.1	77.5	2003	0.76	11.80
72.5	1987	15.5	82.5	2019	0.71	12.03
77.5	2003	15	87.5	2036	0.61	12.49
82.5	2019	14.8	92.5	2052	0.71	12.03
87.5	2036	14.8	97.5	2086	0.55	12.82
92.5	2052	14.8	102.5	2102	0.61	12.49
97.5	2086	14.8	107.5	2118	0.53	12.91
102.5	2102	14.8	112.5	2134	0.67	12.22
107.5	2118	14.7	117.5	2149	1.11	10.12
112.5	2134	15	122.5	2165	0.50	13.05
117.5	2149	15	127.5	2181	0.61	12.49
122.5	2165	14.9	132.5	2197	0.55	12.82
127.5	2181	15	137.5	2213	0.85	11.38
132.5	2197	14.9	142.5	2229	0.32	13.89
137.5	2213	15	147.5	2245	0.32	13.89
142.5	2229	15	152.5	2260	0.74	11.89
147.5	2245	15	157.5	2276	0.87	11.28
152.5	2260	14.8	162.5	2292	0.76	11.80
157.5	2276	14.9	167.5	2308	0.72	11.98
162.5	2292	15	172.5	2324	0.76	11.80
167.5	2308	15	177.5	2340	0.92	11.05
172.5	2324	14.8	182.5	2355	0.55	12.82
177.5	2340	14.9	187.5	2371	0.85	11.38
182.5	2355	14.8	192.5	2387	0.64	12.36
187.5	2371	14.8	197.5	2403	1.05	10.40
192.5	2387	14.9	207.5	2441	0.66	12.29
197.5	2403	15.1	212.5	2460	0.54	12.87
202.5	2422	14.8	217.5	2478	0.69	12.12
207.5	2441	15.1	222.5	2497	1.14	9.98
212.5	2460	15.3	227.5	2516	1.24	9.51
217.5	2478	14.7	232.5	2535	0.86	11.33
222.5	2497	15.7	237.5	2554	0.82	11.51
227.5	2516	15	242.5	2573	1.06	10.36
232.5	2535	15.2	247.5	2591	0.93	10.96
237.5	2554	15.5	252.5	2610	1.04	10.45
238.5	2557	14.7	257.5	2629	1.16	9.88
242.5	2573	15.1	262.5	2648	1.01	10.59
246	2586	14.9	267.5	2667	0.98	10.73
247.5	2591	14.9	272.5	2686	1.33	9.05
252.5	2610	14.6	276.5	2701	1.20	9.68
257.5	2629	14.7	281.5	2719	0.79	11.65
262.5	2648	15	286.5	2738	0.72	11.98
265.5	2659	15.2	291.5	2757	0.81	11.56
267.5	2667	15.6	296.5	2776	0.81	11.56
271.5	2682	15	301.5	2789	0.75	11.84
276.5	2701	15	306.5	2802	1.24	9.51
281.5	2719	15.1	311.5	2815	0.72	11.98
286.5	2738	14.2	316.5	2828	0.75	11.84
288.5	2746	14.2	321.5	2841	0.79	11.66
291.5	2757	14.2	326.5	2854	0.96	10.82
292.5	2761	14.4	331.5	2867	0.97	10.77
296.5	2776	14.2	336.5	2880	1.23	9.56
297	2777	14.6	341.5	2893	0.98	10.73
301.5	2789	13.6	346.5	2906	1.18	9.79
303.5	2794	14.9	351.5	2919	0.96	10.82
306.5	2802	13.8	356.5	2932	0.84	11.42
311.5	2815	14.1	361.5	2945	0.70	12.08
316.5	2828	14.8	366.5	2955	1.84	6.63
321.5	2841	14.8	373.5	2976	0.72	11.98
326.5	2854	14.7	378.5	2989	0.85	11.38
331.5	2867	14.7	383.5	3002	0.97	10.77

Appendix 3.8. continued

core depth (cm)	cal age (BP)	SST (°C) (UK'37)	core depth (cm)	cal age (BP)	$\delta^{18}O_{calcite}$	$T_{\delta 18O}$ (°C) [1]
336.5	2880	14.6	388.5	3015	1.17	9.84
341.5	2893	14.5	393.5	3028	1.27	9.33
346.5	2906	14.3	398.5	3045	0.97	10.77
351.5	2919	14.3	403.5	3061	1.27	9.33
356.5	2932	14.3	408.5	3078	0.73	11.94
361.5	2945	15.1	413.5	3095	1.16	9.89
366.5	2955	15	418.5	3111	1.24	9.51
370.5	2967	14.7	423.5	3128	0.92	11.05
373.5	2976	15.1	428.5	3145	1.12	10.07
378.5	2989	14.8	433.5	3161	1.17	9.84
383.5	3002	15.3	438.5	3178	1.12	10.07
386.5	3010	14.7	443.5	3195	1.06	10.35
388.5	3015	15.1	448.5	3211	1.38	8.82
393.5	3028	15.3	458.5	3245	1.29	9.24
403.5	3061	14.8	463.5	3262	1.51	8.21
406	3070	15.3	467.0	3273	1.16	9.89
413	3093	15.2	473.0	3293	1.02	10.54
413.5	3095	14.9	480.5	3318	1.22	9.61
415	3100	15.1	485.5	3332	1.44	8.54
418.5	3111	14.8	490.5	3352	1.00	10.63
423.5	3128	14.8	495.5	3368	1.82	6.72
426.5	3138	15.1	505.5	3402	1.17	9.84
428.5	3145	15.8	510.5	3418	1.48	8.35
433.5	3161	15.5	515.5	3435	0.96	10.82
434.5	3165	15.3	520.5	3452	1.24	9.47
438.5	3178	15	525.5	3468	1.42	8.63
443.5	3195	14.7	530.5	3485	1.24	9.47
448.5	3211	15.1	535.5	3502	1.30	9.19
453.5	3228	15.9	540.5	3518	1.81	6.77
458.5	3245	15.4	545.5	3535	1.22	9.61
463.5	3262	15.3	550.5	3552	1.20	9.70
470.5	3285	14.9	555.5	3568	1.45	8.48
472.5	3292	14.9	564.0	3597	1.00	10.63
475.5	3302	14.8				
479.5	3315	15.5				
480.5	3318	15.7				
485.5	3332	15.4				
490.5	3352	15.3				
495.5	3368	15.2				
500.5	3385	15.4				
505.5	3402	14.9				
510.5	3418	14.7				
515.5	3435	14.2				
516.5	3437	14.2				
520.5	3450	14.8				
525.5	3468	15.5				
530.5	3485	15.0				
535.5	3502	15.4				
540.5	3518	15.4				
545.5	3535	15.1				
550.5	3552	15.0				
555.5	3568	15.2				
560.5	3585	15.5				

[1] $T_{\delta 18O} = 16.5 - 4.8 \times (\delta^{18}O_{calcite} + 0.22)$